Quantitative monitoring of gas injection, exsolution and dissolution using 4D seismic

Reza Falahat

Submitted for the degree of Doctor of Philosophy

Heriot-Watt University
Institute of Petroleum Engineering

March 2012

Abstract

The main concern in the monitoring of gas injection, exsolution and dissolution is the exact spatial distribution of the gas volumes in the subsurface. In principle, this concern is addressed by the use of 4D seismic data. However, it is recognised that the seismic response still largely provides a qualitative estimate of the moved subsurface fluids; exact quantitative evaluation of fluid distributions and associated saturations remains a challenge still to be solved. It is widely believed that a few percent of gas makes the pore fluid mixture very compressible, so that it cannot be distinguished from a more complete gas saturation using seismic techniques. However, because of the fact that a gas distribution viewed at the reservoir scale is distinctly different from that observed at the laboratory scale, conclusions from laboratory measurements may not, in fact, be wholly applicable. Indeed, it is found in this study that the main factor controlling the seismic response is gas thickness, whilst gas saturation *per se* remains approximately constant. Modelling studies show that, for thin reservoirs (less than tuning thickness), both timeshift and amplitude change attributes have a linear trend with gas volume. In theory, this conclusion does not apply to thick reservoirs, as the amplitude change then becomes non-linear. However, because thick reservoirs are normally combinations of intra reservoir sand and shale, it is anticipated that a linear amplitude response can still be expected in most reservoirs. Reservoir heterogeneity is observed to affect these results by less than 2%. In the modeling, a spurious deviation from linearity is evident with increasing simulation model cell size (especially the vertical dimension). The understanding above is applied to both timeshift and amplitude change attributes in a North Sea gas injection field. Here, seismic scale calibration coefficients are obtained by a volumetric method which aims to calculate gas volume maps using the 4D seismic attributes. The work reveals that the results from the two mapped attributes appear reasonably close but still have regions of disparity. Synthetic data based on the reservoir model and further analysis of the observed data have been able to replicate some of these differences and identify them as due to inter-layer wave interferences and 4D noise.

Similar findings to the above also apply to gas exsolution, in which gas migrates after arriving at the critical gas saturation, and establishes two specific gas saturations in the

reservoir: maximum gas saturation within the gas cap and critical or minimum gas saturation within the oil leg. On the other hand, for the reverse process, in which reservoir pressure builds up, it is noted that it is not only the fluid type that impacts the gas when it goes back into solution, but also other reservoir properties such as relative permeability curves, transmissibility, K_v/K_h, and the injection/production plan. The laboratory-proposed equations for calculation of solution gas oil ratio (R_s) and pressure dependency of the fluid and rock are found to be not directly valid in cases in which the reservoir pressure drops below the bubble point pressure. In this situation, gas evolves, migrates and alters the pressure dependency of the saturated rock and solution gas oil ratio. A compositional change of the gas and oil is found to occur with pressure drop. However, it is observed to have a negligible impact on the seismic domain. Finally, importance is drawn to the role of engineering principles when interpreting dynamic reservoir changes from 4D seismic data. In particular, it is found that, in clastic reservoirs, the principal parameters controlling mapped 4D signatures are not the pressure and saturation changes *per se*, but these changes scaled by the corresponding thickness (or pore volume) of the reservoir volume that these effects occupy. This understanding is validated both with numerical modelling and analytic calculation. This provides a basis for a linear equation that can readily and accurately be used to invert for pressure and saturation changes. The observed seismic data are then inverted for pressure and saturation changes using the principles above. The results show that the simulator does appear to predict the inverted seismic observations fairly accurately. However, there are also some noticeable differences which require some specific updates to the transmissibility multipliers (and hence barriers) and the net-to-gross distribution in the simulation model. This project reveals the ability of 4D seismic to quantitatively monitor the gas injection and exsolution, and highlights the fact that laboratory measures are not directly applicable at the reservoir scale. It can be concluded that the impact of the reservoir scale phenomena needs to be taken into account during time-lapse seismic interpretations.

This thesis is dedicated to

my wife, Masoumeh Gheblehei

Acknowledgments

I would like to express my gratitude to the National Iranian Oil Company (NIOC) and Iranian Ministry of Science, Research and Technology (MSRT) for the financial support. My special thanks go to Dr. Asghar Shams and Prof. Colin MacBeth, my supervisors, for the opportunity of studying within the research team of Edinburgh Time Lapse Project (ETLP). Their understanding, encouragements and technical discussions throughout this PhD program are highly appreciated. I thank BP for permission to use the dataset of An'Teallach gas injection field and Schiehallion oil field. I appreciate all the sponsors of ETLP (BG, BP, Chevron, ConocoPhillips, EnCana, ENI, ExxonMobil, Hess, Ikon Science, Landmark, Maersk, Marathon, Norsar, Ohm, Petrobras, Shell, Statoil, Total and Woodside) for supporting this research. I am grateful to Hamed Amini for provision of software and useful advice and discussions. I thank Schlumberger-Geoquest for the use of their Petrel and Eclipse software.

Further financial support was thankfully received from the SEG Foundation which awarded me the Leon Thompson/BP Scholarship. I thank my examiners Prof. Yanghua Wang and Dr. Andy Gardiner, for making helpful suggestions for improvement. I had the opportunity to meet and share great moments with really nice and smart people; HamidReza, Eric, Fabian, Alejandro, Valeriy, Yesser, Sean, Salako, David, Lu, Ilya, Dhiman, Denis, Sergey, Neil, Mehdi, Pantea, Nader, Hooman, AliReza and Amran, my great friends who have been a source of encouragement. I appreciate all staff and students of the Institute of Petroleum Engineering, Heriot-Watt University.

I am very grateful to my wife, Masoumeh, and my son, Meraj, for their understanding and for always being there for me. This thesis would not have been completed without your love, kindness, friendship and support. I thank my parents for their endless support.

Thanks to God for giving me abundant life, health, happiness and for giving ability to overcome challenges involved in the PhD research.

Reza Falahat, March, 2012

Publications

Part of the work presented in this thesis is also presented in the following publications:

From chapter 4:

- Falahat R., Shams A. and MacBeth C., 2010. Towards quantitative evaluation of gas injection using time-lapse seismic data. 72nd EAGE Conference and Exhibition, Barcelona, Spain.

- Falahat R., Shams A. and MacBeth C., 2011. Towards quantitative evaluation of gas injection using time-lapse seismic data. Geophysical Prospecting, Vol. 59, No. 2, P: 310–322.

From chapter 6:

- Falahat R., Shams A. and MacBeth C., 2011. Adaptive engineering-based scaling for enhanced dynamic interpretation of 4D seismic. 73rd EAGE Conference and Exhibition, Vienna, Austria.

- Falahat R., Shams A. and MacBeth C., 2011. Adaptive scaling for an enhanced dynamic interpretation of 4D seismic data. Geophysical Prospecting, Submitted.

Contents

List of tables

List of figures

Chapter 1

Introduction

In this chapter, a literature review of hydrocarbon gas (mainly methane) is provided, which covers both the 3D and 4D seismic literature. The understanding and assumptions of the geophysical community on the subject of gas are discussed, to reveal the weaknesses and strengths in the previous approaches. After this, 4D seismic is reviewed as a reservoir monitoring tool for different kinds of the gas-related process in a reservoir (e.g., gas injection, gas exsolution, and primary gas cap). A conclusion is reached as to the overall ability of 4D seismic to quantitatively monitor gas in these cases. Subsequent sections focus on equations and techniques which address the main challenges that arise from the treatment of gas saturation in the geophysical literature. The issues arising from this review shape the motivation for the remainder of the thesis. To conclude this current chapter and set up the subsequent chapters, I discuss general suggestions as to how some of the main challenges may be tackled.

1.1 General review of gas from the seismic literature

Natural gas is an enormously light fluid that has a very small bulk modulus. Figure 1.1 shows typical effects of gas saturation on the saturated rock velocity. These examples were obtained either by laboratory measurements (Domenico, 1976) or by a calculation using Gassmann's equation (Han and Batzle, 2002), and highlight an extreme non-linearity in the system. The same trend has been reported for CO_2 (Figure 1.1-c). There is a dramatic drop in the saturated velocity as the first few percent of gas is introduced. The saturated velocity is approximately constant for higher gas saturations, and due to the density effect it can even increases. It is concluded that gas saturation of a few percent has a dramatic effect on the P-wave velocity and this is similar to that of complete gas saturation (the red line in Figure 1.1-b). This suggests that seismic techniques cannot distinguish a water zone with small amounts of gas from economic gas reservoirs with high gas saturation. It is also concluded that 4D seismic is not able to quantitatively monitor the gas saturation variation (Lumley *et al.*, 2008).

In this section, some gas-related terms and concepts from the 3D and 4D seismic literatures are discussed. These are typically written in the context of laboratory data (Figure 1.1). The aim is to be familiar with the literature and understand the main issues and weaknesses in the application of the theory to gas in the seismic domain.

Bright spots

At the 1960s, some strong reflectors and change in reflection characters on seismic sections were reported that formed the basis of seismic sequence stratigraphy. During drilling of these strong seismic events, gas zones were observed, and seismic interpreters started to take them seriously (Chopra and Marfurt, 2007). Considerably larger amplitudes from gas charged reservoir rocks than from nearby oil or water saturated zones are found. Initially, bright spots were interpreted as oil reservoir signals, but it was later realized that these bright spots are the result of free or dissolved gas that cause a low-impedance anomaly (Chopra and Marfurt, 2007). Figures 1.2-a and b demonstrate a bright amplitude blocked by a fault in map and section view respectively, which was interpreted as gas indicator. This bright spot is highlighted in Figures 1.2-c and d which show the amplitude of the peak frequency generated using a matched-pursuit algorithm (Chopra and Marfurt, 2007).

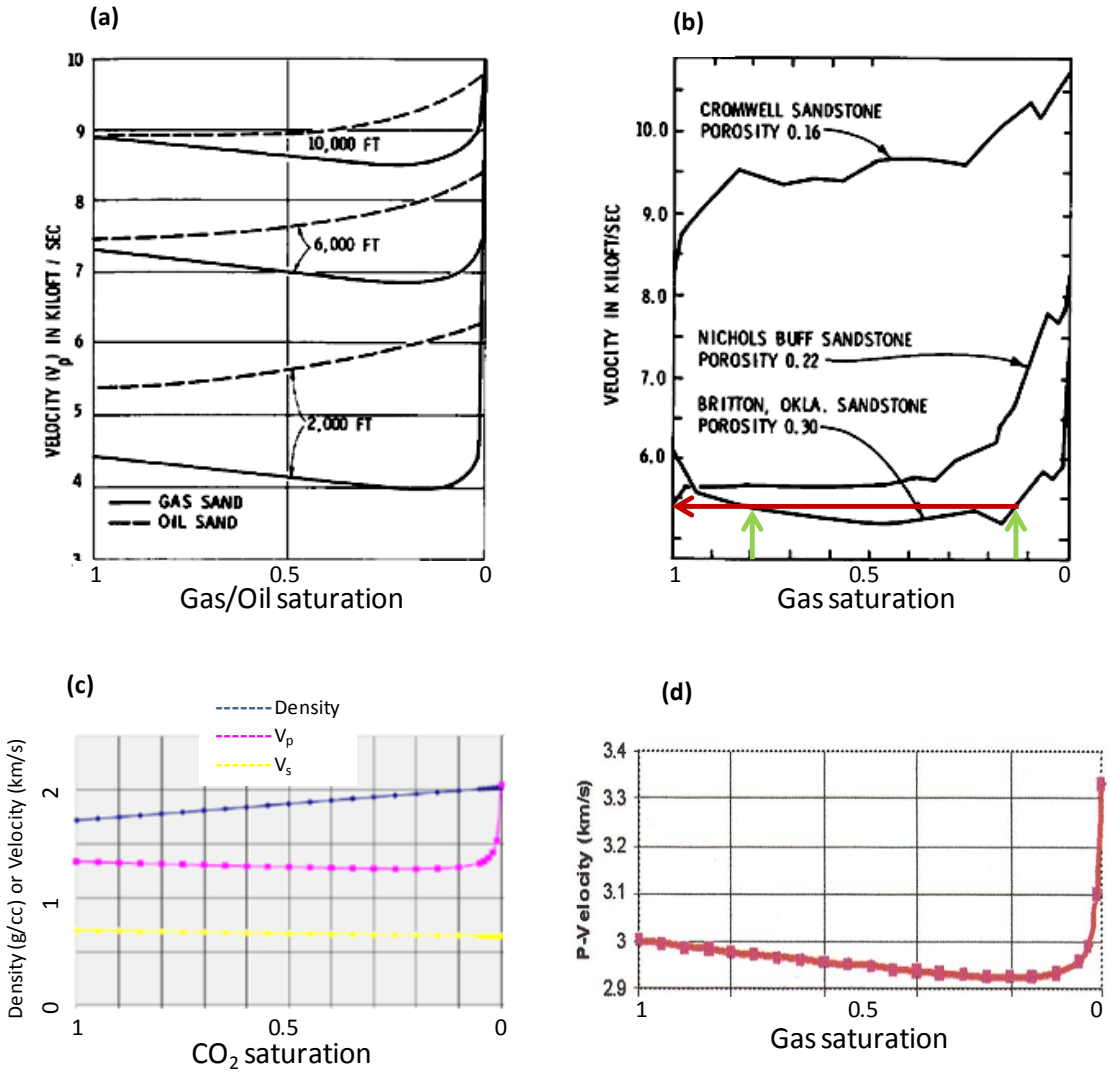

Figure 1.1 a) P-wave velocity as a function of gas or oil saturation, for gas and oil sands at depths of 2000, 6000, and 10,000 ft (Domenico, 1976), b) P-wave velocity in consolidated, porous sandstones versus gas saturation (Wyllie *et al.*, 1956), c) P-wave and S-wave velocity, and density of rocks saturated with CO_2 (in gas phase) at Sleipner (Lumley *et al.*, 2008), and d) Typical effect of gas saturation on the P-velocity of rocks under shallow conditions (Han and Batzle, 2002).

Anomalous behaviour of gas sands and low frequency shadows

Spectral decomposition techniques are occasionally used to detect gas sands (Chopra and Marfurt, 2007). The reason is a possible tuning effect at thin reservoirs or attenuation at the thick reservoirs. Gas charged sands are easily recognised, due to their frequency-dependent behaviour (Burnett and Castagna, 2003). The first example (Figure 1.3-a and b) is from the Alondra field in the Burgos Basin, Mexico (Burnett and Castagna, 2003). The 20m thick

gas sand with porosities between 13% and 18% is not clearly separated on the 20Hz seismic section (Figure 1.3-a), but the same section illustrates a clear signal in 40Hz (Figure 1.3-b). The gas charge makes the reservoir reflection coefficients larger than those saturated by brine. The composite reflection coefficient arising from the thin bed tuning effect reflects higher frequencies, thus making the 40Hz image brighter than the 20Hz image. The time thickness of this sand is close to tuning, so it appears as dipole.

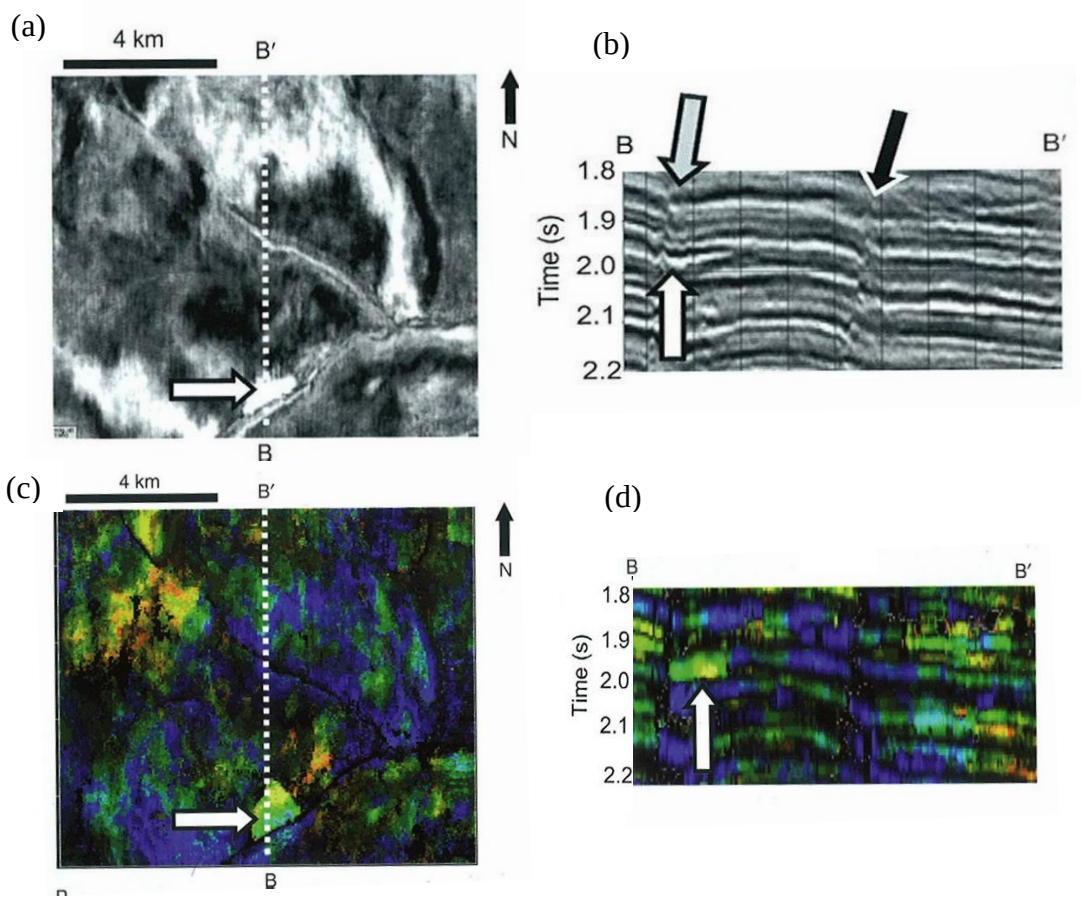

Figure 1.2 a) time slice at t=2000ms through a seismic data with b) vertical seismic section from south Marsh Island, Gulf of Mexico, c) and d) spectral decomposition composite image corresponding to the seismic data shown in a and b respectively (Chopra and Marfurt, 2007).

The second example (Figure 1.3-c and d) is from the Macuspana Basin in Mexico (Burnett and castagna, 2003). Two frequency panels were generated using a wavelet transform that illustrate the reservoir at 25 Hz (Figure 1.3-c) and at 35 Hz (Figure 1.3-d). Gas in this reservoir shifts the resonant frequency to a higher frequency, so this can be detected when

illuminated at the resonant frequency. The reservoir appears continuous on the 25Hz panel, but is discontinuous on the 35Hz. This discontinuity was proven by well data after production.

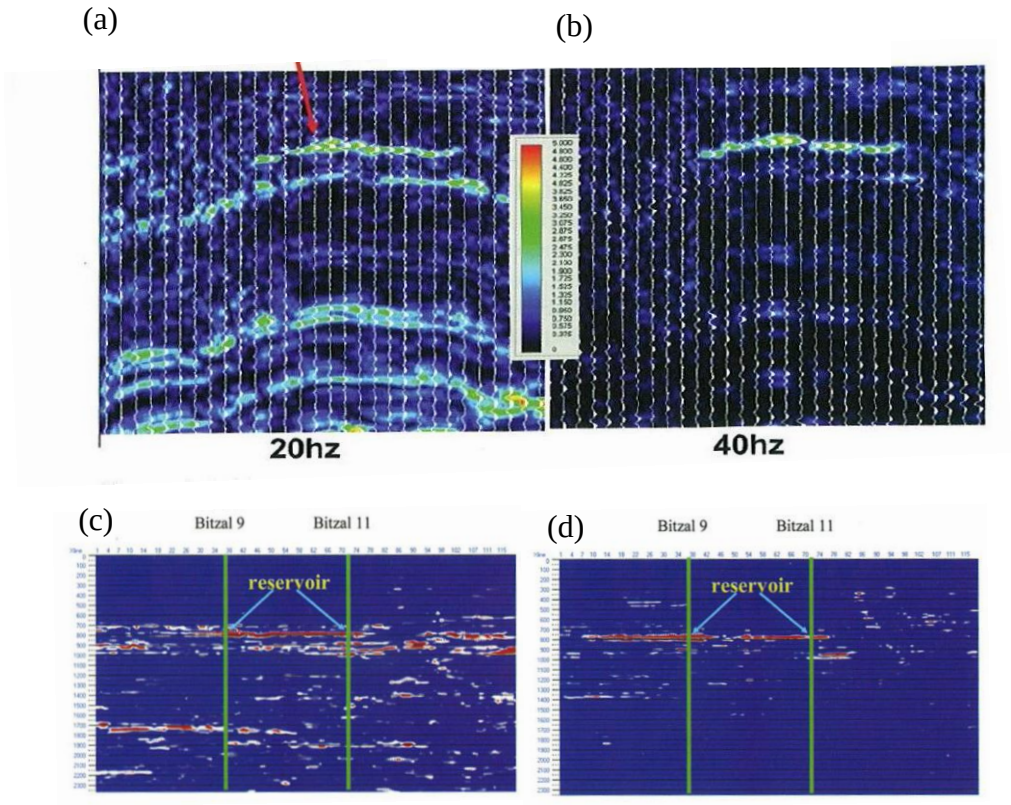

Figure 1.3 a) and b) ISA components of a gas reservoir, Burgos Basin, Mexico at 20 and 40Hz respectively. Iso-frequency panels show a reservoir that is better determined at d) 35 Hz and c) 25Hz (Burnett and Castagna, 2003).

In contrast, low frequency shadows have regularly been observed below gas reservoirs. The term shadows means a lowering of the amplitude spectral content beneath gas reservoirs. The high attenuation of high frequency energy in the gas causes such low frequency shadows. In thick gas reservoirs, energy absorption shifts the spectral energy from high to low frequencies, due to a relatively larger travel path. Consequently, low frequency reflections from below such reservoir have been used as hydrocarbon indicators. Figures 1.4 a and b demonstrate frequency sections generated by wavelet transform for 10 Hz and 30Hz from the Gulf of Mexico (Castagna *et al.*, 2003). Despite the fact that the reservoir

appears bright at 10Hz, a zone of strong low frequency energy below the reservoir can still be seen. Although the reservoir can be observed at 30Hz, the energy under the reservoir is not obvious. However, since the variation of the frequency content has other sources as well (e.g, variable attenuation for different rock types and variable thickness of the layers), the spectral decomposition technique needs to be employed carefully in quantitative analysis.

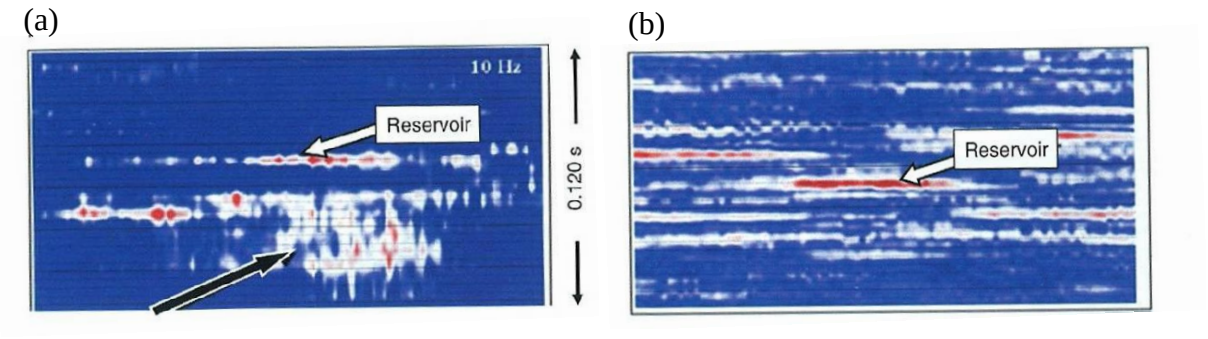

Figure 1.4 Spectral amplitude images at a) 10 Hz and b) 30Hz for an offshore Tertiary clastic section. The black arrow highlights the low frequency energy below the gas reservoir (Castagna *et al.*, 2003).

Gas chimneys

Gas chimneys refer to the regions with a low concentration of gas that has migrated upward from a reservoir. Chimneys are normally observed on seismic data as zones of low coherence reflections. Three main reasons are reported by Chopra and Marfurt (2007) for such a poor data quality. Firstly, there is a considerable absorption of the P-wave energy in the presence of the gas bubbles in the pores. A second reason is relevant to the thin sand layers (less than 0.25m) that are charged with gas migrating towards the surface. The limited lateral extent of gas charged thin layers, which contain very low impedance compared to the surrounding shales, causes scattering of the energy. Thirdly, the presence of gas results in a very sharp drop in P-wave velocity. In shallow sediments (lower pressure zones), this velocity is occasionally less than that of the P-wave velocity in water. As a result, seismic sections display depressions in time, multipathing, and apparent faults. During acquisition and processing, the combination of the reasons mentioned above produce wavefront perturbations that are very hard for a depth migration algorithm to untie. The result is a major loss of signal.

Gas chimneys are good indicators of the presence of source rock (Heggland 2004). They can point to a broken or poor hydrocarbon seal, or a reservoir that is over-charged. Shear waves can be employed to precisely image through a gas chimney, since those are comparatively insensitive to the presence of gas. Heggland (2004) generated a meta-attribute (a combination of attributes) based on coherence, amplitude, and other attributes to map gas chimneys in Green Canyon, Gulf of Mexico. Figure 1.5-a, shows a line through the gas chimney. The chimney is related to zones that are low amplitude and have a low coherence character. Figure 1.5-b shows a 3D image of RMS amplitude extracted along key horizons, overlain with the chimney meta-attribute. Chimneys correlate well with faults on the picked horizons. Figure 1.5-c illustrates another example of a gas chimney from the Lisa Anne prospect, Green Canyon, Gulf of Mexico (O'Brien, 2004).

Fizz water and low gas saturation

Fizz water refers to water with a few percent of dissolved gas. When this gas is free, the rock is defined as a low gas saturated sand. Low gas saturations of up to 25% have been reported. These layers are taken as hazards in drilling shallow sands (Heggland, 2004). Shallow gas-charged channels are considered as over-pressurised gas zones when they are overlaid by impermeable sediments and are not contacted with faults. At the exploration stage, low gas saturated sediments present a strong signal like the high and economical gas saturated sediments, due to the extreme non-linearity shown in Figure 1.1. At this stage, dry holes that are drilled because of such a strong reflectivity in the seismic data are generally explained as low gas saturated sediments, if gas is detected in gas chromatograph logs (O'Brien, 2004, and Chopra and Marfurt, 2007).

A few select examples will be presented here to determine the reasons for assigning strong reflectors to the gas charged sediments. Figure 1.6-a represents the RMS average between top and base reservoir of a channelized system which was interpreted as possible gas charged sands (Oyedele, 2005). However, it could simply be interpreted as a gas free channel that contains a higher impedance contrast. Figure 1.6-b shows the seismic profile and probable stacking pattern within the channel complex.

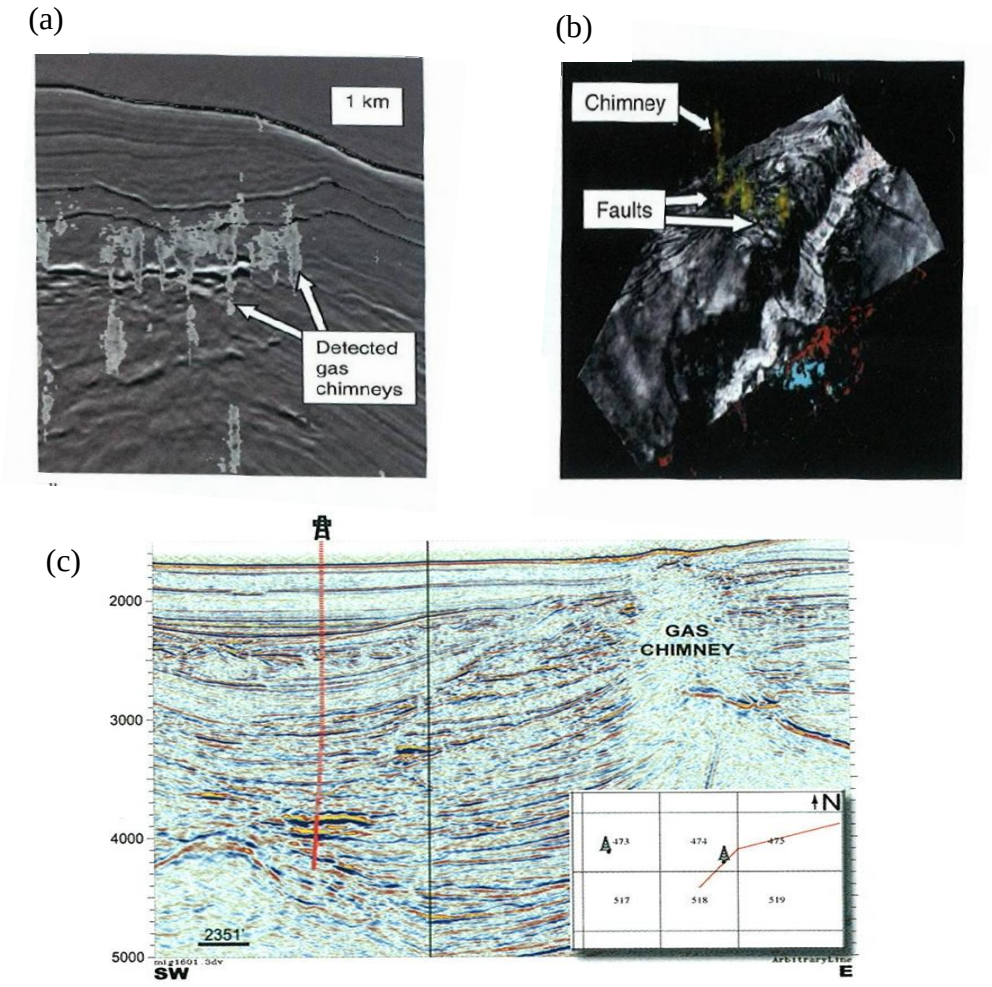

Figure 1.5 a) Vertical seismic section with extracted gas chimneys, b) a 40 ms average absolute amplitude map along a horizon. Chimneys are plotted in yellow and associated with the faults (Heggland, 2004). c) seismic section showing a gas chimney located four miles northeast of the Lisa Anne Prospect, Green Canyon (O'Brien, 2004).

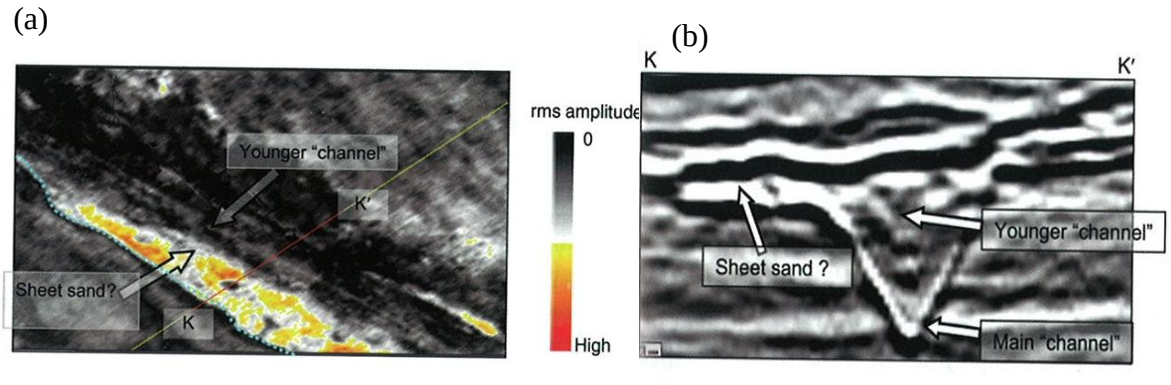

Figure 1.6 a) An RMS amplitude map which highlights the channel with possible low gas saturation, b) A seismic section showing a stacked channel complex (Oyedele, 2005).

The second example of the low gas saturation is chosen from the Lisa Anne prospect, in the Green Canyon, deepwater Gulf of Mexico (O'Brien, 2004). Figure 1.7-a, demonstrates the seismic section along with the drilled wells across the detected bright spots. The strong amplitude at the eastern side was selected as a drilling target but ended up as a dry hole. The logs for the well are presented in Figure 1.7b. The low P-velocity areas (yellow colour) were interpreted as low gas saturated sands. The gas chromatograph log highlights the signature of methane, ethane and propane. Density logs could be a useful tool for confirmation of the results, because of the linear response of the density to the gas saturation variation. However, the density does not show obvious difference between low gas-saturated and water saturated sands, but needs further investigations. AVO analysis can also be useful here. Far angle seismic data should not necessarily provide a strong amplitude response due to the small S-velocity change by gas saturation variation.

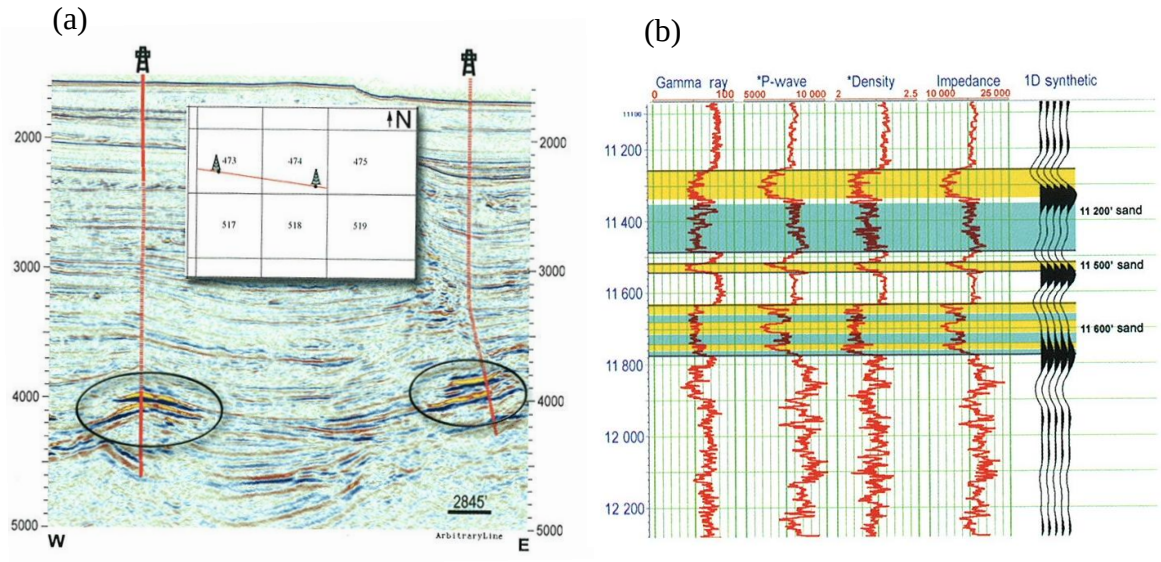

Figure 1.7 a) 3D seismic section across the King Kong/Lisa Anne minibasin, b) Gamma ray, P-wave, Density, P-Impedance and 1D synthetic trace for the Anadarko Green Canyon. Yellow and blue colours are representative of the possible low gas saturated sands and water saturated sands respectively (O'Brien, 2004).

Another question that needs to be addressed regarding the low gas saturation is: where is the gas cap? Due to the physics of gas and gas migration in the geological sense, these sands contain gas saturation close to or below the critical gas saturation, and the gas is not moveable as it is trapped in the pores. However, the remainder of the gas (the higher gas

saturation) will migrate upward due to gravity segregation to form a gas cap over the water column. One possibility that might arise is a gas chimney, which could be generated by the migration of the gas cap along fractures. O'Brien (2004) shows a gas chimney four miles from the drilled well (Figure 1.5-c). However the migration path is not delineated in the seismic data.

It is widely believed that a small volume fraction of the dissolved gas in water drops the P-wave velocity and impedance significantly (Figure 1.8-a, Han and Batzle, 2002). However, recently measured data demonstrate that dissolved gas has a small effect on the P-wave velocity in water (Han and Batzle, 2002). In Figure 1.8-b, both gas-free water and water with dissolved gas of about 6.5 L/L methane were plotted as functions of pressure and temperatures (Han and Batzle, 2002). These data show that dissolved gas has a minor effect on P-wave velocity in water. A possible explanation is that, when pressure is decreased below the bubble point, gas bubbles are liberated to form a gas-water mixture. This free gas phase is expected to extensively lower the fluid mixture modulus. However, measurements by Han and Batzle (2002) show that these exsolved gas bubbles have a small effect on the total gas-water mixture's volume and density at higher pressures. This is due to the low volume and high density of exsolved gas at higher pressures. The gas effect on volume and density gradually increases but only becomes noticeable when pressure is lower than 20 MPa (3000 psi). In addition, the amount of gas that can go into solution has been overestimated in the literature modelling (Figure 1.8-a). Han and Batzle (2002) deduced that a lesser volume of gas can be dissolved in water. Meadows (2008) considered this as negligible for CO_2 injection into an aquifer (for short term 4D seismic monitoring).

As discussed earlier, it is often assumed that gas is so compressible that it has an almost negligible modulus, so a few percent of gas makes a dramatic drop on the fluid modulus (Domenico, 1974). However, it behaves like oil at higher pressures. Figure 1.8-c shows the result of petro elastic modelling from Han and Batzle (2002). Realistic gas properties were used to calculate the velocity and modulus of a gas-water mixture based on Wood's equation. The results show clearly that high-pressure gas (even at higher temperature) is less effective at reducing the modulus of the gas-brine mixture.

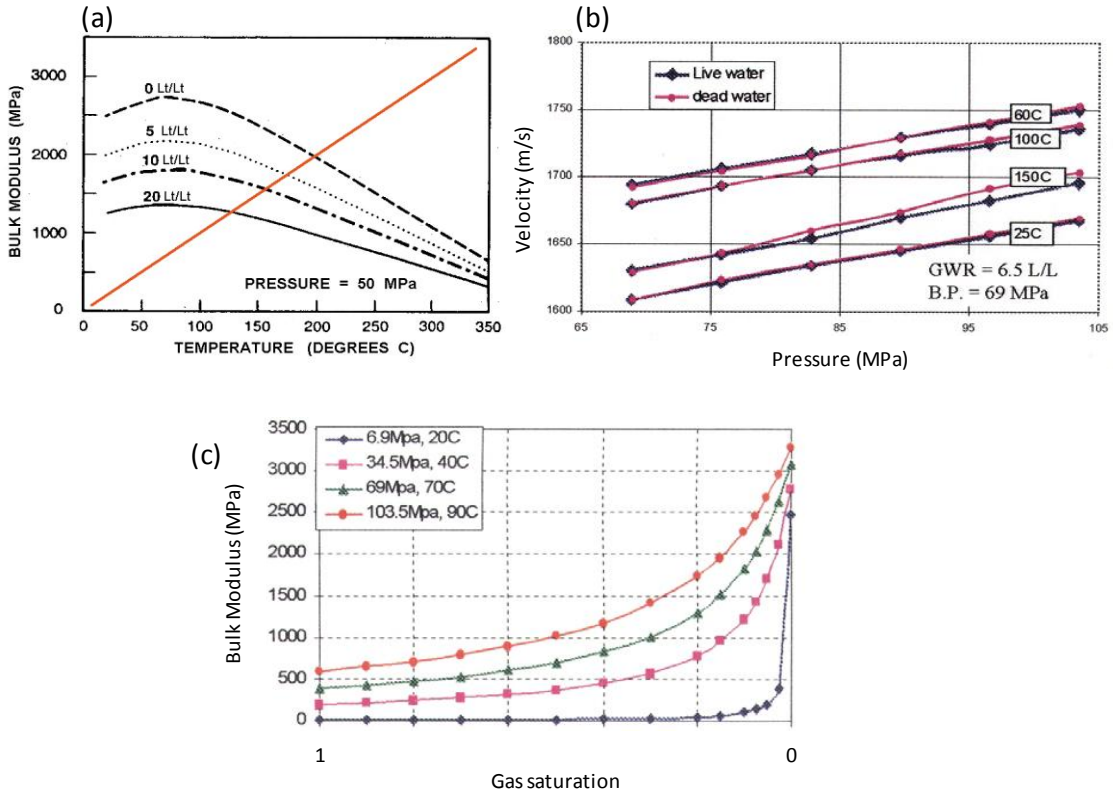

Figure 1.8 a) Calculation of the effect of gas in solution on the water bulk modulus, b) Measurements of "live" and "dead" water velocity at different pressure and temperature conditions, and c) Modulus of gas-brine mixture at in-situ conditions (Han and Batzle, 2002).

Figure 1.9 shows the synthetic modelling results for shallow (lower depth – smaller pressure) and deep (higher depth – higher pressure) fluid properties applied to a log from the Gulf of Mexico (Han and Batzle, 2002). Figure 1.9-a, a gamma-ray log, shows a massive sand zone with a gas cap above the water zone. Saturation conditions are color coded on the log curves: green, red, and blue refers to the normal, shallow fizz and deep fizz water respectively. The water zone can be compared in both shallow and deep conditions for the density, P-wave velocity, P-impedance and the synthetic trace. The water zone with 5% gas saturation shows a clear contact with the gas zone at depth (higher pressure and temperature) in the velocity log and also in the seismic trace. However, it has the same velocity as the gas zone in the shallow area. The same scenario is repeated for the base of the water zone as well. Clearly, seismic cannot distinguish a fizz-water zone from an economic gas reservoir at a shallow depth. However, in deepwater, 5% gas has a very different effect on the *P*-wave velocity (blue curve in Figure 1.9-c).

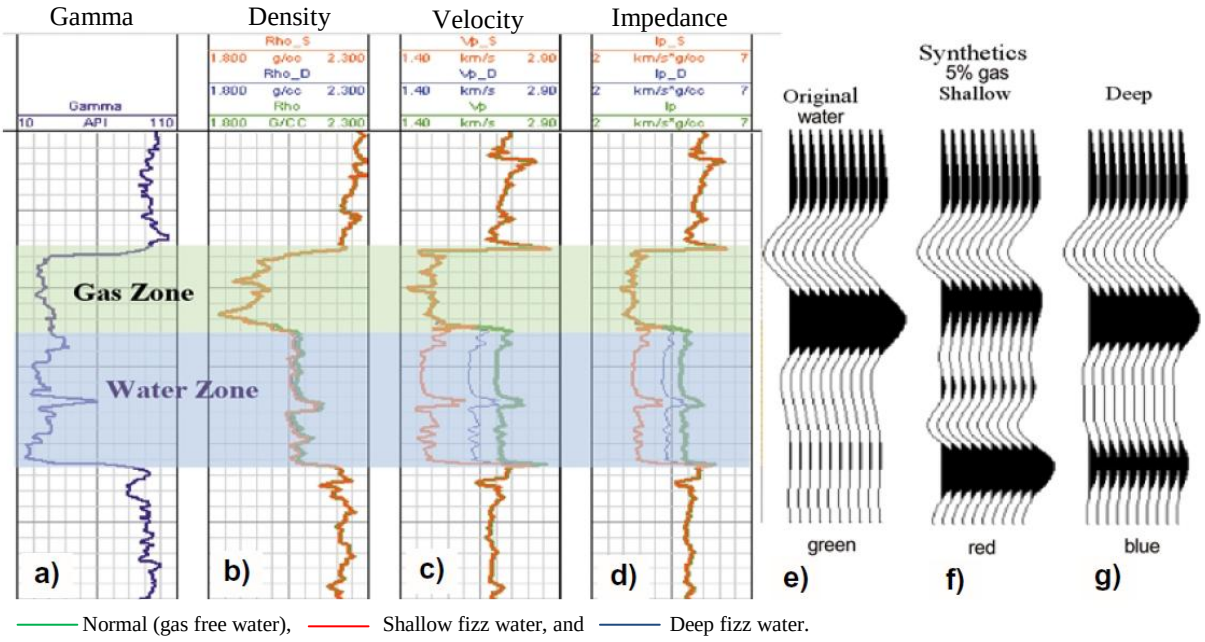

Figure 1.9 a) Gamma ray, b) density, c) velocity, d) impedance, and e-g) synthetic traces calculated for the original water zone log (green curve) and for the 5% gas-saturation effect on the water zone in the shallow and deep conditions (Han and Batzle, 2002).

A brief discussion and conclusion

The seismic literature findings on gas effects are briefly illustrated in Table 1.1. This shows the problems and challenges in the seismic domain which arise from treating gas. These are selected as they address important problems in a qualitative way. It is believed that some of these problems and challenges are not necessarily real, but probably the misunderstandings and forgotten assumptions about the physics of gas.

As a brief conclusion for the discussion provided in this section, blaming fizz water or low gas saturated sediments for false hydrocarbon indicators at depth may not be valid. The gas cap needs to be taken into account in the interpretation of low gas-saturated sands. Finally, gas is not the only reason for all of the unknown events during seismic interpretation. This argument highlights the necessity for a better understanding of gas in terms of the fluid physics, geology, engineering and the related seismic response. We need to understand the gas behaviour under reservoir conditions to be able to talk clearly about the seismic response.

Gas effect	Problems and challenges	Ranking (in terms of problems)
Gas chimney	- Scatters energy incoherency - Gas makes depression in time, multipathing, and apparent faults - Decreases the S/N - Masks the reservoir, and production activities	1
Low gas saturation	- Produces a strong signal - Masks the other signals - Makes hazards in drilling at the shallow sands - End up with dry holes	2
Bright spots	- Presents a strong signal - Misleads the interpreter - Overestimates the reservoir quality and ends up with dry hole - Masks other signals e.g. reservoir activities	3
Unrecognised seismic signal	- Produces some strange sedimentological patterns - Makes apparent faults - Overestimates the fluid effect	4
Processing artefact	- Produces sharp variation on velocity - Makes difficulties during migration	5
Attenuation	- Changes the frequency content - Absorption of the compressional wave energy	6
Dissolved gas in water	- Presents a strong signal - Overestimates the reservoir quality - Makes difficulties during interpretations	7

Table 1.1 Gas effects with problems and challenges for 3D seismic. Note that the items were qualitatively screened based on the problems and challenges regarding gas, in their order of priority (one is the highest).

1.2 Time lapse seismic

As a general statement, the main role of applied geophysics has changed in the last two decades from regional exploration for new fields to reservoir characterisation and

monitoring. Time lapse seismic, as one of the geophysical techniques, has the potential to help reservoir management and recovery improvement plans. 4D seismic, a series of repeated 3D seismic surveys over time, is employed to monitor production related activities in time and space. Production activities change the elastic parameters (velocity and density) of the saturated rocks, and this in turn affects the reflection coefficients at the top or base of the reservoir. These changes are detected by amplitude, timeshift or even frequency-derived attributes. 4D seismic has the potential to provide information regarding fluid movements, barriers and compartments, fault transmissibility and general connectivity. This information helps improve the understanding of well performance and may increase a field's economic life.

By following the general progress of time lapse seismic over the last two decades, three main stages are noticed: the qualitative stage (visual interpretation), semi quantitative stage (model screening) and quantitative stage. By moving from the qualitative stage towards the quantitative one, 4D seismic, as a measurement of the reality in the subsurface, has gradually changed its main objective from being at the service of the reservoir simulation model to being an independent tool for reservoir monitoring and management. There is no doubt that this will probably be the subject of the next decade. Time lapse seismic applicability has been proven for monitoring of water injection in the Draugen and Gannet fields, offshore Norway, which guide the identifying of un-drained compartments (Koster *et al.*, 2000). It has also been used in monitoring heavy oil reservoirs (Sigit *et al.*, 1999; Theune *et al.*, 2003). Gas injection and gas reservoir production are reported to have been successfully monitored (Domunt *et al.*, 2001, Huang *et al.*, 2001, Langlaise, 2005). Besides giving valuable information for hydrocarbon extraction, 4D seismic has also found application in monitoring of carbon dioxide capture and storage projects (e.g. Eiken at al., 2000, Arts *et al.*, 2004, Meadows, 2008).

One of the main challenges of quantitative interpretation of the 4D seismic signal is the noise level. For low repeatability case studies, it is difficult to allocate all the seismic changes to production activities. Another challenge is the long period between repeat surveys. However, with the advent of the life of field (LoF) 4D projects (e.g Valhall, North Sea (Gestel *et al.*, 2008)), there is the possibility to get a higher signal to noise ratio and decrease the time between seismic surveys, although one question will still remain. Have

reservoir activities made significant change in the elastic properties of the reservoir rocks during those few months?

1.3 Gas saturation and thickness in the 4D seismic domain

Amplitude change is the most popular 4D seismic attribute for monitoring gas (Huang *et al.*, 2001, Vidal *et al.*, 2001, Sengupta *et al.*, 2003, Wagner *et al.*, 2004, Meadows, 2008, Lumley *et al.*, 2008, and Ghaderi and Landro, 2009). However, in recent works, timeshift is also employed (Dumont *et al.*, 2001, Meadows, 2008, and Ghaderi and Landro, 2009). For monitoring of the gas using 4D seismic, calculation of the gas saturation (Dumont *et al.*, 2001, Vidal *et al.*, 2001, Huang *et al.*, 2001, Wagner *et al.*, 2004, Floricich *et al.*, 2006, Tsuneyama and Mavko, 2007, and Lumley *et al.*, 2008) or the gas thickness (Sengupta *et al.*, 2003, Meadows, 2008, and Ghaderi and Landro, 2009) are taken into account. Huang *et al.* (2001), in the monitoring of a Gulf of Mexico gas reservoir, linearly related gas saturation to the amplitude change by assuming a patchy saturation (Figure 1.10-a) (patchy saturation refers to the non-uniform or heterogeneous distribution of the fluid throughout the pore space in a reservoir or borehole (Smith *et al.*, 2003)). Using the material balance equation, they thresholded the amplitude change map to highlight the produced gas area. Dumont *et al.* (2001), in the monitoring of a gas storage project in central France, declare that gas saturation is never low in the gas injection experiments. Therefore, the low saturation portion of the plot in Figure 1.10-b that is the most critical part is not included. For the second part of the plot, higher gas saturations, they fit a line which has the opposite trend of the one employed by Huang *et al.* (2001). This highlights the increase of P-wave velocity (the main component on the vertical axes (R_x) is the velocity) with gas (mainly methane) saturation. This trend is due to the density effect, since velocity is proportional to $1/\sqrt{\rho}$. The attribute selected is the normalised timeshift (R_x) described by:

$$\frac{H_t^{\,2}}{\left(H_t + \Delta t\right)^2} = R_x = 0.0788 S_g + 0.7795 \qquad (1.1)$$

where H_t is the time thickness of the reservoir and Δt is the timeshift of the seismic

reflector. Figure 1.10-c, shows the gas saturation at different times. It should be noted that their assumption regarding no low gas saturations during the injection period may not be generalised for other reservoirs. Another issue is that the increasing trend in the second part of Figure 1.10-b, which was selected for fitting the line, has a small gradient in most laboratory-based measurements (e.g. Figure 1.1). A careful consideration for the employment of such a small variation is necessary, as it is probably below the detection limit or repeatability limit of the 4D seismic. The last two examples show two extreme cases in the saturation mixing law, which are arithmetic and harmonic averaging.

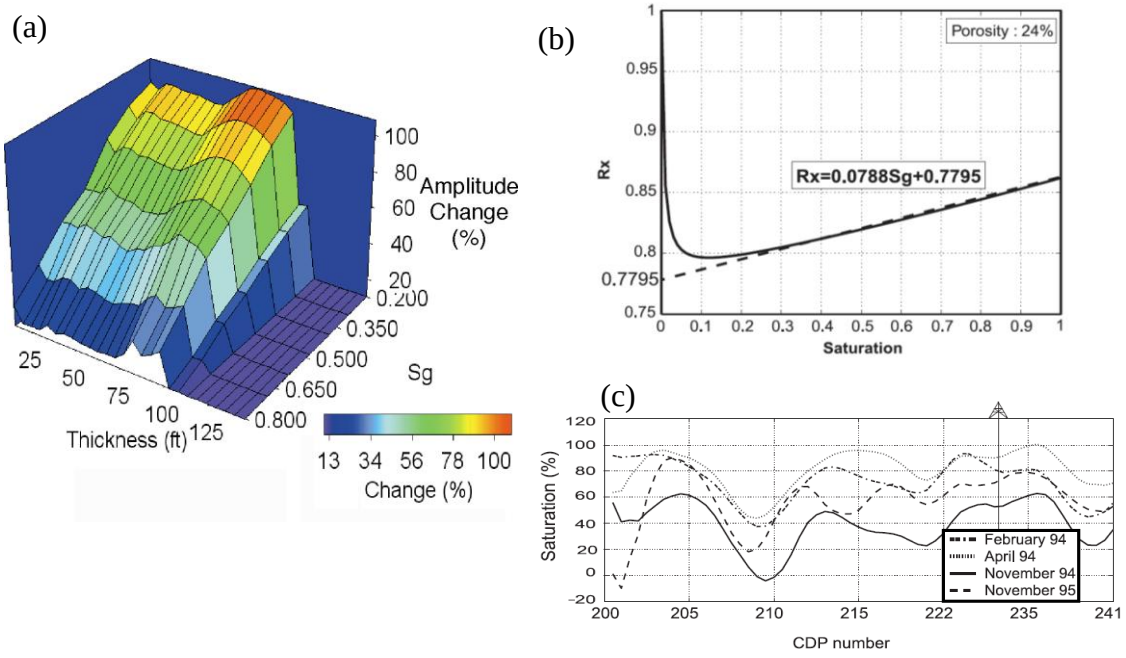

Figure 1.10 a) Relationship between reservoir thickness, gas saturation and amplitude change derived from a "Patchy saturation" model for a frequency of 60 Hz (Huang *et al.*, 2001), b) Rx versus gas saturation and c) gas saturation at different times (Dumont *et al.*, 2001).

Lu and McMechan (2002), Wagner *et al.* (2004) and Tsuneyama and Mavko (2007) obtained gas saturation from amplitude change using rock physics concepts. Lu and McMechan (2002) and Wagner *et al.* (2004) arrived at the gas saturation change by inverting amplitude change to P-impedance change. Wagner *et al.* (2004) assumed harmonic averaging for the low gas saturations and arithmetic averaging for the other saturations in the petro elastic modelling, because they think that, it is somewhere between these two averages. Figure 1.11 shows the P-wave impedance with the inverted gas

saturation map. The inverted gas saturation map (Figure 1.11-b) shows a very large distribution of the exsolved gas due to pressure depletion.

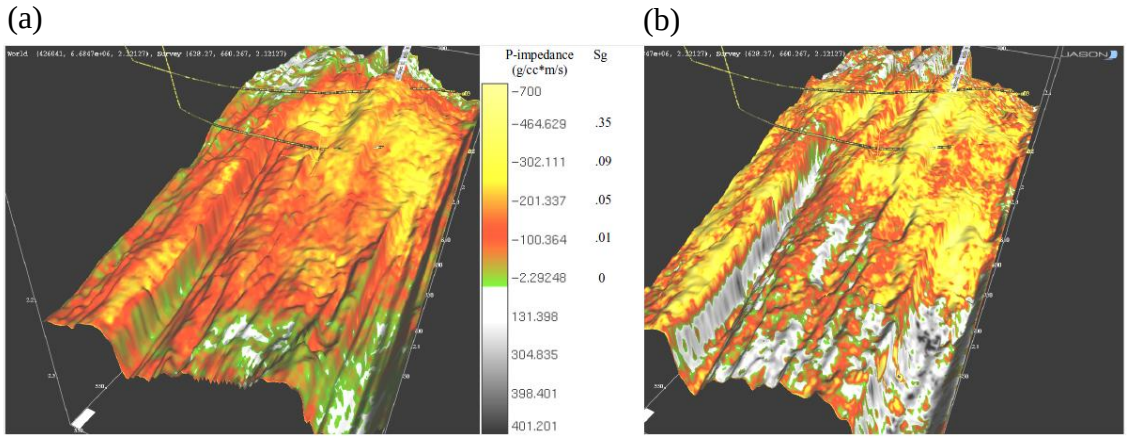

Figure 1.11 a) Change in average acoustic impedance of the reservoir interval, and b) estimated gas saturation (Wagner *et al.*, 2004).

Tsuneyama and Mavko (2007) implemented a workflow based on rock physics to invert the seismic amplitude to the fluid bulk modulus separately for the base and monitor surveys. They then inverted fluid bulk modulus to the water, gas and oil saturation using the harmonic averaging and arithmetic averaging separately, as they believe that, it is somewhere between these two averages. Finally they selected a mean value of the fluid saturations derived from these two methods. Floricich *et al.* (2006) and Lumley *et al.* (2008) included the pressure effect as well, and using the pressure and saturation inversion methods, calculated gas (mainly methane) and CO_2 saturations respectively. Floricich *et al.* (2006) presented an engineering approach based on calibration with production data. Based on rock physics and laboratory data, they proposed the non-linear equation which linearly added pressure, water saturation and gas saturation effects:

$$\Delta A \approx a\left(e^{b\Delta S_g} - 1\right) + c\Delta S_w + d\Delta P^2 + f\Delta P \qquad (1.2)$$

where ΔA represents the change in the seismic attribute; ΔS_g, ΔS_w and ΔP are the changes in the gas saturation, water saturation and reservoir pressure respectively. The constants *a*, *b*, *c*, *d*, *f* are determined by calibration to the engineering data. For the 4D attributes

calibration, ten training wells were selected. For the Schiehallion oil field, North Sea, they employed a combination of five seismic attributes (far amplitude, intra-reservoir time-stretch (time-shifts computed in a window below the reservoir minus the time-shifts computed in a window above the reservoir), near amplitude, full amplitude and instantaneous frequency) using a low validation error. The inverted gas saturation change is demonstrated in Figure 1.12.

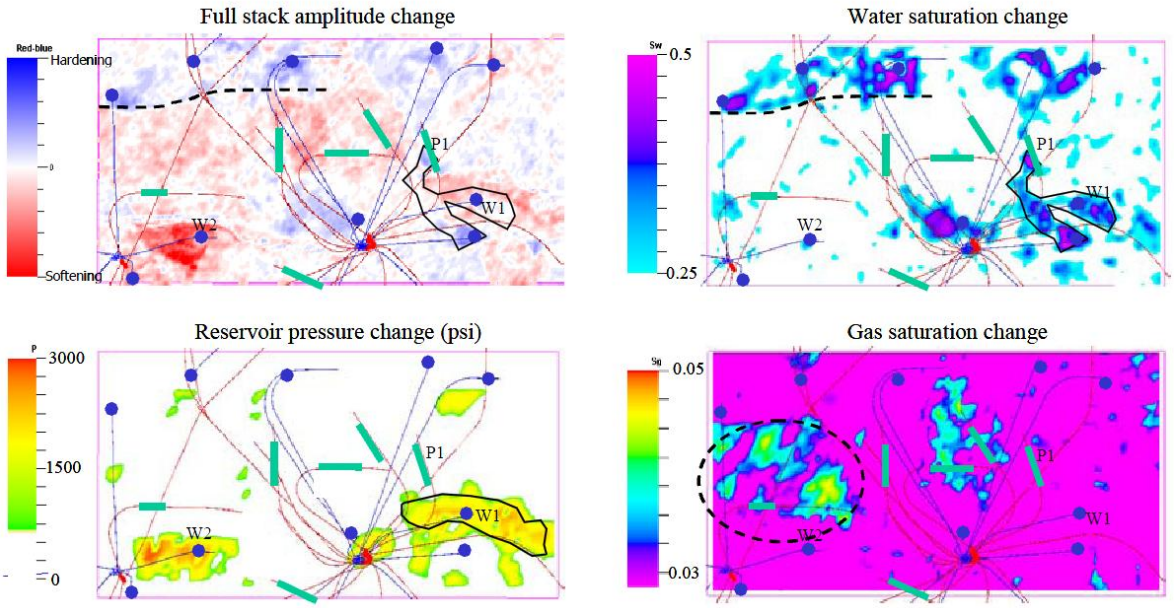

Figure 1.12 Amplitude change and inverted water saturation change, pressure change and gas saturation change respectively for the Schiehallion field, North Sea (Floricich *et al.*, 2006).

Sengupta *et al.* (2003), Meadows (2008), and Ghaderi and Landro (2009) calculated gas thickness instead of the gas saturation (gas thickness is defined here as a thickness of the formation where the gas saturation is above zero percent). Sengupta *et al.* (2003) used the geological trend to downscale the gas saturation log extracted from the upscaled simulation model (Figure 1.13). This downscaled log was employed in a synthetic seismic procedure which has a good correlation with the observed seismic. They used this trend to calculate the gas thickness from the observed 2D seismic. Meadows (2008), in the monitoring of the CO_2 injection into an aquifer, employed 1D modelling for the calculation of the effect of different gas thickness on the timeshift and amplitude change (Figure 1.14-a and b). A

hyperbolic CO_2 saturation height function was used to determine the depth dependent CO_2 saturation for each of the scenarios. He inverted timeshift and amplitude changes to the gas thickness separately and the final proposed map was the average of these maps. Figure 1.14-c and d illustrate the traveltime and amplitude changes. Traveltime difference shows considerable disagreement with the amplitude change map. This disparity will be discussed on Chapter 4. Meadows (2008) also shows that the temperature change in the reservoir range does not have detectable effect on the seismic signal.

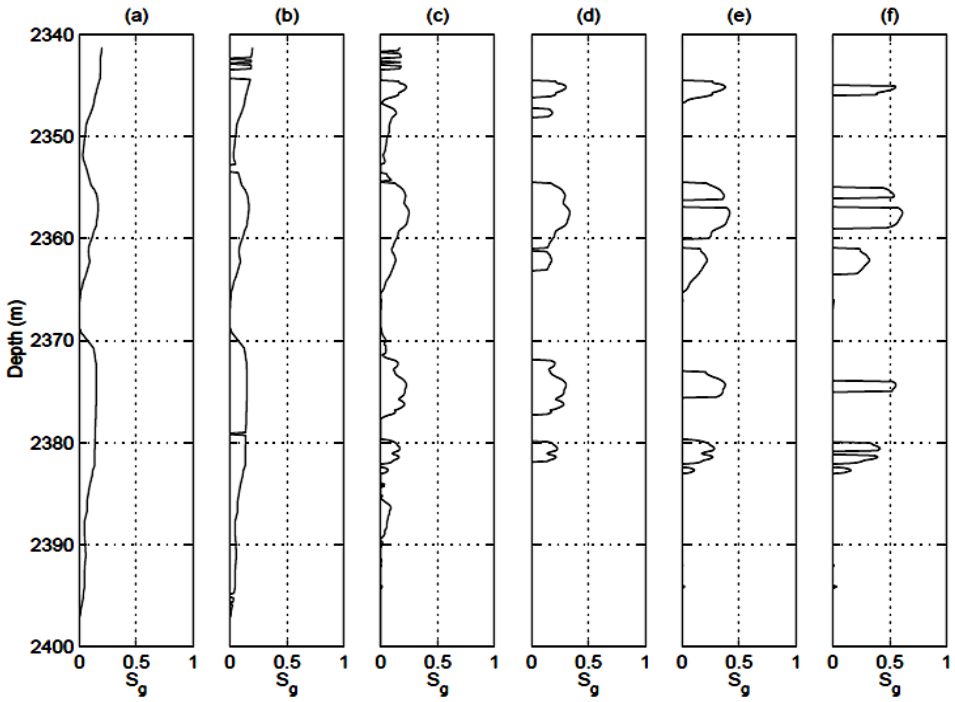

Figure 1.13 Downscaling saturations from the flow simulator. a) S_g extracted from the simulator, and b)–f) estimations of downscaled S_g (Sengupta *et al.*, 2003).

Ghaderi and Landro (2009) developed two equations which relate timeshift and amplitude change with the velocity change and gas (CO_2) thickness change separately. Instead of solving both equations simultaneously to arrive at the gas thickness and velocity change, they assume constant gas thickness and calculate the velocity change by graphical solution. Therefore, the results were constant gas thickness with variable velocity change. They also employed time-shifts with rock-physics principles and assumed two CO_2 saturations (0 and 100%), so the velocity change is constant and they calculated gas thickness change. The

last two examples (Figures 1.13 and 1.14) concern about CO_2, a gas which is different from methane in terms of the physical properties that control the saturation distribution. These examples were selected to discuss the gas thickness definition.

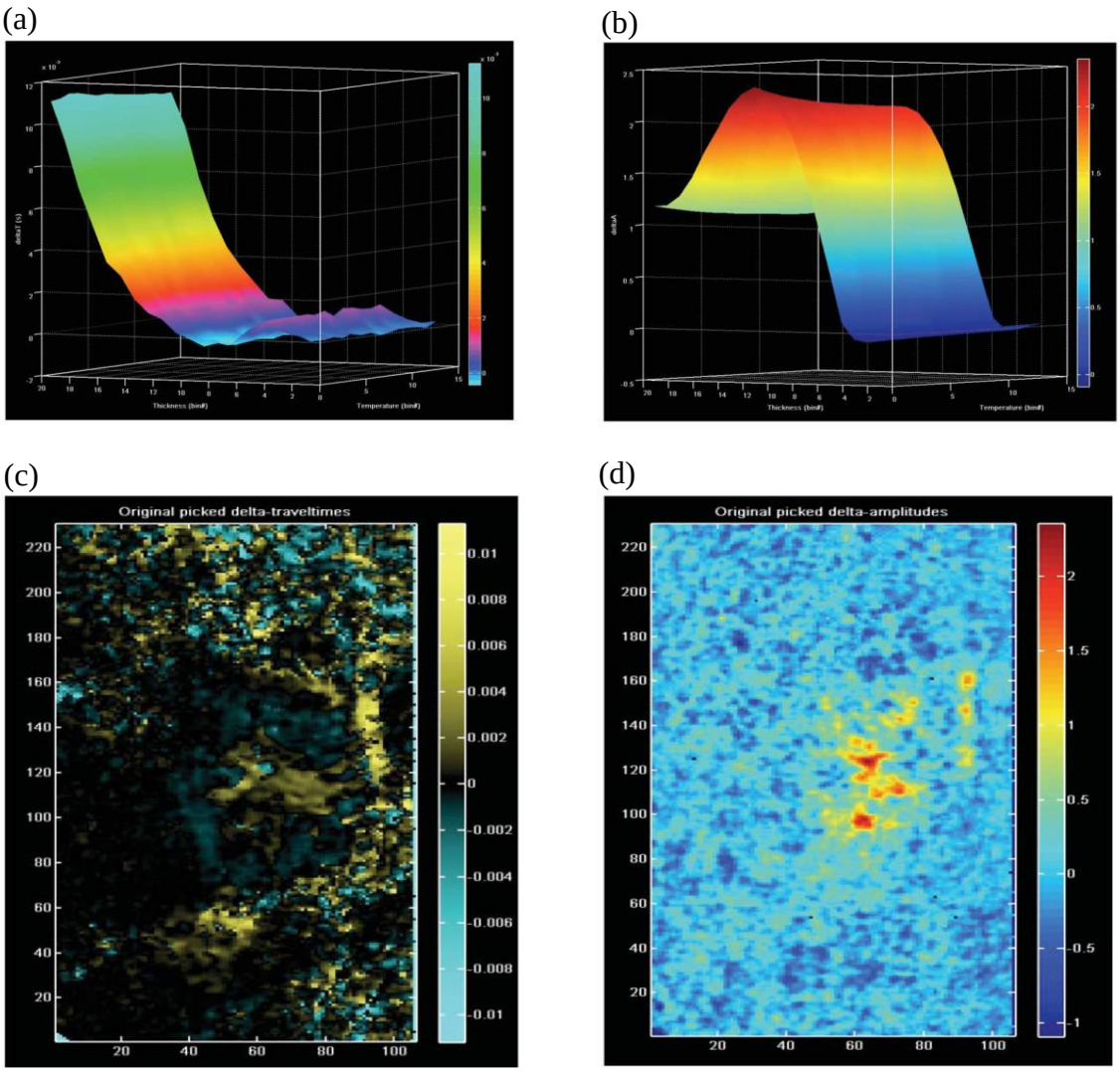

Figure 1.14 Modelled attribute surface of a) traveltime differences, and b) amplitude difference for the sand wedge plotted as a function of CO_2 thickness and temperature gradient number, c) travel time difference Δt, and d) amplitude change for the sand wedge extracted from the 1994 and 2001 near-offset Sleipner image cubes (Meadows, 2008).

The examples provided here highlight the lack of understanding about gas distribution inside the gas thickness. The geological downscaling method (Sengupta *et al.*, 2003), laboratory method of extracting hyperbolic function for vertical CO_2 saturation distribution

(Meadow, 2008) and the method assuming constant gas thickness to calculate the velocity change (Ghaderi and Landro, 2009) lose the engineering aspects and the balance of the forces that drive the fluid flow at the reservoir scale. Beside the geological parameters, engineering aspects (e.g. gravity effect) are very important for gas distribution. As will be discussed in Chapter 3, the vertical distribution of the gas saturation is important in the seismic domain. It seems that the best way is to run a simulation model at a fine scale and then extract the reservoir scale vertical saturation distribution. This topic requires investigation, in order to arrive at a more valid assumption. In addition, the gas saturation described in the literature mainly refers to a depth averaging of the saturation over the reservoir thickness (e.g. Huang *et al.*, 2001, Dumont *et al.*, 2001, Wagner *et al.*, 2004, and Floricich *et al.*, 2006). This does not agree with the gas saturation definition at the laboratory scale.

1.4 Methods of calibration for the proposed 4D seismic equations

The next stage in the monitoring of gas saturation using 4D seismic is the calibration of the proposed methods or equations. These equations contain some coefficients which are required to be calculated or estimated. In general, five methods can be found in the literature for calibration; a) non-seismic tools, b) laboratory measurements, c) Petro elastic modelling, d) production and injection data or simulation model, and finally e) some statistical and advanced methods.

Calibration of the seismic equations with the non-seismic methods such as resistivity logs have been historically taken into account. These methods are based on the empirical fitting of trends to the well logs. Lu and McMechan (2002) fitted a trend for porosity versus P-wave impedance, using well-log data. Then, they made an empirical relationship between P-wave impedance (which can be obtained from the seismic) with the gas or water saturation by employing Archie's equation. Their petro-resistivity model assumes a constant resistivity over the entire reservoir, which is not valid. Therefore, another source of data is required to support these techniques. In addition, gas and oil are not distinguishable using the resistivity data, which is a significant problem.

Calibration of the proposed methods with the laboratory measurements is another approach (Dumont, 2001, Langlais, 2005, Landro, 2001, and etc). However, these measurements are not necessarily applicable at reservoir conditions or in the reservoir context. The presence of some forces, such as gravity effect, at the reservoir scale could render such measurements invalid. It is the balance of several forces that results in the reservoir scale fluid distribution, but these forces are not taken into account in the laboratory scale. This subject is discussed further in Chapter 3.

Calibration with the Petro Elastic Modelling (PEM) is the next method. Huang *et al.* (2001), Sengupta *et al.* (2003), Wagner *et al.* (2004) and Meadow (2008) have employed rock physics equations for calibration of their proposed methods for extraction of gas saturation using 4D seismic. The problem of this method is the number of equations. Gassmann's equation needs some parameters such as the dry bulk modulus, fluid and grain bulk modulus, porosity and saturations, which are not well recognized. Their dependency on pressure and saturation (or even other parameters) are still the subject of research and are not yet well known. In addition, there are some discussions (e.g. Tonnessen *et al.,* 2005) about underestimation and overestimation of the saturation or pressure effects in the petro-elastic model. Therefore, employing these equations leads to a high range of uncertainty.

As mentioned earlier, calibration with the simulation model and engineering data is another possible approach. Sengupta *et al.* (2003) selected the simulation model for determination of the saturation changes in the wells. Due to the scale of the simulation model and lack of correlation, they tried to downscale the gas saturation log using the geological trend. Floricich *et al.* (2006) used calibration with the production data in their pressure and saturation inversion method. The wells were selected for calibration of the proposed non-linear equation. By comparison with the other methods, it seems that calibration with the production data is an in-situ method and avoids scale issues. However, the coefficients in the equations are not constant over the entire reservoir. These coefficients are probably a function of geological properties such as porosity and net-to-gross (Alvarez and MacBeth, 2011).

Some new methods have been used for calibration or education of the equations. Bertrand *et al.* (2005) considered monitoring of the gas-oil contact in a North Sea field by employing

a Neural Network and using time-lapse logs. They educated the neural network to recognise gas saturation change and gas-oil contact. These statistically based methods can be helpful, but the understanding of physical relationships between the elastic properties and the reservoir dynamic properties is a priority in terms of industrial interests and university research.

1.5 Gas saturation in a three-phase system

Three-phase reservoirs are the most challenging cases found in the literature, both in the seismic and engineering domains. Indeed, there are a limited number of published papers and discussions on the monitoring of three-phase system using 4D seismic. Saturation distribution and fluid flow in three phases has not been well-recognised and is still under research, even in the engineering domain. Three-phase relative permeability curves, which control the fluid flow in the reservoir, are still treated as two separate two-phase systems (oil with gas, and oil with water). Gas coming out of solution is totally different from gas injection into an oil reservoir for pressure maintenance, and in turn this is different from reservoirs with an initial gas cap, both in the engineering and seismic domains. The reservoir will even be more complicated if the producing well has a connection with the gas cap and produces gas from the reservoir.

Since the mechanisms of fluid flow and saturation distribution are different for the above mentioned cases (gas exsolution, injection for IOR, and production), their 4D seismic responses are also dissimilar and this needs to be taken into account. For example, for gas injection into an oil reservoir, usually there is no residual gas saturation, whereas, for three phase reservoirs with gas production, there will be irreducible gas saturation at the small scale, and bypassed or trapped gas saturation (S_{gt}) at the reservoir scale. The latter is very important in the seismic domain, due to the extreme nonlinearity of the seismic properties to the gas saturation. For gas coming out of solution, the critical gas saturation makes this scenario different from other types of three phase processes. Ali *et al.* (2008) observed a huge difference between the synthetic and observed seismic in a reservoir with an initial gas cap (Figure 1.15). They changed the end points of the relative permeability curves from 5% (obtained from the laboratory based measurements) to 20%. They then obtained a better

match in the production history match procedure. It is noted that water injection into gas is an imbibition process that needs specification of the trapped gas saturation (S_{gt}) instead of drainage based laboratory extracted value (S_{gc}). In their case study (Ali *et al.*, 2008), a well injected large volumes of water into a gas cap. A weak 4D seismic was detected around this injector (Figure 1.15-a), whilst synthetic data calculated from the simulation model suggested a strong seismic response (Figure 1.15-b). The difference between this expected response and the observed seismic encouraged them to conclude that water injection into a gas-cap would not be well described by drainage gas-oil relative permeability curves. Changing the end points improved the match, but it is still not perfect, and perhaps needs to be updated again.

The interaction between gas/oil and gas/water has not been recognised properly in three phases system in the engineering domain (Firoozabadi, 1999). It seems that reservoir engineers need further tools for a better understanding of three phase fluid flow in the reservoir. 4D seismic is a helpful tool to support them in this aim. It should be taken into account that the role of the 4D seismic is not only to give us saturation and pressure change in the reservoir. It has the ability to support us even in the determination of the end points of relative permeability curves, which is one of the main challenges in the engineering domain (Ali *et al.*, 2008).

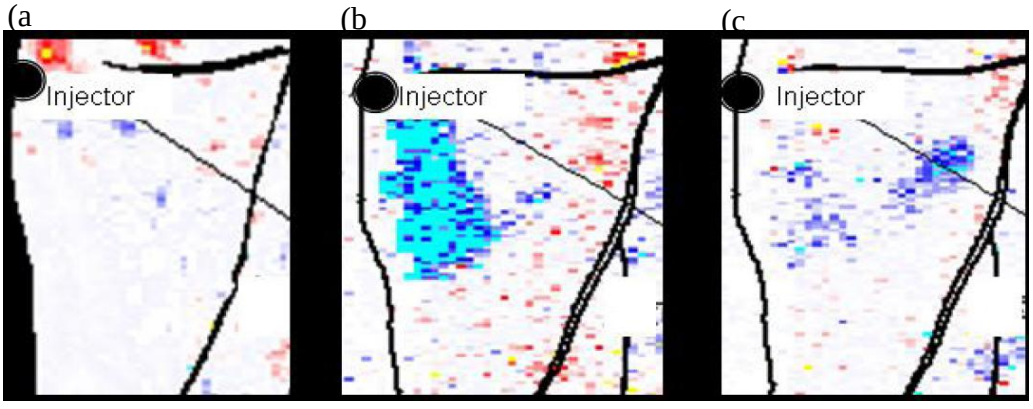

Figure 1.15 Seismic amplitude difference (monitor-base) at base reservoir from a) observed 4D data, b) synthetic from reservoir model with S_{gt}=5%, and c) with S_{gt}=20% (Ali *et al.*, 2008).

As discussed earlier, Floricich *et al.* (2006) proposed the nonlinear Equation 1.2 for the monitoring of a three phase system with the gas coming out of solution. Aarre (2007) estimated the oil-water contact movement and velocity change inside an oil reservoir having gas and water injection. He used the timeshift attribute inside and below the reservoir. He allocated timeshift inside the reservoir to the fluid contact movement and the timeshift below the reservoir to the velocity change due to the reservoir pressure change. It should be taken into account that timeshifts, either inside or below the reservoir, are affected by both the pressure change and the contact movement inside the reservoir, so allocating those timeshifts to only velocity change or only contact movement may not be correct.

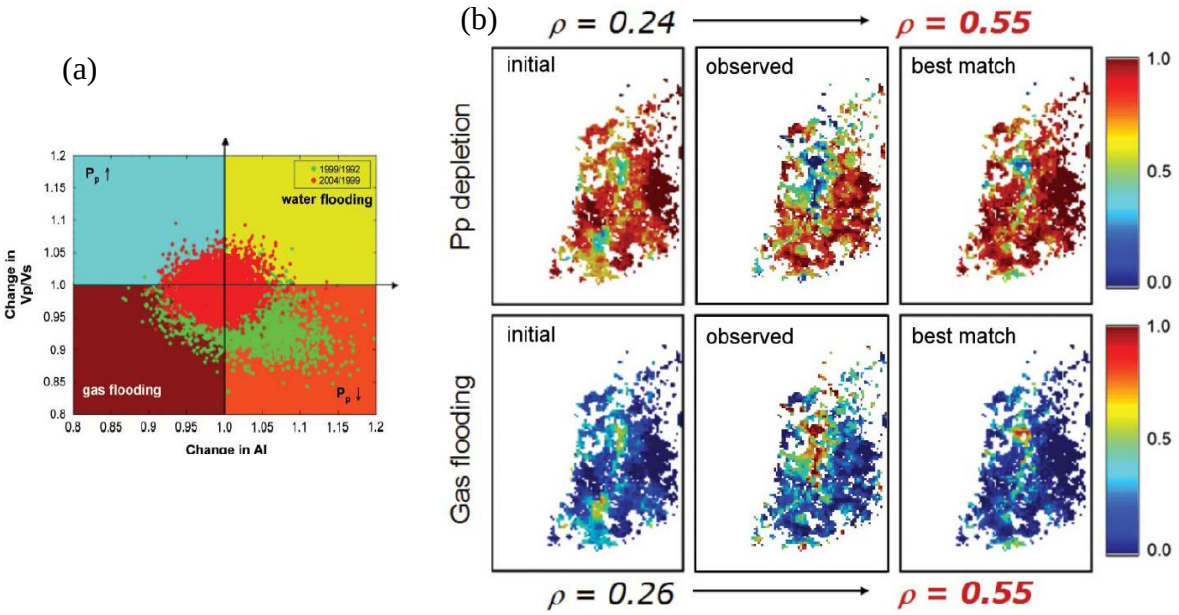

Figure 1.16 a) Classification of the 4D field response using V_p/V_s versus AI changes, b) Proportional maps of the pressure depletion and gas flooding for the synthetic (initial), observed seismic and after best match, respectively (Castro *et al.*, 2009).

Castro *et al.* (2009)**,** worked on a history matching project using 4D seismic in a reservoir with exsolved gas. In the V_p/V_s versus P-wave impedance plot, they divided the cells into four groups: pressure depletion, pressure increasing, gas flooding and water flooding (Figure 1.16-a). The observed seismic data were inverted to the velocity ratio and P-impedance. The inverted cells were later allocated into one of these groups. The number of the cells in each group was vertically added, and then normalised to arrive at the

proportional maps for each group (Figure 1.16-b). This procedure improved the history matching process. However, the gas saturation map (lower row on Figure 1.16-b) follows exactly the trend of the pressure map (upper row on Figure 1.16-b), but with opposite polarity. This is probably not correct due to the different distribution of the pressure and saturation changes. In general, pressure moves faster than fluid, so pressure change anomalies are normally bigger than saturation change ones.

1.6 Relevance of the topic of my research to industry and management

In the above, a question is highlighted: why study gas? What is the benefit of this topic to the reservoir engineering and management team? What are the problems that can be cited regarding gas, for which industry has commercial interest? To answer these questions, a review needs to be done to the engineering domain. This should define problems and challenges that have been reported and for which the engineers are interested in solving by employing seismic data? This topic will be discussed in two stages: exploration and monitoring. The first problem is hazards during drilling. Shallow gas-charged channels that are overlaid by impermeable sediments and are not contacted with faults, are considered as over pressurised gas sands, as the structure is confined and pressure is locally high. Drilling along these channels is obviously risky (Heggland, 2004). Therefore, exploring these sands is vital to avoid drilling through them. These sands, on the other hand, might be assumed as a source of energy, if their reserve is large. Therefore, they have the potential to be suggested as the target for drilling. The quantitative estimation of the gas charged sands seems also to be an important issue.

The second problem is dry or unsuccessful wells at the exploration stages, since drilling a well is extremely expensive. To avoid a dry hole, industry is interested in spending more money in exploration to obtain more accurate data in order to make a proper decision. However, a dry hole could simply be drilled by a misinterpretation of the seismic signals. Gas makes a strong signal, so a few percent of gas can be interpreted as large oil reserves which could be suggested as the target for drilling. The last two paragraphs clearly highlight the need for understanding the accurate and quantitative gas response in seismic data. Gas could scatter energy incoherency, and thus lose the signal. This effect, known as a

gas chimney, degrades the quality of the data and presents difficulties in interpretations (Chopra and Marfurt, 2007). Gas chimneys are normally found at shallow depths, which is consistent with the upward migration of gas. The effect is more significant in 4D seismic as this region is normally not suitable for quantitative monitoring objectives, and is simply deleted out during 4D seismic interpretations (e.g. Ekofisk, North Sea).

To monitor reservoir activities, geological and simulation models are frequently employed. The input parameters (e.g. relative permeability curves, end points and rock/fluid parameters) are typically extracted from laboratory, well, seismic and geological data that are updated during the history matching process. The number of parameters and unknowns is extremely high in this process, especially in a three phase system, so the answers are probably not unique. In addition, the best matched model is not necessarily the most accurate one. Therefore, reservoir engineers are looking for some new tools to extract the reservoir properties (e.g. relative permeability curves, end points and rock/fluid parameters) in the reservoir scale, and do not directly employ the laboratory-measured ones. 4D seismic is a useful tool in this situation and it has even been used for updating the three phase relative permeability curves, estimation of the critical and trapped gas saturation (Ali *et al.*, 2008).

Gas is normally injected to the reservoir for disposal, storage or IOR purposes. The fate of the injected gas is a key point in continuing the project. Gas leakage is one of the challenging issues in injection for disposal. Gas is typically injected into a confined geobody to be kept for a long period. However, when stratigraphical or structural traps are not completely sealed (e.g. due to possible connection via faults), then there would be gas leakage. These connections are not fully known before gas injection. 4D seismic is typically employed for monitoring aims, but if it cannot monitor quantitatively, then such information is of limited value. During gas injection projects for storage, the objective is to reproduce the injected gas. Therefore, knowing the distribution and migration of the injected gas is important. Well information could support management decisions to some extent, but this does not provide spatial data. By recognition of the accurate gas signal in the seismic domain, seismic data act as the main tool for monitoring of the reservoir, so the management team could decide about continuing injection or stopping the project and drilling another well.

Gas is sometimes the best option for IOR (improved oil recovery). It is also used in WAG (water alternating gas) projects. The main aim in these projects is the control of pressure and avoiding bypassed oil. Therefore, water injection is replayed by gas injection in WAG. This process needs knowledge of the pressure regime inside the reservoir and the distribution of oil and injected gas and water. By accessing this understanding, the injection and production plan can be guided properly. Reservoir engineers are interested in extracting these data using reliable tools. By better understanding the gas signal in the seismic domain, 4D seismic data is decomposed quantitatively to support the engineers with the necessary data to optimize the injection and production plan in a WAG project.

Drop of the production rate is one of the main challenges in the engineering domain below the bubble point pressure. Relative permeability of the oil is decreased due to the gas saturation increase. This drops the oil production. In addition, gas arrives at the production well faster than oil due to the higher mobility. It forms a cone shaped accumulation around the production well which prevents oil production. Engineers are interested to control the production drop. But, how is it possible without knowing the volume, shape and position of the liberated gas in the reservoir?

A secondary gas cap can act as another force for production. This normally expands by pressure drop, and is assumed to be one of the driving mechanisms in material balance calculations. To properly include this inside the calculations, accurate measurements of the volume of the exsolved gas is important. Besides that, engineers should also manage the liberated gas. Liberated gas is present in the reservoir and it is not normally forced back into solution by pressure build up. It is produced during the life of the reservoir. Therefore, calculation of the gas in the reservoir is vital to make a plan for the future. Is it sufficiently large enough to produce for sell? Is it possible to re-inject it into the reservoir for pressure control? Are we allowed to burn it considering environmental problems? If we want to dispose of evolved gas, how big is the reservoir we need to find when it has to be close the main reservoir?

Pressure drop and gas liberation is typically controlled by a proper injection plan. The normal plan to stop gas exsolution is water injection. Engineers and the management team are interested to know what happens during water injection. Laboratory-based calculations

highlight dissolution of the liberated gas by pressure build up, whereas considerable volumes of free gas have been reported in the reservoirs. This is not consistent with the PVT equations. In spite of arriving at a pressure above the initial bubble point pressure, gas is produced from the wells. Therefore, the management team are looking for other tools to answer their questions; what happens to the liberated gas after water injection? How much of the exsolved gas dissolves and for how large a pressure build up? Which parameters control the gas dissolution process? Do reservoir rock properties such as permeability and porosity have any effect on the dissolution process, or is it only controlled by pressure and hydrocarbon type? 4D seismic could support them to some extent, but the concepts behind gas signals in the seismic domain need to be updated.

1.7 Motivations

The problems and challenges regarding the gas issue in the oil and gas industry highlights the importance of gas as a subject of interest to the engineers and the management team, as well as encouraging us towards research. It also emphasizes the necessity of using seismic data to handle gas monitoring. Analysis of the seismic literature on gas reveals some misunderstandings that cause problems during quantitative monitoring of gas using seismic data. In the 4D seismic literature, different seismic responses are proposed for the gas saturation variation. The laboratory shows an extreme non-linear seismic response to gas saturation variation (e.g., Lumley (2008), Dumont *et al.* (2001), Rojas (2005)). The linear seismic response was chosen by Huang *et al.* (2001), but a linear response with positive gradient (opposite direction to Huang *et al.*, 2001) was employed by Dumont *et al.* (2001). The exponential relationship between gas saturation and 4D seismic changes was used by Floricich *et al.* (2006). Finally, some intermediate seismic response (between linear and extreme-nonlinear) to the gas saturation variation were proposed by Sengupta and Mavko (2003), Wagner *et al.* (2004) and Konishi *et al.* (2008).

The diversity of these examples highlights the fact that, gas is not handled properly in the seismic domain. It is my belief that it is the reservoir scale gas distribution which is misunderstood. The literature has been supported mainly by laboratory-based measurements, and some strange and possibly invalid relationships were re-applied at the

reservoir scale. It should be taken into consideration that these values are specific to small samples of rock in the laboratory, and clearly cannot be representative of the whole field. There is even doubt on the laboratory procedures used and the preparation procedures required to obtain the data from the rocks and fluids. Knight *et al.* (1998) reported different results (velocity versus gas saturation) for the same sample by changing the frequency. They also observed different results for different saturation histories (imbibitions or drainage). Heterogeneity of the reservoir is not taken into account in the laboratory. Gas movement and distribution is different at the laboratory scale versus the reservoir scale. Furthermore, some forces (e.g. the gravity force), which are negligible at the laboratory scale, are very important at the reservoir scale (especially for gas). Therefore, generalising a statement based on laboratory measurements is not the best approach at the reservoir and seismic scale.

The main question here is: does the seismic response follow a laboratory based trend at the reservoir scale? Is the gas distribution and migration at the reservoir scale the same as the laboratory scale? In the laboratory, a small sample of the rock is injected with gas. Due to the negligible gravity force, gas is homogeneously distributed along the sample. Gas saturation is increased by gas injecting, and elastic properties of the rock are measured against this gas saturation. However, gravity force is the main player at the reservoir scale. Due to the higher density difference of the gas with the water and oil, injected gas migrates toward the upper parts of the reservoir. Gas rapidly makes a gas cap in the upper part. In fact, gas is not distributed homogeneously over the reservoir. This kind of distribution is different from what is seen in the laboratory, and it definitely impacts the seismic response to gas at the reservoir scale. Research needs to be done here to develop seismic scale relationships.

The next issue which was found challenging in both the engineering and seismic domain is gas coming out of solution in depleted reservoirs. The mechanism behind gas liberation is still not well developed in the engineering domain. It is not well understood in the seismic domain either. The gas liberation phenomena are mostly explained by laboratory-based understandings. It is necessary to get familiar with different stages of gas exsolution and try to model the seismic responses at these stages. This understanding could be employed in a more physically consistent interpretation of the 4D seismic. The reservoir scale parameters

(e.g. reservoir heterogeneity) controlling gas dissolution need to be investigated. Pressure dependency of the saturated rock is normally interpreted using laboratory based graphs. However, gas exsolution may alter pressure dependency of the saturated rock below the bubble point pressure. The questions to be emphasized here are: how? Is this trend the same in the gas cap and oil leg? Can the fluid have an important effect on the pressure dependency of the saturated rock? Since the liberated gas is migrated, it is not in contact with oil to be dissolved by pressure build up. Then, the proposed equation to calculate the solution gas-oil ratio (Batzle and Wang, 1992 and MacCain, 1990) is not valid. It is necessary to quantify the deviation of the calculated solution gas-oil ratio from the measured and modeled one, and its impact on the acoustic properties of the fluid. It was also noted that there is a compositional change of the gas and oil during pressure drop. It is necessary to find out the magnitude of this change and the effect on the seismic properties of the gas and oil. After that, we must investigate the accuracy of the black oil model.

As the final issue, gas typically masks the effect of other phenomena on the seismic data. It can swamp events with a small signal. The difference between oil and water, the effect of pressure for example, are usually difficult to detect when a few percent of gas is present. Schiehallion field, Oseberg field and Genesis field, are some examples (Falahat *et al.*, 2011, Castro *et al.*, 2009, and Hodgson *et al.*, 2007) in which gas signal (softening or reduce of the impedance) masks the reservoir pressure drop and reservoir compaction respectively. To overcome this problem, some map-based pressure and saturation inversion techniques have been developed (e.g. Floricich *et al.*, 2006, MacBeth *et al.*, 2004, Castro *et al.*, 2009 and Landro, 2001). The first issue is that a few of them have included gas saturation term. The second, laboratory-based relationships have been used for the gas saturation term. The third and most important issue, depth averaging of the pressure, gas and water saturation changes were related to the map-based 4D seismic attributes in these techniques. However, this is probably not valid at the reservoir scale, by consideration of the physics of the fluid flow. Gravity effects cause water saturation change in the lower part of the reservoir and gas saturation change in the upper part. Pressure change distributes across the entire reservoir thickness. In fact, the thicknesses in which the pressure and saturations vary are not necessarily equal. Those probably are different from the reservoir thickness. These thicknesses change spatially and also with time. Indeed, thicknesses of the pressure and saturation changes are dynamic parameters. As an output, 4D seismic attributes should be

impacted by pressure and saturation changes scaled by their corresponding thicknesses. The influence of thicknesses on the seismic amplitude may be explained to some degree by a tuning effect, as the thickness of the dynamic parameters is generally small and close to the tuning thickness. In addition, the pore volume that is occupied by pressure change is different from that which is occupied by gas and water saturation change. This definitely impacts the 4D seismic signals and needs to be considered in the quantitative interpretations.

1.8 Objectives and thesis outline

Understanding accurate gas migration as well as distribution in the reservoir is the primary objective of this thesis. Using different synthetic and realistic fine scale simulation models, I will try to investigate the gas distribution in the engineering domain. This understanding gives us the knowledge to evaluate gas monitoring using 4D seismic. In fact, by better recognition of the gas behaviour, accurate and reservoir scale relationships between gas saturations and seismic attributes can be easily found. The effect of reservoir heterogeneity (both vertically and laterally) in the seismic domain and also in the engineering domain will be discussed. How can we capture the effect of heterogeneity in the 4D seismic domain? Is the employment of the patchy saturation the correct method in the reservoir scale to cover the heterogeneity? In doing this, the simulation model will be run as finely as possible to obtain a realistic gas distribution in the reservoir. By upscaling the simulation model for different stages, the effect of the upscaling will be investigated in both the engineering and seismic domain. Finally, all of these findings will be used to present a seismic scale technique that calculates the injected gas volume using seismic attributes. This technique will be implemented on a North Sea gas injection case study.

As the second part of my project, I will try to understand the basic concepts and mechanism of the gas exsolution and dissolution process. Which parameters control this process in the engineering domain? What is the effect of the gas liberation on the elastic properties of the liquid and gas? What is the effect of the reservoir heterogeneity on the gas liberation and gas going back into solution? Compositional change of the gas and liquid phases during gas exsolution will be studied to quantify the order of this change and its effect on the acoustic

properties of the gas and oil. Since a constant gas and oil composition is assumed in the black oil model, the liberated gas is modelled by solution gas-oil ratio. It is important to know how valid this concept is by considering the compositional change

All the findings in this project will be used to monitor a depleted and three phase reservoir in the North Sea. Using the synthetic simulation to seismic modelling (generating the synthetic petro elastic model (PEM) and seismic traces using the output of simulation model, and fluid and rock properties), I will try to quantify the effect of the thickness and pore volume occupied by pressure, gas and water saturation change on the 4D seismic signal. In fact, my aim is to improve the pressure and saturation inversion techniques and include the accurate gas saturation term. The achievements will be implemented on the observed seismic to estimate the pore volume scaled dynamic parameters change.

In general, my thesis consists of two parts. The first part, discussed in Chapters 3 and 4, concentrates on the gas injection issue. The second part is presented in Chapters 5 and 6, where the main challenge is gas exsolution and dissolution in the depleted reservoir.

Here are the chapters of my thesis in brief:

Chapter 2 ***The basic concepts of gas in the engineering and seismic domains***

This chapter focuses on a technical discussion specifically about gas. The basic elastic properties of gas will be discussed to get familiar with the physics. The next topic is the understanding of different stages of the gas exsolution process. The effect of gas exsolution on the elastic properties is discussed using the literature. In the next part, gas saturation relations with the elastic properties are analyzed at different scales. The engineering concepts such as capillary pressure, transition zone and mobility are reviewed here to discuss vertical gas distribution, and the meaning of the gas saturation, thickness and volume. The parameters that control the reservoir scale gas distribution are also discussed as the last topic in this chapter.

Chapter 3 ***Fluid simulation and seismic modelling of the gas injection process***

Understanding and modelling of accurate gas distribution in the reservoir and the corresponding seismic response is the primary objective of this chapter. Synthetic fine scale simulation models are built to investigate gas saturation distribution. These models contain different ranges of realistic heterogeneity. The seismic response to injected gas is discussed both analytically and numerically. Simulation to seismic studies are employed to catch the seismic scale relationships between the injected gas and the seismic attributes. The 4D seismic response is illustrated for thin and thick reservoirs separately. Finally, the effect of upscaling on the seismic response is investigated. The aim of this discussion is to evaluate the accuracy of the upscaled simulation models for the monitoring of injected gas in the seismic domain.

Chapter 4 ***Towards quantitative evaluation of gas injection using time-lapse seismic data***

My first case study, An'Teallach, is introduced in this chapter, and a brief qualitative interpretation using 4D seismic, well-logs and injected data is illustrated. A technique is developed here to produce mapped quantitative estimates of the gas volume injected into a clastic reservoir. Pressure effect has been handled properly using the proposed technique. This method uses repeated seismic data, and estimate the volume of the injected gas separately for each seismic attribute that is employed. Despite good results using three accurately repeated seismic surveys, time-delay and amplitude attributes reveal fine-scale differences though large-scale agreement in the estimated fluid movement. These differences indicate disparities in the nature of the two attributes themselves. The same difference was reported in the literature for different case studies. Therefore, an investigation was carried out to find the possible reasons for this disparity.

Chapter 5 ***Gas exsolution and dissolution; basic concepts and seismic response***

The key aim of this chapter is to become familiar with the basic concepts of gas liberation and dissolution. This understanding is of major assistance during the accurate interpretation of the 4D seismic signals. At the next stage, the reservoir-scale parameters controlling the gas dissolution process are investigated. The effect of gas exsolution and dissolution on the

pressure dependency of the saturated rock is then discussed. The R_s (solution gas oil ratio) term and its relationships with the engineering and elastic parameters is one of the interesting subjects that needs to be considered carefully. Finally, as was noticed during the literature review, there is a gas and oil compositional change during gas liberation. The magnitude of this change and its effect on the seismic properties are investigated as the last part of this chapter.

Chapter 6 ***Adaptive engineering-based scaling for enhanced dynamic interpretation of 4D seismic in three phases***

In this chapter, the role of engineering principles in interpreting and estimating dynamic information from 4D seismic data is considered. What are the principal parameters controlling mapped 4D signatures in clastic reservoirs? Are these only pressure and saturation changes, or do they need to be scaled by the corresponding thickness (or pore volume) of the reservoir volume that these effects occupy. Our understanding will be validated both with numerical modelling and analytic calculation. The impact of the gas saturation on the 4D seismic signals will also be included in this procedure. Is the linear approximation of the seismic attributes to the gas volume valid for three phases? Finally, these findings are validated by an inversion procedure for my second case study that ends up with the scaled pressure and saturation changes. These new understandings will be used to propose some areas to be updated in the simulation model.

Chapter 7 ***Conclusions, discussions and recommendations***

This chapter summarizes the findings and provides a view to potential future research. Recommendations introduce some technical challenges that are relevant to my work and worth researching. A variety of opportunities to improve this research is indicated.

Chapter 2

The basic physical properties of gas in the engineering and seismic domains

After the general literature review in Chapter 1, I now present a technical discussion specifically on gas properties. Firstly, the basic definition for gas and the acoustic properties are discussed in order to become familiar with the physics. Next, an understanding of gas exsolution and the different stages of this mechanism follow. Here, the variation of the elastic properties of the oil and the effect of gas liberation is also presented. The relationship between gas saturation and the elastic properties of fluid and saturated rock are discussed at the laboratory, log and seismic scales to outline the knowledge of the geophysicist. The perceived non-linearity of the elastic properties of a saturated rock to gas saturation variation is the centered point of most seismic literature, and is therefore considered important. As mentioned in Chapter 1, this description then highlights misunderstandings at the reservoir scale, and those factors that control the distribution in reality. The engineering literature addresses capillary pressure, transition zones and mobility as important elements in controlling the fluid flow and saturation distribution. A connection between the different ways of thinking in each domain is attempted.

2.1 The origin of the gas

Natural gas, as the gaseous phase of petroleum, normally contains 70 to 99% methane, 1 to 10% ethane and a lower percentage of higher hydrocarbons up to the hexanes. The percentage of carbon dioxide, nitrogen, and hydrogen sulfide, as the typical nonhydrocarbon components, present a wide range of variation from low to 100%. The term dry gas refers to gases that contain less than 0.1 gallon of liquids per 1,000 ft^3, while wet gas refers to gases with more than 0.3 gallons of liquids per 1,000 ft^3. Gas is classified as sweet and sour when it has low and high hydrogen sulfide respectively. Reservoir gas may be observed to be either in the state of free gas or dissolved gas in oil/water. Associated gas refers to gas that occurs with oil as free gas, dissolved in oil, or liquefied gas, whereas non-associated gas refers to the gas that occurs alone as either free or dissolved in water. By comparison with oil or water, gas is very compressible. For example, an equal amount of gas in a reservoir at 600m depth occupies about five times of volume in a reservoir at 3000m depth. Gas is also very mobile, it migrates more easily than oil; so gas is more widely distributed than oil both vertically and laterally (Hunt, 1995).

It has been proven that both the hydrocarbon and non-hydrocarbon constituents have multiple sources. The most important sources of the hydrocarbon gases are: a) methanogenic bacteria, b) all types of kerogens, c) coal, and d) oil in source and reservoir rock. Primary cracking refers to the thermal cracking of kerogen and coal to create methane, whilst the cracking of oil is labeled as secondary cracking (Hunt, 1995). Both organic and inorganic processes would produce non-hydrocarbon gases such as CO_2, H_2S, and N_2. The temperature range for various gases to be formed is demonstrated on Figure 2.1. Bacteria are the origin of about 20% of the methane in conventional reservoirs (Hunt, 1995). From 40 to 55% is assumed to be from the thermal decomposition of oil in rocks and coal. Finally, 25 to 40% is directly made from the thermal decomposition of kerogen.

Methane is formed throughout the entire sedimentary column, while the wet gases, ethane, propane, and butane are made principally in the oil window. These are formed bacterially during diagenesis and thermally during catagenesis and metagenesis (Hunt, 1995). The difference in the temperature of creation of the methane and wet gases originates a vertical distribution: deep dry gas in the metagenesis zone in the deepest part of the basin, overlain

by wet gas in the catagenesis zone and then shallow dry gas on the stable shelf in the diagenesis zone (Figure 2.1). The usual pattern of gas composition in the sedimentary basins is nitrogen plus dry gas on the shallow stable shelf, CO2 plus wet gas within the oil generation window, and CO2, H2S, and dry gas in the deepest section of basin.

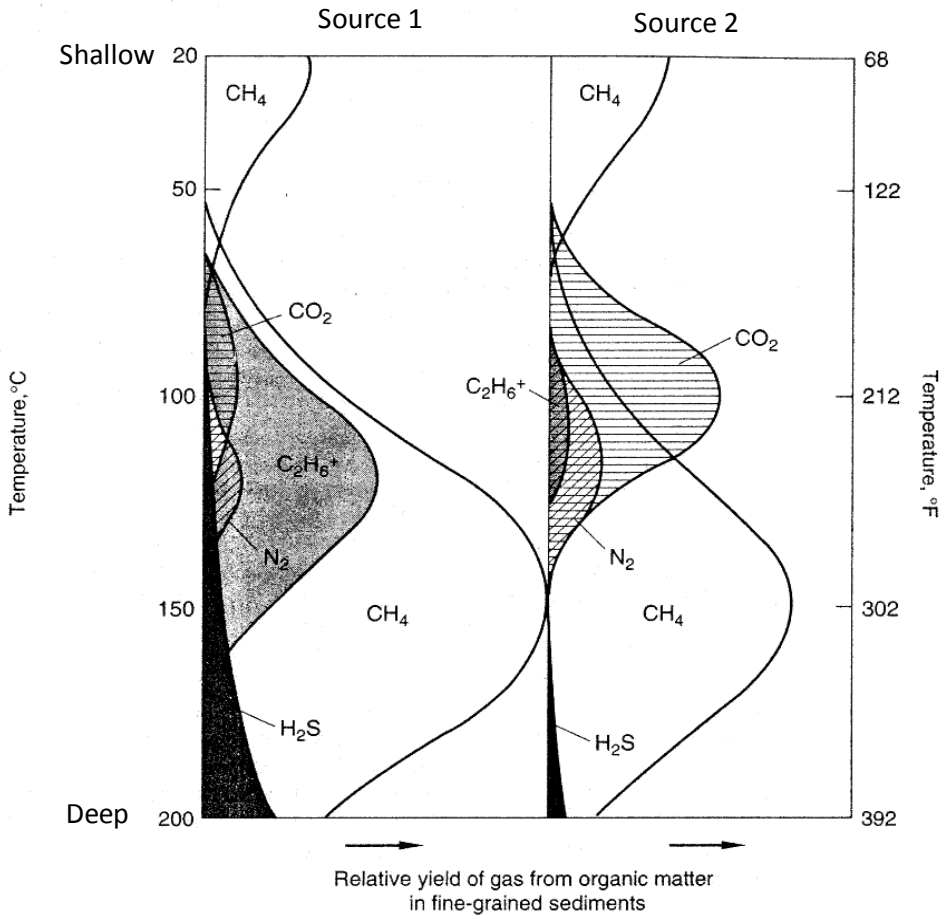

Figure 2.1 The generation of gases from organic material with temperature. The C_{2+} represents hydrocarbon gases heavier than methane (Hunt, 1995).

2.2 The physical properties of natural gas

Gas is defined as a low density and low viscosity fluid that has no independent shape or volume. It expands to totally fill the vessels in which it is contained (McCain, 1990). The equations of state have been developed to characterize gas properties. The ideal gas law

relates the three major parameters of gas, Volume (V), Pressure (P) and Temperature (T); they are put together by the Equation 2.1:

$$PV = nRT. \tag{2.1}$$

where R is the gas constant and n is the moles number (mass of gas divided by molecular weight). Subsequently, gas density can be obtained as shown in Equation 2.2:

$$\rho = \frac{m}{V} = \frac{MP}{RT}. \tag{2.2}$$

where M is the molecular weight. As the petroleum engineer is mostly concerned with gas mixtures, we need to introduce the gas law for mixtures of the ideal gases (Dalton's law of partial pressure):

$$PV = RT.\sum_i n_i \ . \tag{2.3}$$

where n_i are the mole fractions of each gas in the mixture. The specific gravity, G, of a gas is defined as the ratio of the gas density to the air density at standard conditions.

Because an acoustic wave passes quickly through a fluid, the process is adiabatic, not isothermal (Batzle and Wang, 1992) (adiabatic process refers to the cases in which there is no heat transfer to or from the fluid. This process occurs when the container of the system is thermally isolated or the process happens very quickly, so there is no opportunity for considerable heat transfer (MacCain, 1990)). Thus we must consider carefully the adiabatic behaviour of the gas. The behaviour of most real gases does not deviate drastically from the behaviour predicted by an ideal gas law. So the best way of writing an equation of state for a real gas is to insert a correction factor into the ideal gas equation (McCain, 1990). This results in PV = ZnRT where the correction factor, Z, is known as the compressibility factor which is the volume ratio of the actual and ideal gas at the same pressure and temperature.

A further notice is necessary, since the composition of natural gas is variable. The gas and liquid phases are in equilibrium along a pressure-temperature curve for pure components.

The properties of the two phases approach each other by increasing of the pressure and temperature until they combine at the critical point. For mixtures, this point depends on the gas composition. It is referred to as the pseudocritical point with pseudocritical temperature (T_{pc}) and pressure (P_{pc}). Temperature and pressure are normalized or "pseudoreduced" by the pseudocritical values to arrive at the more systematic values (Katz *et al.*, 1959). Using data sets from the various natural gases, Thomas *et al.* (1970) provided the following simple empirical relationship between G and the pseudoreduced pressure (P_{pr}) and pseudoreduced temperature (T_{pr}) (Batzle and Wang, 1992):

$$\begin{aligned} P_{Pr} &= P/P_{pc} = P/(4.892 - 0.4048\ G), \\ T_{pr} &= T/T_{pc} = T/(94.72 + 170.75\ G). \end{aligned} \tag{2.4}$$

The compressibility factor, Z, can now be written in terms of P_{pr} and T_{pr} via the following equation:

$$\begin{aligned} Z = [0.03 + 0.00527(3.5 - T_{pr})^3]P_{pr} + (0.642T_{pr} - 0.007T_{pr}^4 - 0.52) + 0.109(3.85 - T_{pr})^2 \exp \\ \{-[0.45 + 8(0.56 - 1/T_{pr})^2]P_{pr}^{1.2}/T_{pr}\}. \end{aligned} \tag{2.5}$$

The gas formation volume factor (B_g) is defined as the volume of gas at reservoir conditions required to produce one standard cubic foot of gas at surface conditions. A B_g relationship can simply be extracted from the equations of state as below (McCain, 1990):

$$B_g = 0.0282 \frac{ZT}{P} \frac{cu\ ft}{scf}. \tag{2.6}$$

The density of the ideal gas can be obtained from approximation of the equation of state in the typical temperature and pressure range of the exploration stages (Batzle and Wang, 1992):

$$\rho = \frac{28.8GP}{ZRT}. \tag{2.7}$$

This approximation is satisfactory provided that P_{pr} and T_{pr} are not both within around 0.1 of unity. The adiabatic bulk modulus of the gas can be calculated via the following equation:

$$K = \frac{P}{\left(1 - \frac{P_{pr}}{Z}\frac{\partial Z}{\partial P_{pr}}\right)_T}\gamma \ , \qquad (2.8)$$

where γ is the ratio of heat capacity at constant pressure to heat capacity at constant volume, and under exploration stages can be approximated using the following equation (Batzle and Wang, 1992):

$$\gamma = 0.85 + \frac{5.6}{(P_{pr}+2)} + \frac{27.1}{(P_{pr}+3.5)^2} - 8.7\exp[-0.65(P_{pr}+1)]. \qquad (2.9)$$

Shams *et al.* (2007) argue that the approximation proposed by Batzle and Wang (1992) for calculation of heat capacity as well as for gas bulk modulus is weakly composition-dependent. Using the gamma value obtained from the equation of state, they calculated gas bulk modulus for five gases with different compositions, and then compared the ones obtained from the Batzle and Wang (1992) equations. The results illustrate agreement between the two methods for lean gas condensate systems, whereas for richer gases a deviation up to 50% was detected.

Walls and Dvorkin (2005) declare that the Batzle and Wang (1992) equations for the density of methane is valid at very high pressures, but the bulk modulus values at 100 MPa and above will be significantly underestimated. They demonstrate that, as pressure increases from the normal range of 20 to 50 MPa to the high range of 150 to 200 MPa, the bulk modulus of methane rises tenfold from about 0.1 to around 1.0 GPa. The latter values are close to that of oil. For heavier hydrocarbon gases (ethane, propane, butane, and their mixtures) the modulus is even higher. This behaviour affects the seismic response of deep gas sands. Therefore, it needs to be taken into account during the interpretation of deep gas seismic events as well as in forward modelling. Han and Batzle (2002) reported the same behaviour for gas velocity at higher pressures.

Han and Batzle (2000), by including the effect of the pressure and temperature change on velocity, reported that the temperature dependence changes strongly with pressure. At pressures higher than 27.58 MPa, gas behaves like oil, and the velocity drops with an

increase in temperature; whilst, velocity increases with rising temperature at pressures lower than 16.52 MPa. In the region between these pressures, the fluid's wave velocity is independent of temperature.

The approximations proposed by Batzle and Wang (1992) calculate the elastic properties using reservoir pressure, temperature and salinity. These equations are achieved by fitting an empirical relation to the data collected from different reservoirs. These are not necessarily valid at specific reservoir conditions. A large deviation between measured and calculated elastic properties could be observed. These equations have been developed under exploration conditions in which knowledge of the reservoir fluids is not well known (Batzle and Wang, 1992). However, the aim of the monitoring projects is the understanding of changes in the fluid and rock properties, so these approximations are, in fact, not valid. In addition, there is access to production data and good knowledge of the fluids during 4D seismic studies. Most of the properties such as solution gas oil ratio (R_s), oil and gas volume factor have been measured in the laboratory and simulated using the simulation models. Therefore, it is suggested that production data could be employed instead of calculated properties. As will be discussed in Chapter 5, reservoir scale phenomena may cause a large deviation between calculated and simulated values, and an example of this is R_s. Liberated gas has migrated, so it is not in contact with the original oil to be dissolved by pressure build up. The pressure dependence of R_s is not reversible at the reservoir scale, and is opposite to the empirical calculation and laboratory measurement. Instead, these parameters could be extracted from an accurate numerical simulation model or simulated PVT data to get the proper value of the elastic properties.

2.3 Gas in production processes

A large volume in gas reservoirs is normally considered an economical source of energy to be produced, whereas small volumes or gas in solution could be helpful to oil production as one of the driving mechanisms. In dissolved gas drive reservoirs, the reservoir is fully surrounded by impermeable barriers. As the reservoir pressure drops during production, the reservoir's drive energy is mainly provided by expansion of the oil and dissolved gas. In a 'saturated' reservoir in which the reservoir pressure is close to the bubble point pressure,

once oil is produced, the pressure decreases and gas bubbles form in the reservoir. This gas liberation causes the oil to shrink, but the oil shrinkage is more than offset by solution gas expansion, the initial source of drive energy below bubble point pressure. The oil recovery factor is generally low (5 to 30% of the original oil in place) in this mechanism (Hunt, 1995).

In a gas cap drive reservoir, the expansion of initial gas cap by pressure drop is the main source of reservoir energy. The pressure drop rate in this mechanism is slower than in a reservoir producing via a solution gas drive. This rate is dependent on the size of the gas cap. The larger gas caps contain a more gradual pressure decline as oil is produced. Expansion of the gas cap, on the other hand, results in a downward movement in the gas oil contact. It makes a connection between the highest well on structure with the gas cap, ending by gas production instead of oil. Oil recovery from gas cap drive reservoirs is slightly higher than the previous mechanism, typically ranging from 20 to 40% of the original oil in place (Hunt, 1995). If gas production can be minimized, oil recovery increases with the size of the initial gas cap. This can be achieved by controlling the well perforation such that it is as far as possible below the gas-oil contact. The produced gas is commonly returned to the gas cap via gas injection wells in the local high of the reservoir.

Conventional recovery methods generally produce around one-third of the original oil in place. Miscible gas injection has been recently proposed as one of the enhanced oil recovery (EOR) methods. The idea behind miscible flooding using hydrocarbon gases or carbon dioxide is to reduce the interfacial tension between the oil and injected fluids, and control the reservoir pressure. Another benefit of gas injection is to add to oil mobility. As the gas dissolves in the oil phase, the oil swells and its viscosity lowers (Todd, 2007).

The challenging point of the drive mechanisms above is the distribution and migration of the gas. As gas is more mobile than oil, it quickly arrives at the production well and drops the production rate. The size of the primary and secondary gas cap and the gas oil contact movement is also the subject of discussion in the reservoir engineering domain. Production management and well design plan is mostly dependent on gas migration and distribution in these cases. By understanding and measuring the gas-fluid contact movement and the history of the exsolved gas, the production plan could be changed to prevent lowering of the

oil production rate. However, the spatial distribution of the gas is not well understood in the reservoir.

Beside gas injection for EOR, gas can be injected for storage or disposal purposes. Gas storage has recently been taken into account for control of supply and demand. In addition, the gas production could be higher than that required for the market, so gas needs to be stored for the future. Gas is typically stored in a depleted reservoir or a sealed subsurface reservoir. Gas is also disposed inside underground reservoirs to avoid air pollution (e.g., CO_2 disposal). The Sleipner field in Norway is a good and successful example of such disposal (Meadow, 2008). Gas disposal may be viewed as an economical and emergency solution for the small amounts of produced methane in oil reservoirs. Generally, there are five short or long term solutions for a small amount of produced gas. Flaring, which is not environmental friendly. Export, or conversion to power and then export, are other solutions which normally are non-economical and suitable for the long term. Re-injection is another solution, but it may affect the reservoir pressure and change the production plan. This is particular true for compartmentalized reservoirs for which there is possibility of a dramatic increase of the pressure inside the injection compartment. Furthermore, the volume of produced gas may be higher than the necessary volume for injection. Therefore, disposing of the produced gas into another structure is probably the only solution for some situations. A suitable structure close to the main reservoir is chosen for this purpose. There is a possibility of re-producing the injected gas for marketing aims if a proper structure is selected and then the reservoir is monitored during the injection period. There are some issues that need to be taken into account regarding the selection of the gas injection structure. The first subject is the reservoir quality and connectivity. In addition, a large aquifer must be connected to any disposal location to control over-pressurizing the structure. Reservoir depth and pressure regime are also important in terms of expenses associated with the injection equipment. Gas migration should be predicted and monitored to prevent leakage. Leaked gas can arrive at shallower depths or even at the surface. It could also arrive at the reservoir close to the injected site. It may affect the tools (e.g., seismic signal) for exploring the new targets in the area. Injectivity is another issue which is associated with the reservoir pressure and rock properties. It could become important if gas injectivity is hampered by poor relative permeabilities, low NTG and low rock permeability. Finally, selection of a proper trap could support the management team when

planning the re-production of the disposed gas for marketing aims in the future.

Most of the items above need to be monitored during the injection period. The possibility of leakage, migration of the gas towards the main oil reservoir or towards the surface, connection to an aquifer for pressure control are some examples that need to be controlled during the injection and a few years afterwards. Re-producing the gas, especially from the storage sites, is possibly an important objective for these projects. For better planning for re-production, knowledge of the spatial distribution of the subsurface gas is vital. The management team is interested to know where the injected gas goes. The possible connection of the injected layers via faults needs to be monitored. The trapped gas or irreducible gas saturation should be measured in-situ. These are some questions in the engineering domain which have not been properly treated yet.

2.4 Gas exsolution and dissolution

Without proper pressure support, reservoir production will end as pressure depletes. Due to the negative effects of pressure depletion on the production rate, it is prevented by an injection plan such as water or gas injection. However, the compartmentalized structure of the reservoir may prevent pressure support from reaching non-connected geobodies. As mentioned earlier, pressure drop below bubble point pressure results in gas coming out of solution (Dake, 2002).

What is the mechanism of the gas liberation process under pressure drop? Phase diagrams may provide some valuable information. Figure 2.2 represents the phase diagram for a multicomponent fluid system. In Figure 2.2-b, above the bubble point line the hydrocarbon is a liquid. It is gas below the dew point line. Gas and liquid co-exist in the area between these two lines, but the ratio of the liquid to gas is varied as a function of the pressure. These lines, named as quality lines, converge at the critical point. On the pressure-volume curve (Figure 2.2-c), higher change in the pressure results in a small change in volume for the pressures higher than bubble point. This is due to the low compressibility of the liquid. At the bubble point pressure, otherwise called vapour pressure, the first hydrocarbon molecules leave the liquid and produce gas bubbles. More liquid is vaporised as pressure

declines and the system expands. Only a few drops of liquid remain at the dew point pressure. Further pressure drops results in gas expansion. By following the highlighted blue line in the Figure 2.2-b, the system is above bubble point pressure at point (a), therefore the fluid is 100% in the liquid phase. By moving along the highlighted line at constant temperature, pressure drops. Once pressure arrives at the bubble point pressure, fluid compounds are broken and lighter components, say C_1 (methane) shift to the gas phase, and some gas bubbles come out of solution (stage two in the Figure 2.2-a). If we continue the pressure drop, more gas will be exsolved; these bubbles are connected together and arrive at the critical saturation, and are then movable. These connected bubbles start to migrate upward due to the gravity effect and form a gas cap (stage three in the Figure 2.2-a). By continuing pressure drop, more light components shift from the liquid phase to the gas phase, therefore the volume of the free gas cap increases (Todd, 2007).

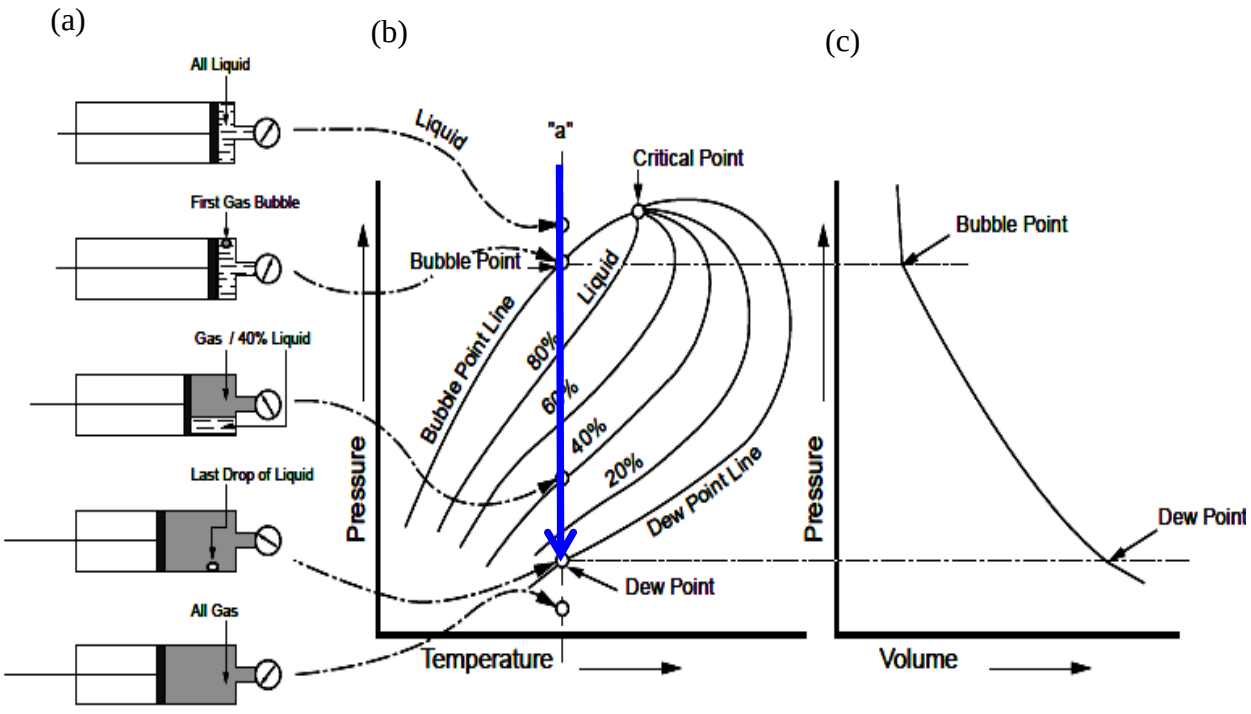

Figure 2.2 Phase diagram for a multicomponent fluid system (Todd, 2007).

Different types of hydrocarbon (black oil, volatile oil, gas condensate, wet gas and dry gas), have different phase diagrams. However, for comparison only, these are presented on

Figure 2.3 in one diagram. It should be highlighted that, each fluid type contains different scales. For black and volatile oil, the story is nearly similar, but volatile oil can release more gas than black oil. The region of liquid and gas coexistence for black oil is bigger than that for volatile oil. At the area between C_p (critical temperature) and X_5 (circondentherm temperature) on Figure 2.3, a gas condensate field exists. The gas phase exists above the dew point line (above the phase envelope). Heavier components shift from the gas phase to the liquid phase by pressure drop, so the amount of liquid increases. Further pressure drop results in the reduction of the liquid by re-vaporisation. Wet gas contains some fluid at separator conditions (on the surface), but dry gas, which has a lesser fraction of Ethane to Hexane (C_2-C_6), always remains outside the two phase envelope (Todd, 2007).

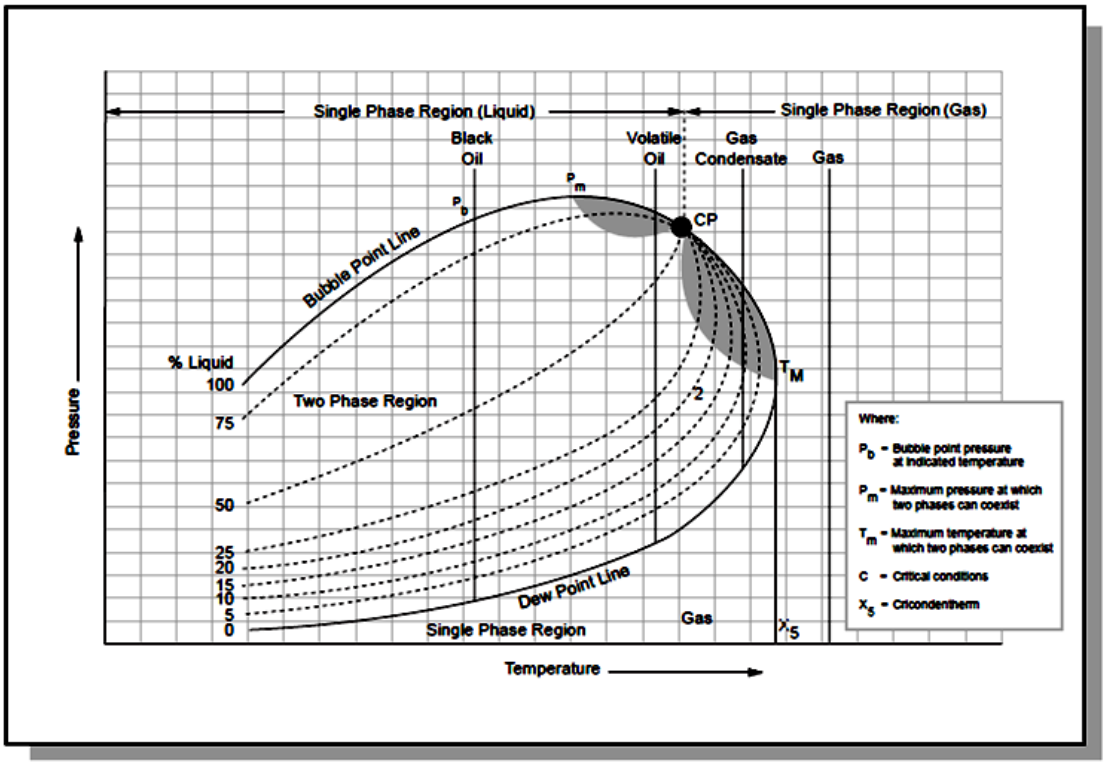

Figure 2.3 Phase diagram for reservoir fluids (black oil, volatile oil, gas condensate and gas) (Todd, 2007). Phase behaviour of these fluids is presented as a function of temperature and pressure. Note the fluid and gas phase area of each reservoir fluids.

There are two basic liberation mechanisms at the laboratory scale: (a) Flash liberation**:** the liberated gas is kept in contact with the liquid until equilibrium is established. (b)

Differential liberation: evolved gas is gradually separated from contact with the liquid, and the liquid is in equilibrium with the liberated gas over a finite pressure range (Dake, 2002). These two scenarios can be modelled at the reservoir scale. At a pressure close to the bubble point, gas saturation is below critical gas saturation, therefore it is not moveable and the whole of the evolved gas is in contact with the original oil (flash). Once bubbles are connected and migration occurs, the gas is no longer in contact with the original oil (differential).

Each component (C1 to Cn) has its own phase diagram as well as bubble point pressure. The total phase diagram for a hydrocarbon is a curve fit to the phase diagrams of the components. Phase diagrams of the ethane-normal heptane system are demonstrated on Figure 2.4 as an example. Pressure is dropped along the blue line at a constant temperature close to our case studies (as an example). The bubble point pressure of C_1 will be reached at the first step. Therefore liberated gas is mainly C_1. By continuing the pressure drop, the bubble point pressure of C_2 and C_3 will be reached at the second and third step, so liberated gas is the mixture of C_1 to C_3, and so on…. This is easily highlighted that, the composition of the liberated gas changes from lighter components at the primary steps to the heavier components at the next steps. Also, the composition of the oil changes (Danesh, 1998). Therefore, assuming a constant gas composition in 4D seismic studies may not be valid.

The Peng-Robinson equation of state is a most popular equation employed to calculate the percentage of each component (C_1 to C_n) in the gas or liquid phases at different pressure and temperatures. But, due to oil and gas production, the simulation model needs to be run in a compositional package (Multi-component system) to detect accurate compositional changes. In the black oil model (two-component system), constant composition for gas is assumed without considering the compositional change of the gas and oil. In this modelling, the solution gas oil ratio (R_s) is simply employed to represent the gas coming out of solution. Below the bubble point pressure, R_s is a function of pressure (Equation 2.10).

$$R_s=2.03G[P.\exp(0.02878API-0.00377T)]^{1.205} \quad (2.10)$$

There is only an initial value of the gas gravity factor (G) and oil API for that relationship. R_s is decreased and increased by pressure drop and build up respectively (Figure 2.5). Therefore, this process can be assumed to be reversible, whereas in reality it may not be reversible if compositional change is included. In addition, some other factors (e.g. gas migration) may prevent this reversible process. This topic is discussed in detail in Chapter 5.

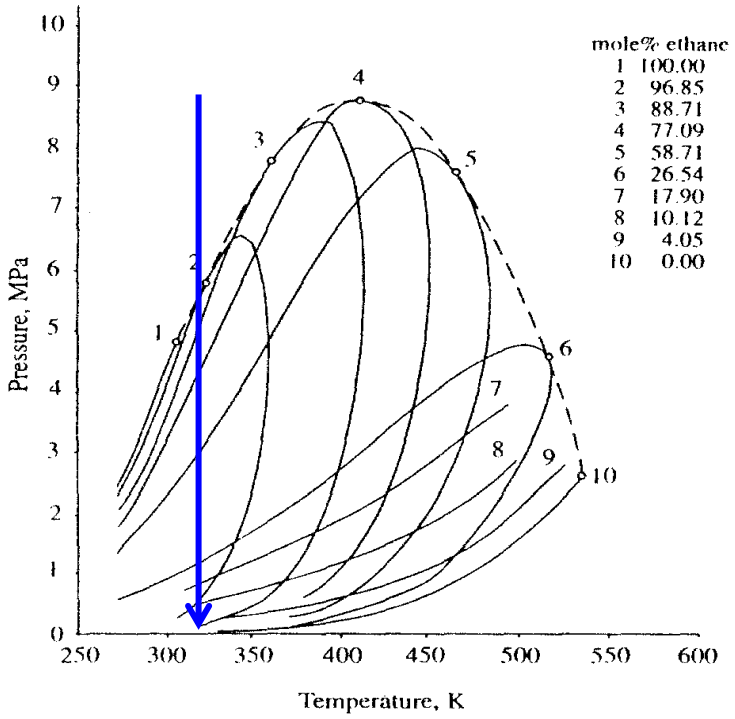

Figure 2.4 Phase diagram of ethane-normal heptane (Danesh, 1998).

2.5 The effect of gas exsolution on the physical properties of hydrocarbon fluid

The effect of dissolved gas on the acoustic properties of the oil has not yet properly been documented. Hwang and Lellis (1988) reported the extensive decrease in bulk modulus and density, and Clark (1992) observed a significant decline on the ultrasonic velocity by increasing the gas content in several oil samples. Batzle and Wang (1992) (after Wang *et al.*, 1988) suggested the following equation for calculation of the live oil velocity in m/s:

$$V = A - B \times T + C \times P + D \times T \times P \tag{2.11}$$

where P and T refers to the pressure and temperature respectively, and A, B, C and D defines as:

$$A = 2096\left(\frac{\rho'}{2.6-\rho'}\right)^{1/2} \quad , \; B = -3.7 \quad , \; C = 4.6 \quad , \; D = 0.0115\left[4.12\left(1.08\frac{1}{\rho'}-1\right)^{1/2}-1\right], \text{ and}$$

$$\rho' = \frac{\rho_o}{B_o}\left(1+0.001R_s\right)^{-1}$$

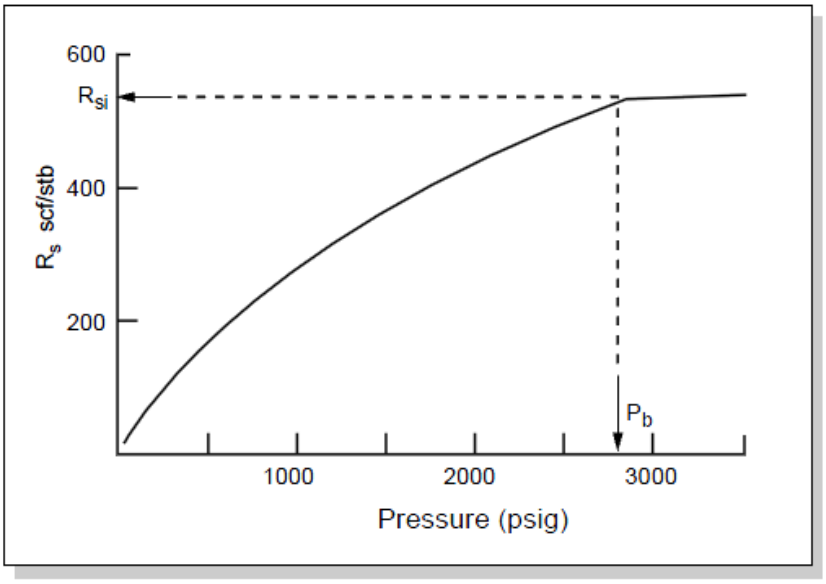

Figure 2.5 Typical solution gas-oil ratio of black oil as a function of pressure at constant reservoir temperature (after McCain, 1990).

R_s and B_o are the gas oil ratio and oil volume formation factor respectively. Han and Batzle (2000) using 70 gas-free (dead) and gas-charged (live) oil samples, suggested that the velocity model developed by Batzle and Wang (1992) overestimates the solution gas-oil ratio effect on the velocity of hydrocarbon liquids. Using these laboratory measurements, they noticed that the parameters in Equation 2.11 (A, B, C and D) are not constant, so they suggested the following equations respectively:

$$A = V_{PO} = 1900.3 \times \rho_{PV}{}^{0.6477} - 256.2 \qquad (2.12)$$

$$B = 3.044 + 0.012 \times \left(141.5 / \rho_{PV} - 131.5\right)$$

$$C = 3 + 0.031 \times \left(141.5 / \rho_{PV} - 131.5\right)$$

$$D = 0.3356 \times \exp\left(-4.036 \times \rho_{PV}\right)$$

$$\rho_{PV} = \rho_o \times \left(1 - \rho_{PV}\right) + \varepsilon \times \rho_a \times \rho_{PV}$$

$$\rho_a = 0.61731 \times \left(10^{-0.00326API}\right) + \left(1.5177 - 0.54349 \times \log API\right) \times \log G$$

where ρ_{PV} is pseudo density, ρ_a apparent liquid density, V_g volume fraction of apparent liquid gas and ε=0.113. The true density of live oil can be obtained by including the mass of dissolved gas:

$$\rho_G = \left(\rho_T + 0.0012 G R_s\right) / B_o\right) \qquad (2.13)$$

where $\rho_T = \rho_P / \left[0.972 + 3.81 \times 10^{-4} \left(T + 17.78\right)^{1.175}\right]$ and

$$\rho_P = \rho_o + \left(0.00277P - 1.71 \times 10^{-7} P^3\right)\left(\rho_o - 1.15\right)^2 + 3.49 \times 10^{-4} P.$$

The first equation considers the effect of dissolved gas, the second and third equations convert the first equation from the surface conditions to the reservoir temperature and pressure respectively.

Han and Batzle (2000) evaluated the effect of gas on oil in terms of pressure and temperature. They noticed that:

a) temperature is more important for heavy oil, so velocity rises with depth, but pressure is significant for light oil, so velocity drops with depth,

b) highly pressurized gas behaves like light oil. Therefore, the difference between gas and oil is very small at higher pressure, and separation of the gas and oil may not be realistic,

c) by examination of wave propagation near the bubble point, they found that the acoustic waves are not sensitive enough to the bubble point pressure. As a result, the acoustic wave does not detect any noticeable phase transition between gas and oil.

Contrary to the above, Firoozabadi (1999) reported a significant change in the wave velocity and fluid compressibility close to the bubble point pressure with liberation of a few bubbles of gas.

In final remarks to this discussion, it seems that simply employing R_s in the seismic domain as a correction factor for the live oil may not cover the complicated behaviour of the gas coming out of solution. This is because the gas composition changes step by step during this process and also the seismic response of the gas around the bubble point pressure is probably close to the liquid. Furthermore, the method and conditions which are selected for the calculation of R_s in the laboratory are not valid at the reservoir scale. In the laboratory, some oil sample is selected and then pressure is changed to measure the solution gas oil ratio at different pressures. Liberated gas is in contact with the oil, so gas can go back into the solution by pressure build up. However, at the reservoir scale, the exsolved gas may has migrated towards the upper part of the reservoir and also to the well. At the lower part of the reservoir, there is no gas in contact with the oil to be dissolved by pressure build up, so R_s cannot be increased. Therefore, applicability of these equations (e.g. Wang *et al.*, 1988, Batzle and Wang, 1992, Han and Batzle, 2000) is questionable at the reservoir scale. This topic is discussed in detail in Chapter 5 in order to see which parameters control the dissolution process and how much deviation from these equations can be observed at the reservoir scale. In addition, the effect of the gas and oil compositional change is investigated to quantify the magnitude of these changes, and its impact on the acoustic parameters. Is it acceptable to assume the effect is negligible, and finally how accurate is the black oil modelling below the bubble point pressure?

2.6 Gas saturation relations in the elastic wave domain

By comparison with oil, the specific properties of gas, such as gravity effect, pressure dependency, higher density difference with brine, relative permeability, capillary pressure etc., make it different in both the engineering and seismic domain. Gas saturation relations or the seismic response to gas saturation variation is one of the most challenging subjects in the seismic literature. In general, the relationship between gas saturation and seismic

attributes or elastic properties can be discussed at three major scales: the laboratory scale, log scale and seismic scale.

Laboratory scale

By selecting different samples from different reservoirs and measuring the wave velocity change versus brine saturation in the laboratory, Domenico (1976) arrived at a highly non-linear behaviour by increasing gas saturation (Figure 1.1). Dumont *et al.* (2001), Rojas (2005) and Lumley *et al.* (2008), reported the same response for methane and CO_2 respectively (Figure 1.1). These laboratory-based measurements clearly indicate the harmonic averaging in the fluid mixing stage. Based on these graphs (Figure 1.1), there is a dramatic drop in the saturated rock wave velocity for a few percent changes in the gas saturation in the primary stages (from zero to around 15%), followed by an approximately constant response for higher gas saturations. This means that, for higher saturations, seismic is not able to detect any change due to the gas saturation variation. The seismic response is approximately the same for gas saturations of 20% and 80%. Employing the same conclusion, Lumley *et al.* (2008) concluded that quantitative monitoring of gas saturations higher than 20% is impossible. It should be taken into consideration that, in the laboratory, values are specific to small samples that obviously cannot be representative of the whole field. There is even doubt on the laboratory procedures employed and the preparation procedures to get the reality of the rocks and fluids. Knight *et al.* (1998) observed different plots (velocity versus gas saturation) for the same sample by changing the frequency. They also reported different plots for different saturation history (imbibitions or drainage). Heterogeneity of the reservoir is not taken into account in the laboratory. Gas movement and distribution is different in the laboratory scale versus the reservoir scale. Furthermore, some forces such as gravity force are negligible at the laboratory scale, but are very important at the reservoir scale (especially for gas). Therefore generalising a statement based on the laboratory measurements is not valid at the reservoir and seismic scale.

Log scale

At the log scale, the harmonic saturation mixing law, arithmetic saturation mixing law or a weighted trend between those have been employed (Mavko *et al.*, 2003). However, the most renowned log scale relationship between gas saturation and elastic properties is the Brie's empirical mixing law (Brie *et al.*, 1995):

$$K_{fl} = \left(K_w - K_g\right)S_w^{\ e} + K_g \qquad (2.14)$$

where K_{fl} is the fluid bulk modulus and e is a calibration constant. When e = 1, Brie *et al.*'s formula is the same as the Voigt or arithmetic average. As e increases, the patchy saturation of Brie *et al.* arrives at the uniform saturation (or harmonic), and is identical to a uniform saturation at e = 40. Brie *et al.* (1995) showed that most well data fit the mixing law with calibration constants between e =2 and e = 5. However, other e values are possible, depending on the degree of consolidation and the frequency of measurement. Gei and Carcione (2003) proposed the following calibration constant e for the mixing law of Brie *et al.* (1995):

$$e = \left(\frac{f_o}{f}\right)^{0.36} \qquad (2.15)$$

where f_o is a reference frequency and f is the measurement frequency. There is no clear definition for the reference frequency. By considering the average measurement frequency of North Sea surveys, e cannot possibly reach at 40, thus harmonic averaging is not achievable. The results are not compatible with the laboratory based results. In 4D seismic interpretations, e is not well-recognised, and guessing a value for e without repeated gas saturation well-logs may be misleading. e is perhaps not constant either vertically or horizontally. Equation 2.14 has also been employed in CO_2 injection monitoring. Konishi *et al.* (2008) applied harmonic, arithmetic and Brie's method to a CO_2 geological storage project and assert that the arithmetic saturation and Brie's equation gives a reasonable value. Their result show good agreement with the CO_2 saturation calculated from neutron log (the blue points in Figure 2.6). They introduced, for the area, the following equation:

$$M_{patchy} = \left(\frac{\left(1 - S_g / S_{gc}\right)}{M_w} + \frac{S_g / S_{gc}}{M_{gc}} \right)^{-1} \qquad (2.16)$$

where M_w is water saturated modulus, and M_{gc} is the partially CO_2 saturated modulus at the critical saturation (S_{gc}). In fact, they adjusted the original equation by normalising it with the critical gas saturation. Their modified equation is shown by the green colour in Figure 2.6. Using well-log data, Konishi *et al.* (2008) obtained an approximately linear seismic response to the gas saturation which is completely contradictory to the Lumley *et al.* (2008) statement. However, without considering the reason for this linearity, they simply employed patchy saturation to explain their observations.

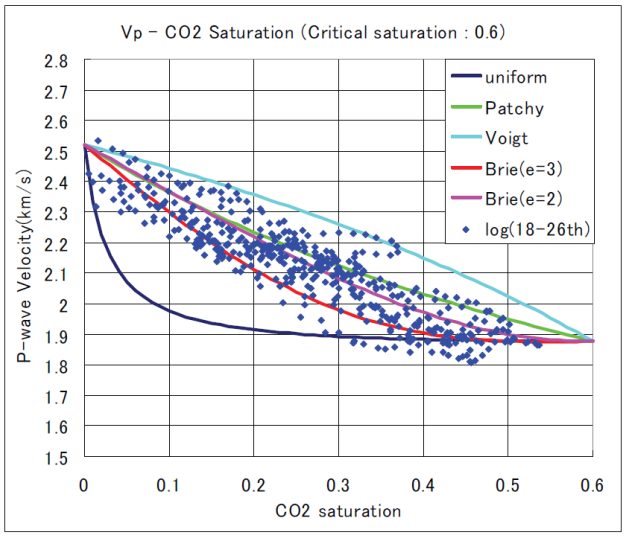

Figure 2.6 Theoretical curves for each saturation state with the observed data in blue point (Konishi *et al.*, 2008).

Seismic scale

In the seismic literature, different seismic responses are proposed to be due to the gas saturation variation. An exponential relationship between gas saturation and 4D seismic attributes was used by Floricich *et al.* (2006) (Equation 1.2 and Figure 1.12). The linear seismic response was chosen by Huang *et al.* (2001) (Figure 1.10-a). The linear response

with positive gradient (the opposite direction to Huang *et al.*, 2001) was employed by Dumont *et al.* (2001) (Figure 1.10-b). Finally some intermediate seismic response (between linear and extremely nonlinear) to the gas saturation variation was proposed by e.g. Sengupta and Mavko (2003) and Wagner *et al.* (2004). These examples highlight the fact that there is not a good and correct understanding about 4D seismic response to the gas saturation variation at the reservoir scale.

The main reason for employing these relationships is the increase of heterogeneity at the seismic scale by comparison with other scales. The homogeneous distribution of saturation arrives at the equilibrium over geologic time. This equilibrium distribution is probably disturbed during drilling, production, and injection. Smith *et al.* (2003) assert that the return to equilibrium may require time frames longer than those encountered during logging or between seismic surveys. Thus, based on this non-uniform distribution of the fluid, they proposed application of arithmetic averaging for fluid mixing that is called "patchy saturation". This name has also been used by others (e.g. Mavko *et al.*, 2003). In the monitoring of a Gulf of Mexico gas field, Huang *et al.* (2001) state that initial attempts using a uniform Gassmann fluid substitution model did not sufficiently predict the observed seismic response. Consequently, they used a patchy saturation model to better describe observable differences in the seismic data.

Knight *et al.* (1998) observed a velocity versus saturation plot similar to the laboratory measurements. They employed a homogeneous distribution of saturation and petrophysical properties in their modelling. For another model that contains multiple distributed patches (every patch has different petrophysical properties and saturation distribution), they obtained a plot which is close to arithmetic average. They suggested the patchy modelling for use at the reservoir scale. They employed two fully saturated patches, a water saturated patch with 100% water saturation and a gas saturated patch with full gas saturation (the gas is air in their modelling). To achieve the saturation distribution at every geological unit, they used some empirical sets of equations which relate the saturation distribution directly to the permeability and porosity. These empirical equations, however, are probably not valid at the reservoir scale (Morrow and Melrose, 1991). It is the balance of forces (injection force, gravity force and pressure gradient) that produce the saturation distribution

in the reservoir. It is not only the porosity and permeability that controls the fluid distribution.

By running the simulation model, calculation of the elastic properties and upscaling, Sengupta and Mavko (2003) concluded that gas injection can give rise to patchy saturation, and mixing law is close to the upper boundary with different end points (Figure 2.7). Using the result of this modelling and modifying Gassmann's equation (1952), they proposed the calculation of bulk modulus at the residual oil and gas points (K_{or} and K_{gs}) by Equations 2.17-a and b. Saturated bulk modulus at saturations between S_{gs} and $1\text{-}S_{or}$ (at the intermediate saturation values) can be obtained using the Equation 2.17-c as a modified bulk modulus.

$$\frac{K_{gs}}{K_{\min} - K_{gs}} = \frac{K_{dry}}{K_{\min} - K_{dry}} + \frac{K_{gas}}{\phi(K_{\min} - K_{gas})} \qquad (2.17\text{-a})$$

$$\frac{K_{or}}{K_{\min} - K_{or}} = \frac{K_{dry}}{K_{\min} - K_{dry}} + \frac{K_{f2}}{\phi(K_{\min} - K_{f2})} \qquad (2.17\text{-b})$$

$$\frac{1}{M_{MP} + \frac{4}{3}\mu} = \frac{S_{f1}}{M_{gs} + \frac{4}{3}\mu} + \frac{S_{f2}}{M_{or} + \frac{4}{3}\mu} \qquad (2.17\text{-c})$$

where $1/K_{f2}=(1\text{-}S_{or})/K_{gas}+S_{or}/K_{oil}$. K denotes bulk modulus; μ, φ and S refer to shear modulus, porosity and saturation respectively. The subscript "*min*", "*gs*" and "*or*" refers to the grain, gas saturated, and residual oil respectively and $S_{f1}=(S_{gas}+S_{or}\text{-}1)/(S_{or}\text{-}1)$ and $S_{f2}=1\text{-}S_{f1}$. It should be noted that they employed Hill averaging for the upscaling procedure, which can be converted to the Vogit (or arithmetic) averaging in an approximate form (Sengupta and Mavko, 2003). The linearity observed by them is probably due to this approximation. The most renowned equation for upscaling of the velocity is the Backus (1962) averaging.

Wagner *et al.* (2004) concluded that the end points for gas saturation are not 0 and 100 percent, these are S_{gm} (minimum saturation for the gas movement) and $1\text{-}S_{wc}$. These values were 15% and 70% respectively in their case study. By including these end points instead of 0 and 100 percent, they obtain that the harmonic and arithmetic averages are close

together. They then used harmonic averaging for gas saturation less than 15% and more than 70%, and arithmetic averaging for gas saturation between 15 and 70%.

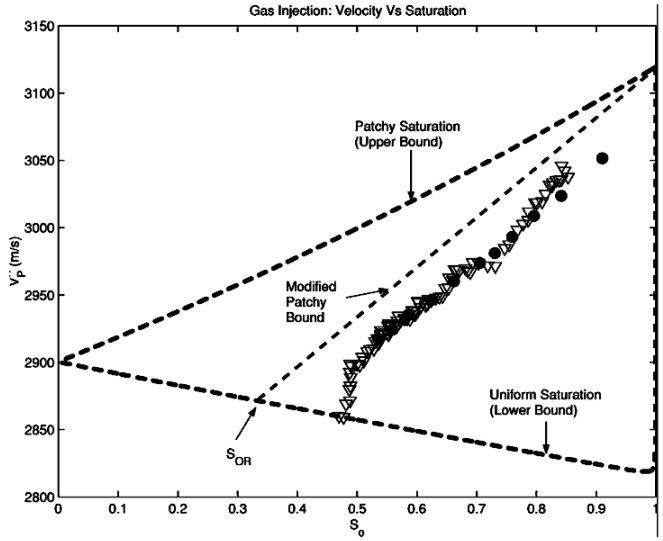

Figure 2.7 Velocity (m/s) versus gas saturation (Sengupta and Mavko, 2003).

The idea behind the patchy saturation is that there are some parts fully (100%) saturated by water, oil or gas respectively. These fully saturated parts are then mixed by Equation 2.18 which is Hill averaging.

$$\frac{1}{K+\frac{4}{3}\mu}=\frac{S_w}{K_{wsat}+\frac{4}{3}\mu}+\frac{S_o}{K_{osat}+\frac{4}{3}\mu}+\frac{S_g}{K_{gsat}+\frac{4}{3}\mu} \qquad (2.18)$$

where K and μ are the average effective bulk and shear moduli of the rock. K_{wsat} , K_{osat} , and K_{gsat} are the bulk moduli of the rock saturated with water, oil, and gas, respectively. This calculation mixes the fully saturated bulk and shear modulus in fraction (f) or saturation (S) form. However, it should be taken into consideration that the fully saturated idea is incorrect by taking the irreducible water saturation into account. By including that, the question is still there, how we mix irreducible water saturation with the oil and gas to calculate the fluid bulk modulus?

Another issue in the engineering domain is whether we are allowed to interpret heterogeneity in the reservoir as a patchy saturation? At the reservoir scale, if the geobodies are connected together, gas will migrate upward due to the gravity effect. This may take a while but, over the 4D seismic timeline, it will stabilise. Our synthetic modelling discussed in the Chapter 3 shows that the equilibrium in the saturation distribution is reached sooner than expected. It takes less than 6 months, even for the heterogeneous models. For the cases with no connections between geobodies, gas may be trapped as separate accumulations or layers with separate seismic responses. Therefore, in the engineering domain, the idea behind patchy saturation seems to be invalid at the reservoir scale. Instead of finding the correct gas migration and distribution at different scales in the engineering domain, simply the word "patchy saturation" has been employed. Arithmetic averaging or patchy saturation may not be applicable at the seismic domain as well by considering the wave propagation. In the seismic domain, arithmetic averaging is typically used where waves propagate parallel to the layer, while if it is vertical or close to the vertical with the layer then harmonic averaging is used.

The argument provided here highlights the lack of a proper understanding about the gas saturation distribution and subsequently the accurate seismic response for the gas saturation variation. Obviously, the gas distribution at the seismic scale is not the same as laboratory scale and log scale. It does not necessarily follow the petrophysical distribution at the reservoir scale. Assuming a patchy saturation at the reservoir scale to generalise laboratory scale relationships seems to be invalid.

2.7 Gas saturation; the physical meaning in the engineering domain

From the above, understanding the saturation distribution at the reservoir scale is an important issue (Figure 1.1). The aim of this topic is to find what the meaning of the gas saturation is at this scale, how much variation exists, and how closely it follows our initial expectations. This saturation distribution is well defined in the capillary pressure related texts. Therefore, I will briefly discuss the vertical saturation distribution using the parameters which affect capillary pressure curves.

Capillary pressure is defined both in terms of density difference and in terms of interfacial tension as below:

$$P_c = \frac{2\sigma Cos\theta}{r_c} == gh(\rho_w - \rho_o) \qquad (2.19)$$

where
P_c = capillary pressure
σ = surface tension
θ = contact angle
r_c = radius of the tube
h = height of interface
ρ_w = the density of water
ρ_o = the density of oil

For a distribution of tubes, the capillary pressure causes a distribution of wetting fluid into the tubes. The capillary increase starts from around free water level (FWL), the point of zero capillary pressure. Figure 2.8 illustrates the behaviour for capillaries and together with the related capillary pressure curve. It is important to note that the different radii contain different capillary pressure and heights to which the water moves up into the oil zone.

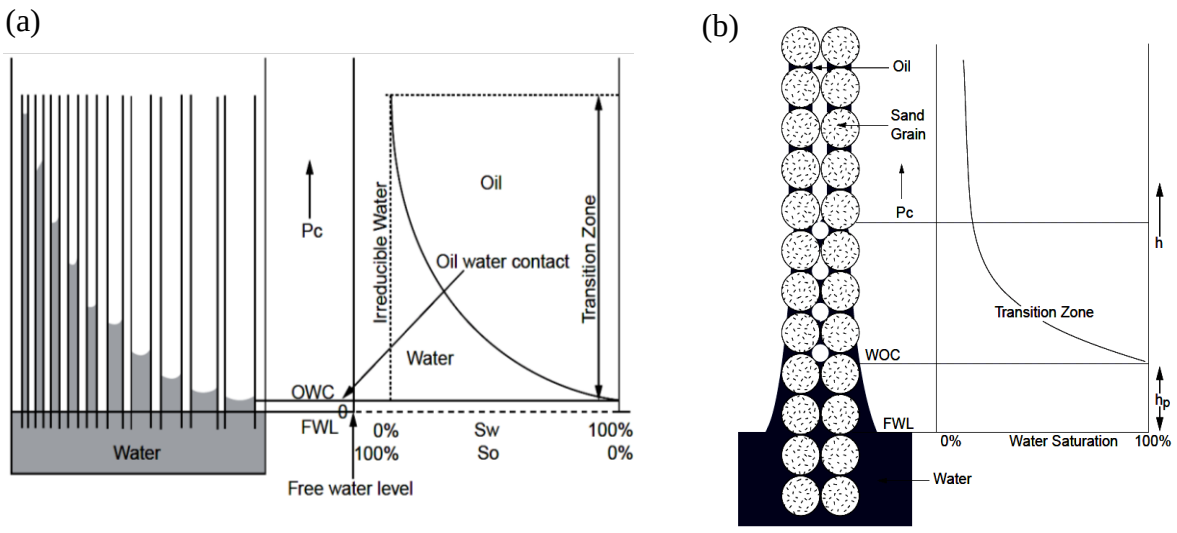

Figure 2.8 Capillary pressure curves for a) tube and b) porous media (Todd, 2007).

Above the hydrocarbon-water contact, water saturation decreases with increased height. Typically, there is a zone of 100% water saturated rock at the bottom of the reservoir. The

100% water saturation can also be observed some height above the free water level (h_p in Figure 2.8-b) corresponding to the largest pores of the rock. The upper limit of this height is called water oil contact (OWC). Above the WOC, since the larger pores do not support the water by capillary action, the water saturation reduces. Both the oil and water co-exist and the water saturation decreases with increased height and arrives at the irreducible water saturation. The distance between the hydrocarbon-water contact and the irreducible water saturation is named the transition zone. Water saturation is constant ($S_{w\text{-}ir}$) above the transition zone and capillary pressure becomes independent of the height. The transition zone is the only part of the reservoir with saturation variation, so it is important to know its magnitude and which parameters control it.

The height of the transition zone is proportional to capillary pressure (Equation 2.19), which is related to the size of the pores and their distribution (r_c), interfacial tension (σ), the wettability and inversely proportional to the fluid density difference ($\Delta\rho$). The size of the pores and their distribution have a significant effect on the shape of the capillary pressure graph, and subsequently on the height of the transition zone. Todd (2007) compares two cases with different pore connectivity. Case 2 contains well connected pores, while case 1 has the small range of connecting pore sizes. Figure 2.9-a compares the two cases. As is expected, the irreducible water saturation is reached at low capillary pressure in case 2, which represents a small transition zone height.

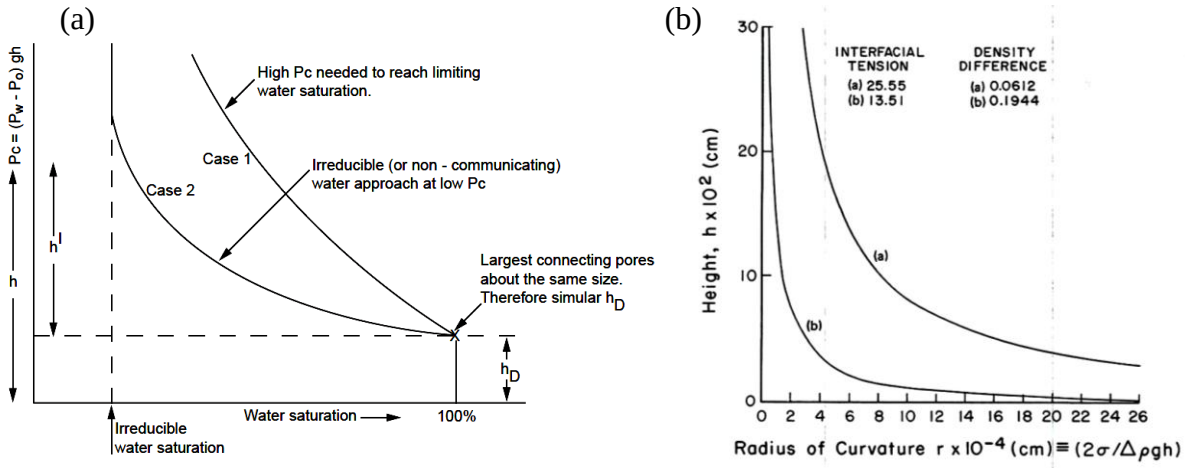

Figure 2.9 a) Capillary pressure curves for different rocks (Todd, 2007) and b) height versus mean radius of curvature (Morrow and Melrose, 1991).

Morrow and Melrose (1991) presented an argument about the increasing trend of permeability and porosity by increasing the pore size. They plotted the height of the transition zone versus the radius (Figure 2.9-b). The height, in general, drops with increased pore size. The other parameters such as the density difference and interfacial tension can also amplify this effect and produce a sharper trend which will be discussed below. To conclude the effect of the pore size and its distribution, for reservoirs with medium to high permeability and effective porosity, we expect a sharp capillary graph and a small transition zone.

Another parameter which is important for the height of the transition zone is the density difference between hydrocarbon and water. As a general statement, large density differences (e.g. between light gas and water) significantly reduce the transition zone and conversely, small density differences (e.g. between water and heavy oil) dramatically increase the transition zone (Figure 2.9-b and Figure 2.10). For the case of gas injection or gas coming out of solution, the large density difference between gas and water or between gas and oil may cause a significantly smaller transition zone.

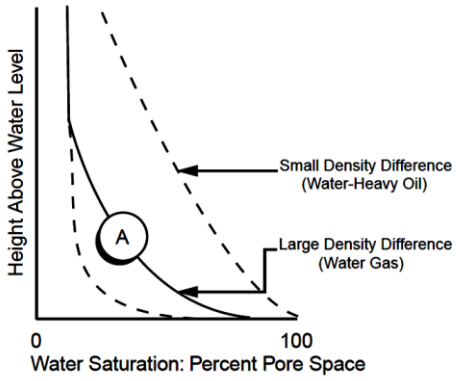

Figure 2.10 The effect of density difference on the capillary pressure curve (Todd, 2007).

Saturation history influences the capillary pressure versus water saturation curve and therefore the magnitude of the transition zone. In general, a slightly sharper capillary pressure curve for drainage saturation than for the imbibitions is expected (Morrow and Melrose, 1991), although the opposite trend has been reported in some cases. Rock wettability affects the capillary pressure curve and therefore the transition zone. High

interfacial tension spreads the transition zone, while low interfacial tension decreases it (Morrow and Melrose, 1991, and Todd, 2007). The several sets of published interfacial tension data for gas-water systems do not agree with each other (McCain, 1990, Danesh, 1998). The same result has been reported for oil-water systems. In general, interfacial tension between gas and water is higher than that between oil and water. Opposite to above has also been reported (Firoozabady, 1990 and Danesh, 1998). An important subject for gas-water interfacial tension (IFT) is that it decreases with increased pressure and temperature. A lower IFT is expected at reservoir conditions (higher pressure - Figure 2.11-a). On the other hand, oil-water IFT increases with pressure increase (Figure 2.11-b), so a higher oil-water IFT is predicted at the reservoir conditions (higher pressure). This probably is the reason for some contradictory results at reservoir conditions. In addition, the presence of the other components affects the IFT value. Gas contains a considerable amount of ethane, propane etc., and water salinity, and on the other hand, shows a wide range in different oil fields which definitely affects the IFT graphs (Tiab and Donaldson, 2004). Therefore, generalizing a statement for the IFT value is difficult. Unfortunately, we do not have access in our case-studies to an IFT data-set to obtain knowledge of the effect of interfacial tension on the magnitude of the transition zone.

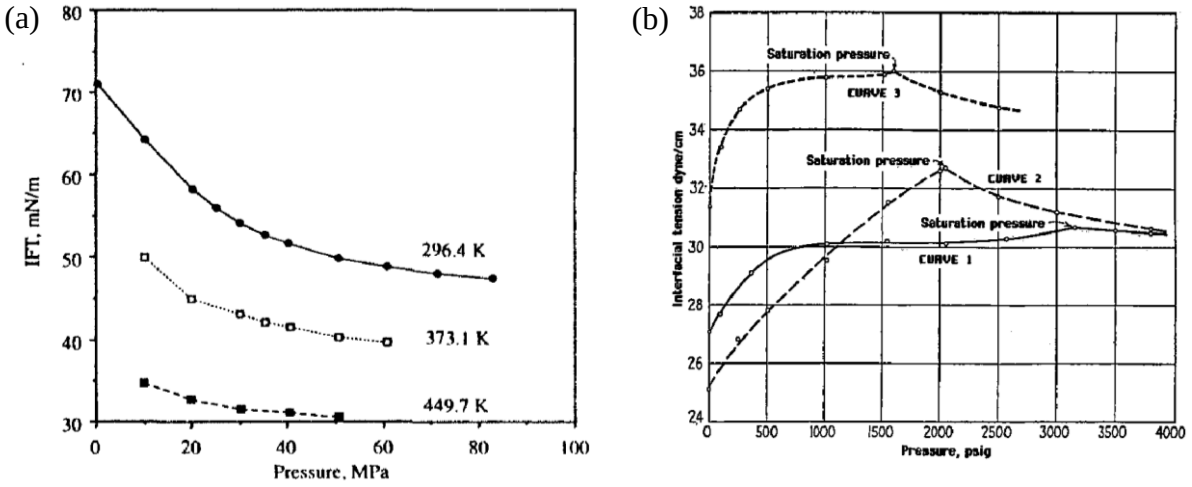

Figure 2.11 Interfacial tension between (a) water and gas (Danesh, 1998) and (b) water and oil (MacCain, 1990).

Contact angle (θ in Equation 2.19 that represents how the fluid spreads over the solid surface) is the other parameter which affects the height of the transition zone. Neutral contact angle (around 90 degree) makes a sharper capillary pressure curve with a tiny transition zone. This angle is dependent on the type of the rock and the composition of the fluids and gas, so generalizing any statement is difficult. The lack of data from our case studies prevents the need to discuss this further.

As a result of the above discussion, a small height of the transition zone is expected for the case of gas injection or gas out of solution in a reservoir that contain a medium to high porosity and permeability. In these cases, the higher density difference between gas (mainly methane) and water (for case of the gas injection) and oil (for case of gas coming out of solution), and also a good pore size connections cause a negligible transition zone. However, the validity of this assumption needs to be tested in different case studies (Chapter 3 and 5). For gas injection into an aquifer, injected gas migrates toward the upper part of the reservoir due to the gravity effect. The gas saturation is the maximum gas saturation ($1-S_{wir}$) within the gas cap. The lower part of the reservoir contains 100% water saturation (Figure 2.12). Inside a specific thickness in the upper part of the reservoir (gas thickness), the magnitude of the gas saturation is constant. It is the gas thickness which varies horizontally. There are higher gas thicknesses around the injection well and a small thickness far from the well. The gas thickness is increased by continuing the gas injection (Figure 2.12-b and c), but the gas saturation is approximately constant in that layer. Thus, in fact the main player in the seismic domain is gas thickness, and gas saturation *per se* remains approximately constant. For appropriate detection of this behaviour, a very fine scale simulation model is necessary to catch a sharp transition zone. This is because of the fact that cells around the gas-water or gas-oil contact will present a large variation of gas saturation in the upscaled simulation models. This unrealistic variation definitely affects the seismic properties of the saturated rock.

By considering gas behaviour at the reservoir scale, the definition of ‘gas saturation’ is challenged and may need renamed. It seems that the gas thickness has more physical meaning at the reservoir scale. It is also a good representative of the changes of the injected gas in the reservoir. However the magnitude of the maximum gas saturation (or irreducible water saturation on the other hand) is mainly dependent on the rock type, and different

reservoirs contain different values (Morrow and Melrose, 1991). Therefore, for comparison of the injected gas between reservoirs, it is possibly better to employ gas thickness multiplied by maximum gas saturation, and consider injected gas in volumetric form. Therefore, gas volume or gas thickness may be the proper words, rather than gas saturation *per se* at the reservoir scale and in the seismic domain. It will be seen later how this directly affects the seismic response.

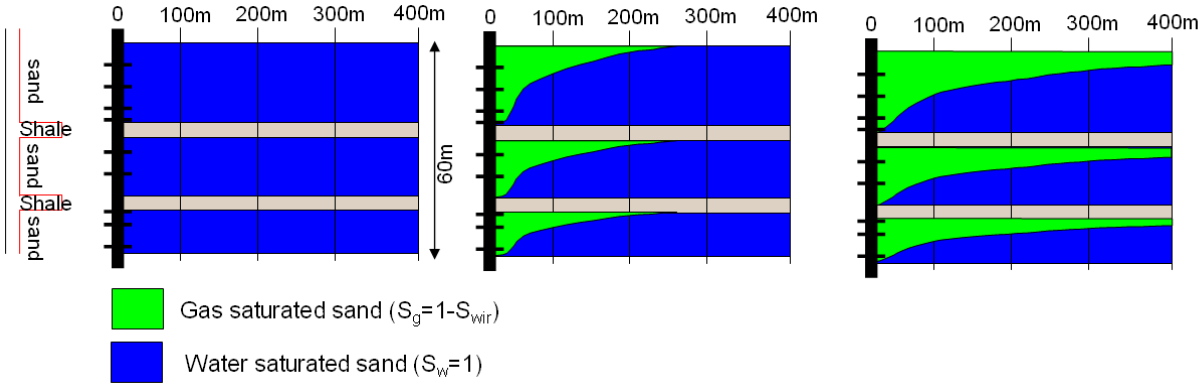

Figure 2.12 Schematic illustrating injected gas movement in three homogeneous sand reservoirs (a) before gas injection, (b) after a short time of gas injection, and (c) after a longer period of gas injection.

The next discussion is about the magnitude of the maximum gas saturation. As the process of gas displacement of the water or oil proceeds, the final saturation reaches a limit determined by the irreducible, immobile water saturation (S_{wir}) for the rock. This irreducible water saturation is a function of a number of interrelated factors such as the surface area of the pore space, clay content and placement, grain shape, grain arrangement, wettability, temperature and pressure. However, there is also a recognised empirical correlation with the permeability and effective porosity, and a number of correlations exist in the literature (for example, Timur, 1968, Wyllie and Rose, 1950, Torskaya *et al.*, 2007). In general, these references empirically correlated the irreducible water saturation to the permeability and effective porosity via the Equation 2.20 with different coefficients (a, b and c):

$$k = a\frac{\varphi^{b}}{S_{wi}^{\ c}}. \qquad (2.20)$$

However, the applicability of these empirical relationships is questionable for different reservoirs. Various examples can be found in the literature with approximately the same range of the porosity and permeability (moderate to good range), but different magnitude of the irreducible water saturation (Burdine, 1953, Corey, and Rathjens, 1956, Morgan and Gordon, 1970, Keelan, 1976, Holditch, 1979, Fulcher *et al.*, 1985, Lal and Brandt, 1988, Mulyadi *et al.*, 2001, Kumar *et al.*, 2004 and Pentland *et al.*, 2008). In these references, the irreducible water saturation is from 10% to 80% for the moderate to good permeability range. Morrow and Melrose (1991) declare that these empirical correlations are naive because they do not take the mechanism and scaling law that govern retention of irreducible saturation into account. They proposed using the capillary pressure curve or the relative permeability curves for determining the S_{wir}, and, therefore, the maximum gas saturation.

At the reservoir scale, the absolute value of maximum gas saturation is influenced by the relative permeability curves, and the balance of viscous, gravitational and injection forces. The heterogeneity of the reservoir can affect the saturation distribution also. However, our simulation results for synthetic models with different heterogeneity (vertically and laterally) and real case studies for gas injection and gas coming out of solution illustrate a narrow distribution around the maximum gas saturation. This topic is discussed in the next chapters.

2.8 Summary

The purpose of this chapter is to present a technical discussion about gas. After providing a basic definition of the gas, the PVT relationships and elastic properties of the gas were reviewed. The mechanism of the gas coming out of solution was discussed. Different stages of gas exsolution with the effect of compositional change were taken into account. Subsequently, the effect of gas liberation on the elastic properties of the oil was presented. The gas saturation relationships with the elastic properties were discussed at the laboratory scale, log scale and seismic scale to discover the geophysicists understanding of gas saturation. A lack of a proper understanding of the gas distribution at the reservoir scale was observed. This is the main reason for employing different relationships to monitor the gas injection or gas coming out of solution in the literature. This subject encouraged us to

review the concepts of reservoir engineering such as the capillary pressure and transition zone, to become familiar with the true gas saturation distribution. We observed that gas saturation can be considered approximately constant inside a specific thickness (gas thickness). The terms gas thickness or gas volume are suggested as substitute for gas saturation.

Chapter 3

Fluid simulation and seismic modelling of the gas injection process

An accurate understanding of the gas distribution in a reservoir as detected through the seismic response is our primary objective. It has already been mentioned in previous chapters that we do not expect all of the tools and concepts from the laboratory scale to apply at the seismic/reservoir scale. To investigate this further, different synthetic fine scale simulation models, with a range of heterogeneities, are generated. Then, the seismic attribute response to injected gas is studied analytically and numerically. The 4D seismic response is considered for both thin (below the tuning thickness) and thick reservoirs. The seismic response is generated at different scales to discuss the accuracy of the upscaled simulation models for monitoring of the injected gas.

3.1 Introduction

We have established in previous chapters that the link between the gas distribution and the seismic response is still challenging to determine. We have already seen that application of the laboratory-based non-linear response of the seismic properties to the gas saturation variation (Domenico, 1976) suggests that seismic is not useful for monitoring of the gas saturation variation in gas injection (Lumley, 2008). However there is the suggestion that this response may not correspond to the proper physics, especially when monitoring 4D seismic (Huang *et al.,* 2001, and Konishi *et al.,* 2008). A critical aspect of gas monitoring is the scale at which the study is performed. Our understanding of the way in which gas is distributed in the reservoir, based on the fluid physics and simulation modelling for two phases (gas and water) and three phases (gas, oil and water), encourages us to revise our models for determining the seismic response. After the process of gas injection or exsolution, the gas will migrate to the upper parts of the reservoir due to the gravity effect. Thus, we assume approximately constant gas saturations inside a gas volume (or thickness) based on the physical properties of the gas. The transition zone between gas and water, or gas and oil (which is the main saturation change area) is less than a meter for most clastic reservoir under consideration here, and hence can be assumed negligible. Below the transition zone, the gas saturation is zero for gas injection. For accurate detection of the transition zone, a very fine (horizontal and vertical) scale simulation model is vital. In industry models, which are fairly coarse vertically (normally more than 2m), the large vertical cell thickness prevents the proper detection of the transition zone and does not allow a proper description of the gas saturation distribution. To analyse this effect further, gas injection into an aquifer is focused on this chapter.

Figure 3.1 describes the problem of scale for the description of gas. This diagram shows a number of differently scaled simulation models, and their corresponding gas distributions (Figure 3.1-a, c, e and g). During immiscible gas injection with the aim of storage or disposal, gas is injected into an aquifer, so that the initial water saturation is 100%. Once it is injected, the gas will migrate upwards and establish a zone with maximum gas saturation. As the injection process continues, the gas accumulation increases in thickness (Figure 3.1-a, left to right). The primary controlling parameter at the reservoir scale is now the

thickness of the gas volume. In this scenario, the velocity of the saturated rock remains constant (the pressure effect will be discussed later), and the seismic response to the injected gas volume is in fact linear for both timeshift and amplitude change attributes. This is because these attributes respond directly to the thickness changes occurring below the tuning thickness. Figure 3.1-b demonstrates variation of the base reservoir timeshift versus the injected gas volume (there is a similar plot for the amplitude). The elastic properties for this model study correspond to our first case study (Chapter 4). The harmonic saturation law is employed for each reservoir cell when determining the effects of fluid mixing (gas and water). Despite this, the output of the fine scale simulation clearly shows a linear seismic response to the injected gas volume (thus agreeing with the observations of Huang *et al.*, 2001 and Konishi *et al.*, 2008). However, these authors chose to employ an arithmetic fluid mixing law to explain their observation, as it appears to them to be more appropriate to explain their results using patchy saturation term.

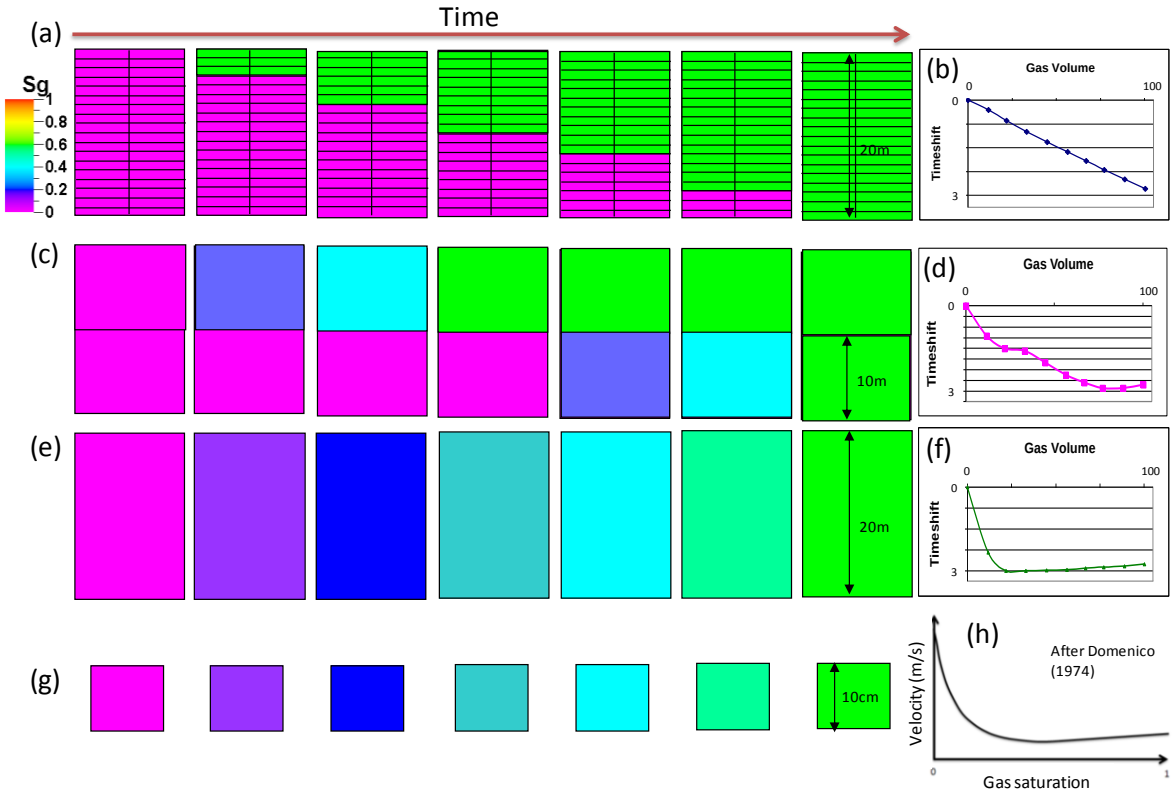

Figure 3.1 The gas saturation distribution at different scales and the seismic response for each corresponding scenario (refer to the text for more description).

Since the upscaled model normally used in the industry for practical purposes, it may not be appropriate for deducing the correct seismic response. A natural question arises as to the exact accuracy of this coarse scaled computation. To tackle this, firstly the total vertical thickness of the reservoir is divided into only several cells (e.g., two or three) (see Figure 3.1-c). The same gas volume as in the Figure 3.1-a example is injected at each stage (left to right). The cell is too thick to be filled by a small gas volume at the primary stages. The gas saturation increases in the upper cell and arrives at the maximum gas saturation by the fourth step. It is followed by the gas saturation increasing in the bottom cell to arrive at the $S_{g\text{-}max}$ at the last step. The seismic response is plotted in Figure 3.1-d. This graph illustrates the effect of the saturation variation - it looks like the combination of two laboratory driven plots. Thus, unlike the fine scale cells (which are also, of course, reality), where the thickness grows gradually (saturation fixes), the incomplete saturation changes the response into a more non-linear response.

For the next stage, the entire layer thickness is taken as one cell and the same gas volume as in the Figure 3.1-a and c examples is injected. Due to the lack of the gravity effect at this scale, gas is homogenously distributed across the entire cell (Figure 3.1-e – left to right). It is exactly similar to the procedure in the laboratory. A sample of the rock is selected and injected with gas (Figure 3.1-g). The gas saturation now varies from zero to the maximum gas saturation during the injection. Now, in this scenario the only controlling variable is gas saturation as the gas thickness is constant (this is not, of course, reality). The anticipated and well known non-linear response is now obtained for both (Figure 3.1-f and h). This clearly highlights the need for employing the fine scale simulation model to produce the accurate gas distribution and seismic response. Another conclusion is that, by employing an upscaled model in synthetic seismic modelling, the results may show considerable deviation from the observed seismic.

3.2 Description of dataset for case study

For the remainder of this chapter, I will discuss different simulation models of reservoir heterogeneity and assess their seismic response. As a guide to this model building procedure, I employ the properties and conditions of the An'Teallach field (BP internal

reports, Lamers and Carmichael, 1999 and Freeman *et al.*, 2008). A more detailed discussion of this dataset will be provided in Chapter 4, in which a method is presented to monitor injected gas volume using the 4D seismic.

Our dataset consists of repeated seismic surveys shot over a turbidite reservoir lying at 2km depth in the North Sea, into which methane was injected. Previous detailed evaluation of well and seismic data by the operator of the field has allowed the group to be sub-divided into a number of sequences. The sands are generally clean, fine to medium grained, varying with porosity by only a few percent, with a mean of 27%, and a slightly wider range of permeability from 225 to 600mD (Lamers and Carmichael, 1999 and Freeman *et al.*, 2008). The three main sands of interest are the T31-sst1, T31-sst2 and T28-sst1, and these are separated by a background of pelagic mudstones (Figure 3.2-d). The sands of T31-sst1 are very thick bedded sandstones, with a high net-to-gross, whilst the other two sands show varying degrees of shale interbedding and hence amalgamation. Inside the selected structure of interest to our study, each sand body remains hydraulically isolated although some cross-flow is thought to occur at fault locations. These sands are approximately parallel and are underlain by the base conglomerate, a key marker for seismic interpretation (see Figure 3.2). Our study area is limited by the channel boundary at the east and west, and by faults in the north and south.

Data from a single injection well drilled into the area of interest is available. Injection started in 1998 and continued for the period of the seismic monitoring (Figure 3.3-a). The baseline seismic data were shot in 1993, and three seismic monitor surveys were acquired thereafter in 1999, 2000 and 2002, after 25, 37 and 53 billion cubic feet (BCF) of gas injection respectively. Because of the need to maintain pressure, daily injection gradually decreased after 1999 and this ensures that the average reservoir pressure was held approximately constant during the acquisition of the monitor surveys (see Figure 3.3-b). As each sand body is well connected both vertically and laterally, pressure equilibration was rapidly established, controlled by the bounding faults and channel edges, and the pressure at the well also reflects that of field in general.

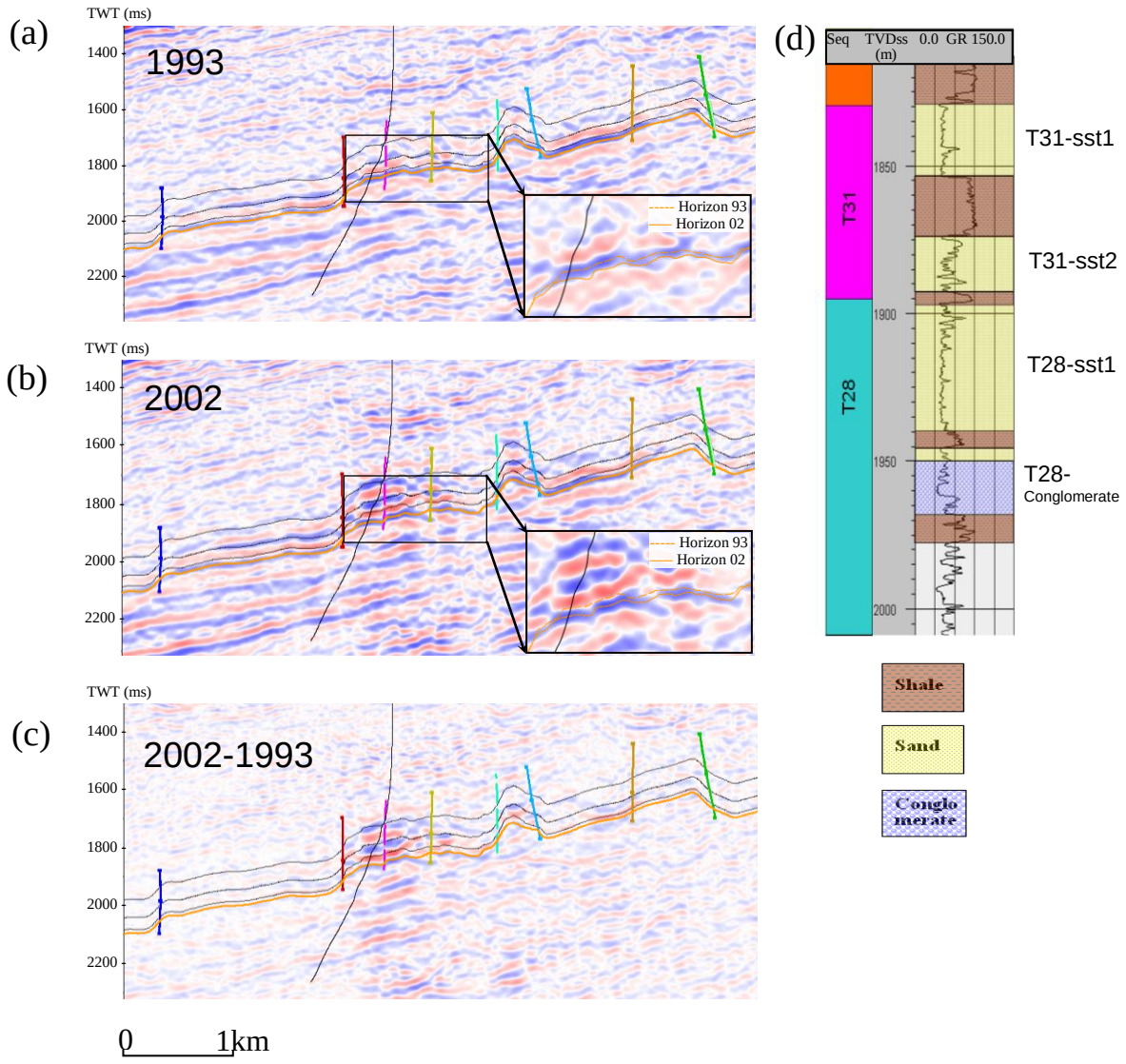

Figure 3.2 (a), (b) and (c) NW (left) – SE (right) seismic sections for the area of interest, at the baseline in 1993 (before gas injection) with horizons and faults, at 2002 after four years of gas injection and their difference. The orange horizon corresponds to the base conglomerate layer picked in the time-shift analysis. Inset in (a) and (b) show the base conglomerate in baseline and monitor surveys. (d) gamma log and interpretation of the main T28-ss1, T31-sst1 and T31-ss2 sands of the reservoirs of interest.

3.3 Synthetic simulation study for detection of the gas saturation distribution

To study the gas saturation distribution at the reservoir scale, some simulation models with different heterogeneity are built. All of the properties such as engineering, petrophysical -

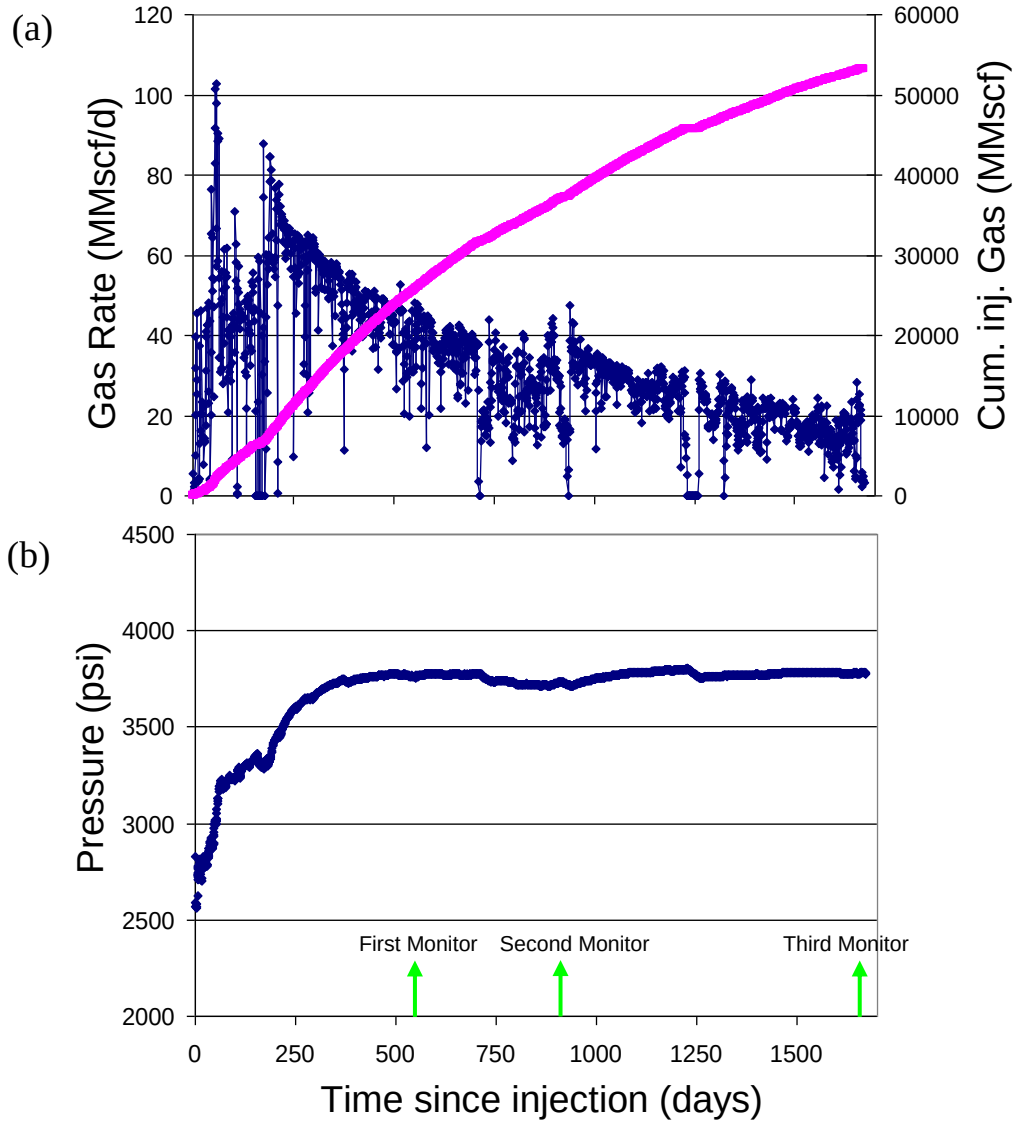

Figure 3.3 Gas injection data: (a) gas rate (in blue) with cumulative volume of injected gas (in red) and (b) reservoir pressure together with the times of the monitor surveys.

and geological data were chosen from the An'Teallach simulation model which was provided by the operators, BP. The aim is to run the simulation model at the fine scale (cell size set to 6.5*6.5*0.5m). The model dimensions are 800*800*19m. This small model is selected to be able to run the simulation model in an appropriate time for research analysis. The first model considered is a homogeneous one. Net to gross, porosity and permeability were obtained from the first layer (T31-sst1) of the An'Teallach simulation model (0.9, 0.27 and 600md respectively) and homogeneously distributed across the entire reservoir.

K_v/K_h is 0.1 (from the original model). All the other engineering data are selected from the original simulation model. For the pressure maintenance, a connection to an aquifer is built from the north-west side of the model. Initial water saturation is 100% across entire the reservoir. A constant gas injection rate is designed by considering the ratio of the reservoir pore volume to the original model pore volume, and relation to the injection rate. The pressure change is approximately constant across the entire reservoir (there is a small gradient of 70 psi per 800m which is undetectable in the seismic domain). All of the parameters above are chosen to accurately honour the true subsurface gas movement.

Figure 3.4-a shows the gas saturation after 8 months. This 3D view clearly demonstrates a high gas thickness around the injected well and smaller thickness far from the well. Gas saturation seems to be approximately constant inside the gas volume itself, but there is a minor fluctuation. Figure 3.4-b shows the gas saturation histogram. There is a standard deviation of the gas saturation inside the gas thickness of 0.04 with the average saturation of 0.52. Figure 3.4-c gives the vertical gas saturation along the highlighted lines in red, blue and green respectively on Figure 3.4-a. This graph clearly shows (in agreement with our previous expectations) that gas saturation is zero in the lower part of the reservoir with a sharp and thin transition zone. Above the transition zone, gas saturation shows a small variation about the maximum gas saturation.

Absolute values of gas saturation are strongly influenced by the relative permeability curves defining the rock, and also the balance of viscous, gravitational and injection forces. Indeed, for the fluid flow simulation, above it has been shown that the gas saturation state is likely to change slightly near to the injector (due to the small pressure gradients) and at the top of the reservoir (due to the gravity force), followed by a sharp change at the gas-water transition zone as a consequence of capillary forces. Constant gas saturation inside the gas volume is an accepted engineering principle. The small variation of the gas saturation around the maximum gas saturation has a negligible effect in the seismic domain (Figure 3.4-d).

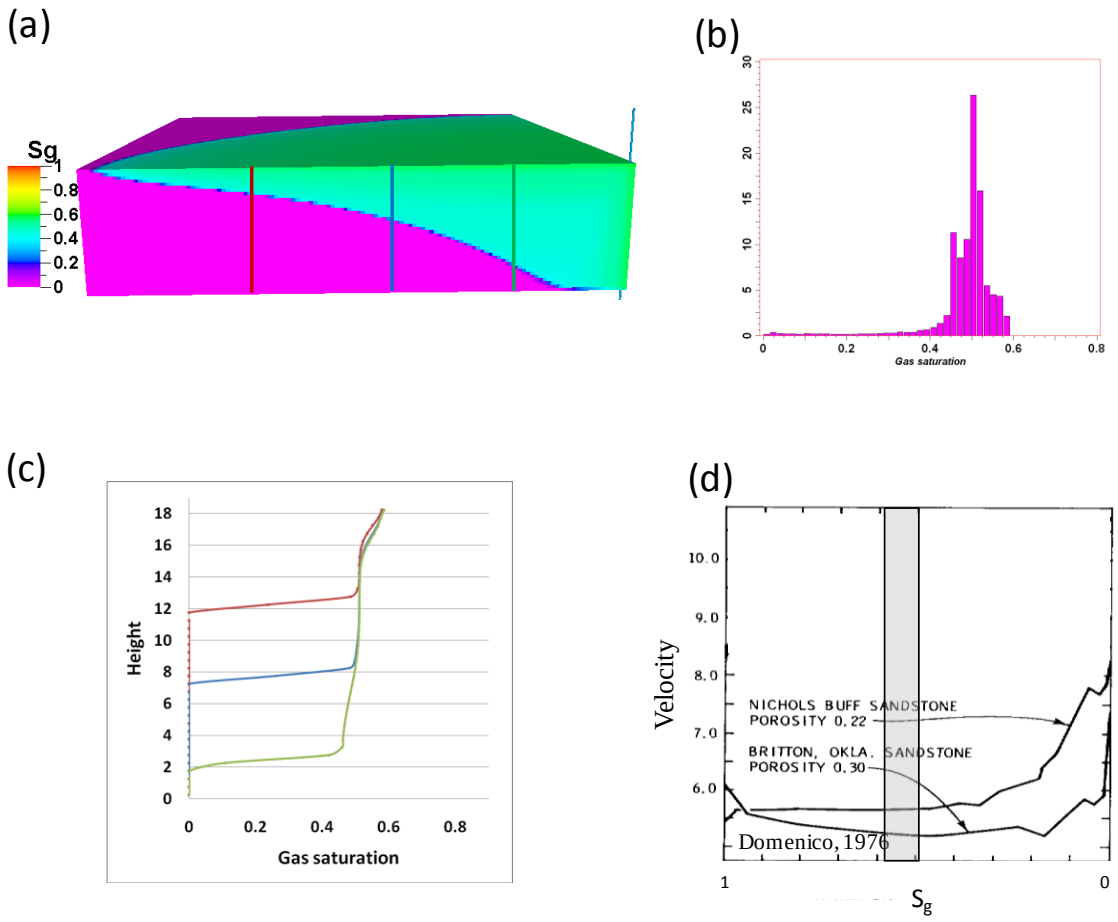

Figure 3.4 Gas saturation distributions in the synthetic homogeneous model. a) 3D view from the simulation model, b) histogram of the gas saturation, c) vertical section of the gas saturation along the three highlighted lines in the (a), and d) velocity versus gas saturation with the highlighted gas saturation variation range (Domenico 1976).

One of the possibilities is that, by increasing the heterogeneity, there will be a wider range of gas saturation which may break this earlier assumption (constant gas saturation inside the gas thickness). This topic will be investigated by employing heterogeneous models. The size of the models as well as the cell size is the same as the homogenous model. There are three hydraulically isolated sands with permeabilities of 600, 400 and 200mD from top to bottom, separated by impermeable intra-reservoir shales. Net-to-gross in the sands is 0.9, 0.84 and 0.75 respectively and the porosity is fixed at 0.27. These values are selected from the three layers of the An'Teallach model. Also, a constant gas injection rate was assigned based on the pore volume fraction of the original model. The simulation model indicates

rapid fluid movements in the top layer and a slow movement at the bottom, which is consistent with the gravity effect. Figure 3.5 repeats the same plots and results as in Figure 3.4 for this model. The standard deviation for gas saturation is 0.05 with an average of 0.52 after 8 months of injection. Since the average gas saturation inside the gas thickness is approximately similar for the different layers, so the same scenario as the last model is repeated inside every layer. The vertical gas saturation section (Figure 3.5-c) highlights a small variation of the gas saturation inside the gas thickness. The vertical heterogeneity for the range of our case studies increases the gas saturation variation by only 1% (Figure 3.5-b).

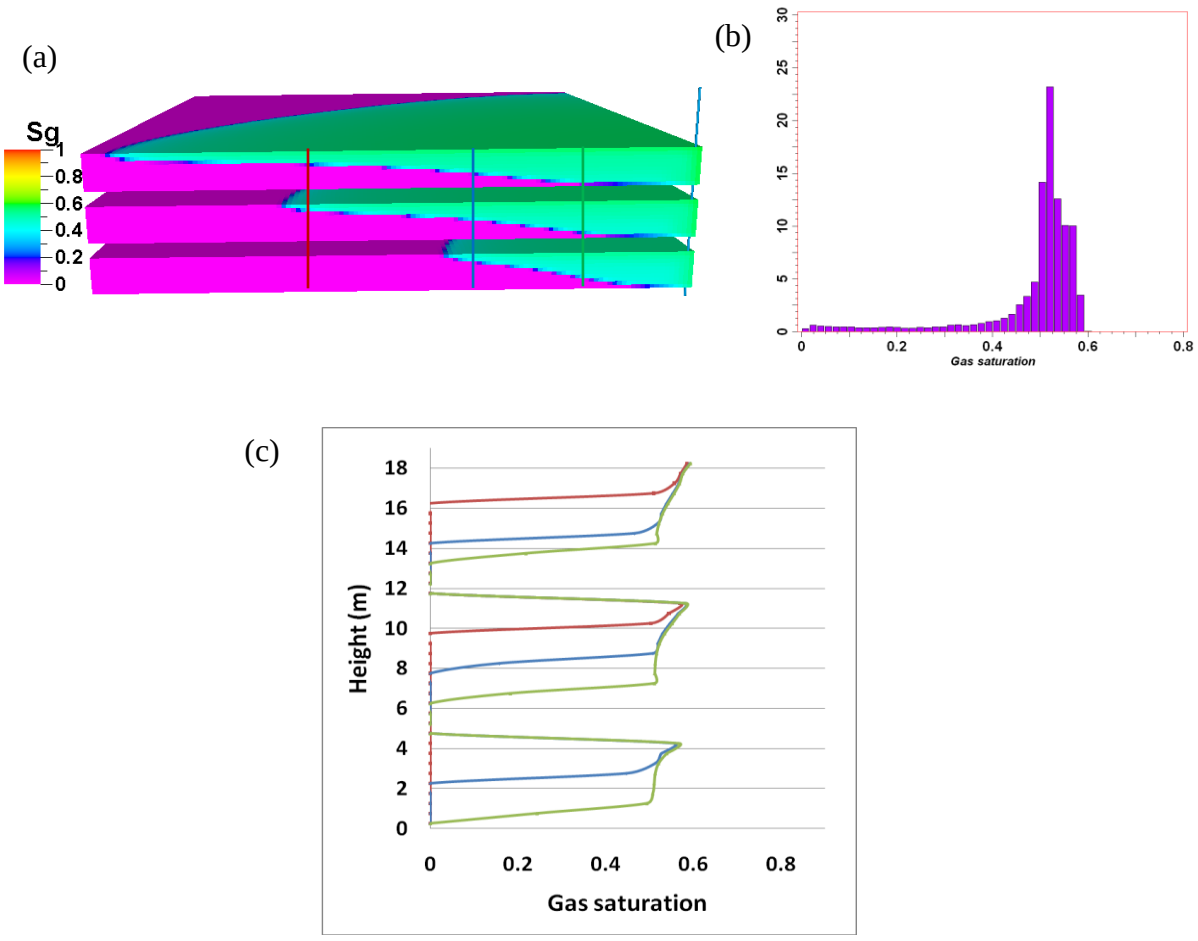

Figure 3.5 Gas saturation distributions for the synthetic vertical heterogeneous model. a) 3D view from the simulation model, b) histogram of the gas saturation, and c) vertical section of the gas saturation along the three highlighted lines in (a).

For the third scenario, a heterogeneous (both vertically and horizontally) model was built with porosity distributed randomly in the range of 0.26-0.28 (the porosity variation is very small in the original simulation model as well). The permeability is distributed using the revised version of Pickup and Sorbie (1996), giving a range of 50-800md. Net-to-gross is distributed randomly with the same geostatistical properties as porosity in the range of 0.4 to 1.0 (Figure 3.6). The other properties such as saturation table and PVT data are obtained from the original simulation model of An'Teallach. The entire reservoir is assumed to be one facies and a fixed set of engineering data are used throughout (similar to the simulation model of An'Teallach). Figure 3.7 shows the gas saturation distribution as a 3D view, with the histogram and vertical sections along three highlighted lines. By comparison with the previous models, there is a slightly higher amount of saturation variation inside the gas thickness. However at the seismic survey time (e.g., more than 6 months for a repeat), gas saturation will have stabilized and have a small range of variation. The standard deviation of the gas saturation is 0.07 and the average is 0.52 after 8 months of injection. The vertical profile of gas saturation (Figure 3.7-c) demonstrates the degree of variation and the extent to which it is affected by the heterogeneity in terms of the effective porosity and permeability. This plot highlights the fact that, the normal heterogeneity in the range of a typical North Sea type reservoir does not make a big variation in the gas saturation distribution.

The above results can also be generalised for the reservoirs with the high value of porosity, NTG and permeability (this was investigated by building different models). However, we have reservations about the applicability for reservoirs with very low permeability (e.g. tight gas reservoirs). The engineering data which are used in our synthetic modelling cannot be employed in these types of reservoirs. They have a specific behaviour for the capillary pressure curve and relative permeability curves that may affect the gas saturation distribution. However, it should be taken into account that the reservoirs with medium to good connectivity were generally chosen for gas injection projects with the aim of storage or IOR (otherwise they will be uneconomical). Therefore, our assumption can be generalised in most of the gas injection projects for storage, disposal or reservoir pressure maintenance aims.

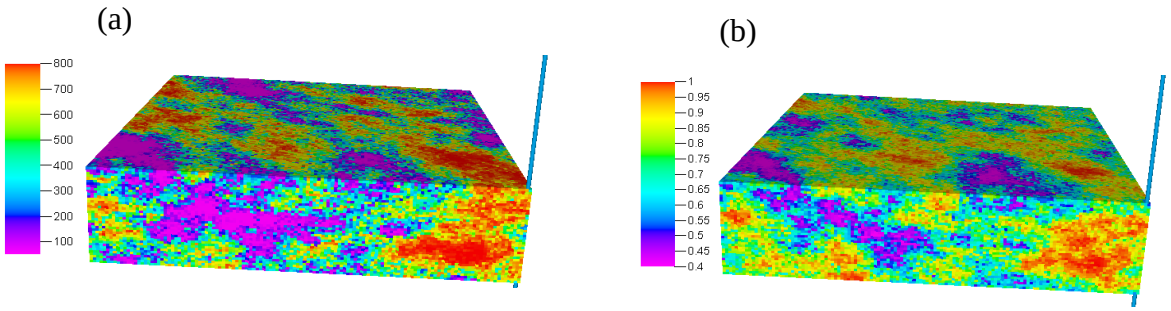

Figure 3.6 The variation of the a) permeability and b) NTG inside the heterogeneous model. These ranges were selected from the original case study.

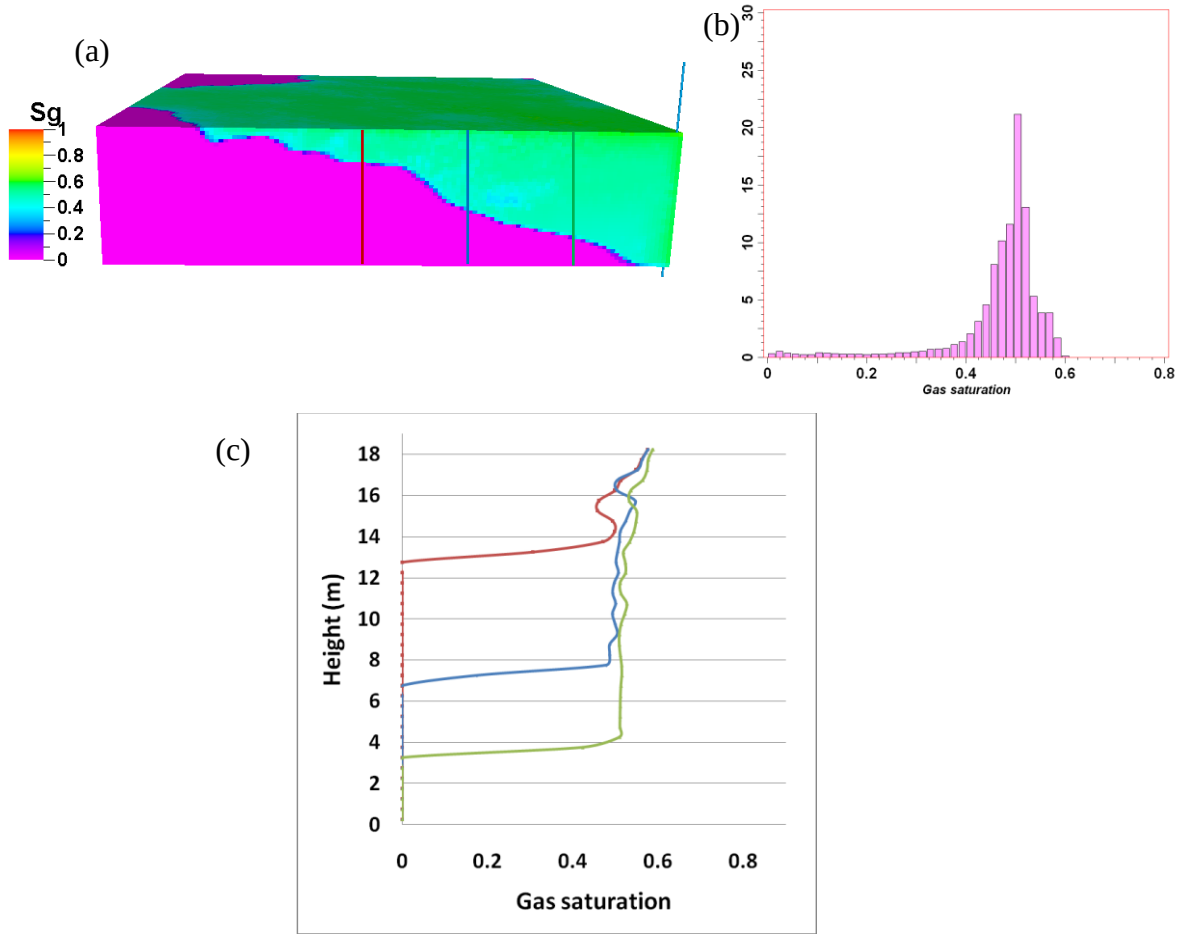

Figure 3.7 Gas saturation distributions in the synthetic heterogeneous model. a) 3D view from the simulation model, b) histogram of the gas saturation, and c) vertical section of the gas saturation along the three highlighted lines in the (a).

3.4 The seismic response to injected gas – analytical modelling

By excluding pressure effects, the results above suggest seismic modelling can be performed with two saturated velocities (and densities), a gas saturated and water saturated velocity. The two most popular 4D seismic attributes (timeshift and amplitude change) are selected to extract relationships between the derived seismic attributes and injected gas volume. Figure 3.8 shows a homogeneous sandstone reservoir of porosity φ, thickness H and uniform distribution of net-to-gross, before and after gas injection. The gas is uniformly distributed inside the gas thickness (h_g).

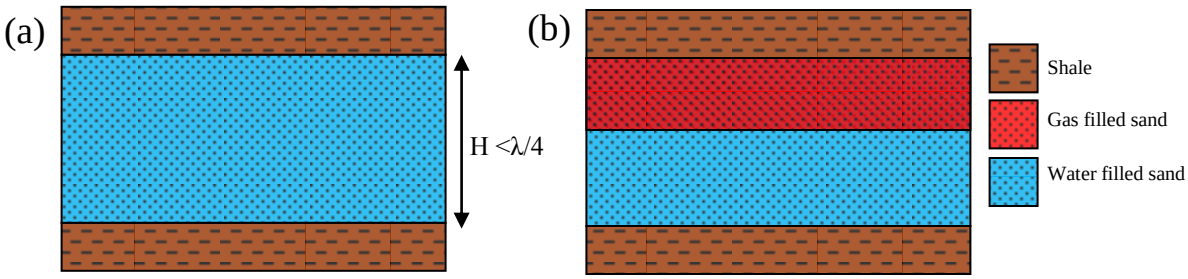

Figure 3.8 A sand layer model surrounded by shale a) before gas injection and b) after gas injection.

For normal incidence, the two-way time change after gas saturation changes is:

$$\Delta t = 2.\left(\frac{H}{V} - \left(\frac{h_g}{V'} + \frac{(H - h_g)}{V}\right)\right) = 2.\left(\frac{V' - V}{VV'}\right)h_g \qquad (3.1)$$

where V' and V are the velocity of the saturated rock with the maximum gas saturation ($S_{g\text{-}m}$) and 100% water saturated respectively. As the saturations are approximately constant, so the velocities are also constant. The only variable in the right hand side is the gas thickness (h_g). This simple equation highlights the linear relationship between injected gas thickness and the timeshift attribute. The gas thickness can be converted to the gas volume via Equation 3.2 to observe the same linear relationship with the injected gas volume.

$$V_g = h_g.\Delta x.\Delta y.NTG.\phi.S_{g-m} \tag{3.2}$$

here the V_g is the gas volume and Δx and Δy are the size of the block. An identical relation to (3.1) is possible for amplitude change as well. Using the basic physics, the reflection coefficient (R) for the composite of two reflectors (Figure 3.8-a) can be written as:

$$R(\theta)_{comp} = R(\theta)_{Top} + R(\theta)_{Base} e^{i\omega\Delta t_N} \tag{3.3}$$

where ω is the angular frequency and $\Delta t_N = 2\left(\frac{H}{V}\right)$. This leads to:

$$R(\theta)_{comp} = R(\theta)_{Top} + R(\theta)_{Base} e^{i\omega 2\left(\frac{H}{V}\right)}.$$

Here, assuming that the reservoir is thin relative to the seismic wavelength ($\lambda/H >> 1$), ω is so small by comparison with the wavelength. Therefore, for the exponential the first order term in the expansion can be used because the high order terms will provide only a small contribution to the total response:

$$e^{i\omega 2\bar{T}} \approx 1 + i\omega 2\overline{T} \quad . \tag{3.4}$$

Therefore, the reflectivity will be converted to:

$$R(\theta)_{comp} = R(\theta)_{Top} + R(\theta)_{Base} + R(\theta)_{Base} i\omega 2(\frac{H}{V}). \tag{3.5}$$

This equation can be transformed to the time domain:

$$A_{comp} = \{R_{Top} + R_{Base}\}s(t) + \{R_{Base} 2(\frac{H}{V})\}s'(t) \tag{3.6}$$

where S(t) and S'(t) are the wavelet and its time-derivative respectively. Assuming that the property contrasts at the top and base reservoir and at the gas-water contact are small, Equation 3.6 leads to the following equation:

$$A_{comp} = \left\{\left(\frac{Z_w - Z_{sh}}{2\bar{Z}}\right) + \left(\frac{Z_{sh} - Z_w}{2\bar{Z}}\right)\right\} s(t) + \left\{\left(\frac{Z_{sh} - Z_w}{\bar{Z}}\right)\left(\frac{H}{V}\right)\right\} s'(t) \qquad (3.7)$$

where Z_{sh} and Z_w are the shale and water saturated sand impedance respectively, finally $\bar{Z}$ is the average impedance. Assuming identical shales above and below the reservoir (log analysis suggests this to be a reasonable assumption) and rearranging Equation 3.7, the next equation can be obtained for the base case (before gas injection):

$$A_{comp-b} = \left\{\left(\frac{Z_{sh} - Z_w}{\bar{Z}}\right)\left(\frac{H}{V}\right)\right\} s'(t) \ . \qquad (3.8)$$

For the monitor (after gas injection), the same scenario can be repeated to arrive at:

$$A_{comp\_m} = \left\{\left(\frac{Z_w - Z_g}{\bar{Z}}\right)\left(\frac{h_g}{V'}\right) + \left(\frac{Z_{sh} - Z_w}{\bar{Z}}\right)\left(\frac{h_g}{V'} + \frac{(H - h_g)}{V}\right)\right\} s'(t) \qquad (3.9)$$

where Z_g is the gas saturated sand impedance. In these equations, the subscripts *m* and *b* refer to the monitor and base respectively. In terms of 4D, this gives:

$$\Delta A = A_{comp\_m} - A_{comp-b} = \qquad (3.10)$$
$$\left\{\left(\frac{Z_w - Z_g}{\bar{Z}}\right)\left(\frac{h_g}{V'}\right) + \left(\frac{Z_{sh} - Z_w}{\bar{Z}}\right)\left(\frac{h_g}{V'} + \frac{(H - h_g)}{V}\right) - \left(\frac{Z_{sh} - Z_w}{\bar{Z}}\right)\left(\frac{H}{V}\right)\right\} s'(t) \ .$$

This equation can be rearranged as:

$$\Delta A = h_g \left\{\left(\frac{Z_{sh} - Z_g}{\bar{Z}.V'}\right) - \left(\frac{Z_{sh} - Z_w}{\bar{Z}.V}\right)\right\} s'(t) \ . \qquad (3.11)$$

This is a same equation as for timeshift, with the difference in the coefficients. There is only one variable (gas thickness) on the right hand side. The amplitude change is now directly proportional to the thickness of the gas accumulated between surveys (or volume of the gas via Equation 3.2).

Interestingly, in Equation 3.11, the wavelet appears in first derivative form (this is validated by numerical computation). Figure 3.9 illustrates the synthetic trace obtained for gas thicknesses from zero (top left) to the total reservoir thickness of 20m (bottom right). A 25Hz Ricker wavelet with the elastic properties of the An'Teallach has been employed for the synthetic seismic modelling. Detail of this procedure will be discussed in the next section; however the expected shape of the trace should be noted. The magnitude of its amplitude is, of course, linearly proportional to gas thickness.

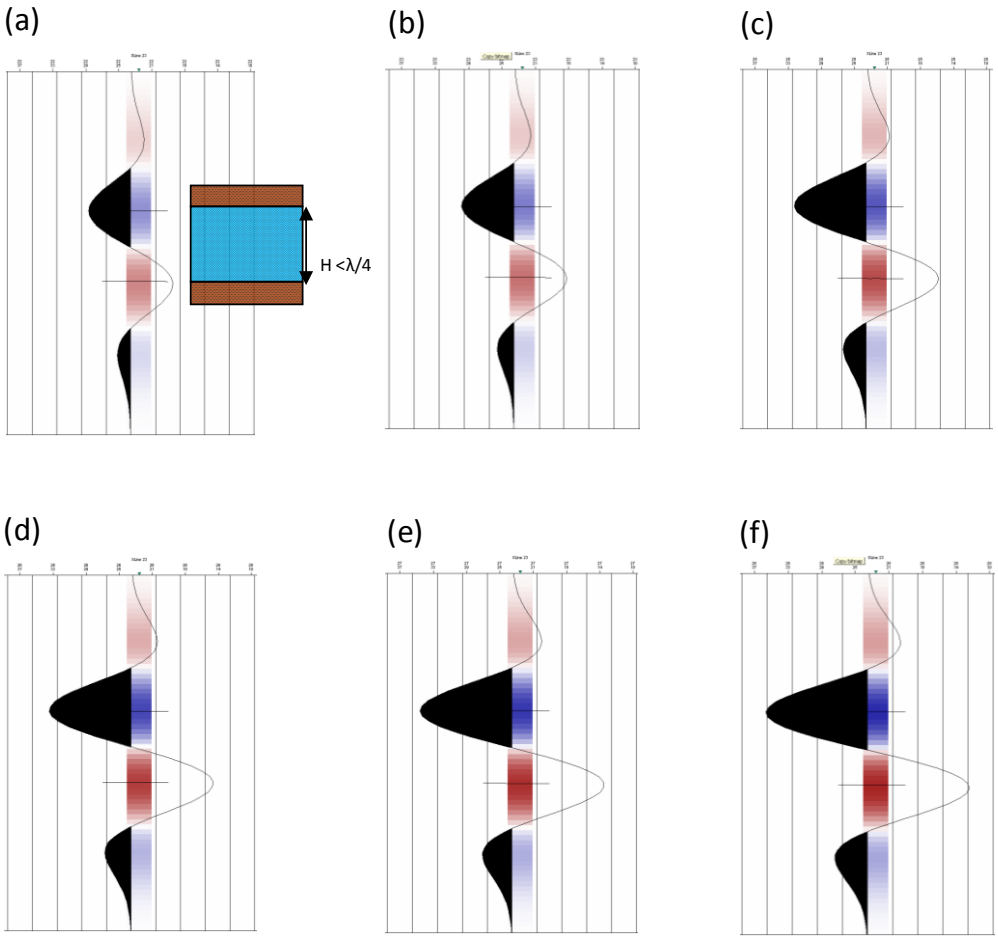

Figure 3.9 Synthetic trace obtained for gas thicknesses from zero (a) to the total reservoir thickness (f).

3.5 The seismic response to injected gas – numerical modelling

For numerical modelling of the seismic response to the injected gas volume, three models with a different range of heterogeneity have been selected. The details of these models were discussed earlier. For the elastic properties of the model, An'Teallach well logs have been employed and the saturated P-velocity, S-velocity, density and other necessary data have been extracted. Following Amini *et al.* (2011), matrix bulk modulus and density were calculated using Gassmann's equations. MacBeth (2004) equations have been used for the stress sensitivity analysis. The main parameters have been changed to arrive at an acceptable match with the well log data. Obviously the variability of the well log data is higher than that of the synthetic seismic data, but the averages are matched. A wavelet was extracted after well tie analysis.

The ETLP (Edinburgh Time Lapse Project) simulation to seismic (Sim2Seis) code (Amini *et al.*, 2011) is employed for producing the 3D synthetic seismic cube separately for the base and monitor seismic. An important issue which needs to be mentioned is that harmonic averaging, a common choice, is selected for the fluid mixing (Figure 1.1). For the calculation of timeshift, a synthetic event below the reservoir is picked in both the base and monitor, and the two-way times subtracted. For the amplitude change, the RMS average a few millisecond around top reservoir is calculated separately in both the base and monitor. Subtraction of these RMS maps gives the amplitude change. This procedure protects us from timeshift effects on the amplitude change (Domes, 2010).

Figure 3.10 shows the results plotted against the injected gas volume for the first model (homogeneous) (a and b), for the second model (vertical heterogeneous) (c and d) and for the third model (heterogeneous) (e and f) respectively. The seismic response (both timeshift and amplitude change) to the injected gas is linear for the models with quite different ranges of heterogeneity. However, by increasing the heterogeneity, some scatter appears in the plots for both attributes. A fitted line for the third model has an R^2 of 0.98 for both timeshift and amplitude change (Figure 3.10-e and f). This clearly highlights the fact that, the heterogeneity in the range of our case study (a North Sea example) does not break the linearity in the system. Despite using the harmonic averaging for the fluid mixing, the

seismic response is not non-linear. These results conform to the notion that Equations 3.1 and (3.11) represent, the main variable for producing the 4D seismic response is the gas thickness or gas volume change.

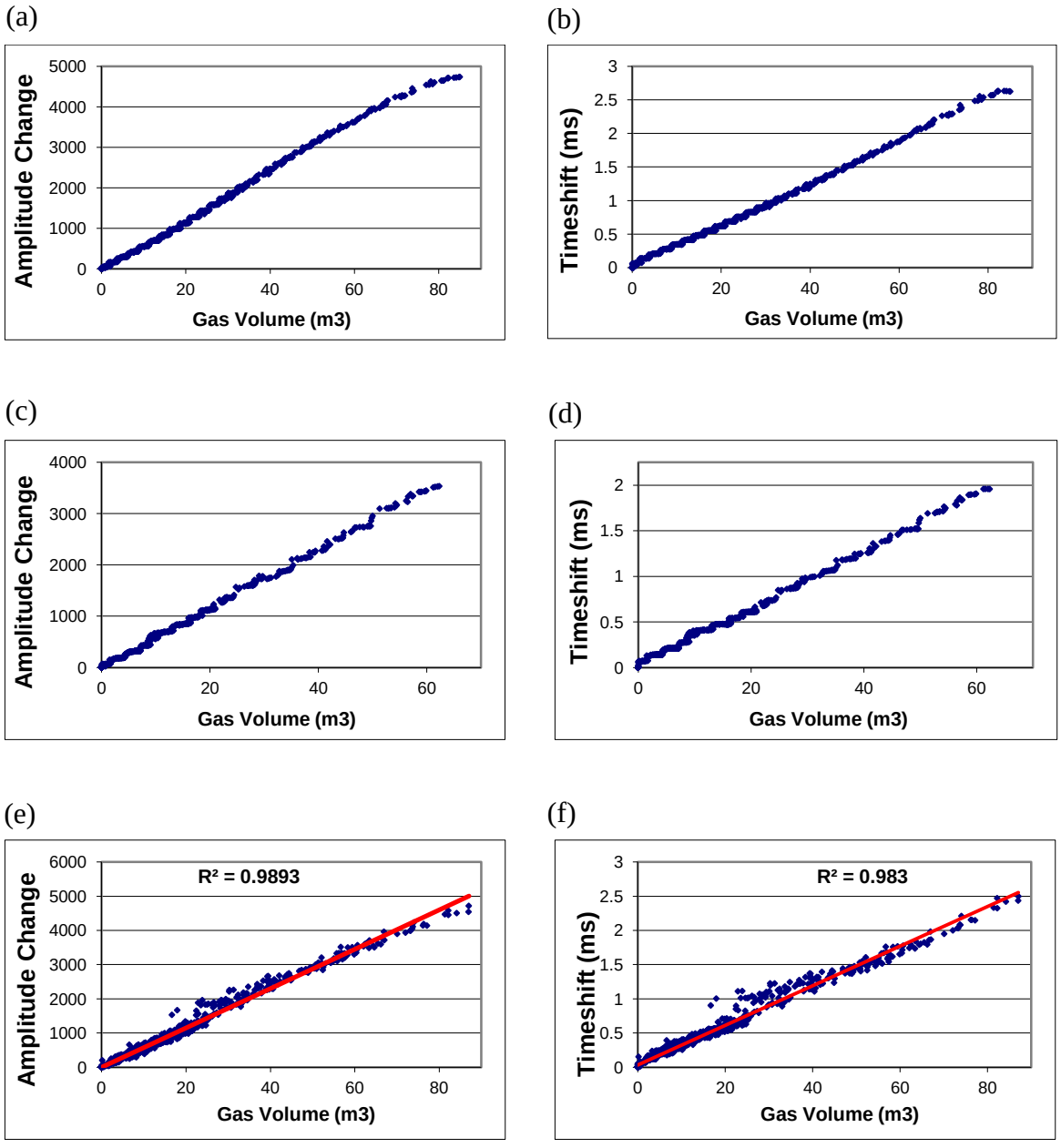

Figure 3.10 Seismic attributes (timeshift and amplitude change respectively) versus injected gas volume for a) and b) homogeneous model, c) and d) vertical heterogeneous model, and e) and f) heterogeneous model. The linear response of the 4D seismic attributes versus injected gas volume is confirmed for these models.

The subject that was discussed above does, however, cover thin reservoirs only (thin, here, means below tuning thickness. It is case dependant, but tuning thickness is approximately 30 m in my case studies). The main question here is: what is the 4D seismic response for thick reservoirs? Is it possible that the proposed linearity will be broken for a thick reservoir? It should be taken into account that even thick reservoirs are usually made of repeating sequences of sand and shale. For a very clean sand, the whole of the reservoir can be assumed to be one layer, but for the real cases, the whole reservoir is a repetition of the sand and shale or other geological layers, such as conglomerate, evaporates and etc.

For investigation of the above subject, different thick 1D models are built (Figure 3.11). The total thickness is 200m but with different structure or architecture of the shale and sand. The first model contains 140m sand in the middle, surrounded by shales at the top and bottom. This is a very clean and thick sand. The second model is a combination of two sands surrounded by shale. Finally, the third model contains five sands surrounded by shales. The thickness of the sand and shale layers in model 3 is randomly selected to have variable sand thicknesses and with different positions. The cell thickness is set to 1m. A constant porosity and net-to-gross are distributed over entire the sand layer (the same value of the T31-sst1 in our case study-An'Teallach). The constant gas saturation (maximum gas saturation) was distributed inside the gas thickness. The reservoir is fully water saturated for the base case. After that, gas thickness starts to increase from the top to the base of the sand layers. For the models with different sands, the gas thickness is separately increased inside every layer whilst maintaining the same ratio to the sand thickness. The assumption behind this kind of modelling is that the gas is separately injected into every layer, but the injection rate is proportional to the layer thickness. Different gas thicknesses were produced to be representative of different injection stages.

The same petro elastic parameters as in An'Teallach are chosen, and sim2seis modelling produces the seismic traces. For the timeshift, an event below the reservoir was selected to calculate travel time difference between base and monitors. For the calculation of amplitude, the RMS (root mean square) average covering the top to the base of the reservoir was selected to cover the variation of the entire reservoir. In this case, the trough at the top of the reservoir is only the representative of the activities close to the top. There are other peaks and troughs for the rest of the layers, especially for model 3 (but with

interference effects). Given the small amplitudes involved, the RMS amplitude is approximately equal to the sum of the individual root mean square amplitudes for each reservoir sand, and hence the summation of the gas accumulation thicknesses. Subtraction of the RMS averages gives us the desired amplitude change. The timeshift and amplitude change are plotted versus gas thickness for different models. Because the porosity, NTG, S_g and cell dimensions are constant, so gas thickness is representative of the gas volume here.

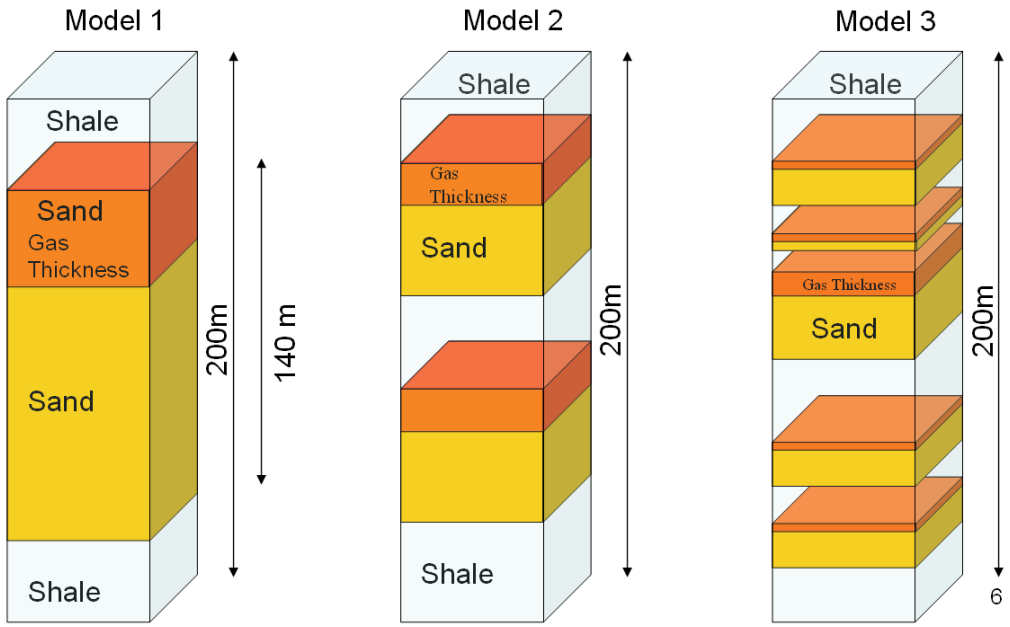

Figure 3.11 The architecture of the 1D models that were employed in the synthetic seismic studies.

Figure 3.12-a and b shows the timeshift and amplitude versus gas thickness for the first model. It can be clearly seen that the timeshift illustrates a linear response for the injected gas. It is because of the fact that timeshift below the reservoir is representative of the change over the entire vertical reservoir thickness. As discussed in the last section, timeshift is proportional to the gas thickness change. It is independent from the reservoir thickness. Amplitude change response is complicated (Figure 3.12-b). It can be interpreted in the same way as a wedge model. For gas thicknesses below the tuning thickness, the amplitude change indicates our anticipated linear response. After this stage, amplitude change decreases and arrives at the true value. In the last stage, for the higher gas thicknesses, the peak at the base of the gas thickness interferes with the peak of the base of

the sand, so that a second maximum is observed on Figure 3.12-b. It can be briefly concluded that the behaviour of the amplitude change for a thick reservoir cannot be easily captured and parameterised. In this case, the top reservoir amplitude change is representative of changes over only the upper part of the reservoir. It does not contain useful information on the reservoir thickness. However timeshift is found to be a valuable attribute for the thick reservoir.

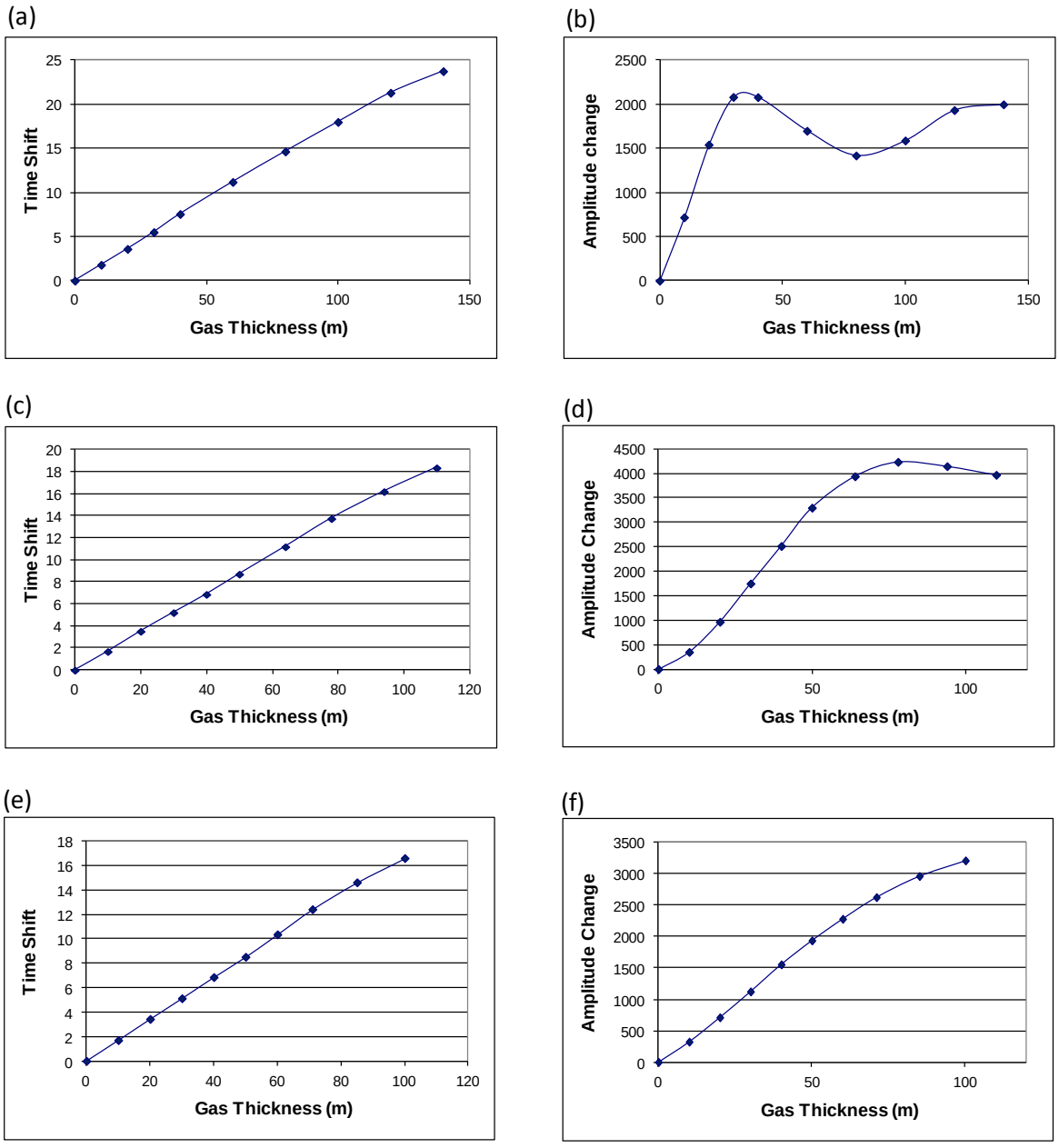

Figure 3.12 Seismic attributes (timeshift and amplitude change respectively) versus gas thickness of the 1D modelling for a) and b) model 1, c) and d) model 2, and e) and f) model 3.

For the second model, the timeshift shows a linear response again (Figure 3.12-c), because it is independent of the reservoir architecture. The amplitude change response is interesting (Figure 3.12-d). The tuning thickness of the upper sand and lower sand are added, so the linear part of the graph is enlarged. In the same way as the first and second model, timeshift versus gas thickness demonstrates a linear response in the third model (Figure 3.12-e). The interesting issue for the amplitude change here is that it also illustrates a linear response for the gas thicknesses from zero through to the total sand thickness. This is due to the interference of the different peaks and troughs, which increases the tuning thickness and creates a linear relationship even for a thick reservoir. Thick reservoirs in the North Sea are normally a combination of a few sand and shale packages. This behaviour originates from the depositional environment during geological time, especially in turbidity reservoirs that are a repetition of different flows and layers (Link, 2001). The third model in the above study is close to my case study (An'Teallach).

In the reservoir engineering domain, the effect of intra-reservoir shales may be neglected. The fluid flow is the main objective (and a minimum run time for simulation model), so that the thin shales are considered along with sand using the net-to-gross (NTG) concept. By combining shale and sand, we lose intra reservoir reflectors that are important in the seismic domain (Folstad and Schoenberg, 1992). By taking account of this concept in the seismic, the interference effect (or tuning effect) will create the linear 4D seismic response even for thick reservoirs (e.g. model 3). Our suggestion is to include the intra-reservoir shales in both the geological and simulation models.

The next issue is the comparison of the timeshift and amplitude change attributes. It seems that timeshift is more stable than amplitude change. It is independent from the reservoir architecture, while amplitude change shows a variable response for different reservoir architectures. It is also possible to have both destructive and constructive effects in the amplitude change response. Timeshift is more robust and it contains a simple physical meaning and is easy to interpret. However, the calculation of timeshift is a challenging subject. Picking the base reservoir is one of the methods of calculation, but there is the possibility of reservoir activities affecting a base reservoir reflector. Ghaderi and Landrø (2009) suggested selection of an event below the reservoir to circumvent this problem. This horizon should be below enough to be not affected by the base horizon. Very below

horizons are not suggested, due to the loss of the signal in the deeper area. as the aim of the processing, but it should not be very below Other methods such as cross correlation based methods were discussed by them, but the picking method was proposed because it produced answers close to the real timeshift. The detection limit of the timeshift is one of the main problems regarding this attribute. Calculation of the timeshift below 0.5 ms is probably not reliable, while a considerable velocity change (or a gas thickness change around 2.5m) is necessary to make a 0.5 ms timeshift (or a gas thickness change around 2.5m). Therefore, timeshift around 0.5 ms is not small enough to be disregarded. As a conclusion, timeshift is a good and robust attribute, but it should be treated with care. A detailed discussion will be provided in the next chapter on timeshift and amplitude change attributes and their lack of agreement.

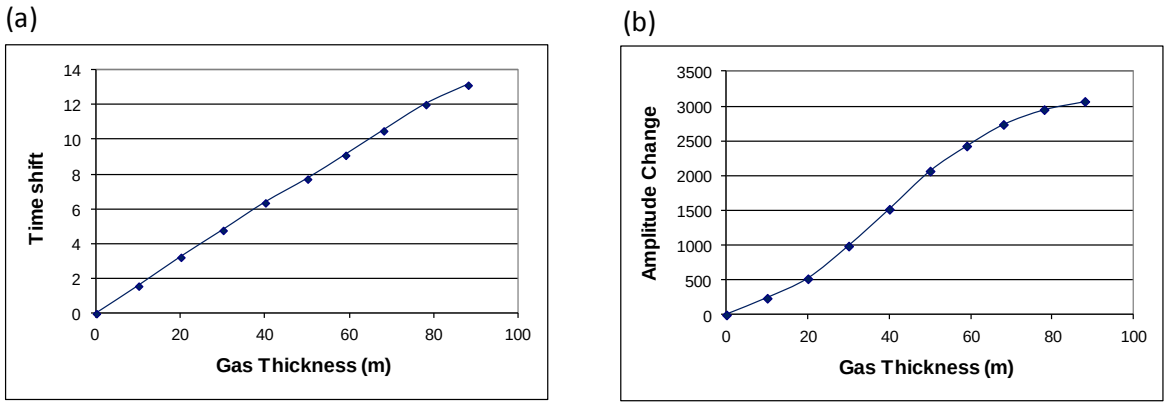

Figure 3.13 a) Timeshift and b) amplitude change versus gas thickness for the 1D modelling of An'Teallach.

For synthetic seismic studies, the injection well in the centre of the area of interest (the only well which is present in the injected area) is selected. Figure 3.2 gives the description of the layers (sand, shale and conglomerate) and observed seismic response to the layering before gas injection and after. The total net sand thickness is around 90 meters. Gas thickness increases from the top to the base of the sand layers. It is separately increased inside every layer whilst maintaining the same ratio to the sand thickness. The elastic properties and the input data for the petro elastic modelling of the layers is extracted from the well data using the iterative approach that was discussed earlier. Figure 3.13 represents the output of the synthetic seismic modelling. The same as the third model in the last 1D discussion,

timeshift (Figure 3.13-a) shows a clear linear trend. Amplitude change response (Figure 3.13-b) is also close to being linear. As Figure 3.2-b shows, the sands remain approximately parallel over the entire injected area, therefore the linear 4D seismic response for both timeshift and amplitude change can be generalised across the entire area.

3.6 The impact of model upscaling in the seismic domain

As discussed earlier and presented in Figure 3.1, gas saturation immediately arrives at the maximum gas saturation at the top of the reservoir for the fine scale model and then starts to increase the gas thickness. However, gas saturation cannot arrive at the maximum gas saturation in the primary stages for the upscaled models. More gas injection would be needed to increase the gas saturation of a large cell to the maximum gas saturation, so a gas saturation variation is observed during the gas injection process in the upscaled model. Detection of a realistic gas saturation distribution is not possible with the upscaled model. The question here is: how much error or deviation from the realistic seismic response is expected by upscaling the model? To answer the question, vertical and horizontal upscaling is taken into account. For the vertical upscaling study the An'Teallach 1D model used earlier is considered. For the fine case, the vertical cell size is 1m. Gas thickness is increased inside the sands from the top to the base of each sand layer. Ten time steps are chosen - the first case is considered as a base case, when the sand is fully water saturated. Gas thickness rises during the other steps to arrive at the full sand thickness by the 10^{th} step. During the upscaling stages, the vertical thickness of each cell is set to 2m, 4m, 6m, 10m and the full sand thickness of 25m (in average) respectively. In each time step, the same volume of gas is injected into these differently upscaled models. For example, the gas volume for the first time step (first point in Figure 3.14) is $233m^3$ for all of the models. These models can now be compared in terms of the injected gas volume. The aim is to see the effect of the cell thickness.

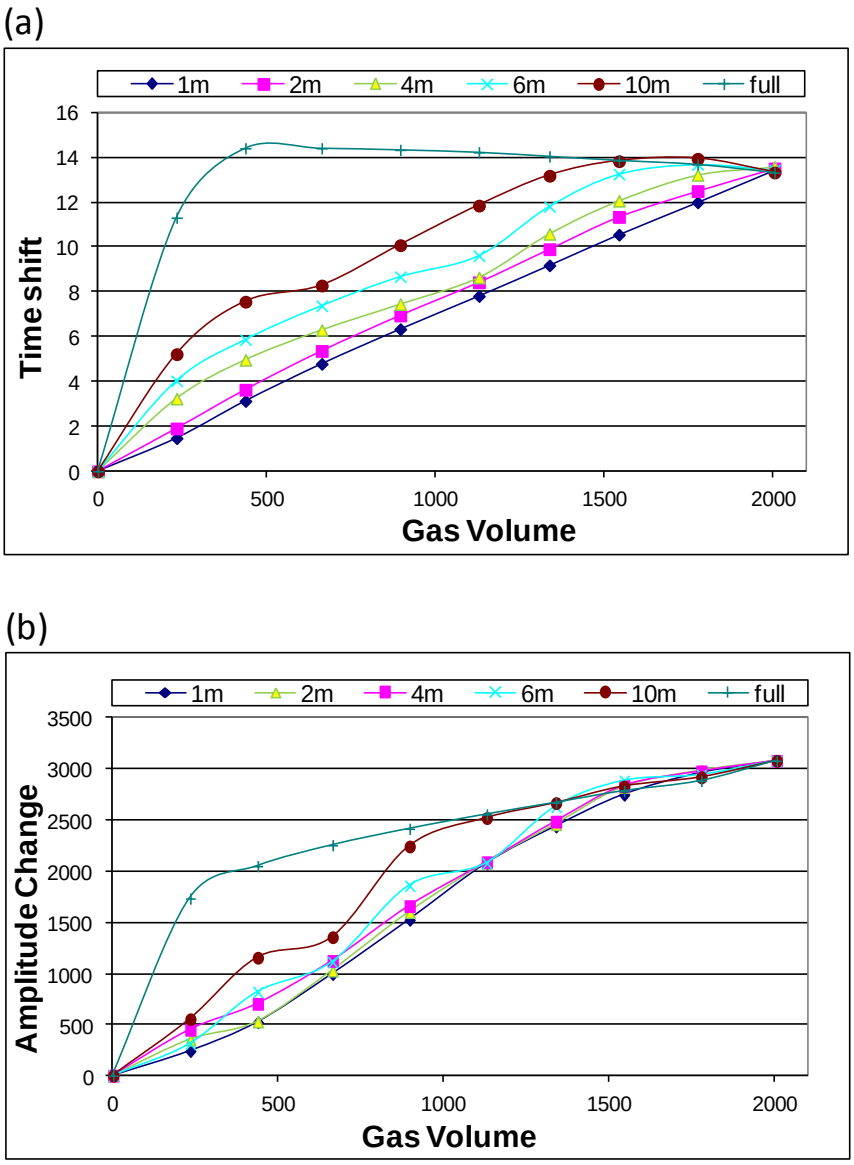

Figure 3.14 a) Timeshift and b) amplitude change versus gas volume for different cell thicknesses.

Figure 3.14 illustrates the timeshift and amplitude change versus gas volume. The clear linear seismic response for the fine scale model is observed as a reference with our earlier studies. There is a deviation from linear to non linear by increasing the cell size for both timeshift and amplitude change. The deviation becomes increasingly non-linear with cell size. For timeshift, it becomes nonlinear quite quickly due to its direct inverse dependence on velocity. Amplitude change is affected by both velocity and density. The density response with gas saturation is always linear. This suggests there should be less deviation

for the amplitude. The fine scale seismic response is taken as the base case. The deviation from this line is considered as the error for every cell thickness. Figure 3.15 shows the error for the timeshift and amplitude change. For timeshift (Figure 3.15-a), the error is less than half a millisecond for cell thicknesses of up to 2m. Half a millisecond is considered as the ultimate detection limit for timeshift in the 4D seismic literature. Therefore, 2m can be taken as the maximum cell thickness we are allowed to use in the simulation models, whose aim is to accurately monitor gas injection in the seismic domain. In the next step, the error was converted to the percentage form (by subtracting from the base case and dividing by it). The average error calculated for each cell thickness is given in Table 3.1. The average error for cell thicknesses of more than 2m is higher than the average non-repeatability for North Sea seismic surveys. Therefore 2m can again be assumed as the maximum limit for cell thickness in the simulation model built for monitoring of the gas injection. Note, however that, the upscaling error for amplitude change is less than that for timeshift, in terms of absolute values. Therefore amplitude change does not give further complications.

Obviously, running the simulation model with 1m cell thickness (or even less) is our priority so as to minimise the error. However, due to the computational limitations, it is very difficult and time consuming to run a realistic simulation model with thin cells. Our investigations suggest 2m as a maximum allowable cell thickness. For cells larger than this thickness, the accuracy of the model is questionable in the seismic domain given the non-repeatability range of the 4D seismic. Note, however, that the accuracy range for timeshift calculation or seismic repeatability is not a fixed value. Obviously, with the development of new technologies in 4D seismic acquisition and processing (e.g. LoF projects), repeatability ranges even less than 10% have been reported. The second issue that needs further attention is that, by employing 2m as a vertical cell thickness in the simulation model, there is still considerable error (9.5% for timeshift and 6.08% for amplitude change). This error is not negligible and could be important in some cases. Therefore a more careful consideration of the vertical cell size is vital. Considering the rapid development of computational systems and with the presence of parallel calculation, running a real simulation model at the fine scale seems to be possible in the near future.

The investigation of the horizontal upscaling based on the 3D synthetic model shows some scattering in the seismic response by increasing the cell size horizontally. Scattering is

especially related to the cells in the gas front and at the gas-water contact. As this type of upscaling does not change the trend of the seismic response to injected gas, it is not as important as the vertical upscaling. However, an attempt should be made to make the cell size as small as possible. Average scattering error arrives at 10%, when the cell size is 25*25m. Therefore, it is proposed as the maximum horizontal cell size in the simulation model, whose aim is to accurately monitor gas injection.

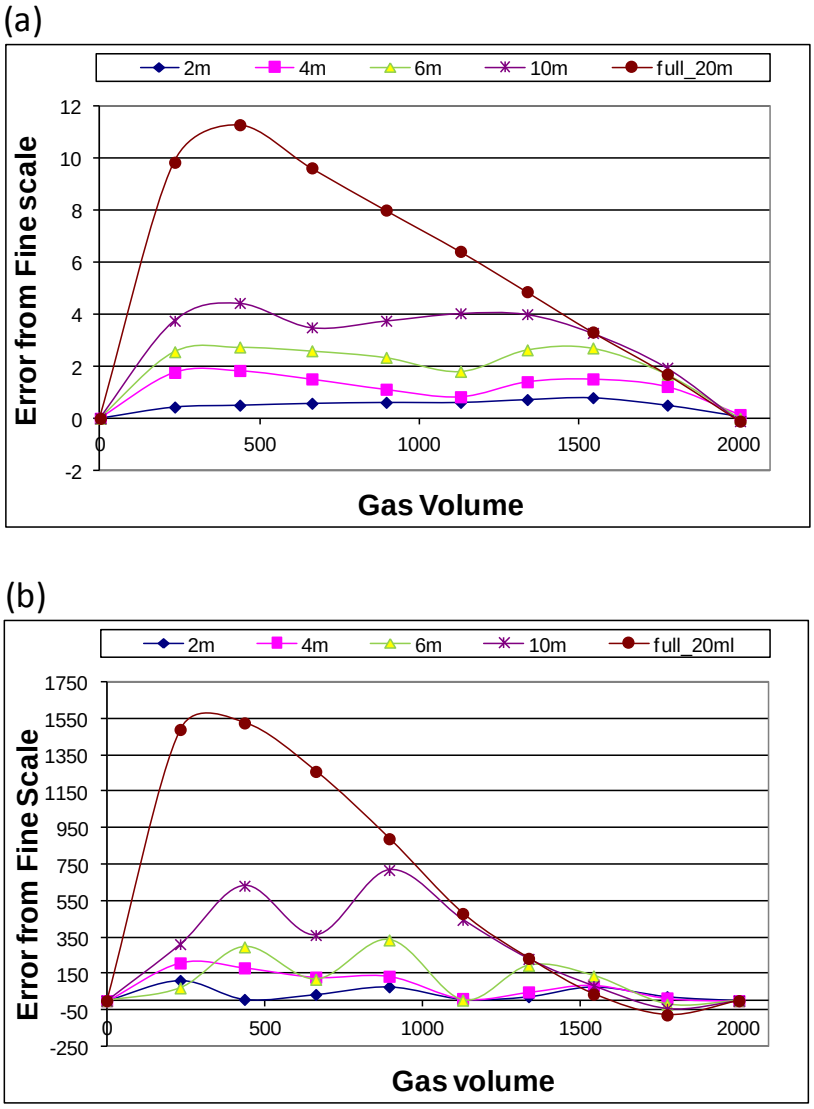

Figure 3.15 Error (deviation) of different models from the fine scale model for: a) timeshift and b) amplitude change versus gas volume for different cell thicknesses.

Cell Thickness	Average error (%) - timeshift	Average error (%) – amplitude change
2	9.50	6.08
4	27.88	14.89
6	44.30	16.21
10	66.87	36.62
20	153.22	112.92

Table 3.1 Average error referenced to the fine scale model for the timeshift and amplitude change, and for different cell thicknesses.

The above upscaling problem is more challenging in the seismic domain than in the engineering domain. The main purpose during history matching of the simulation model is the fluid flow. This flow is controlled by some changes in the simulation model such as vertical equilibrium switches, pseudo relative permeability and capillary pressure curves, and changing the transmissibility. These solutions fix the same saturation front in the upscaled model as the downscaled one, but the saturation variation is still there for the upscaled model. This variation is not an important issue for the engineers, but it prevents detection of the accurate seismic response. As another issue, the simulation model and seismic data are normally converted into 2D maps to be compared, and make some seismic interpretations and reservoir model updates. This situation is the same as the completely upscaled model, in which the total reservoir thickness is assumed as one cell. As the gas saturation variation is observed in these maps, geophysicists are encouraged to employ the laboratory extracted non-linear seismic response. Using the gas thickness or gas volume terms instead of gas saturation in the reservoir scale will solve this misunderstanding.

3.7 Summary

Investigation of seismic scale gas saturation distributions was performed in this chapter. Gas saturation is found to be approximately constant inside the gas volume (or thickness).

Thus, the main parameter that induces 4D seismic change is gas thickness. It was also observed that reservoir heterogeneity does not affect this conclusion significantly. Analytical and numerical modelling in the seismic domain for thin reservoirs (less than tuning thickness) highlights a linear seismic response to the injected gas thickness or volume for both timeshift and amplitude change attributes. However, for thick reservoirs amplitudes become non-linear. It is the architecture of the reservoir which decides the amplitude response. Because of the fact that the thick reservoirs are normally the combination of intra reservoir sand and shale, a linear amplitude response can therefore be expected in most reservoirs. We observe a deviation from the linear response with increasing simulation model cell size (especially the vertical dimension).

Chapter 4

Towards quantitative evaluation of gas injection using time-lapse seismic data

Of particular concern in the monitoring of gas injection for the purposes of storage, disposal or improved oil recovery is the exact spatial distribution of the gas volumes in the subsurface. In principle, this requirement is addressed by the use of 4D seismic data, although it is recognised that the seismic response still largely provides a qualitative estimate of moved subsurface fluids. Exact quantitative evaluation of fluid distributions and associated saturations remains a challenge to be solved. Here, an attempt has been made to produce mapped quantitative estimates of the gas volume injected into a clastic reservoir. Despite good results using three accurately repeated seismic surveys, time-delay and amplitude attributes reveal fine-scale differences though large-scale agreement in the estimated fluid movement. These differences indicate disparities in the nature of the two attributes themselves, which can be explained by several possible causes. Of most impact are the effects of processing and migration, wave interference effects and noise from non-repeatability of the seismic surveys. This subject highlights the need for a more careful consideration in 4D acquisition, amplitude processing and use of true amplitude preserving attributes in quantitative interpretation.

4.1 Description of dataset

An'Teallach is a turbidite reservoir to the west of Shetland, lying at 2km depth in the North Sea, into which methane is injected into water-bearing sands for disposal. It is on the south-west of the Schiehallion field and south east of Foinaven (Figure 4.1). In this project, the known well volume of the light immiscible gas (table 4.1) injected into a saline aquifer. This aquifer is a set of highly porous reservoir sands known to be reasonably homogeneous. This selected structure for the gas injection is a local high, which is confined by the channel boundary and the fault system.

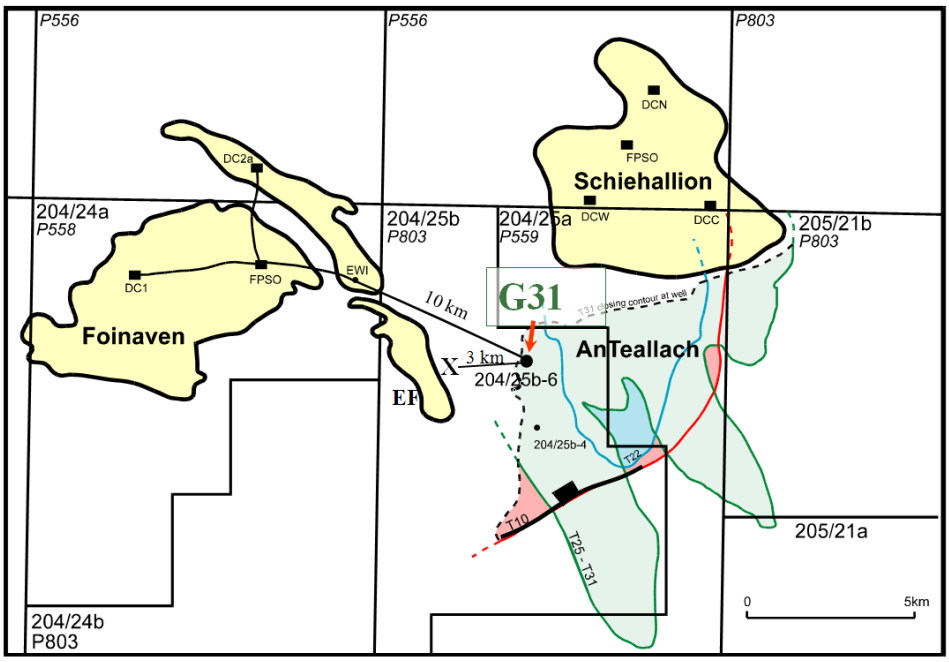

Figure 4.1 Location of the AnTeallach field to the west of Shetland, North Sea (BP internal report).

The multiple reservoir sands of the area sit within the Vaila Formation of the Paleocene Faroe Group. Previous detailed evaluation of well and seismic data by the operator of the field has allowed the group to be sub-divided into a number of sequences. It is these sandstone bodies that form the reservoir into which gas was injected. The sands are generally clean, fine to medium grained (Lamers and Carmichael, 1999 and Freeman *et al.*, 2008). The three main sands of interest are the T31-sst1, T31-sst2 and T28-sst1, and these are separated by a background of pelagic mudstones (Figure 4.2). The sands of T31-sst1 are

very thick bedded sandstones, with a high net-to-gross, whilst the other two sands show varying degrees of shale interbedding (Lamers and Carmichael, 1999). Inside the selected structure of interest to our study, each sand body remains hydraulically isolated although some cross-flow is thought to occur at fault locations. These sands are approximately parallel and are underlain by the base conglomerate, a key marker for seismic interpretation (see Figure 4.2). Well tie analysis shows not perfect correlation coefficient (65%) which can be because of the deviation of the well (Chopra and Marfurt, 2007).

Time frame

summary

----1993------	Base line 3D survey acquired
February 1998	Gas Injection start-up
August 1999	1st monitor 3D @ 19 months / 25 BCF
August 2000	2nd monitor 3D @ 31 months / 37 BCF
August 2002	3rd monitor 3D @ 55 months / 53 BCF

Table 4.1 Summary of the data set.

Data from a single injection well drilled into the area of interest is available. Injection started in 1998 and continued for the period of the seismic monitoring. The baseline seismic data was shot in 1993, and three seismic monitor surveys are acquired thereafter in 1999, 2000 and 2002, after 25, 37 and 53 billion cubic feet (BCF) of gas injection respectively (Table 4.1). Figures 4.2-a, b, c and d demonstrate the general seismic quality. The resultant time lapse responses have a high repeatability, defined by a low value for the normalised root mean square (NRMS) non-repeatability metric. Figure 4.3 illustrate the NRMS maps for the 600 millisecond above the reservoir for 1999-1993, 2000-1993 and 2002-1993 respectively. The average, mode and standard deviation of the NRMS maps are 0.23, 0.19 and 0.09 for 1999-1993, 0.25, 0.21 and 0.10 for 2000-1993, and 0.28, 0.24 and 0.11 for 2002-1993 respectively. Figure 4.3 highlights the bad repeatability for the central to the south-east and good repeatability range for the remainder of the area.

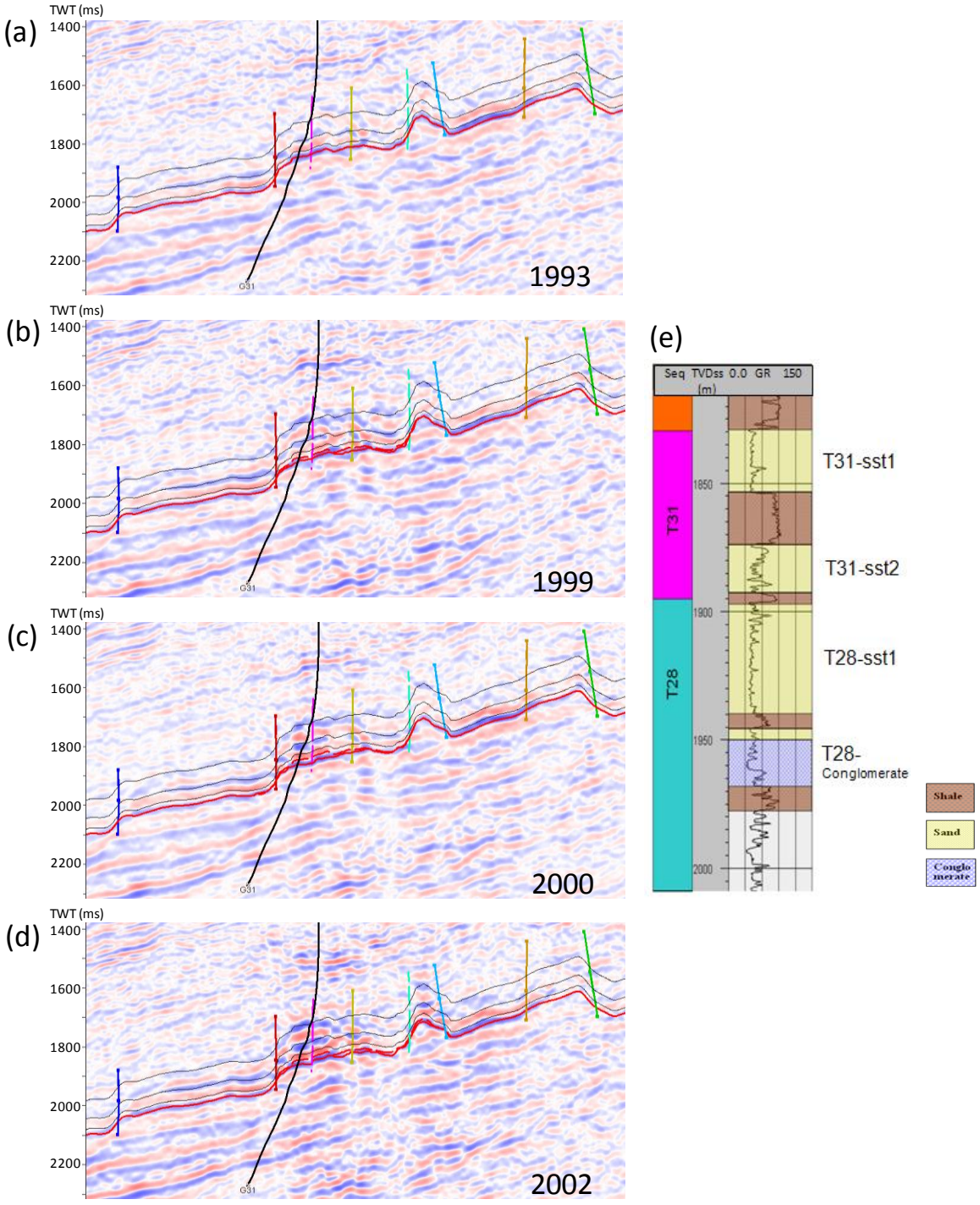

Figure 4.2 (a), (b), (c)and (d) NW (left) – SE (right) seismic sections for the area of interest, at the baseline in 1993 (before gas injection) with horizons and faults, at 1999 after one year, at 2000 after two years, at 2002 after four years of gas injection. The red horizon corresponds to the base conglomerate layer picked in the time-shift analysis. (e) gamma log and interpretation of the main T28-ss1, T31-sst1 and T31-ss2 sands of the reservoirs of interest.

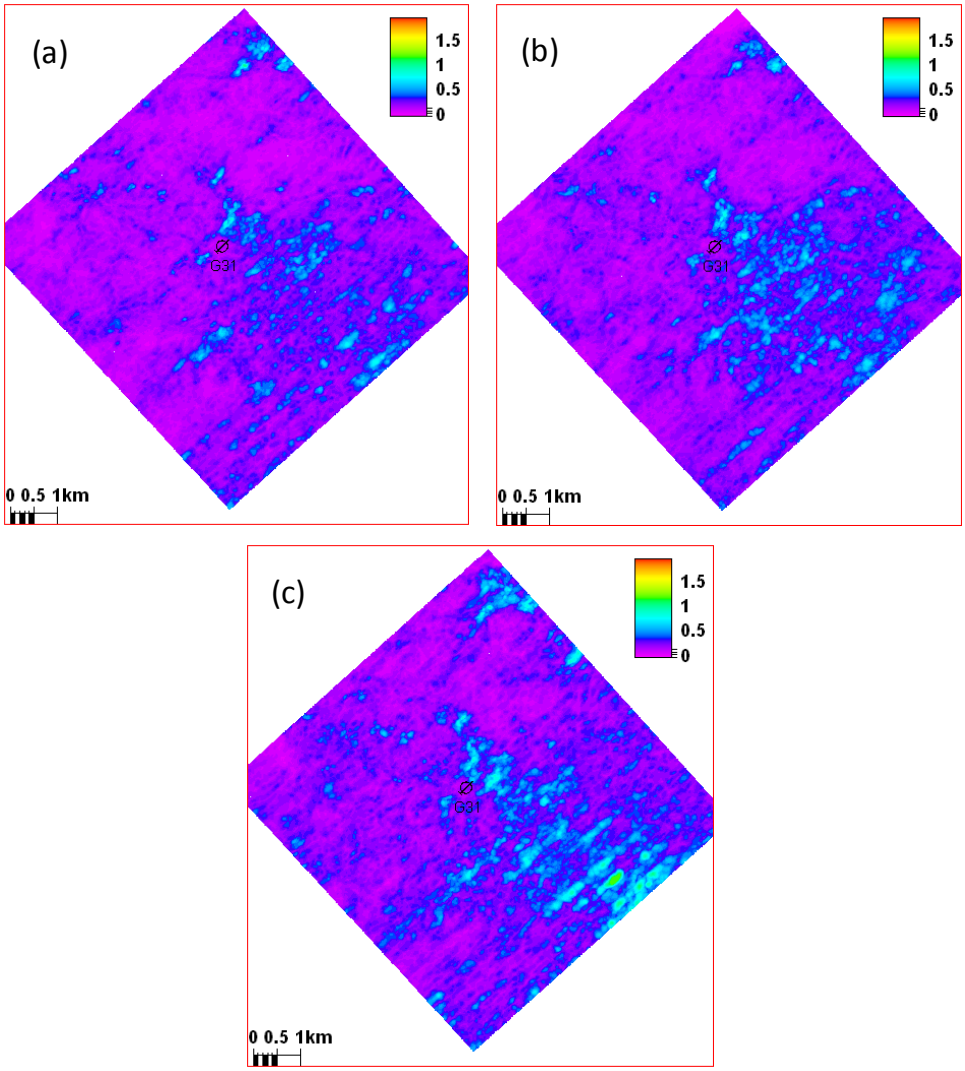

Figure 4.3 NRMS maps for the 600 millisecond window above the reservoir for (a) 1999-1993, (b) 2000-1993, and, (c) 2002-1993 respectively.

In the portion of the structure where the well is drilled, there lie the three distinct and fairly homogeneous (T31-sst1, T31-sst2 and T28-sst1) sands, into which the gas was injected (Figure 4.2-e)). Because of the need to maintain pressure, daily injection gradually decreased after 1999 and this ensured that the average reservoir pressure is held approximately constant during the acquisition of the monitor surveys. As each sand body is well connected both vertically and laterally, pressure equilibration is rapidly established, controlled by the bounding faults and channel edges, and the pressure at the well also reflects that of the field in general. Thus, the time-lapse changes visible between the 1999,

2000 and 2002 surveys are mainly due to gas volume or saturation increases. However, any seismic time-lapse changes taken relative to the baseline survey shot in 1993 also contain the start-up pressure effect. Because of the small contrast between sand and shale (in terms of the P-Impedance), the trough at the top of the reservoir is not sharp on the seismic (1993 in Figure 4.2). After gas injection, however, the density and velocity of the gas saturated rock is significantly smaller than the water saturated sand and shale. Therefore, injected sands are more obvious after gas injection (Figure 4.2-b, c and d). The red horizon that is representative of the base conglomerate shows timeshift by gas injection. This timeshift will be used for quantitative monitoring in the next stages.

The structure that was selected for the gas injection is shown on Figure (4.4-a). This horizon is the base conglomerate in time with the highlighted area around the well. This area is a local high which is suitable for gas injection due to the gas gravity effect. The study area is limited by the channel boundary from the east and west, and by faults in the north and south (Figure 4.4-b).

At the primary stage of gas injection (Figure 4.4-c) gas migrates towards the east and north east of the injection well. This is consistent with the gravity effect by including the reservoir geometry. At the next stage, gas arrives at the boundary of the channel towards the east side, so that gas thickness increases in that region. Gas, after that, migrates towards the south (Figure 4.4-d and e). The magnitude of the 4D seismic anomalies rises with increasing gas volume in the selected region. The area of the anomaly grows with time as well, and represents gas migration towards new areas of the field. The northern fault seems to be sealed, as there is no sign of gas leakage from this fault. The qualitative interpretation of the 4D seismic maps highlights the ability of the 4D seismic data to monitor injected gas. The increase of both magnitude and the area of the 4D seismic anomalies encourage developing a quantitative method for the measurement of the injected gas volume. The 3D gas body that was extracted from the 4D seismic energy attributes (Figure 4.4-f) is also used for better visualization of the injected gas.

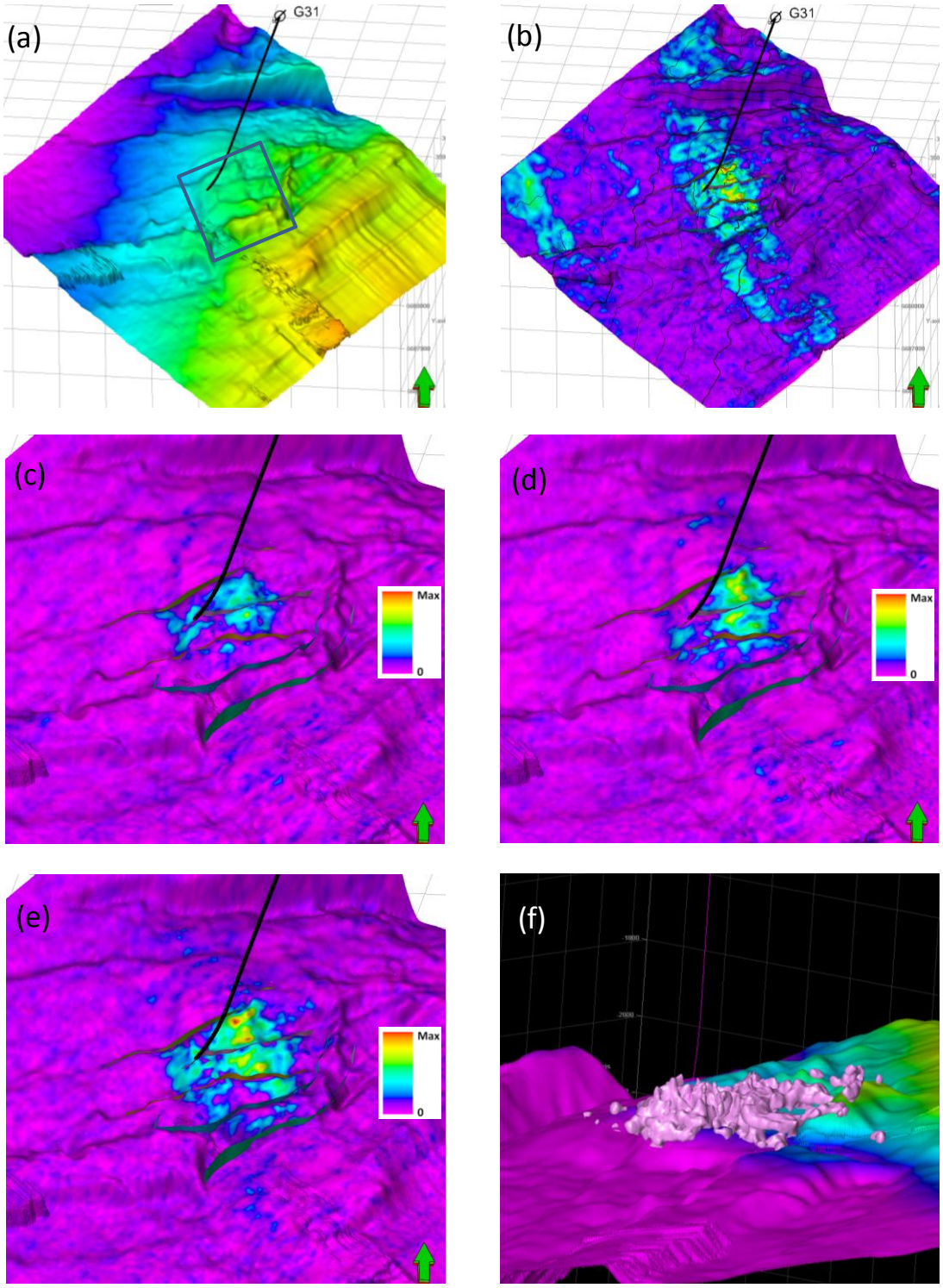

Figure 4.4 (a) Base conglomerate horizon in time, with highlighted structure for the gas injection, (b) RMS average for a window from top reservoir to the base at 2002 which clearly represents the channel boundary. (c), (d) and (e) are difference of the RMS maps for a window from top reservoir to the base at 1999, 2000 and 2002 with the base seismic (1993). These maps overlaid on the base reservoir for better visualization of the injected gas anomalies on the 4D seismic derived maps. (f) 3D body of the injected gas at 2002 extracted from the energy attributes of the 4D seismic data.

4.2 Volumetric analysis using time shift attributes

A stable reference reflector, which appears as a zero-phase trough on the seismic, is chosen for the analysis corresponding to the base of the conglomerate layer (see Figure 4.2). This reflector is below the reservoir and is chosen to avoid the effects of tuning influencing the results (as explained in Ghaderi and Landrø, 2009). The field operator provided an interpreted pick for this reflector, derived from the baseline seismic. The reflector is then manually re-picked on each of the monitors using the baseline interpretation as a guide. Subtraction of the resultant picks from the two surveys then gives the required time-shifts that can be mapped across the area of interest around the injection well.

Time-shifts of up to 26ms are observed, corresponding to a velocity slow-down in the reservoir, due to the presence of gas. During the picking procedure, only an occasional degradation of the signal is noticed (perhaps due to residual multiples or thinning of the layer), but this has little impact on the overall results. There is no obvious sign of a change of event character when extending beyond the reservoir zone. The data are well cross-equalized, as can be observed by the clean difference section in Figure 3.2-c, indicating that the influence of non-repeatability effects on these picking procedures is low. Indeed, analysis (described below) has shown that events picked above the reservoir on the baseline and monitor seismic vary only by a fraction of a millisecond.

Following the strategy of Huang *et al.* (2001), we threshold the resultant time-shift maps to allow us to define robust contiguous areas influenced by the changes in gas volume. The time-shift changes remaining after the thresholding procedure describe an area, $\sum$, of change on the map. For each cell within this area, the corresponding time-shift, Δt, is related to the change in the in situ gas volume ΔV_g sampled through the reservoir interval and within the cellular area $\Delta x \Delta y$ via

$$\Delta V_{gas} = \left\{ S_g . \phi . NTG . \frac{VV'}{2(V - V')} \right\} \Delta t(x, y) . \Delta x . \Delta y, \qquad (4.1)$$

where V *is* the seismic wave velocity with no gas and V' the seismic wave velocity in the

cell in the presence of the gas saturation S_g. ϕ and *NTG* are the sand porosity and net-to-gross respectively, and combine to give the effective porosity $\phi_{eff} = \phi.NTG$. S_g is a strong function of rock properties for flow, particularly the relative permeability curves.

By integrating (4.1) over $\sum$, an estimate of the total volume of injected gas for each seismic time-lapse period can be obtained. As the reservoirs are fairly homogeneous and their petrophysical properties are known to vary only slowly across $\sum$, then the spatial integral of S_g and ϕ_{eff} can be approximated by their average. This is justified, as inspection of the operator's simulation model shows that the net-to-gross distribution is very narrow across the area of interest, with a standard deviation of approximately 0.1. Numerical simulations have shown that the gas saturation for the reservoir is narrowly distributed, with a mean close to the maximum attainable value of $S_g^{\max}$ (see Chapter 3). These assumptions lead to a formula for the gas volume injected relative to the initial gas volume V_{gas}*(initial)*

$$V_{gas} = V_{gas}(initial) + \left\{ S_g \phi_{eff} \frac{VV'}{2(V - V')} \right\}^{mean} \iint_{\Sigma} \Delta t(x, y) dxdy, \qquad (4.2)$$

which predicts that the integration of the time-shift changes observed from the seismic data are directly proportional to the total volume of injected gas V_{gas} for a chosen survey time period.

One modification to this is required when time-shifts between the (pre-injection) baseline and any of the monitor surveys are being considered. This is because the total measured time-shift, Δt, in this case now includes a constant time-shift Δt_{pr} due to the effect of a pressure increase on the rock frame and fluids prior to 1999 but after 1998, such that $\Delta t = \Delta t_{gas} + \Delta t_{pr}$ and the time-shift due only to gas saturation Δt_{gas} is slightly masked. This effect essentially adds a positive constant, *a*, to Equation 4.1 as both increase in pressure and gas saturation soften the reservoir (this was also tested numerically using the simulation to seismic analysis (Sim2Seis)).

In practice, the combination of constant factors multiplying the integrand in Equation 4.2 and the pressure factor *a* are not known *in situ* with certainty, but can be estimated directly from the data, by calibrating the time-lapse seismic with the known well injection data. Thus, the three combinations of integrated time-shift from the 2002-2000, 2002-1999 and 2000-1999 signatures are cross-plotted against the injected volumes independently from the 2002-1993, 2000-1993 and 1999-1993 signatures (Figure 4.5-a). An initial common noise threshold of 0.5ms is used for the time-shift maps prior to integration, and this is refined upwards until the points in the cross-plot follow a straight line and both sets of points for the monitor-monitor and baseline-monitor combinations have identical gradients. This is

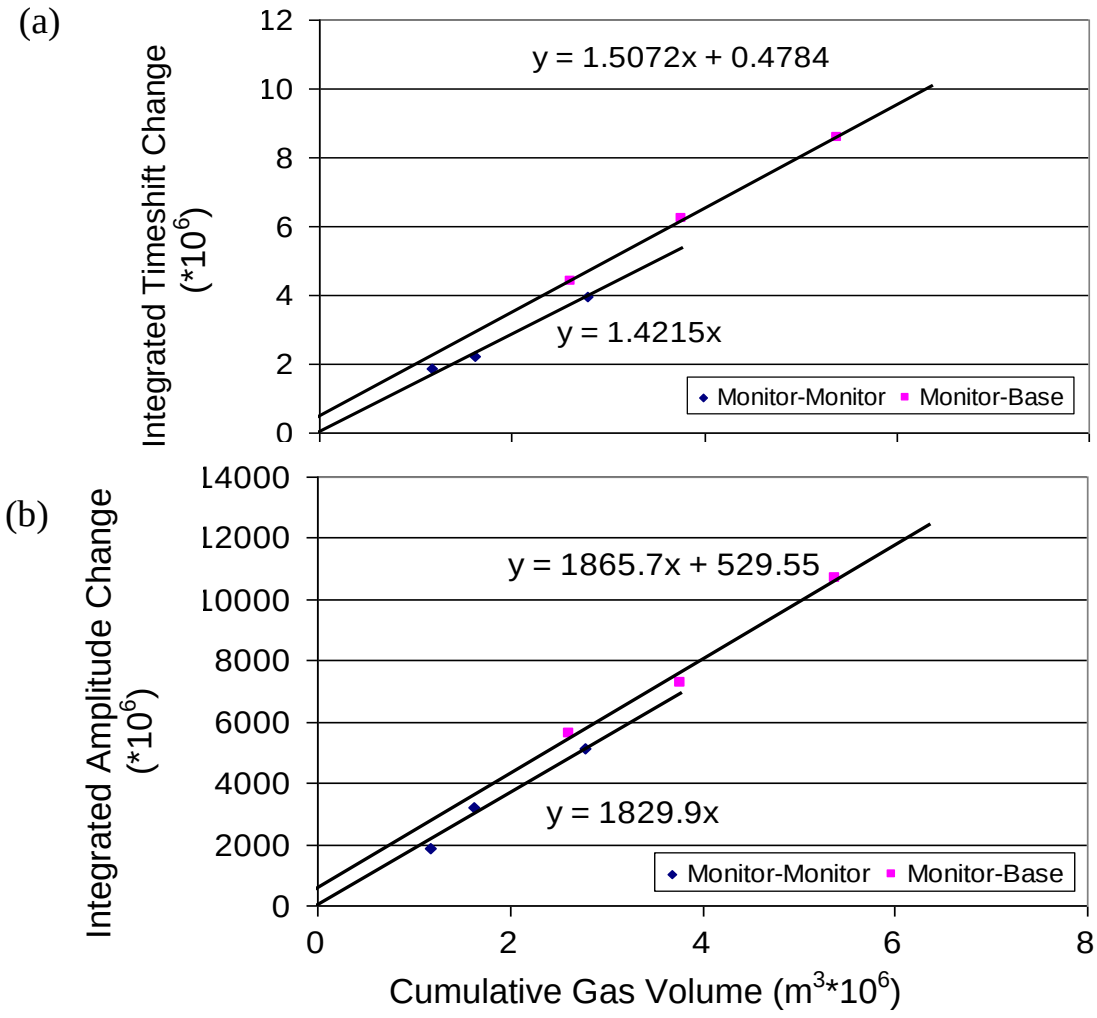

Figure 4.5 Total injected gas volume versus: (a) integrated time-shift; (b) integrated amplitude. Data points are for the differences formed by the baseline-monitor combinations 1999-1993, 2000-1993, and 2002-1993; and the monitor-monitor combinations 2000-1999, 2002-2000, 2002-1999.

achieved by finding the maximum of an objective function that optimizes the fit of the points to each line and the degree to which both resultant lines are parallel. Based on this function, the optimal threshold can be determined that is accurate to within 5%.

It is observed that the points involving the baseline survey display an offset corresponding to the pressure effect anticipated above, whilst the points generated between monitor surveys lie on a straight line which passes very close to the origin (there is no condition to intersect the origin in our technique). The offset due to the pressure effect contributes on average 19% (or 4ms) to the total time-shift (for a 1000psi pressure increase). The common gradient of the lines now gives us an estimate of the calibration coefficient (the factor in the curly brackets multiplying Δt in Equation 4.1 and the integrand in Equation 4.2) that can be applied to the time-shift $\Delta t(x,y)$ at each location and to the baseline-monitor attribute maps to convert them into a gas volume variation $V_{gas}(x,y)$ with appropriate correction for the pressure effect. As a quality control check, it is found that an estimate of the calibration factor using approximate values from the field match the final derived value quite well. The gas volume distribution predicted in this way for the 2002 survey is shown in Figure 4.6-a.

4.3 Volumetric analysis using amplitude attributes

A similar relation to Equation 4.1 is also possible for amplitude attributes. Each reservoir sand is below tuning thickness, as the thickness of the individual sands is between 20 and 39m (from log interpretation), compared with the seismic wavelength at the reservoir level of 185 meters. The gas thickness, h, can be written in terms of the seismic amplitude. Here, assuming that the reservoir is thin relative to the seismic wavelength ($\lambda/H >>1$), then the underlying mathematics from tuning analysis may be used. This leads to an expression relating gas thickness h to the time-lapsed root mean square amplitude change $\Delta A = A_{MON} - A_{BL}$ (see Chapter 3 for detail):

$$\Delta A = h_g \left(\frac{Z_{sh} - Z_g}{\overline{ZV}'} - \frac{Z_{sh} - Z_w}{\overline{ZV}} \right) S'_{RMS} \qquad (4.3)$$

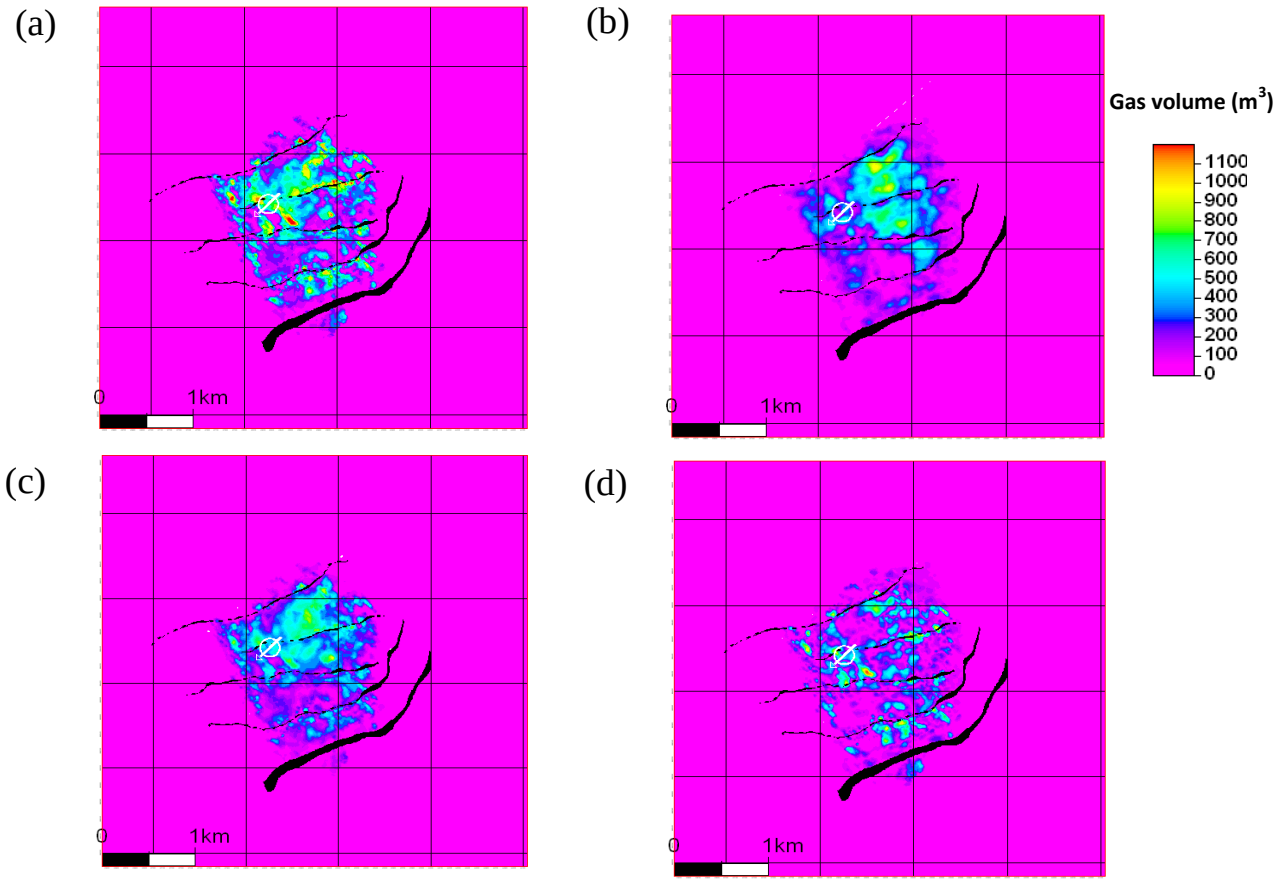

Figure 4.6 Gas volume maps (in m^3 for each cell) for the period up to July 2002, estimated from: (a) time shift attributes; (b) amplitude attributes. (c) the average estimated gas volume map; and (d) the difference of the maps in (a) and (b).

in terms of the shale impedance Z_{sh}, water-saturated sand impedance Z_w, gas-saturated sand impedance Z_g, average impedance $\overline{Z}$, and the root mean square amplitude S_{RMS} of the time-derivative of the wavelet *s(t).* Equation 4.3 can now be used to replace *h* in the gas volume definition by the observed amplitude change. Thus, their time-lapsed seismic root mean square amplitude is directly proportional to the thickness of the gas accumulated between surveys. Here, the difference of the root mean square amplitudes is chosen as it significantly reduces intra-reservoir time-shift effects. The amplitude equivalent of Equation 4.1 is

$$\Delta V_{gas} = \left\{ S_g . \phi_{eff} \cdot \frac{VV' \overline{Z}}{V(Z_{sh} - Z_g) - V'(Z_{sh} - Z_w)} \right\} \Delta A(x, y). \Delta x. \Delta y, \qquad (4.4)$$

where *c* is a constant of proportionality that converts tuned amplitude to time-thickness, and is a function of impedances in the sand and shale, and the fixed velocities *V* and *V'* (see also Chapter 3).

The *in situ* volume of gas injected can now be calculated in a similar manner to those from the time-shifts, and the term in the curly brackets in Equation 4.4 estimated empirically using the cross-plots. In practice, a root mean square amplitude average is selected in a window between top and base of the reservoir interval. Given the small amplitudes involved, this is approximately equal to the sum of the individual root mean square amplitudes for each reservoir sand, and hence the summation of the gas accumulation thicknesses. Furthermore, assuming (as before) that the pressure effect on the amplitudes is linearly additive, pressure can be treated using an identical workflow to the time-shifts.

The amplitude threshold is initially set at 5% of the maximum, and then adjusted upwards as before until the points in the cross-plot follow a linear trend (Falahat et al., 2011). In this process the lower limit amplitude threshold is required to avoid introducing the spatially broad background noise level. The final cross-plot results are shown in Figure 4.5-b, which also reveal the anticipated small vertical offset due to the pressure effect on the time-lapse signatures, contributing in this case to 13% of the total amplitude. After determining the corresponding calibration coefficient linking V_{gas} to ΔA in a similar manner to the previous section, the resultant gas volume derived from the amplitude for 2002 can now be mapped in Figure 4.6-b.

Comparing the gas volume maps of Figures 4.6-a and 4.6-b, together with their corresponding average and difference, the time-shift and amplitude attributes are observed to yield different results. Indeed, differences between amplitude and time-delay based interpretations are expected and are commonly observed (Figure 4.7). For example Meadows (2008) shows significantly different maps for CO_2 injection into a clastic reservoir, and Ng *et al.* (2005) show major differences in maps for the injection of a miscible gas and solvent into a carbonate reservoir, but conclude that the time-delays appear to agree more clearly with their well activity. Finally, Mehdizadeh *et al.* (2010) found different amplitude and time-shift maps in seismic monitoring of an in-situ

combustion process in heavy oil. They concluded that the time-shift map was noisy relative to the amplitude.

In our example, the two maps do appear to be reasonably close but there are still regions of disparity. For example, there is a region of no gas change in the southern part of the amplitude map which is not present in the timeshift map. Also, in general, the amplitude map possesses lower spatial frequencies. Around the well, gas volume anomalies are shifted towards the east and north east in the amplitude map relative to the time-shift map. Both maps possess roughly the same geometric outline consistent with the flow simulation predictions (see the next section). The results also show an excellent correlation with the known fault system and the edges of the channel to the west and east. Whilst the signals appear to terminate at the fault to the north, there is, however, a gap between the southernmost edge of the gas volume and the southern fault. The latter observation can be explained using the simulation model as a combination of structural and gravitational effects. Gas is accumulated in a local high in this area. However, it is the fine-scale details between the time-shift and amplitude maps that differ greatest, with a general mismatch of many of the local high and low gas concentrations. As the calibrations using the well injectivity data and material balance as described above are found to be excellent, the differences between maps must be due to the inherent nature of the attributes themselves. These differences are discussed further in the next section.

4.4 The possible reasons for a disparity between timeshift-derived and amplitude-derived gas volume maps

There are a number of reasons why the estimates of gas volumes derived from the amplitude and time-shift maps do not match exactly. These attributes are different average measures of the gas saturated reservoir sands, and the variation cannot be simply related to errors in the picking of the time-shifts or in evaluating the amplitudes. Some possibilities are:

(a) the amplitudes respond to local changes in density and velocity, whereas the time-delays respond only to a depth-averaged velocity. If density and velocity are uncorrelated, then there will be differences in the attributes;

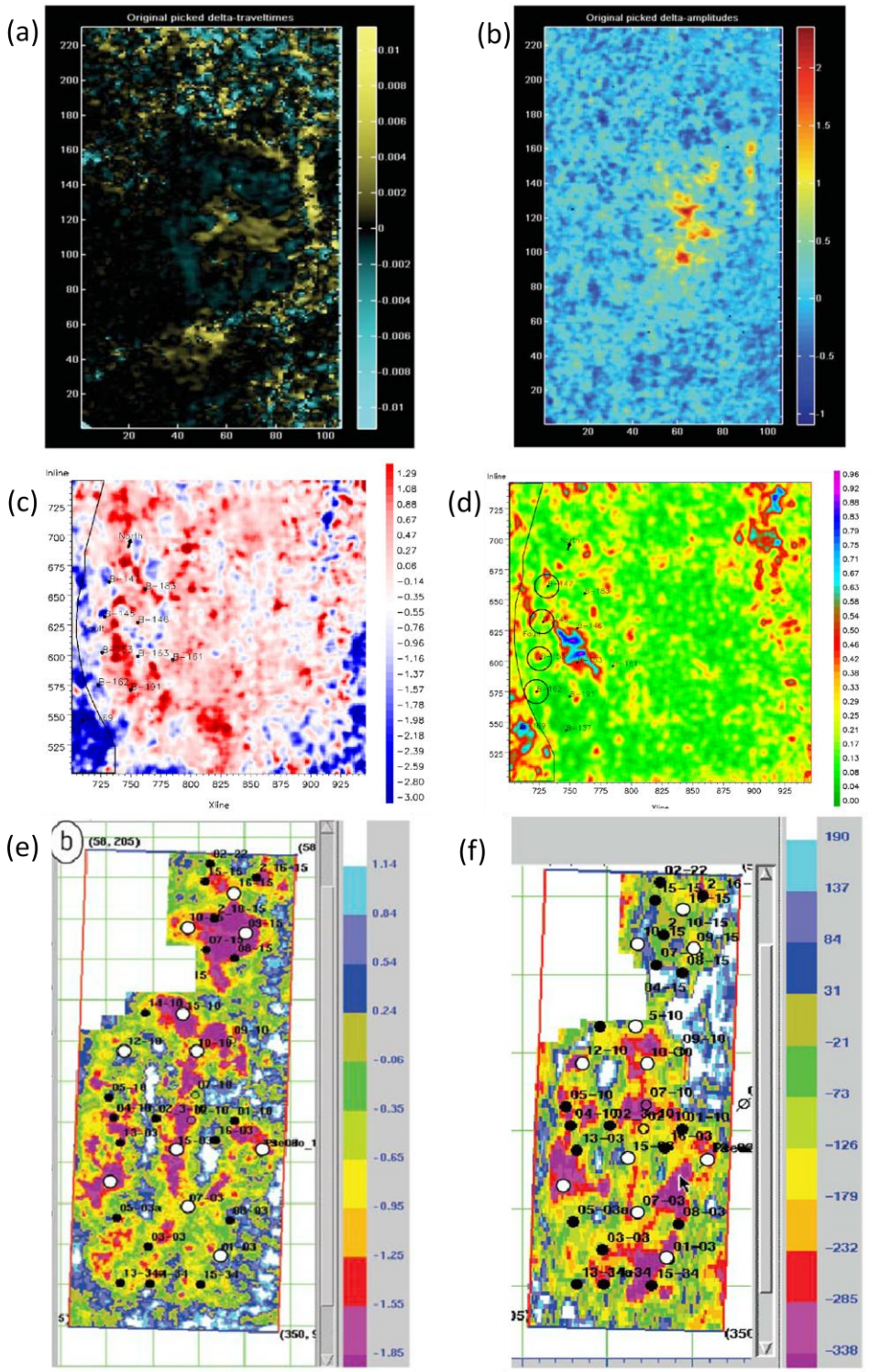

Figure 4.7 (a) Travel time difference and (b) amplitude change for the sand wedge extracted from the 1994 and 2001 near-offset Sleipner image cubes (Meadow, 2008). (c) Map of average timeshift inside the reservoir and (d) Map of RMS difference for the reservoir level (80 ms time window) (Mehdizadeh *et al.*, 2010). (e) Time-delay map and (f) impedance between 1987 and 2002 (arithmetic mean). The injection wells are shown in white (Ng *et al.*, 2005).

(b) the amplitudes may be affected by variable thin bed tuning effects;
(c) lateral variations in the phase or frequency of the seismic wavelet;
(d) errors arise due to acquisition (and processing) non-repeatability which superimpose the uncertainty already present in the evaluation of the amplitude and time shifts;
(e) the seismic amplitudes are sensitive to the choices made during processing such as the choice of a particular velocity model or migration algorithm. These possibilities are discussed in more depth below.

To aid in the understanding of the origin of the differences between the attributes, a simulation model is built from which seismic data are modelled, amplitudes and time-delays extracted and gas volumes estimated as in the previous section. The simulation model for the area of interest is built based on the petrophysical and geological characteristics of a larger model provided by the operator of the field. The field model is, however, too coarse for our studies as it was intended to cover a larger area, so a finer scale model is required. The base conglomerate (see Figure 4.2), a key event on the seismic, is picked, converted to depth and displaced upwards by 30m to provide the base of the reservoir lowermost reservoir sand. (The conglomerate layer is included later in the seismic modelling, but not in the simulation model). As the other seismic data picks are unclear, the additional layers of the model are developed by extrapolating the well picks for the top and base of each sand layer. Five faults are also identified from the seismic interpretation and added to model. The overall size of the final model is 2900x2400x143m, with a cell size of 25x25x2m. Properties are distributed in the model according to those extracted from the coarse-scale field model. This uses knowledge that the porosity in the sands is fairly uniform both horizontally and vertically. Permeability ranges from 225 to 600md, and it is constant laterally across each sand, but varies from sand body to sand body. Net to gross follows the channelised system established in the original model. Finally, the PVT (pressure-volume-temperature behaviour) tables and relative permeability data from the original model are used. The final resultant predictions of gas saturation from this simulation model are shown in Figure 4.8.

(a) To investigate the first possible explanation for the mismatch of amplitude and time-shift attributes, P-wave impedance (I_P) is plotted against velocity (V_P) from the wireline

logs (using the density and sonic logs) (Figure 4.9). Separate cross-plots are made for each individual shale and sand layer. For these data, a small, 1 to 2%, fluctuation about a linear trend line is noted. As it is likely that the lateral variability in subsurface properties is smaller than the vertical variability, then this result indicates that lack of correlation between I_P and V_P is an insufficient reason for the observed differences between attributes.

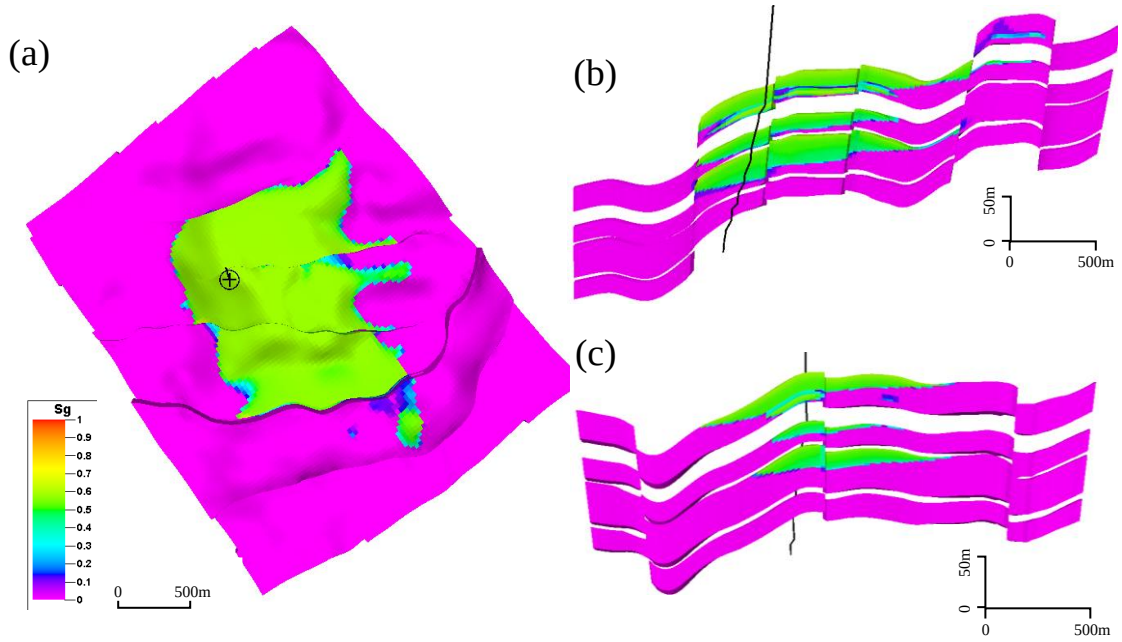

Figure 4.8 (a) Gas saturation for upper layer predicted from the flow simulation model for July 2002. Model section is shown corresponding to (b) the NW(left) – SE(right) seismic sections in Figure 4.2 and (c) perpendicular to the seismic section. Well locations and vertical trajectories are marked for reference.

To check that this point remains valid for the gas saturated sands, the water saturated log values are adjusted by Gassmann fluid substitution (Mavko *et al.*, 2003) to represent those for the gas saturated case. Note that the injected gas volume fills the sands and settles quickly into a saturation state governed approximately by the maximum gas saturation $S_g = 1\text{-}S_{wir}$ (see Chapter 3) between seismic surveys. Figure 4.10 shows the resultant cross-plots after gas saturation and that a predominantly linear correlation between I_P and V_P remains, despite the range in I_P - V_P space covered by the data (on average a coefficient of variation

for I_P and V_P from 12% to 26%). Varying the gas saturation by 10% either side of the mean does not affect this result.

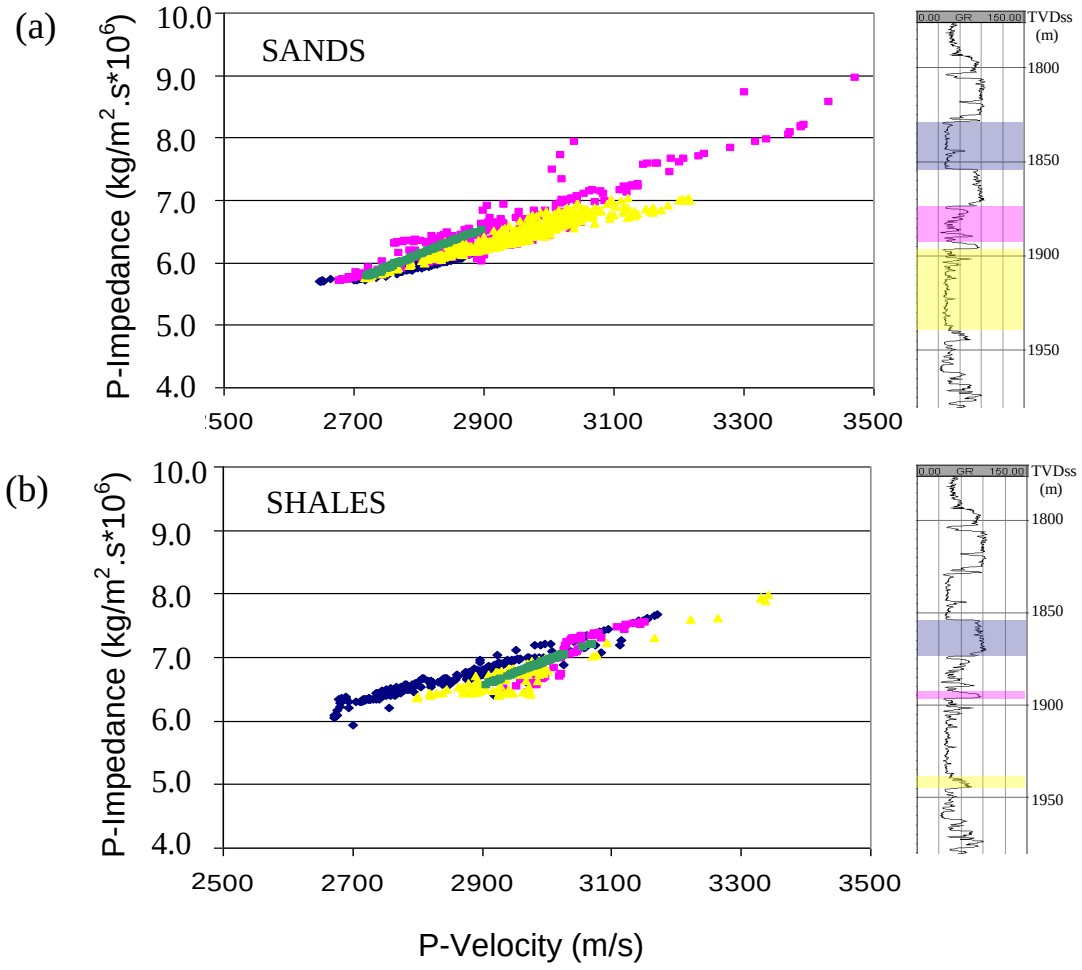

Figure 4.9 P-wave impedance against P-wave velocity from well-log data for (a) reservoir sands; (b) shales. Different sand and shale layers are colour coded (blue, red and yellow) on the well log (right) and cross plots (left) to separately present each sand and shale body. Green points indicate properties of the sands and shales respectively used in our simulator to seismic modelling, showing their degree of calibration with the well data.

(b) Another possibility for consideration is that the root mean square amplitudes are influenced by constructive or destructive wave interference effects, and the time-delays are not. To examine this, synthetic seismic are modelled directly from the simulation model; the root mean square amplitudes and time-shifts are then calculated and the gas volume estimates obtained in a similar manner to the observed data. An essential component of this modelling involves using the I_P-V_P cross-plot to calibrate the rock matrix values (bulk

modulus and density) for the simulator-to-seismic calculations. These values are adjusted until there is a match between the log values and those obtained from each cell of the simulation model (as shown in Figure 4.9).

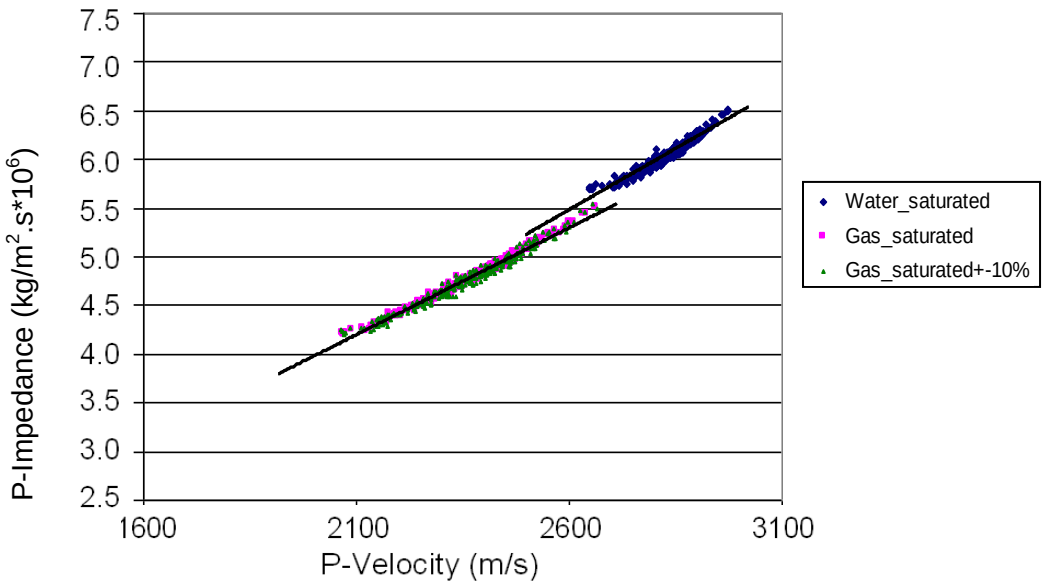

Figure 4.10 P-wave impedance plotted against P-wave velocity for the upper T31 sand. Water saturated points (blue points) shift to red points by changing from water to gas. Green points –gas saturation is varied randomly by 10% from 1-S_{wir}.

Pressure and saturation changes are calculated using flow simulation, and then convolutional modelling applied to generate the synthetic traces, using a wavelet derived from the observed data. Next, the traces are subjected to the same cross-plot volumetric analysis as that carried out on the observed data in the previous section. The results of this procedure are shown in Figure 4.11, and indicate several differences between the estimated spatial distributions across the area of interest.

It appears that amplitude estimates are reduced relative to those from the time-shifts due to intra-reservoir wave interferences. For example, in the southern part of the reservoir there is a reduction in amplitude due to a gas volume concentration, which is completely contradictory to what is expected. Inspection of this region indicates that this is a zone of gas lying below a shale barrier which prevents upward movement into the top of the

structure. Here, time-shifts are more reliable as destructive interference results from the particular thicknesses of these layers.

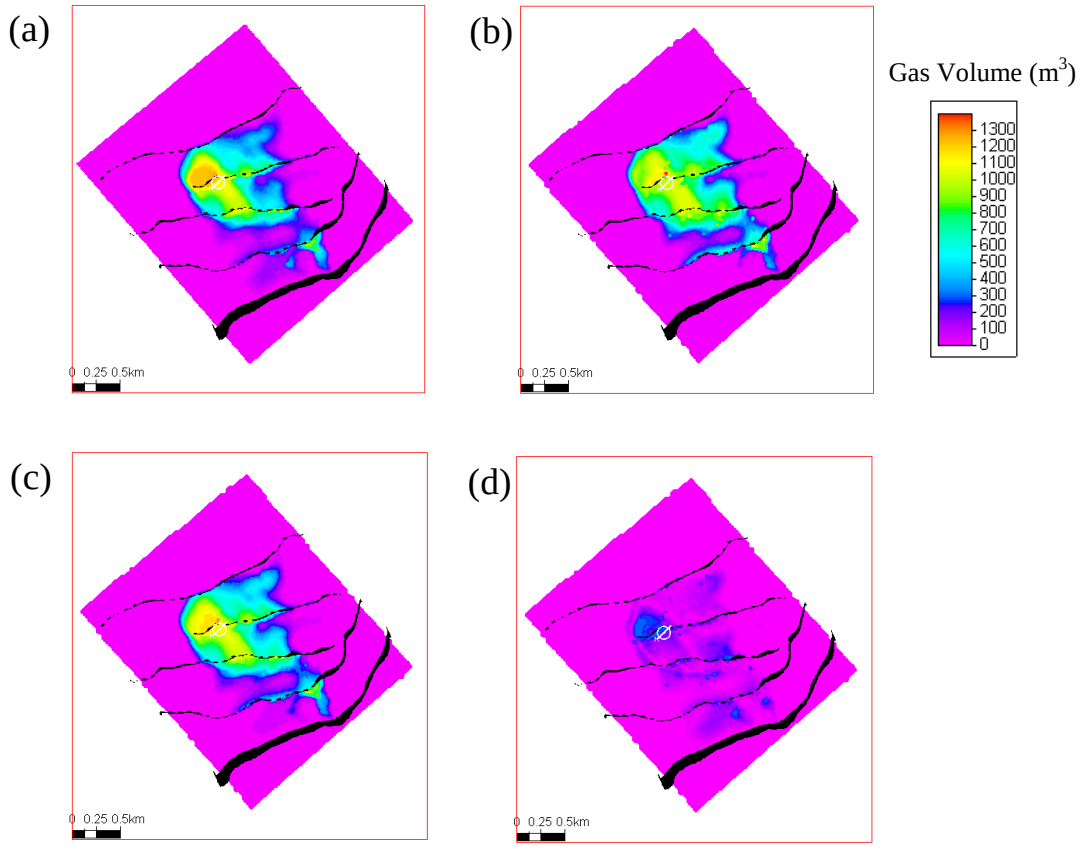

Figure 4.11 Gas volume maps (in m^3) for the period up to July 2002, estimated from: (a) synthetic time shift attributes, (b) synthetic root mean square amplitude attributes. (c) The average estimated gas volume map; and (d) differences of the maps.

Additionally, it is observed that there is a correlation between the thickness of the gas-water transition zone and departures of the amplitude from that expected from our modelling in Chapter 3. This is probably due to the larger variability of gas saturation values in this zone creating a more non-linear seismic response. It is anticipated that, in practice, variations might also arise in the observed data due to reservoir thickness. Furthermore, our convolutional modelling does not capture the effects of intra-bed multiples or that of wave conversions. Acquisition offset range variability has also been tested in the modelling, and

it is observed that the reservoir does not show strong amplitude variations with offset and that the estimates closely resemble the normal incidence results.

(c) Lateral changes in the seismic wavelet across a survey, and also between seismic surveys, are other probable reasons for the gas volume differences. These may arise due to a variety of processing- or acquisition-related causes.

To investigate wavelet effects, we pick and window a second reference horizon at approximately 700ms above the reservoir. Timing, phase and amplitude differences of this event are analysed between the baseline and monitor surveys. Time-shift variations between vintages are observed to be on average 0.05ms, with a standard deviation of 1.47ms. The mean phase rotation between surveys is -0.8 degrees, with a standard deviation of 15 degrees. The final measure is a cross-correlation coefficient taken between wavelets evaluated in a 300ms window, and across the entire survey area, giving a value of 0.93. This analysis confirms that the different vintages of data are well cross-equalised and inter-survey differences (in, for example, statics) should not contribute significantly to the observed disparity in the volume estimates. Further to this study, the seismic wavelet used to generate the synthetic data is varied by ±10 degrees in phase and ±5Hz in frequency. This simulates changes that may arise due to processing and acquisition. Such variations are found to shift the resultant pattern of volume estimates slightly, and the effects are not large enough to cause the major discrepancies that are apparent between the observed amplitude and time-shifts.

(d) Another reason for differences in the gas volume maps could be the presence of seismic noise or non-repeatability noise in the 4D data. Time-lapse seismic attributes are particularly susceptible to non-repeatability of the acquisition geometry when in the presence of overburden heterogeneity (Domes, 2010). To consider this, we map non-repeatable noise from the 4D seismic by calculating the normalised root mean square amplitude of the difference data for a range of window sizes above the reservoir and away from the reservoir pressure and saturation changes. These windows are from 400 to 600ms, 600 to 800ms, 800 to 1000ms, and 400 to 1000ms in size (see Figure 4.12). Interestingly, the various maps show a consistent pattern of high level (> 60%), low spatial frequency noise to the north-east and east, and a smaller noise level elsewhere.

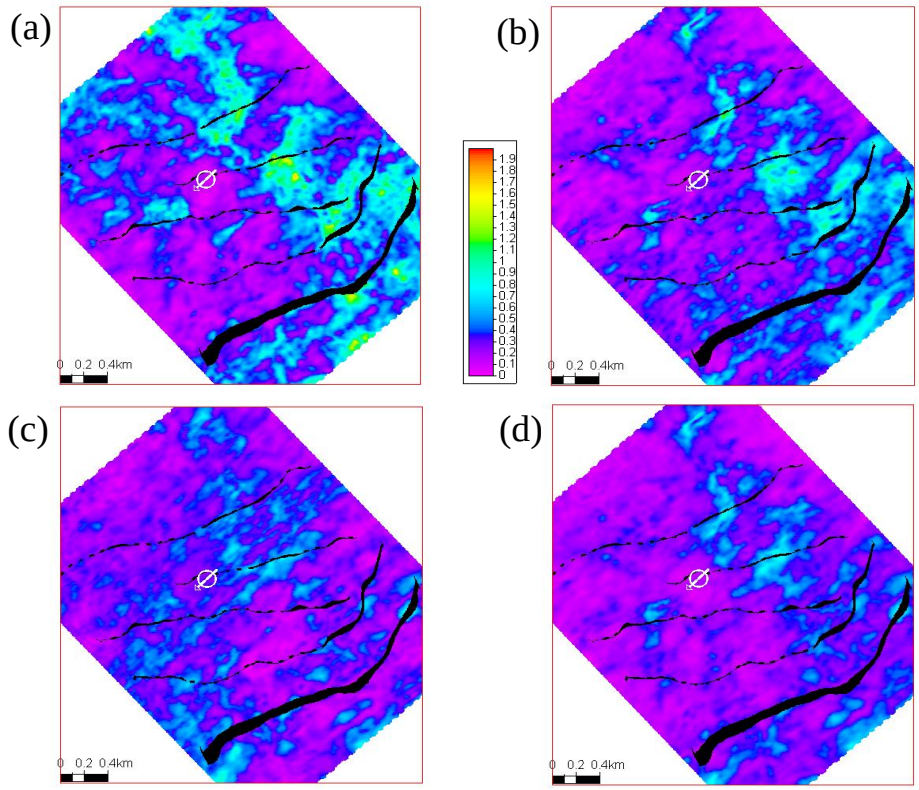

Figure 4.12 Normalised root mean square amplitude maps for a window (a) 400 to 600 ms; (b) 600 to 800 ms; (c) 800 to 1000ms; and (d) 400 to 1000ms in size above the reservoir. These maps assess the impact of acquisition non-repeatability of the seismic.

The noise map for the 400 to 1000ms and 400 to 600ms windows (Figure 4.12-d and a) are chosen for our analysis as those could be the statistical measure of the noise in different aspects. This is now rescaled to the average amplitude of the synthetic traces, and then added to the synthetic amplitude map to simulate an observed dataset (Figure 4.13). Comparison of the noise contaminated synthetics with the observations indicates some similarities in general character, particularly with the repositioning of the major anomalies. Overall, the noisy synthetic amplitude maps compare well in character with those obtained from the observed data. It appears therefore that this non-repeatability noise could be a major contributor to the mismatch.

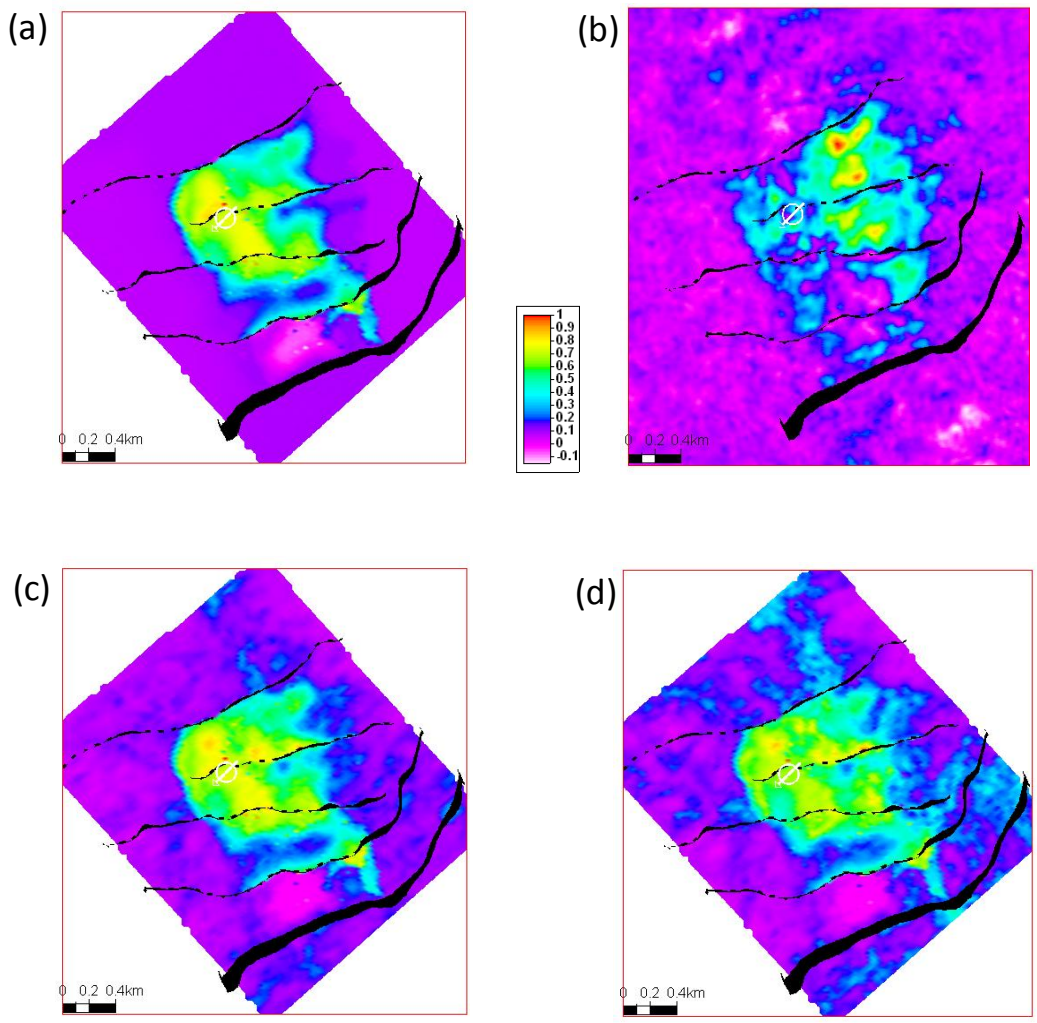

Figure 4.13 Root mean square amplitude maps of the difference volume at top reservoir for: (a) synthetic seismic, (b) observed seismic, (c) and (d) synthetic seismic with noise from a window 400 to 1000ms and 400 to 600ms above the reservoir respectively.

To investigate the impact of time-shifts, the time-shifts previously analysed for the second shallow reference event at 700ms are normalised and then added to the time-shifts from the synthetic data (the same procedure as for the amplitudes) (Figure 4.14). It is observed that this creates a low level, high spatial frequency noise, but in this case noise has very little impact on the time-shift maps.

(e) The final reason for the observed mismatch is seismic processing. Whilst the processing noise due to non-repeatability of acquisition and processing algorithms throughout the -

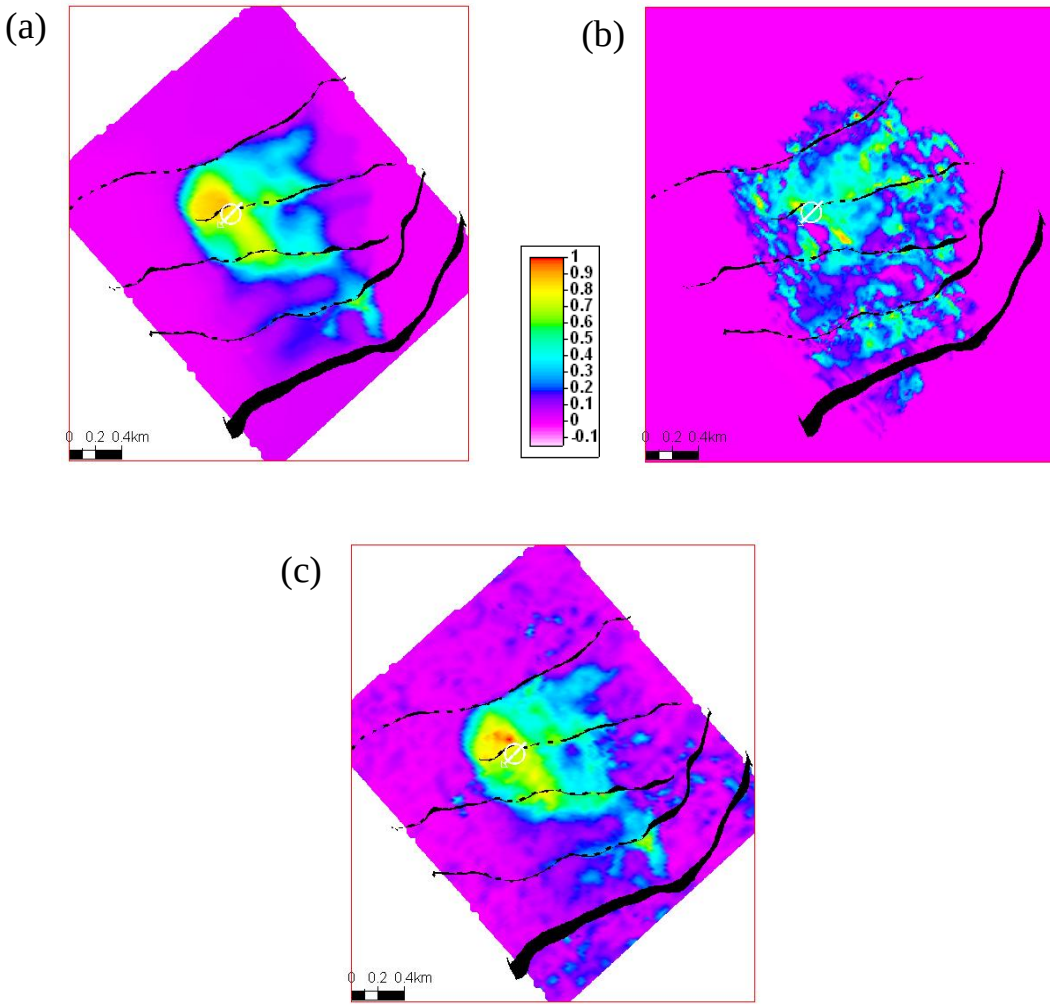

Figure 4.14 Time-shift maps from (a) synthetic seismic, (b) observed seismic, (c) synthetic seismic with noise from a horizon at approximately 700ms above the reservoir added. The scale bar is adjusted so that a comparison with Figure 4.13 can be made.

workflow may add to the overall 4D noise levels, seismic amplitudes in general are affected by the choice of velocity model and migration algorithm (Kvalheim *et al.*, 2007). Amplitudes may shift laterally or vertically depending upon the velocity model and underlying structural dips. The choice of migration combined with the heterogeneities in the velocity model can alter the spatial frequency content, continuity and smoothness of the amplitude maps (Figure 4.15). Inspection of the maps in Figure 4.6 and the south-east dip of the structure in the area of interest, suggests structure as a possible cause of movement in the main amplitude changes.

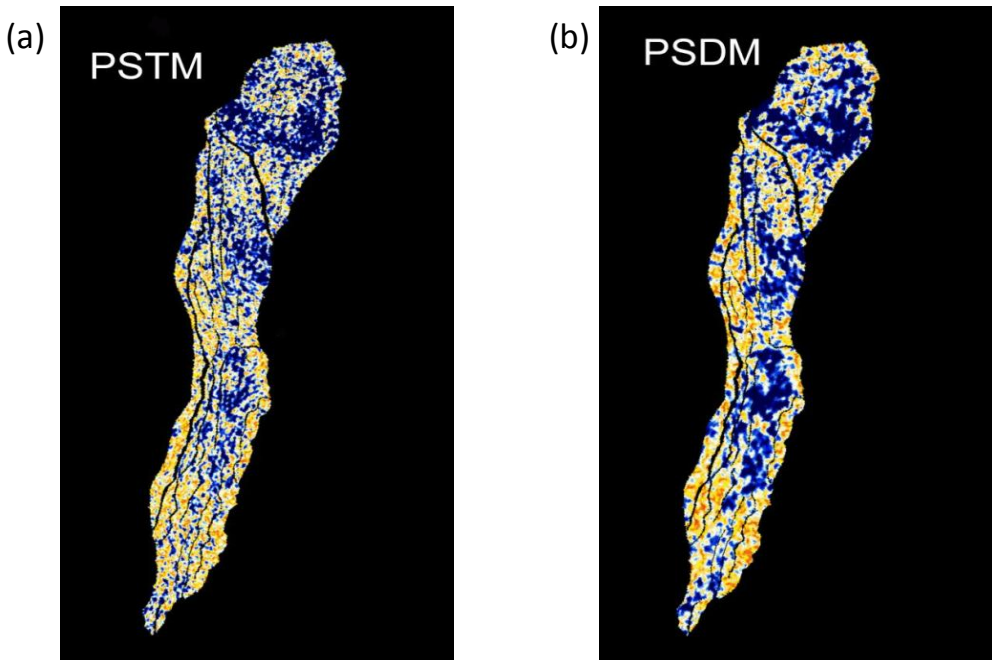

Figure 4.15 The attribute maps show the remaining oil column in the Statfjord Formation (Brage oil field) and are taken from the initial (a) PSTM and (b) PSDM processing (Kvalheim *et al.*, 2007).

In additional, Domes (2010) indicates that overburden heterogeneity may also have some considerable influence on the 4D seismic amplitudes and should be taken into account, although insufficient information is available on the overburden characterisation to assess this further. However it is clear that overburden heterogeneity such as channels, faults, or velocity changes due to geomechanical activity can have a significant effect on the amplitudes and time-shifts. The impact of these effects is not easily predictable from 4D seismic repeatability metrics and, ideally, should be taken into account in the velocity model when using a full pre-stack depth migration (Domes, 2010).

4.5 Summary

A surprising result of the flow simulation component of our study is that the saturation values for injected methane occupy a fairly narrow range. As a consequence, there is a direct linear relationship between the injected gas volume and both seismic amplitude differences and time-shifts of the reflector below the reservoir. Indeed, analysis of field

data confirms that this relation is very accurate in practice, yields good quality volumetric gas distribution maps, and also allows easy separation of pressure effects. The technique which is introduced in this chapter is applied to both timeshift and amplitude change attributes. The seismic scale calibration coefficients are obtained by the proposed volumetric method, which calculates gas volume maps using the 4D seismic attributes. In our example, the two maps do appear to be reasonably close, but there are still regions of disparity. In general, the amplitude map possesses lower spatial frequencies. Around the well, gas volume anomalies are shifted towards the east and north east in the amplitude map relative to the time-shift map. Both maps possess roughly the same geometric outline, consistent with the flow simulation predictions. The results also show an excellent correlation with the known fault system and the edges of the channel to the west and east. However, it is the fine-scale details between the time-shift and amplitude maps that differ greatest, with a general mismatch of many of the local high and low gas concentrations. As the calibrations using the well injectivity data and material balance are found to be excellent, the differences between maps must be due to the inherent nature of the attributes themselves. Synthetic data based on the reservoir model and further analysis of the observed data have been able to replicate some of these differences and identify them as due to inter-layer wave interferences and 4D noise; however there are still some remaining variations that cannot be adequately explained. An examination of previous studies on this topic points to inaccurate choices made during the processing and migration of the seismic product as a possible explanation. As a disparity between the results of amplitude and time-shift attributes has also been seen elsewhere by other researchers, there is a need to carefully evaluate the impact of decisions made during acquisition and processing on quantitative interpretation of 4D seismic, particularly when used for reservoir engineering purposes.

Chapter 5

Gas exsolution and dissolution - basic concepts and seismic response

Mechanism of gas liberation by pressure drop and its effect on the seismic properties are investigated in this chapter. The basic concepts of the gas exsolution and dissolution are reviewed using the literature, and are modelled with different synthetic simulation models. The aim is to understand the gas flow and distribution at the reservoir scale that is important for the 4D seismic modelling. The effect of reservoir scale parameters on gas dissolution is also discussed here. Is it only the fluid type that impacts the gas when it goes back into solution, or do other reservoir properties such as relative permeability curves and transmissibility impact this phenomenon? Gas liberation may alter the laboratory-based stress sensitivity of the sand. Therefore, the effect of gas exsolution on the pressure dependency of the fluid and rock is discussed as the next subject. The solution gas oil ratio (R_s), as an important parameter in the petro-elastic modelling, is normally calculated using the laboratory proposed equations. The accuracy of these equations and the effect of the reservoir scale phenomena are investigated in this chapter. Finally a compositional change of the gas and liquid phase during gas liberation were seen from the literature. The magnitude of this change and its effect on the overall seismic properties is discussed as the last part of the chapter.

5.1 Introduction

Without proper pressure support, reservoir production ends up with pressure depletion. Pressure drop below the bubble point pressure causes gas to come out of solution (Dake, 2002). This gas exsolution mechanism can be explained using a phase diagram (Figure 5.1). Above the bubble point line, the hydrocarbon is a liquid. It is a gas below the dew point line. Gas and liquid co-exist in the area between these two lines, but the ratio of the liquid to gas is varied as a function of the pressure. At the bubble point pressure, called also vapour pressure, the first hydrocarbon molecules leave the liquid and make gas bubbles. As the system expands, more liquid is vaporised. Only a few drops of liquid remain at the dew point pressure. Further pressure drops results in gas expansion (Todd, 2007).

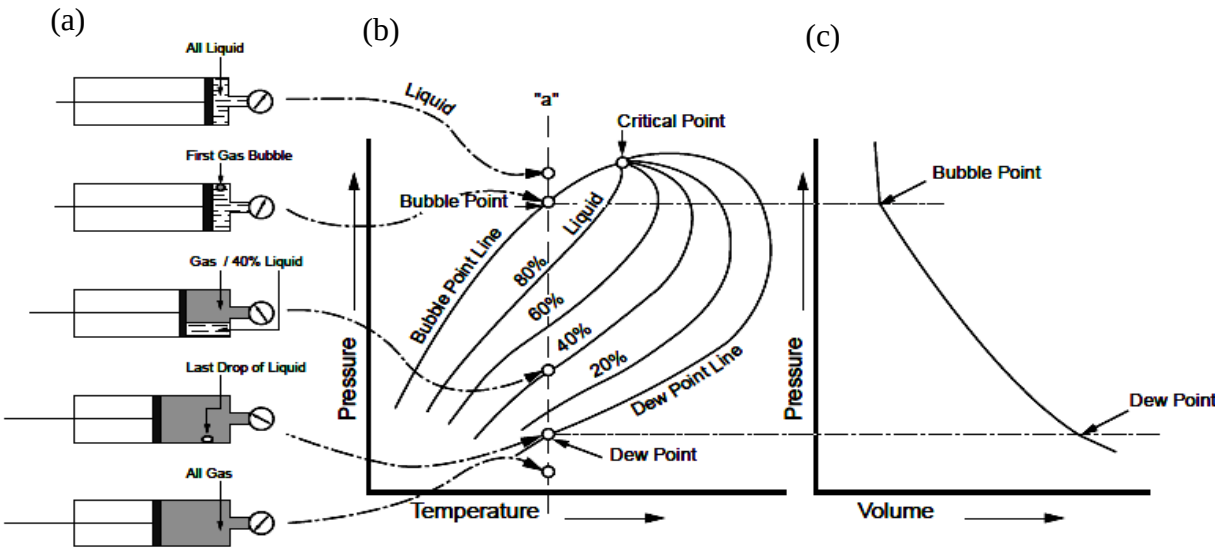

Figure 5.1 Phase diagram for the multicomponent fluid system (Todd, 2007).

As discussed on Chapter 1, gas liberation causes a decrease of oil saturation, that causes a drop in the oil production rate. Oil production rate decrease is one of the main challenges in the engineering domain below the bubble point pressure. Gas liberation also alters the main inputs to the simulation model, that makes considerable uncertainty in the simulation results. On the other hand, calculation of the exsolved gas volume is important, to be able to include its impact on the material balance equations as well as on the gas management (sell, re-inject or dispose). Seismic could be a way of addressing some of these questions,

but how? Is the gas signal in the seismic domain useful, and can it help us with liberated gas management? In the seismic domain, gas normally makes sharp signal which dominates the 4D seismic. Liberated gas softens the 4D seismic signal (reduces the impedance), as against hardening (increase of impedance) due to the pressure depletion or water injection. For a proper interpretation of the 4D seismic observations, it is important to know the pore scale and reservoir scale gas liberation processes.

5.2 Synthetic modelling of gas exsolution

Pore scale and reservoir scale schematic modelling

Assume a small piece of the reservoir at a pressure above bubble point (Figure 5.2-a). Gas saturation is zero, water is the connate water saturation, and oil saturation is the initial which is $1-S_{wc}$. After pressure drop, some bubbles are evolved. Gas saturation is below critical gas saturation (minimum movable saturation) and oil saturation is slightly decreased, but water saturation is still constant at S_{wc} (Figure 5.2-b). After more pressure drop, more gas bubbles are liberated. These bubbles connect together and then gas arrives at the critical saturation. The gas bubbles now start to move upward or towards the wellbore due to the gravity force or pressure gradient (Figure 5.2-c). Migrated gas makes a gas cap at the top of the reservoir. Gas saturation is around maximum gas saturation on the gas cap (Figure 5.2-d), but it remains about critical gas saturation on the oil leg. Therefore, two sets of gas saturation exist on the reservoir.

The same story is valid on the reservoir scale. Figure 5.3 shows a part of the reservoir under different stages of the pressure drop. Gas bubbles are liberated, connected and migrated to make a gas cap at the top of the reservoir (Figure 5.3-a, b and c). By continuing pressure drop, the thickness of the free gas cap is increased (Figure 5.3-d). It is also possible for gas to arrive at the well bore, so some part of the gas is probably produced (Figure 5.3-e). Therefore, the size of gas cap may decrease in spite of the gas liberation. At the seismic survey time, pressure has dropped, so production rate has decreased and probably gas can no longer be released (Figure 5.3-e). Therefore, the system stabilises at two gas saturations ($S_{g\text{-}max}$ in the gas cap and $S_{g\text{-}cr}$ in the oil leg). Once the pressure is built up by water

injection, the gas in the oil leg which is in contact with initial oil is dissolved rapidly (Figure 5.3-f). Some part of the gas in the gas cap possibly goes back into solution, but a considerable volume of free gas is still present in the reservoir despite arriving back at the initial bubble point pressure. The discussion and schematic modelling that were provided here are based on some synthetic and a real simulation models.

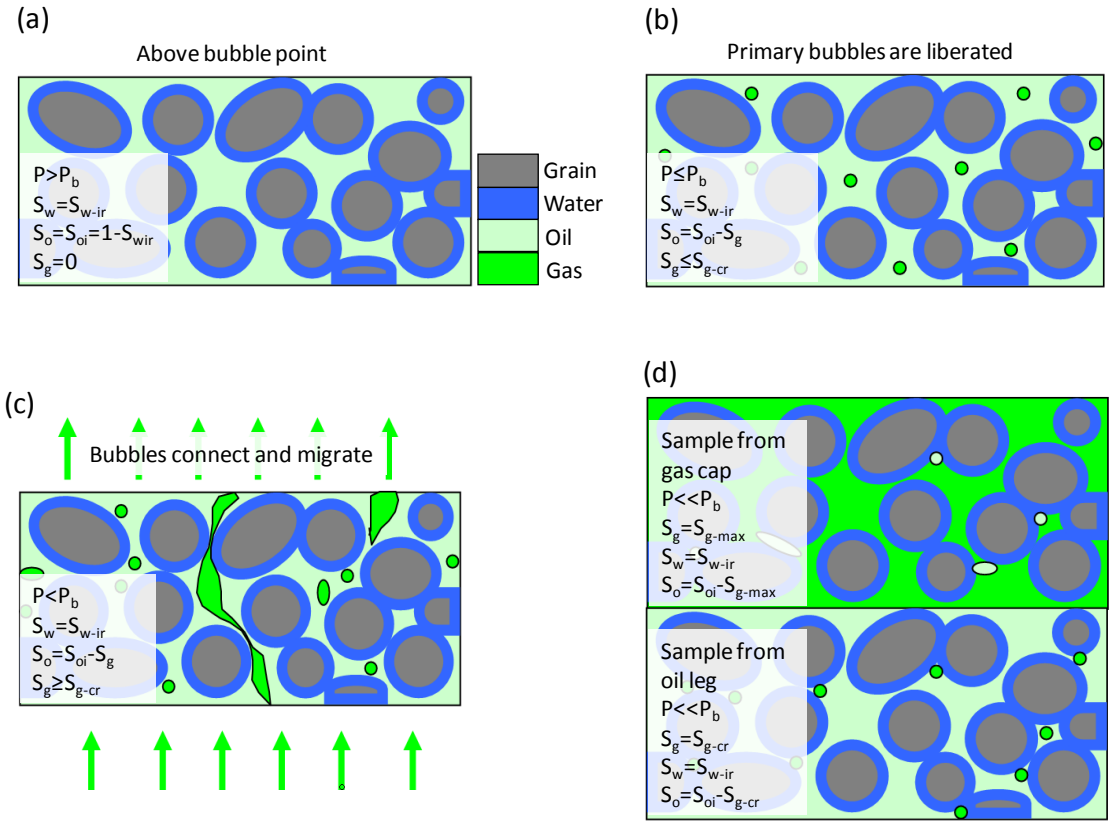

Figure 5.2 Pore scale schematic model of pressure drop and gas out of solution a) initial case - before pressure drop, b) pressure has slightly gone below the bubble point, c) pressure drop has been continued and more gas bubbles have exsolved, and d) at the seismic survey time, production rate has decreased and probably gas will no longer be released.

Gas saturation distribution

The discussion of Chapters 2 and 3 can be generalized for gas coming out of solution also. It was shown in previous chapters that gas saturation remains constant inside a specific thickness, termed the gas thickness. For the gas injection case, gas thickness is the only

parameter which is varied and increased by gas injection. This was the main reason why the 4D seismic response is linear for the injected gas volume. Our synthetic modelling shows that this kind of distribution may be valid for the gas exsolution stages. Indeed, as gas migrates to the upper parts of the reservoir during gas exsolution, the gas cap thickness is increased and gas saturation remains constant inside the cap itself.

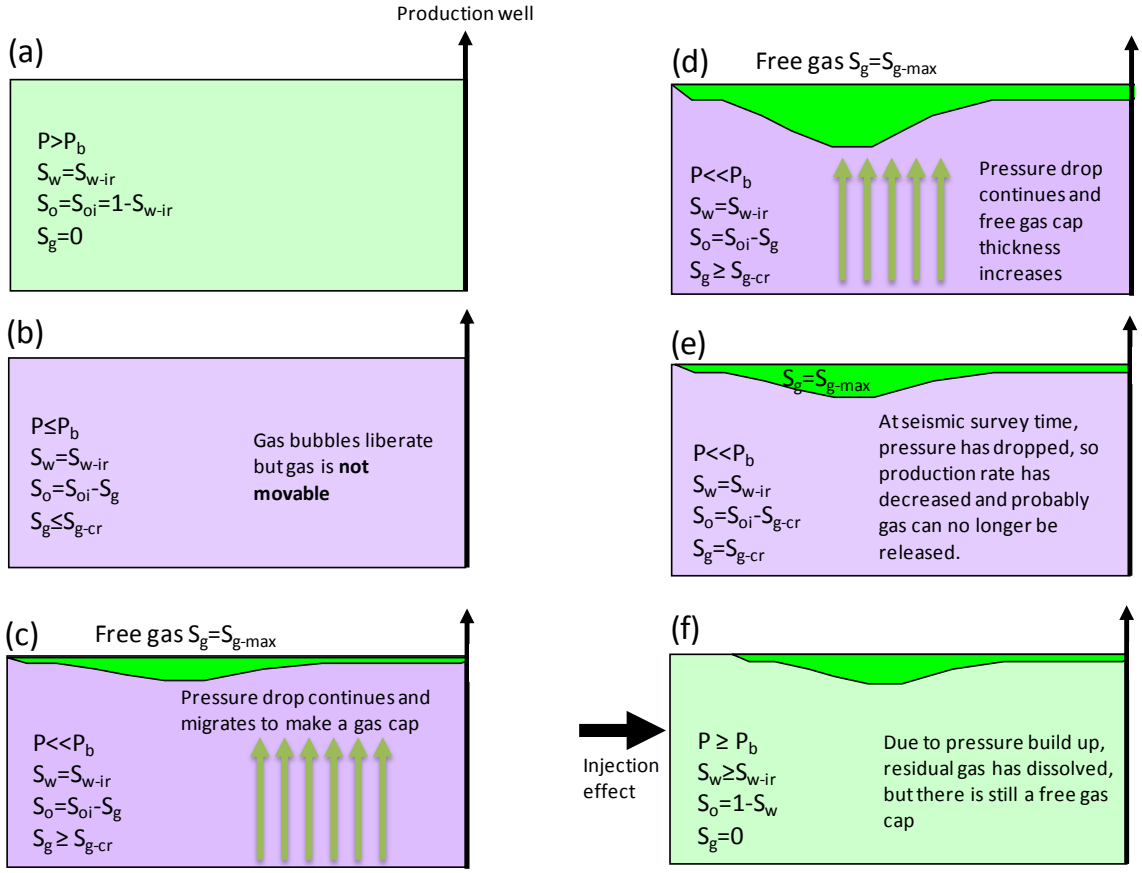

Figure 5.3 Reservoir scale schematic model of pressure drop and gas out of solution a) initial case, b) pressure has slightly dropped below the bubble point, c) gas cap has been formed, d) the size of gas cap has been enlarged, e) the gas has arrived at the production well, f) pressure build up causes gas dissolution.

This particular understanding is investigated using realistic simulation models with a range of heterogeneity. The story of the models was guided by a sector from the Schiehallion field. The initial pressure was around the bubble point pressure. Production started in 1998 and, as there were no connected pathways to the water injection well, pressure dropped by

up to 1500 psi during the first four years. PVT tables and the petrophysical properties are extracted from our case study to generate a homogeneous fine grid synthetic model. The size of the model is 800*800*19m, with a cell size of 12.5*12.5*0.18m (430000 cells). Figure 5.4 illustrates the resultant gas saturation distribution for the variety of times. After arriving at the bubble point pressure, the components of the oil are immediately broken down and gas is exsolved. Interestingly, for repeat times smaller than 6 months, gas saturation does not reach the maximum gas saturation in the gas cap. This observation highlights the time required for the gas migration and stabilisation at the gas cap, and also perhaps the cell thickness. Because the volume of migrated gas in the upper part of the reservoir is not big enough during the primary stages to fill the cells, a perceived variation of the gas saturation is apparent. This may be solved by choosing a smaller cell thickness; however for computational reasons the cell size remained coarser than is needed. Note, however, that this point is not an important issue when working with the 4D seismic time lines.

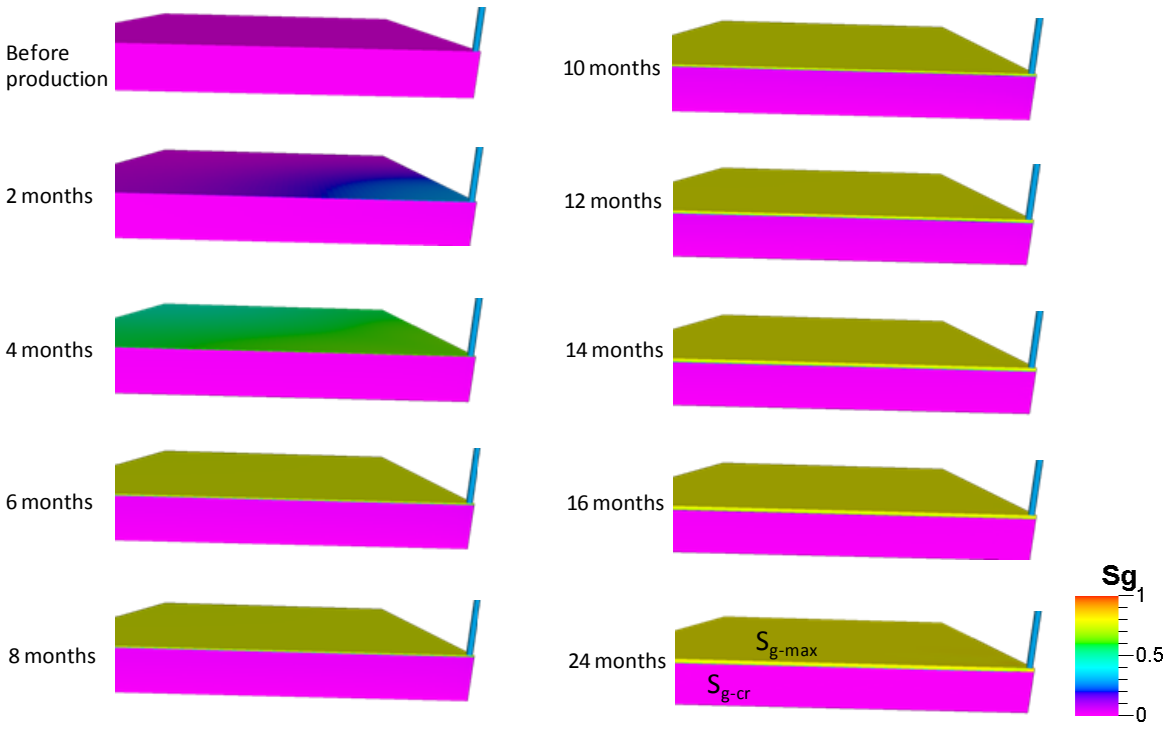

Figure 5.4 Gas saturation distributions for a homogeneous synthetic model, for a variety of times after pressure depletion.

For the second stage, a vertical heterogeneous model is built. There are three layers with different petrophysical properties, but not connected vertically. The production well produces from these layers, so that pressure drops inside the layers. The liberated gas migrates vertically inside the layers and is trapped at the top of the layers. There are separate accumulations of gas inside every layer. The story of gas saturation is the same as for the homogeneous model for every layer (Figure 5.5-a). In fact, it is a repetition of three homogeneous models.

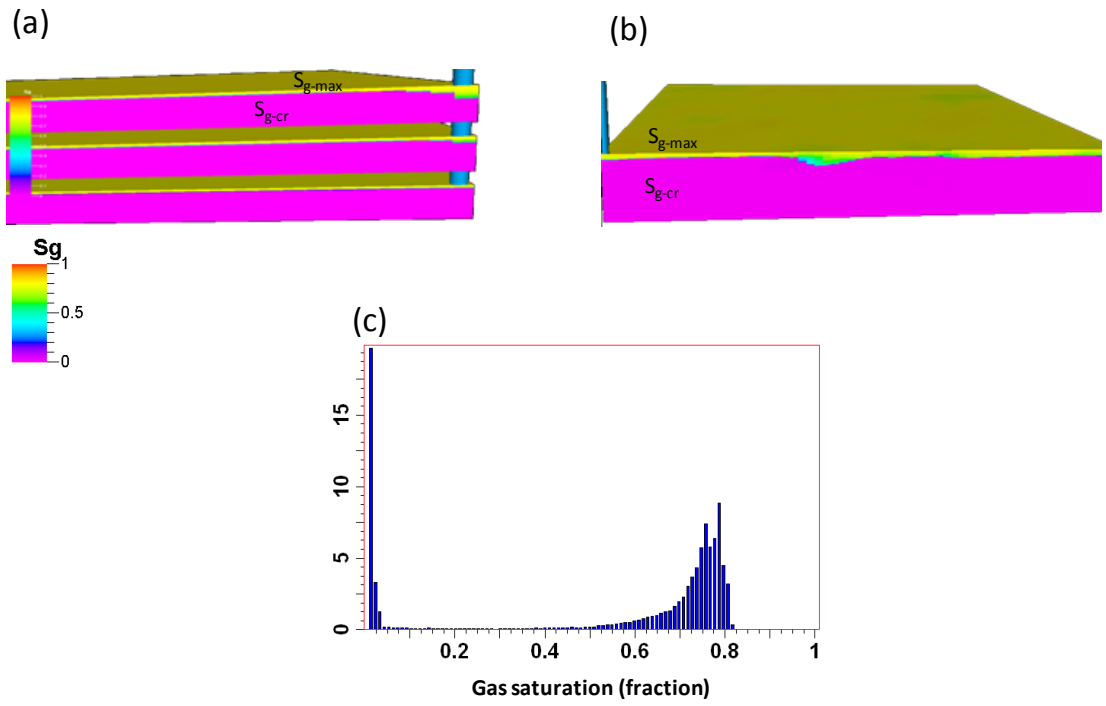

Figure 5.5 Gas saturation distributions after 24 months of production for: a) vertically heterogeneous model, b) vertically and horizontally heterogeneous model, and c) histogram of the gas saturation for the heterogeneous model.

The third model that contains the heterogeneity in the range of my case study confirms the saturation distribution (Figure 5.5-b). There are two accumulations of gas (Figure 5.5-c) with a narrow saturation distribution. One is around the minimum gas saturation and the other is roughly at the maximum gas saturation. The average saturation is 0.2% with a standard deviation of 0.36% in the oil leg. The average and standard deviation of the saturations are 76% and 5.5% respectively for the gas cap. The same histograms are

observed for both homogeneous and vertically heterogeneous models (first and second model considered), but for these models, the saturation contains an even narrower distribution around the maximum gas saturation. Therefore, Chapter 3 can indeed be generalized to gas liberation – a nonlinear gas behaviour need not be invoked, as only two end member saturations determine the seismic behaviour in addition to the gas thickness. The variation of the signal in the 4D seismic data is entirely due to thickness variation.

5.3 Gas dissolution

In field management, pressure drop is usually controlled by water injection. The aim of water injection is mainly pressure support and pushing the oil towards the production well. Therefore, pressure builds up during water injection. The questions that may be highlighted here are: is gas dissolved again by pressure build up? If the reservoir pressure has arrived at the initial value, could all of the liberated gas go back into solution? If not, how much goes back into solution and which parameters control this phenomenon? Is hydrocarbon type the only factor that controls dissolution (as indeed PVT engineers care about)? These are some important questions for both the engineering and seismic domains. The answers will affect the 4D seismic interpretations.

In the engineering domain, some interesting attempts have been made to answer these questions. There are many references which include this discussion (for example, Danesh, 1998). They mainly consider the hydrocarbon effect only. PVT engineers have presented interesting discussions about the solubility of the gas inside oil and water. These are laboratory scale observations which are already included in the simulation models. However, there are some reservoir scale phenomena which affect the solubility of the gas in oil. To investigate this subject at the reservoir scale, a homogeneous model is built. The cell size is set to 12.5*12.5*1.7m, with these grids chosen to save computational time. The petrophysical parameters are extracted from the Schiehallion case study. In the model, there is a production well in the south which produces for two years, then this well is shut and another well in the east injects water for another two years. During the production period, pressure has dropped gradually to around 1500psi. However, during the injection stage pressure built up to arrive at the initial pressure (Figure 5.6-a and b).

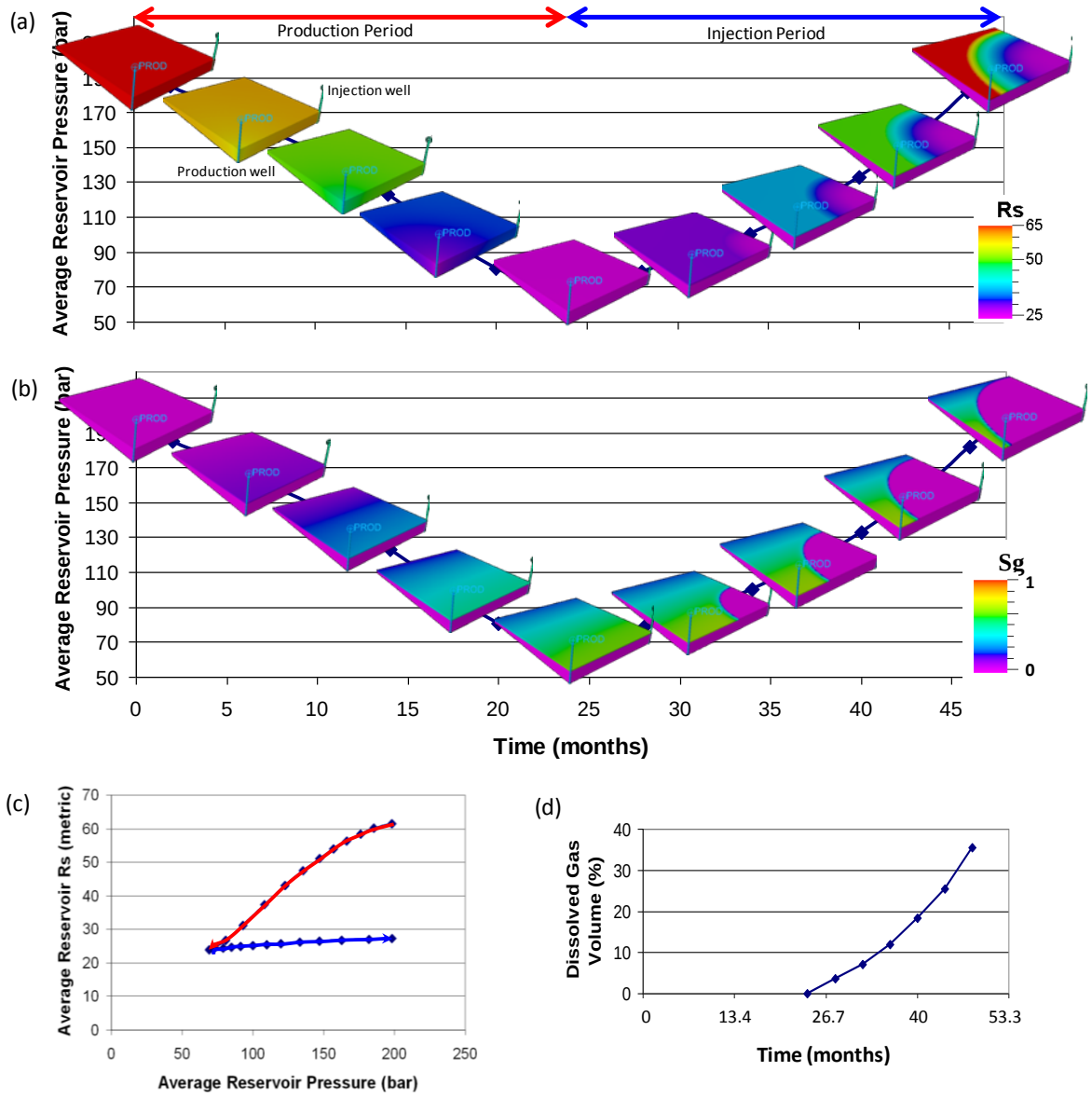

Figure 5.6 Average reservoir pressure versus time for a period of production and injection. a) R_s variation and b) gas saturation variation from the simulation model is overlain on the pressure plot. c) average R_s variation for the period of production (red line) and injection (blue line). d) percentage of the dissolved gas volume for the period of the injection.

As gas comes out of solution during production, R_s (the solution gas-oil ratio) decreases gradually (Figure 5.6-a production period). The R_s value is approximately constant across the entire reservoir during every stage. After injection, pressure arrives back at the initial value but is R_s able to go back to its initial value? There are some issues that need to be

taken into account: a) once the pressure starts to increase, residual gas saturation in the lower parts of the reservoir dissolved in the oil, but cannot significantly change R_s because critical gas saturation (S_{g-cr}) is small. b) in the upper part of the reservoir, two necessary conditions for the dissolution process already exist: pressure build up and free gas. The gas dissolution process as well as the R_s variation is reversible. They return along the same line as the exsolution stage (Figure 5.6). c) in the area close to the water injection well, water has moved the gas in the model. Therefore, in spite of pressure build up, R_s is not able to increase, because there is no free gas in this part of the reservoir. Comparison of the laboratory based plot of R_s versus pressure variation with the output of the simulation model highlights the fact that they both follow the same trend during pressure drop. R_s decreases with pressure drop along the red line in Figure 5.6-c but, on build up, the behaviour is completely different. It returns to the initial value along the red line in the laboratory, while it shows a very small increase (blue line) at the reservoir scale. This is due to the contribution of gas production and lack of dissolution (because of gas migration). Therefore, the R_s graph and gas dissolution process cannot be reversed at the reservoir scale.

Figure 5.6-b represents the gas saturation at both the production and injection stages. Once pressure increases, residual gas will dissolve immediately. This is due to the change of the hydrocarbon composition and the phase diagram. Some of the gas in the gas cap has dissolved and the rest has been pushed towards the left part of the model by the injection well and compressed. First of all, despite the fact that pressure arrives back at the initial value (which is around the bubble point pressure), the gas has not dissolved completely and there still is some free gas. The question may now be asked: what is the volume of free gas or, on the other hand, how much of the gas volume has been dissolved? Visual observation tells us that the free gas volume is small (around 25%) by comparison with the total liberated volume. Although this means that 75% of the evolved gas has dissolved, the pressure effect needs to be included. Because pressure compresses the gas, the gas occupies a smaller volume at the higher pressure. After conversion of the gas volumes to the surface conditions, only 35% of the gas has now dissolved and there is 65% free gas in the reservoir. Figure 5.6-d shows the dissolved gas percentage with time.

Parameters controlling the gas dissolution process

Some questions are highlighted from above: which parameters control the dissolution process? Is it only fluid type that controls this process or are there some other reservoir scale parameters that affect the dissolution process? Finally, how big is the effect? The main parameter is fluid type, which has been taken into account in most of the PVT and phase behaviour literature. It could be concluded from these references that, for lighter oils, a higher volume of the gas can be liberated by pressure drop, and a smaller volume of the gas can be dissolved by pressure build up. On the other hand for the heavier oils, a smaller volume of the gas is liberated by pressure drop, and a higher volume of the gas can be dissolved by pressure build up (Danesh, 1998 and MacCain, 1990). In the 4D seismic interpretations, however, we are dealing with a specific reservoir and a narrow variation range of hydrocarbon type. Therefore this parameter is not important in 4D seismic interpretations.

There are some reservoir scale parameters that may affect the dissolution process, so those should be taken into account during 4D seismic interpretations. These parameters are difficult to measure spatially, so they could be the source of the uncertainty in the quantitative or qualitative monitoring of the reservoir activities. Some of the reservoir scale parameters will be discussed here. The same simulation model as used earlier is employed here, but a different range of the parameters is involved to build different cases:

1- K_v/K_h is one of the key parameters. It is difficult to define spatially, while it contains considerable variation in clastic reservoirs (Link, 2001). To tackle this, three different cases are selected that contain high (1), average (0.1) and low (0.01) K_v/K_h value respectively. The result for the gas dissolution percentage is presented in Figure 5.7-a. The blue and red lines which represent the average and high K_v/K_h respectively show a very small difference. This means that increasing K_v/K_h does not affect the volume of the dissolved gas. However, there is considerable deviation for the low K_v/K_h (green line in Figure 5.7-a). The percentage of dissolved gas volume is considerably higher for small K_v/K_h. Investigations with the simulation model tell us that it is harder for gas to move towards the upper part of the reservoir in this case. Therefore, a large volume of gas is in contact with the original oil.

Subsequently, there is higher opportunity for this liberated gas to be dissolved by pressure build up. The dissolved gas volume becomes up to 65% in this scenario.

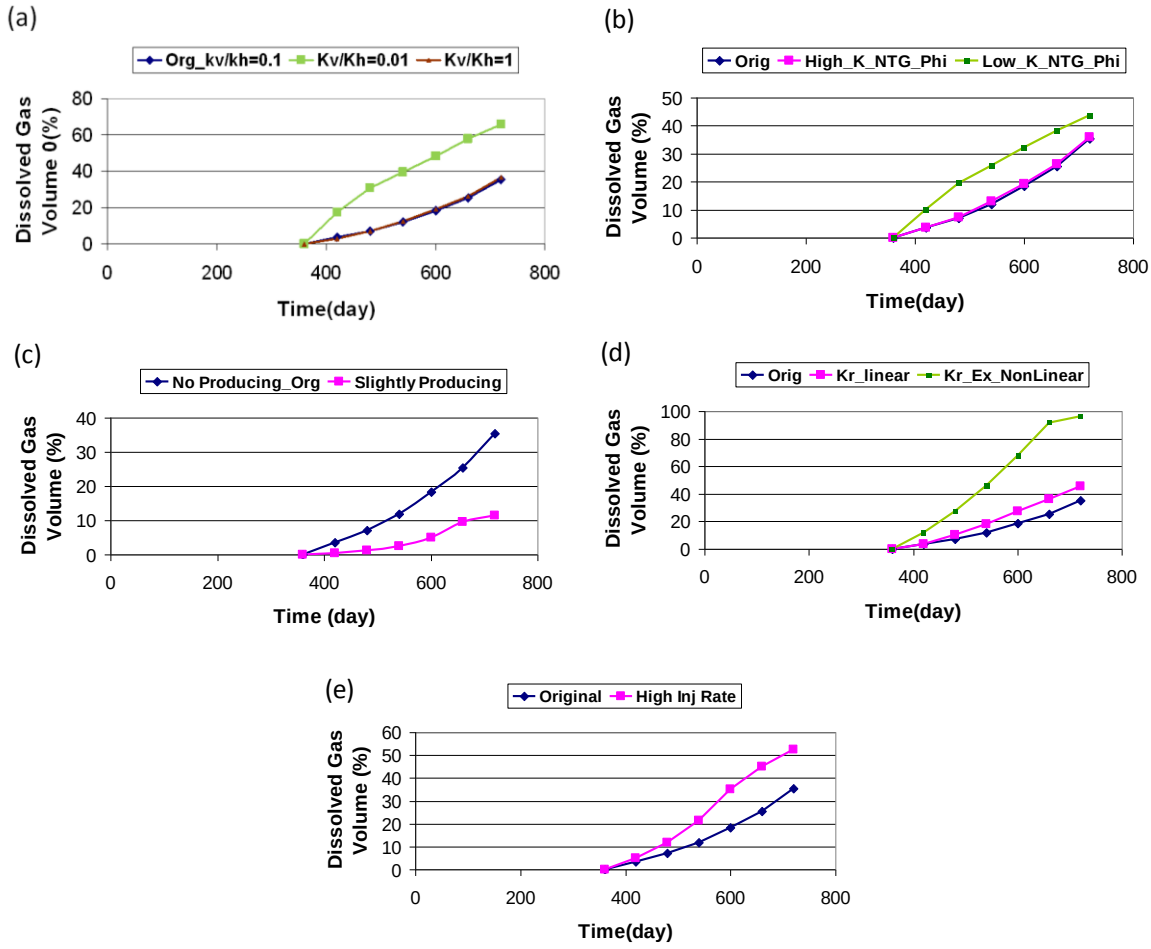

Figure 5.7 The effect of the reservoir scale parameters on the gas dissolution process, a) K_v/K_h, b) transmissibility index, c) production rate in the second half of the reservoir life, d) relative permeability curve, and finally e) injection rate for the second half of the reservoir life. Vertical axis in these plots is the volume of dissolved gas divided by the total exsolved gas at the end of production period in the percentage format.

2- The second parameter is transmissibility: permeability, net-to-gross and porosity are chosen to be the representative of the transmissibility. Three values for the transmissibility are allocated: high (800), average (150) and low (3.45) transmissibility (the values are permeability times NTG times porosity). The results for gas dissolution are presented at Figure 5.7-b. By comparison with the blue and purple lines which are representative of the average case and higher transmissibility respectively, only a small difference is observed. Therefore, increasing the

transmissibility does not affect the volume of the dissolved gas. However, the model that contains the low values of the joint permeability, net-to-gross and porosity product show an increase in the dissolved gas volume (green line). Once again, gas migration decreases for the low transmissibility case because it is hard for gas to move. Therefore a large amount of gas is in the contact with the original oil, and there is an opportunity for gas to be dissolved by pressure build up. Dissolved gas volume is up to 45%. The results show that, the effect of transmissibility is less pronounced than the K_v/K_h effect.

3- The effect of production rate is the third parameter discussed here. Two cases are chosen to be investigated. a) the original case in which there is no production in the second half of the reservoir's life (injection part), and b) production well is slightly open during the injection period. In this case, the injection rate should also be increased to stabilise the pressure to the same level as in the first case. Figure 5.7-c compares the two cases. For the second case with production at the pressure build up period (red line), there is a sharp drop in the volume of the dissolved gas. This is because of the fact that most of the liberated gas has been produced and there is no opportunity to be dissolved again.

4- One of the important, but challenging, set of parameters is the relative permeability curves. There is always some debate about determining the reservoir scale relative permeability curves. Normally, one set of curves are allocated for the entire reservoir, even though it is a function of many parameters (for instance rock type). Therefore, it may affect the gas dissolution process and subsequently the 4D seismic interpretations. Three cases were designed for this aim. The first is the original case which uses the Schiehallion field relative permeability curves. For the other two cases, linear and extremely non-linear (exponential) curves are employed respectively (Figure 5.7-d compares the results). A high increase in the dissolved gas volume (up to 96%) is observed when extreme non-linear relative permeability curves are employed (green colour). The reason is that end points in the relative permeability curves contain higher values in this case, so the critical gas saturation is very high. Higher critical gas saturation prevents a liberated gas migration. The

result of this scenario is that most of the liberated gas is in the contact with original oil. Therefore, there is higher opportunity for gas dissolution by pressure build up.

5- The last parameter to be discussed here is the injection rate. The water injection rate is increased to obtain a higher pressure range than the original case. The reservoir pressure rises to 3600 psi, while the initial pressure for the original case is 2900 psi. It can be seen in Figure 5.7-e that increasing the reservoir pressure by more injection enlarges the gas dissolution slightly. However, despite arriving at 700 psi higher than the bubble point pressure, 47% free gas remains in the reservoir. Therefore, the dissolution rate can only be slightly improved by increasing injection rate, and it could not dissolve all of the liberated gas.

In conclusion, it appears that hydrocarbon type is not the only parameter that controls the dissolution process. There are some reservoir scale parameters that have significant effects. Smaller K_v/K_h and transmissibility, and extreme non-linear relative permeability curves increase the volume of the dissolved gas. These parameters are, therefore, very important during interpretation of the 4D seismic signal. During this interpretation, more careful attention to these reservoir scale parameters and correlation of specific 4D signals to the dissolution effect is necessary. On the other hand, the effect of these parameters on the 4D seismic response can be used to indirectly extract parameter estimates from the seismic data to update the simulation model. For instance, the laboratory extracted relative permeability curves are normally used in the simulation model (or sometimes upscaled), but we could possibly achieve the reservoir scale relative permeability curves by employing of these concepts. This might even provide some information about the areal distribution of the transmissibility, to be used during updating of the simulation model. This latter point is not attempted in this thesis, and is proposed as a future research topic.

5.4 Seismic response to gas exsolution and dissolution

I now consider whether seismic is able to discriminate the different stages of the gas liberation and dissolution? This question will be discussed for the laboratory scale and reservoir scale separately. The same segment of the Schiehallion field as in the previous

sections is used for this work. All of the necessary parameters for synthetic seismic modelling, such as pressure, saturation and petroelastic modelling parameters, are extracted from that particular segment, and in-house ETLP simulator to seismic code applied (Amini *et al.*, 2011). The result is illustrated on Figure 5.8-a, where scenarios 1 to 4 represent the gas liberation stages, and scenario 5 to 7 demonstrate the gas dissolution period. There is a very small change of gas saturation from scenario 1 to 2 due to the small value for the critical gas saturation (0.2%) in our case study. Therefore only a small change in V_p can be observed. By continuing the pressure drop, we arrive at scenario 3 in which the gas saturation is approximately constant at around $S_{g\text{-}cr}$, but there is pressure drop. Pressure drop increases the impedance (hardens the 4D seismic signal), which is the opposite of the gas saturation effect. A sample from a gas cap located in that sector of Schiehallion is used to simulate the historical evolution of the gas cap (scenario 4). There is considerable decline of the P-wave velocity due to a gas saturation change, but only a small increase due to the pressure drop (see Figure 5.8-a).

To simulate various injection period scenarios, the production well is shut and water injected from the injection well (Figure 5.8-a, scenarios 5 to 7). Immediately after injection, pressure builds up so that the critical gas saturation in the oil leg is dissolved. Scenario 5 is chosen in which there is no gas, but pressure is at a minimum. An increase in velocity is observed for this scenario. Water injection continues and pressure reaches the initial value at scenario 6. A location inside the gas cap is selected in which there is no pressure change, but gas saturation is the maximum gas saturation. The signal at the location is a large fall in velocity due to the pure gas saturation signal. When the initial pressure is reached, there is no gas in the oil leg and the area close to the water injection well. A point is selected from this area to represent scenario 7. Velocity is now close to the initial value, but there is a very small deviation due to the R_s history. As discussed earlier, R_s could not reach its initial value and this affects the elastic properties of the saturated rock.

At the reservoir scale, initially reservoir pressure is above or close to the bubble point pressure, oil saturation is $(1\text{-}S_{wc})$ and there is no gas. With a slight pressure drop, gas bubbles are liberated. Gas saturation is at the critical value throughout the entire reservoir. Scenario 2 represents this stage, in which there is a small decrease in velocity (Figure 5.8-b). The liberated bubbles connect and migrate upward to make a free gas cap. Despite a

small gas thickness for scenario 3, the pressure drop is not big enough to cancel out the gas saturation signal. At the next stage, pressure continues to drop. More gas is liberated to increase the thickness of the gas cap. Scenario 4 represents this, and confirms that the gas -

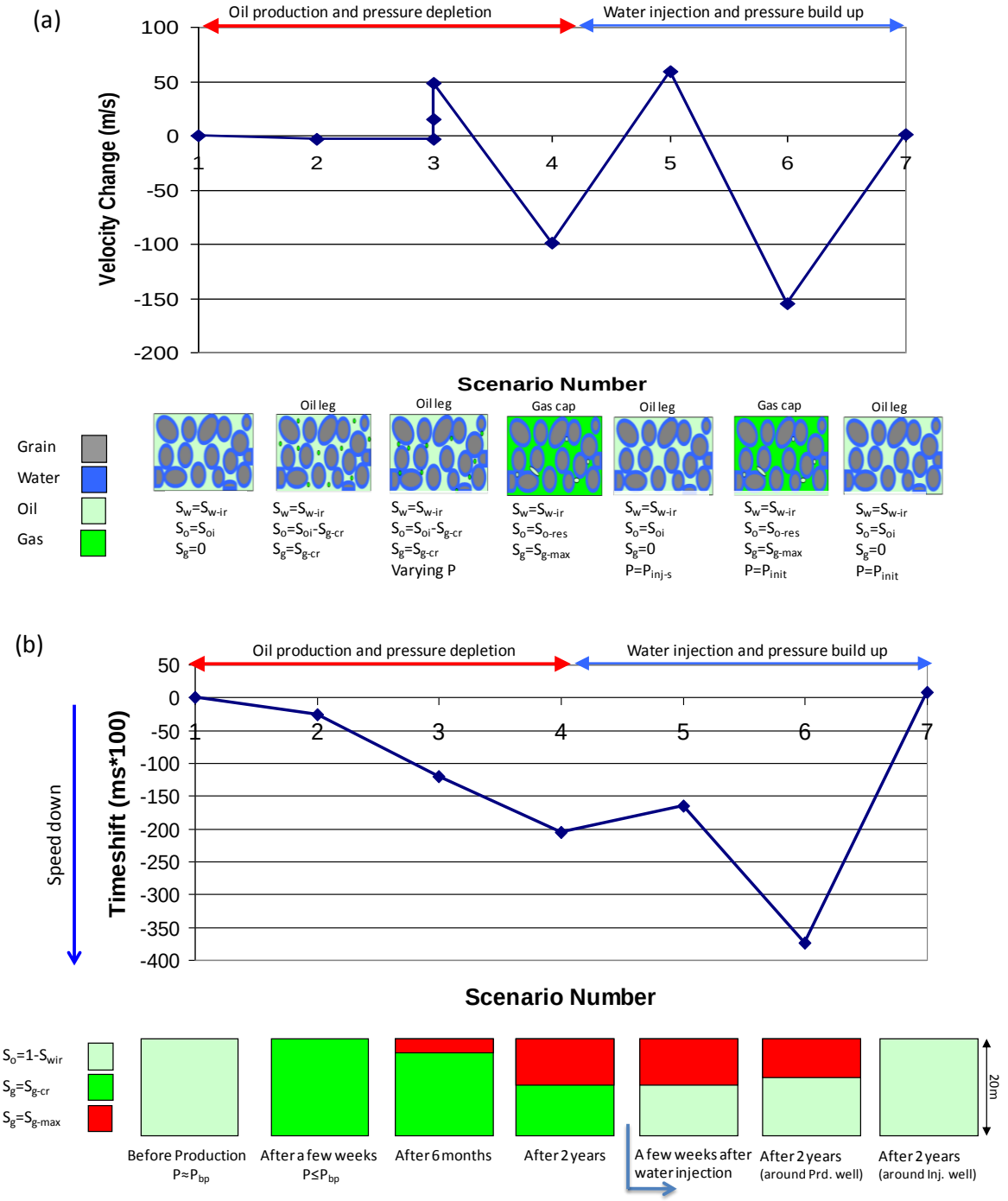

Figure 5.8 The 4D seismic signal for different scenarios and stages during gas exsolution and dissolution for: a) the pore scale, and b) the reservoir scale.

saturation signal dominates. However, a hardening (impedance increase) due to the pressure drop obscures observation of the true gas saturation signal for scenario 4.

At the injection stage, once pressure has increased, the critical gas in the oil leg dissolves. The lack of critical gas saturation in the oil leg is the only difference between scenario 5 and 4, because pressure has not built up enough. In this case, if pressure support is not taken into account during 4D seismic interpretation, this signal might be interpreted as due to a lower gas thickness when compared to scenario 4. At stage 6, pressure has arrived back at the initial value. The thickness of the free gas cap decreases slightly due to gas dissolution, and there is no critical gas saturation. The seismic signal at this stage is completely due to the free gas cap, and represents the maximum velocity decrease. Scenario 7 is based on the location between the injection and production well, in which there is no gas (either free or critical), and there is no pressure change by comparison with the initial case (scenario 1). A small 4D seismic signal can be observed for this scenario which is due to the R_s variation. In this area, R_s has not reached its initial value, and this affects the seismic properties.

Figure 5.8 clearly illustrates the ability of seismic to discriminate the different stages and scenarios of the gas exsolution and dissolution process. The timeshift is more than 0.5ms for each of the scenarios - this could be assumed as a 4D seismic detection limit. Velocity change is also more than 10% for the scenarios, and this can be taken as a non-repeatability range for the well-acquired and processed 4D seismic data. However, scenario 2 shows a small 4D signal that is difficult to be distinguished with seismic data. This is due to the small magnitude of the critical gas saturation in our case study. Therefore, it could be concluded that, except for critical gas saturation, scenarios of gas exsolution and dissolution could be monitored accurately by the 4D seismic data. Higher values of critical gas saturation could be present in other fields. For example, critical saturations of up to 20% have been reported (Ali *et al.*, 2008). In this case, a significant seismic response can be expected in these areas due to the known non-linear response of velocity change to the gas saturation variation. For the last recommendation, the pressure regime needs to be carefully considered when trying to interpret gas exsolution and dissolution signals. That is because of the fact that the overall seismic signal for gas saturation is probably overestimated or underestimated, if the pressure regime is not properly understood and treated.

5.5 The effect of gas exsolution and dissolution on the pressure dependency of the seismic properties

Generally speaking, the pressure effect on the 4D seismic signals is interpreted using the laboratory based data (Landro, 2001, Mavko *et al.*, 2003, MacBeth, 2004, Han and Batzle, 2004, Tsuneyama and Mavko, 2007). Laboratory measurements illustrate the increasing trend of the seismic properties of the saturated rock with pore pressure drop (Figure 5.9-a) (note that effective pressure is, in simple form, equal to the overburden pressure minus pore pressure). However, after a specific pressure, this trend is largely constant (green highlighted area in Figure 5.9). The same trend has been reported for P and S velocity (Figure 5.9-b), saturated and dry bulk and shear modulus (Figure 5.9-c). Gas out of solution may alter the pressure dependency of the saturated rock, but by how much? In the laboratory, this is difficult to simulate and measure effectively. Here we analysis this –

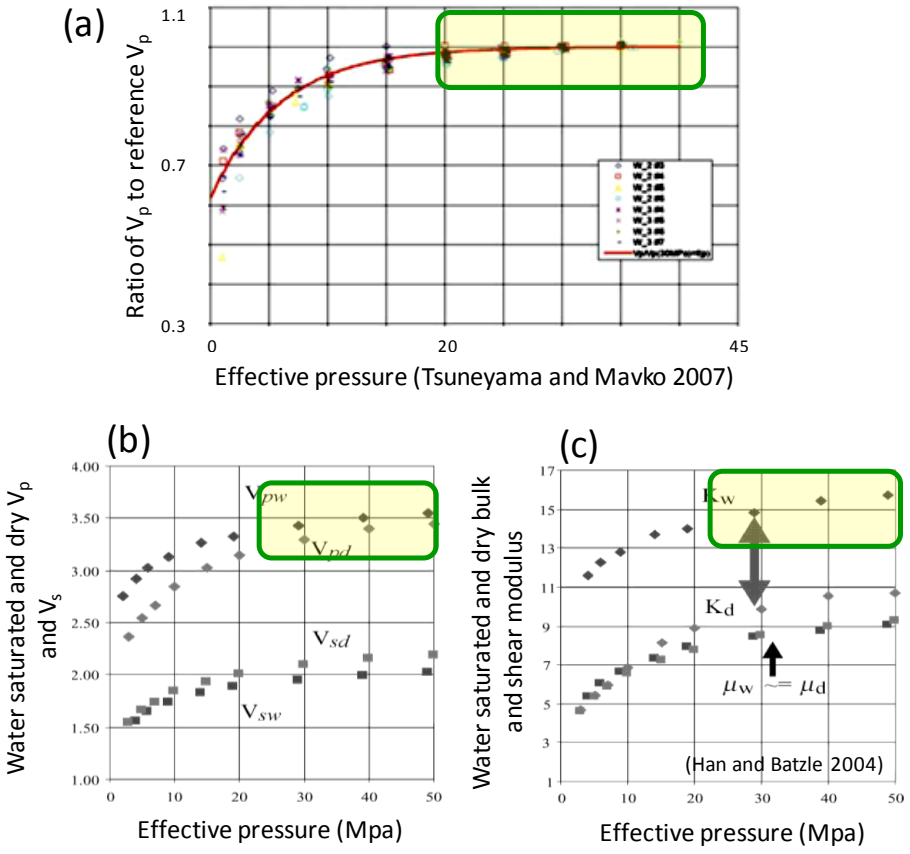

Figure 5.9 a) Ratio of V_P to reference V_P, b) water saturated, and dry V_P and V_S, and c) water saturated, and dry bulk and shear modulus versus effective pressure. Green highlighted area refers to the non-sensitive area of the seismic properties to the pressure variation.

mechanism in more depth. This study is once again guided by a sector of Schiehallion field. Pressure drop with considerable associated gas volume exsolution has occurred since 2002. The liberated gas is observed on the 4D seismic map as a softening signal (reduction of the impedance) (Figure 6.4). Two locations from the oil leg and gas cap are chosen for the calculations.

Gas exsolution effect in the oil leg

The first step is the density variation for the location within the oil leg. As is normal, gas and water density decreases with pore pressure drop (Figure 5.10-a and b). However, the pressure dependency of the oil is complicated. There are two effects on the oil density variation (Figure 5.10-c). The first one is the pressure compressibility effect, which decreases the oil density with decreasing pore pressure (red line). This effect drops oil density by up to 1.2%. The second and most important factor is the effect of gas liberation. Below the bubble point, the lightest components of the oil are exsolved, so oil is heavier step by step as pressure drops (due to the decrease of R_s). This effect leads to an increasing trend of oil density with pore pressure drop (green line). It raises oil density by up to 4.1%, which is bigger than the compressibility effect of the oil. By mixing these two effects together, a rising trend of oil density with pore pressure drop is observed (blue line in Figure 5.10-c). The density of the oil is increased by up to 3% with a pore pressure drop of 2000 psi. By linearly mixing oil, water and gas, the fluid density follows the oil density trend (Figure 5.10-d), as oil saturation dominates the oil leg. By assuming a negligible variation of the dry rock density with pressure change (MacBeth, 2004 and Meadows *et al.*, 2005), the saturated density follows the pressure sensitivity of the oil (Figure 5.10-f). This clearly shows that the effect of R_s dominates the density of the saturated rock.

The next step is pressure sensitivity of the bulk modulus for a location in the oil leg. As with density, the bulk modulus of the gas and water decreases with pore pressure drop. However, there are two effects on the oil bulk modulus variation. The pressure compressibility effect, causing a fall by up to 15% (red line in Figure 5.11-c) and the gas liberation effect, causing an increase of the oil bulk modulus by up to 25% (green line) with pore pressure drop of 2000 psi. The later effect is dominant and a predominant increase in oil bulk modulus can be observed with pore pressure drop. Oil bulk modulus increases with pore pressure drop by up to 9%. Gas, water and oil bulk moduli are mixed harmonically

according to their saturation, so the fluid bulk modulus demonstrates a decrease with pore pressure drop (Figure 5.11-d). By employing the stress sensitivity of the dry bulk modulus proposed by MacBeth (2004), the opposing behaviour of the fluid and dry bulk moduli is observed (Figure 5.11-e). In the end, the fluid and rock are mixed together using Gassmann's equation (1952) to obtain the saturated bulk modulus. For a small pore pressure drop (effective pressure less than 30 MPa), the pressure dependency of the dry rock is dominant, and so the saturated bulk modulus follows the trend defined in the literature (Figure 5.11-f). However for higher pressure drops (effective pressure more than 30 MPa), fluid pressure sensitivity is dominant, and the saturated bulk modulus is decreased contrary to that suggested in the literature (Figure 5.9).

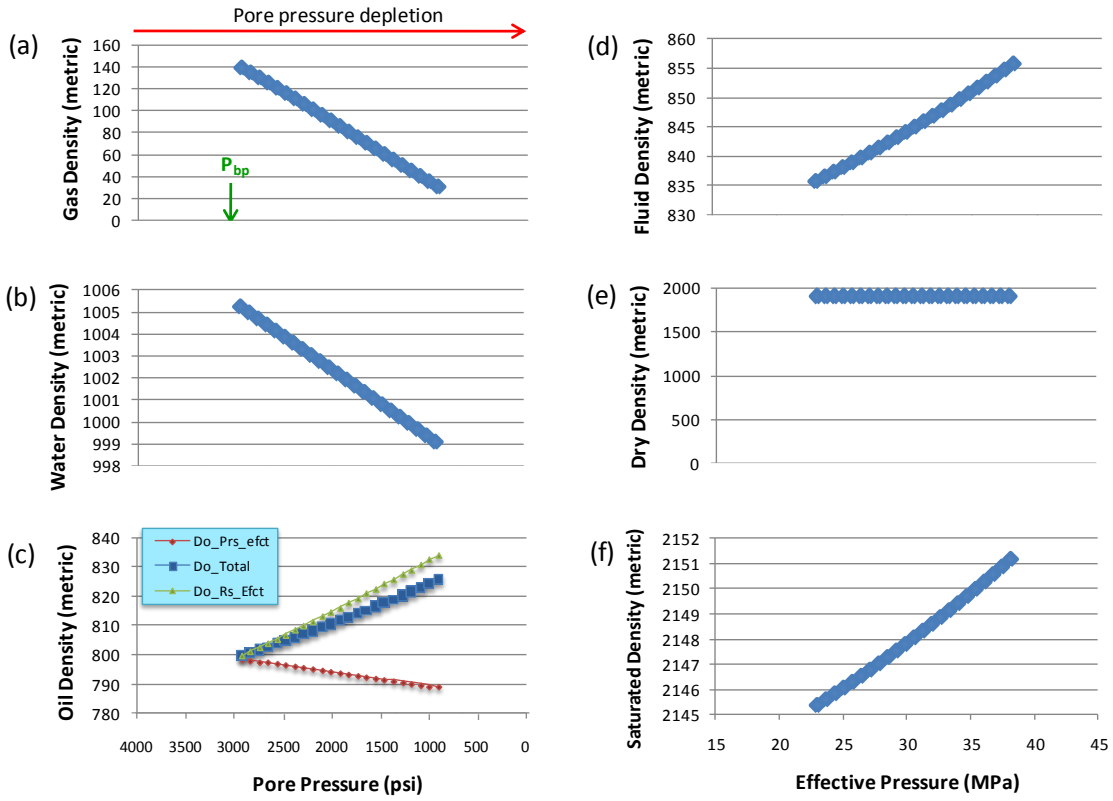

Figure 5.10 The density of a) gas, b) water, c) oil, d) fluid, e) dry (non-saturated rock), and finally saturated versus pressure for a sample from oil leg.

Finally, the P-velocity and impedance are calculated and compared with the laboratory results (Figure 5.12-a and b). As observed in both plots, pressure dependency of the dry rock is dominant for a small pore pressure drop (for an effective pressure less than 32.5

MPa). This follows the trends cited in the literature. However for higher pressure drops (effective pressure more than 32.5 MPa), fluid pressure sensitivity is dominant, so the saturated bulk modulus is decreased. It should be noted here that there is no saturation change in our study, and the variation in all of the plots provided in this section is due only to the pressure. Because the scenario is at the reservoir scale, this behaviour may not be detectable in the laboratory.

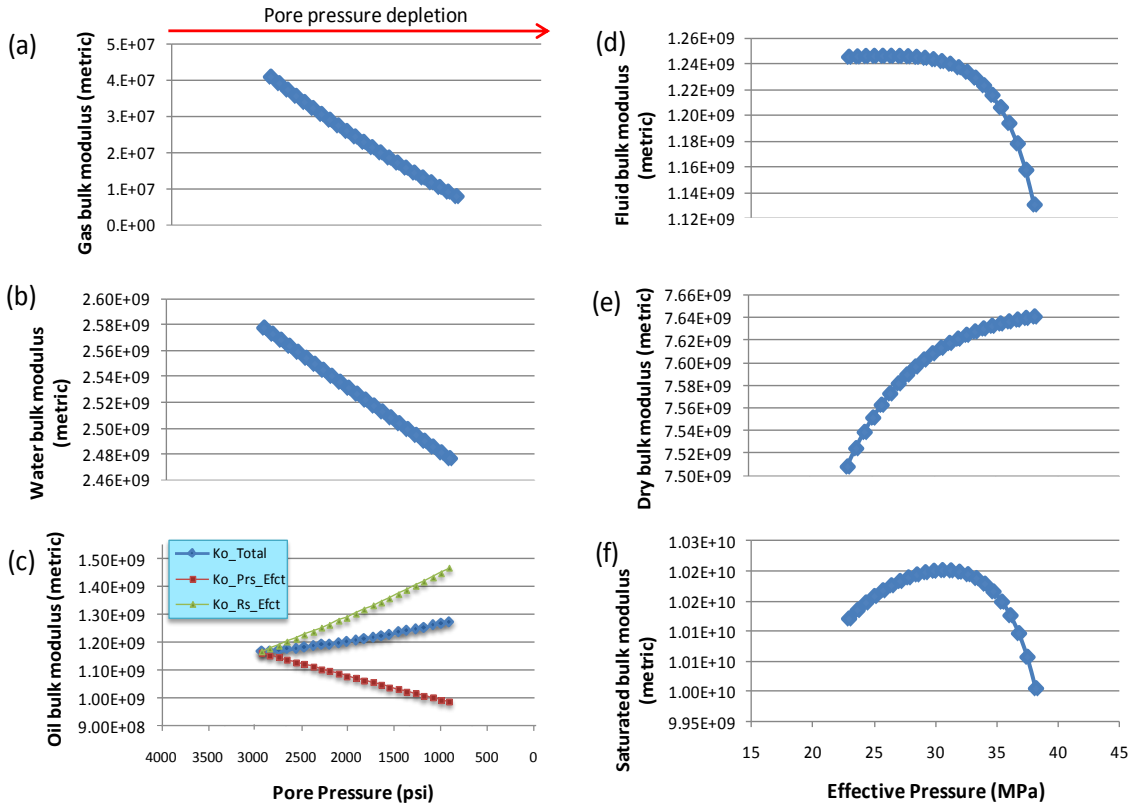

Figure 5.11 The bulk modulus of the a) gas, b) water, c) oil, d) fluid, e) dry (non-saturated rock), and finally saturated versus pressure for a sample from oil leg.

Gas exsolution effect on the gas cap

What is the story for the gas cap? A sample located in the gas cap is selected to investigate the impact of the gas exsolution further. Gas, water and oil density follow the same variation as discussed. Pressure dependency of the oil is opposite to that for gas and water (previous section). However, fluid density follows the gas and water variation. This is

because of the higher gas saturation and low oil saturation in the gas cap (gas saturation is around 76%, which is maximum gas saturation in our case study). By assuming a negligible variation of the dry density with pressure change, the saturated density follows the pressure sensitivity of the gas and water. Therefore, the gas effect in the gas cap is a dominant element of the pressure dependency of the saturated density.

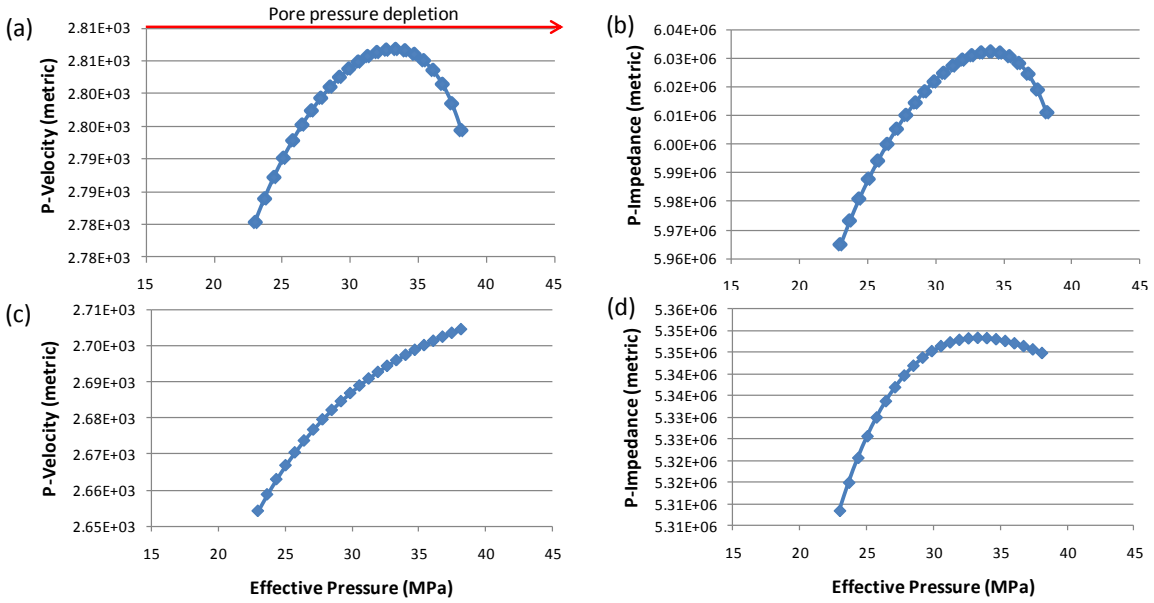

Figure 5.12 a) P-velocity and b) P-impedance variation with effective pressure for a sample from oil leg. c) and d) are the same properties respectively for a sample from the gas cap.

The same sensitivity analysis was performed for the bulk modulus. Gas, water and oil bulk modulus follow the same variation as discussed for the oil leg. The fluid part was mixed with the rock frame using Gassmans's equations (1952). In a similar way to the sample from the oil leg, the pressure dependency of the dry rock is dominant for small pore pressure drop. However for higher pressure drops, fluid pressure sensitivity is dominant, so the saturated bulk modulus decreases. However the second part of the plot is not as strong as for the oil leg. There is a very small drop at the end. The final stage is calculation of the P-velocity and Impedance. As can be seen in both plots (Figure 5.12 c and d), fluid has small effect on the pressure dependency of the saturated rock within the gas cap. It slightly reduces the saturated bulk modulus at higher pressure drops. Table 5.1 summarizes the achievements of this section.

As discussed earlier, the pressure effects on the 4D seismic signals are interpreted using the laboratory based understanding (Landro, 2001, Mavko *et al.*, 2003, MacBeth, 2004, Han and Batzle, 2004, Tsuneyama and Mavko, 2007). Laboratory measurements give an increase of the seismic properties (velocity and bulk modulus) of the saturated rock with pore pressure drop (effective pressure build up). However, after a specific pressure, these properties are approximately constant. We have noticed in this study that this is not valid in some cases in which the reservoir pressure drops below the bubble point pressure. In this situation, gas evolves and alters the pressure dependency of the saturated rock. Generally speaking, it is accepted in the seismic literature that reservoir pressure drop hardens the 4D seismic signal (increases the P-impedance). However, our investigation suggests that a softening 4D seismic signal can be observed for reservoir pressure drop. It is the initial reservoir pressure that plays an important role here. This is important, as understanding the pressure signal in the 4D seismic data is a challenging subject (Mondal, 2010). It is possible that, for higher pressure drops below the bubble point pressure, we might detect no change or even the opposite change to that expected in the 4D seismic literature (Figure 5.12).

General conclusions	The pressure effect on the fluid and rock has different signs.
	Gas exsolution causes the fluid effect to be an important parameter for the pressure dependency of the saturated rock.
	Because the scenario is at the reservoir scale, this behaviour is not detectable in the laboratory.
Specific conclusions	**For oil leg:** the pressure dependency of the fluids is higher than that of the rock on the pressure dependency of the saturated rock. This alters the seismic response to the pressure change.
	For gas cap: the fluids have a small effect on the pressure dependency of the saturated rock. These slightly decrease the P-impedance.
Conclusion from the table	Pressure dependency of the gas exsolution effect is a function of saturation.
	Because of the presence of discrete two types of gas saturation (maximum and critical gas saturation), gas effects are easy to handle in seismic interpretation.

Table 5.1 Summary of the discussion on the pressure dependency of the saturated rock.

5.6 Validity of the R_s equation for calculation of the seismic properties

In black oil modelling, R_s (solution gas-oil ratio) is normally employed to simulate different stages of the gas exsolution and dissolution process. Equation 5.1 was proposed to calculate the R_s at different pressures (McCain, 1990, Batzle and Wang, 1992, Danesh, 1998 and Todd, 2007):

$$R_s = 2.03G\left[P.e^{(0.02878API-0.00377T)}\right]^{1.205} \quad (5.1)$$

where G, P, T and API refer to the gas gravity, reservoir pressure and temperature, and oil density in the API system respectively. Figure 5.13-a is the typical shape of the R_s variation with pressure change. Because of the gas liberation with pressure drop, solution gas-oil ratio is reduced. The main parameter in the equation is pressure change, as the others are approximately constant in the black oil model. This equation is at the centre of the Petro Elastic Modeling (PEM), so the validity is an important issue.

Figure 5.13-b compares the calculated (blue line) and measured R_s (red line) versus pressure. For calculation of R_s, the proposed equation was employed. Measured R_s is extracted from the Schiehallion PVT data. A very small deviation is observed in this plot, but we need to know its importance. Another key parameter which is dependent on R_s is B_o (oil volume factor) that is defined (McCain, 1990, Batzle and Wang, 1992, Danesh, 1998 and Todd, 2007):

$$B_o = 0.972 + 0.00038\left[2.4R_s\left(\frac{G}{\rho_o}\right)^{1/2} + T + 17.8\right]^{1.175} \quad (5.2)$$

where ρ_o is the initial oil density at surface conditions. Figure 5.13-c compares the calculated and the measured B_o. A small deviation can be observed in this plot also. The effect of this deviation on the seismic parameters needs to be investigated here.

To understand the effect of the mentioned deviation on the seismic domain, two of the most important elastic parameters are calculated here. Figure 5.14-a compares the oil bulk modulus which is calculated using measured R_s and B_o (red line), and calculated R_s and B_o

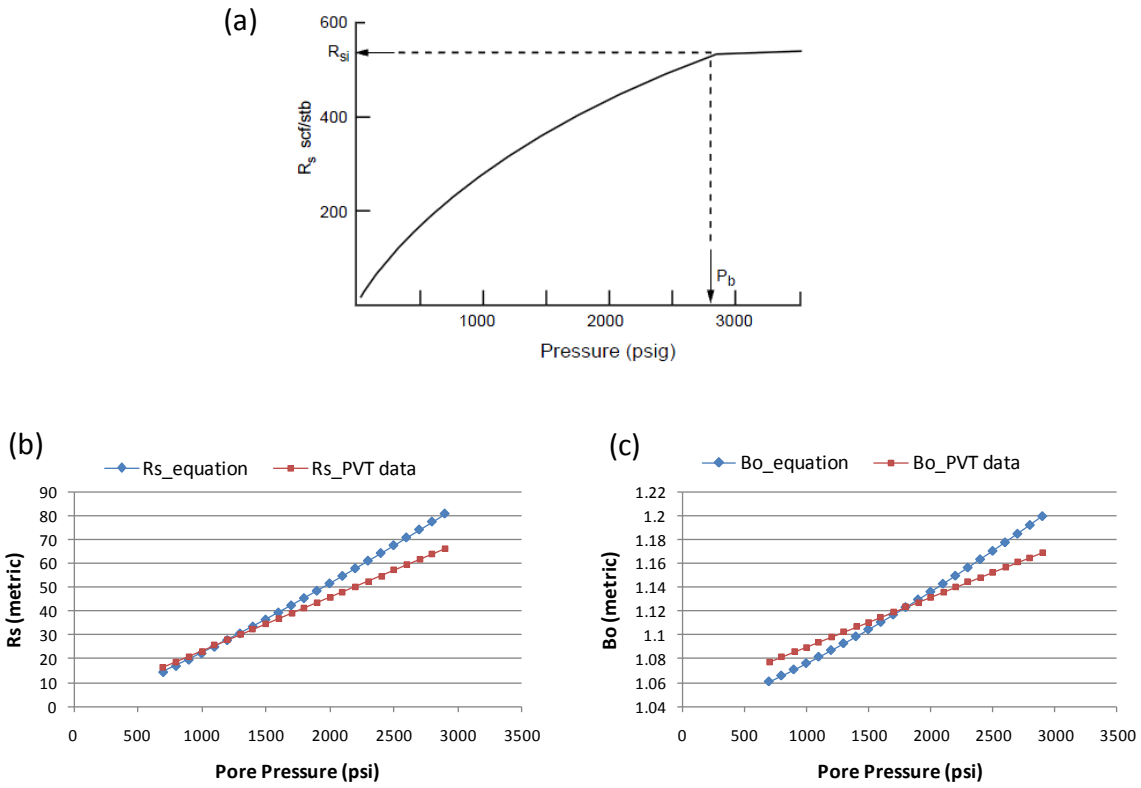

Figure 5.13 a) typical shape of R_s as a function of pressure (McCain, 1990, Batzle and Wang, 1992, Danesh, 1998 and Todd, 2007), b) R_s and c) B_o variation by pore pressure. Blue line is calculated using the proposed equations, while the red line is extracted from the PVT measurements.

(blue line). For computation of the oil bulk modulus and density, the proposed equations by Batzle and Wang (1992) are employed. There is a deviation by up to 30% between these two lines (orange arrows). The important issue is that the calculated R_s and B_o overestimates the pressure effect on the oil bulk modulus by up to 100%, which is not negligible (compare the length of light and dark green arrows). The second parameter is the oil density. As can be seen in Figure 5.14-b, there is a deviation by up to 25% between these two lines. The calculated R_s and B_o overestimates the pressure effect on the oil density by up to 90%. As was discussed in the previous section, oil pressure dependency is the main controlling factor for the saturated rock's pressure dependency in the oil leg.

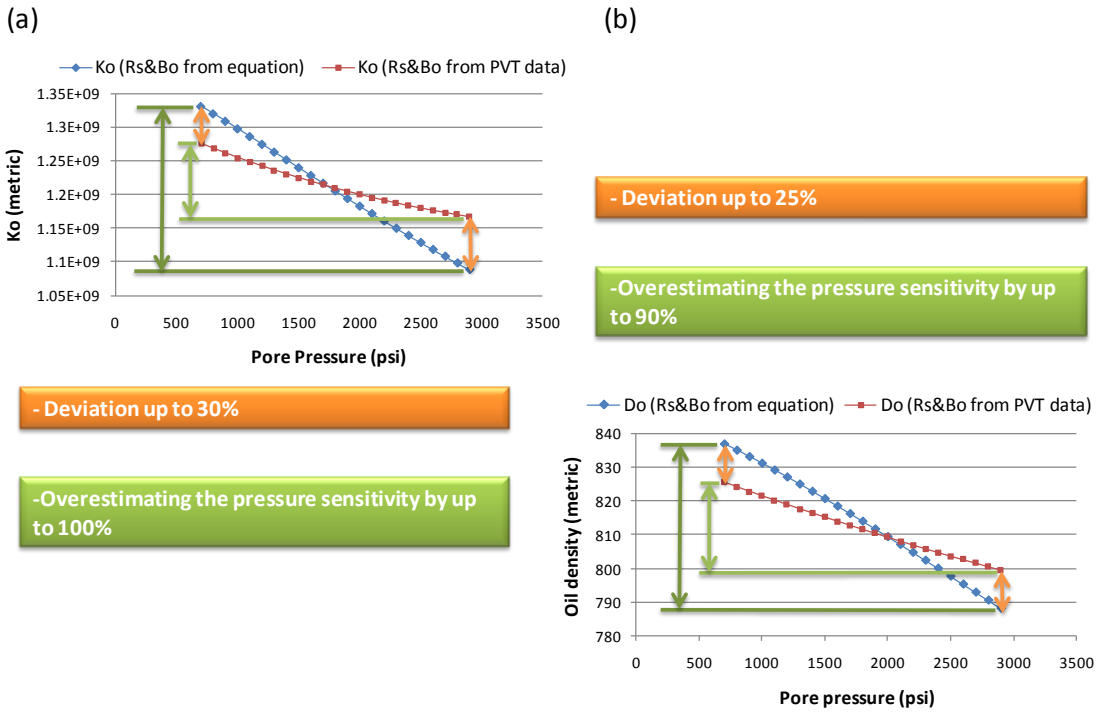

Figure 5.14 a) Oil bulk modulus and b) oil density variation with pore pressure. Oil density and bulk modulus are calculated using calculated R_s and B_o (blue line) and measured R_s and B_o (red line).

The next question is the validity of the R_s equation during the gas dissolution stages. In the laboratory, R_s is measured at different pressures. As presented on Figure 5.13-a, R_s decreases by pressure drop and increases by pressure increase. This process is reversible. However, the story is different for the reservoir scale versus the laboratory scale. To investigate this subject, the synthetic simulation model that was discussed in section 5.3 and presented in Figure 5.6 is employed. At the production period (pressure drop stage), gas comes out of solution and R_s decreases gradually (Figure 5.6-a). It follows the red line on Figure 5.15-a and green line on Figure 5.15-b for the gas cap and oil leg respectively. In fact the trend and story are the same as predicted in the laboratory.

For the injection period (pressure build up), the R_s behaviour is different for the gas cap and oil leg. Within the gas cap, we already have two necessary conditions for the dissolution process: pressure build up and free gas. Therefore the conditions are the same as the laboratory and gas has dissolved. In this case R_s increases back to the original value (Figure 5.15-a). The scenario is slightly different for the oil leg. As discussed earlier in section 5.3,

once the pressure starts to increase, residual gas saturation within the oil leg is dissolved but this cannot change R_s by a large amount. The same scenario occurs for an area around the injection well, because the injection force pushes the gas towards the western part of the reservoir, and there is insufficient gas to be dissolved. Therefore, the R_s variation in Figure 5.15-b is slightly raised during the first step, then is constant with pressure build up (blue line on Figure 5.15-b). It does not follow the same line as the exsolution stage. R_s never arrives back at the original value and there is a big deviation. Therefore, the laboratory based Equation 5.1 is not valid at the reservoir scale during the injection period.

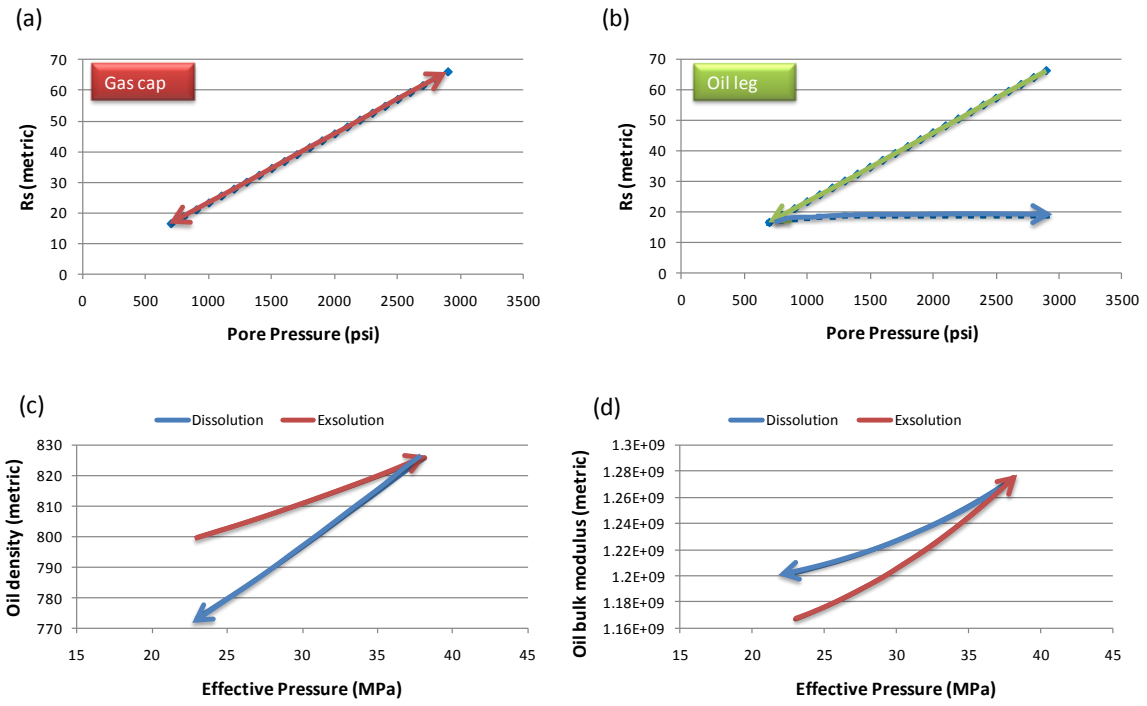

Figure 5.15 R_s variation with pore pressure for a sample from a) gas cap and b) oil leg. c) oil density and d) oil bulk modulus versus effective pressure variation for pressure drop (exsolution) and pressure build up (dissolution) period.

The question to be highlighted here is: how much does this phenomenon affect the seismic properties of the oil. For this, two samples from the oil leg and gas cap of the Schiehallion oil field simulation model were chosen to be separately discussed. For the sample from the oil leg, oil density increases along the red line with pore pressure drop (Figure 5.15-c). However, for water injection period (pressure build up), the oil density does not follow the

same path as at the exsolution stage (blue line on Figure 5.15-c). Therefore, the pressure dependency of the oil density is significantly different during the gas exsolution and dissolution stages. The same scenario occurs for the oil bulk modulus (Figure 5.15-d). During water injection for pressure build up, the oil bulk modulus does not follow the same path as at the exsolution stage (blue line and red line respectively). However, this pressure dependency is reversible for a sample from the gas cap.

Table 5.2 summarises the discussion above about the solution gas oil ratio. Our investigations highlight the need for careful interpretation of the 4D seismic signals for a reservoir in which pressure has gone below the bubble point pressure. That may prevent employing the same stress sensitivity for the saturated rock for the pressure drop and pressure build up scenarios when below the bubble point pressure. It is also suggested that the measured R_s and B_o values, or simulated ones (using a numerical simulation model) can be directly used during seismic forward modelling (simulation to seismic modelling). This is because the proposed equations for the calculation of the R_s and B_o contain considerable error during the gas exsolution stage. They are not even valid at the reservoir scale during gas dissolution stages.

At the gas exsolution stage	The R_s equation with pressure introduces up to 30% error in the properties of the oil.
	The R_s equation increases the pressure sensitivity of the oil by up to 100%
At the gas dissolution stage	The R_s equation with pressure is not valid at the gas dissolution stage.
Main conclusion	The seismic properties of the oil do not follow the same path on pressure build up (dissolution) as pressure drop (exsolution).

Table 5.2 Summary table of the discussion about the validity of the R_s equation.

5.7 The effect of the hydrocarbon compositional change on the seismic properties

As was mentioned in Chapter 2, there is composition change in both oil and gas during the gas exsolution stages. The normal phase diagram for the fluid is a composite curve fit of the phase diagrams for the components, say C_1 to C_n. Different phase diagrams as well as

bubble point pressures exist for different components. For example, from the ethane-heptane system (Figure 5.16-a), the bubble point pressure of C_1 is the highest of all, and therefore the bubble point pressure will be reached rapidly by a pressure drop. Therefore liberated gas is mainly C_1. With more pressure drop, the bubble point pressure of C_2 and C_3 is reached at the second and third steps also. Then, the liberated gas will be a mixture of C_1 to $C_{3,}$ and so on. Thus, the composition of the liberated gas changes from the lighter components at the primary stages to the heavier components at further steps (Danesh 1998). In addition, the composition of the oil changes as well. It is lightest at the initial pressure, and becomes progressively heavier with pressure drop, because it releases its lighter components. Figure 5.16-b illustrates the behaviour of a hydrocarbon above the bubble point pressure that is converted to gas and liquid phases by passing through the bubble point pressure, as discussed above. This understanding highlights the conclusion that assuming a constant gas and oil composition in 4D seismic studies may not be valid.

In black oil modelling, the above scenario is simulated using the R_s concept. Here, a binary system is designed (oil and gas), and gas exsolution stages are simulated using different solution gas oil ratios. Figure 5.16-c shows the process of gas exsolution from black oil model concepts. The initial oil contains a specific solution gas ($R_{s\text{-}i}$). Arriving at the bubble point pressure, part of the solution gas has evolved, but the rest of the gas is still in the liquid phase. Constant gas composition has been assumed for the gas phase. Thus, with pressure drop, more gas is exsolved and R_s decreases as the liquid phase releases the solution gas. Therefore the volume of the free gas is enlarged, while the solution gas (R_s) is reduced. The challenging question is: how accurately can the R_s concept cover the compositional change of the liquid phase?

By taking into account the above discussion, some important questions can be raised here:

- How much is the compositional change of the gas and oil?
- How big is the effect of the compositional change on the elastic properties of the gas and oil?
- Can we use the R_s concept to correct this change for oil (black oil modelling)? Because industry is not interested in the complication of reality, we need to quantify the order of the deviation and error by employing the black oil model to decide about the applicability of black oil modelling. Compositional modelling is difficult,

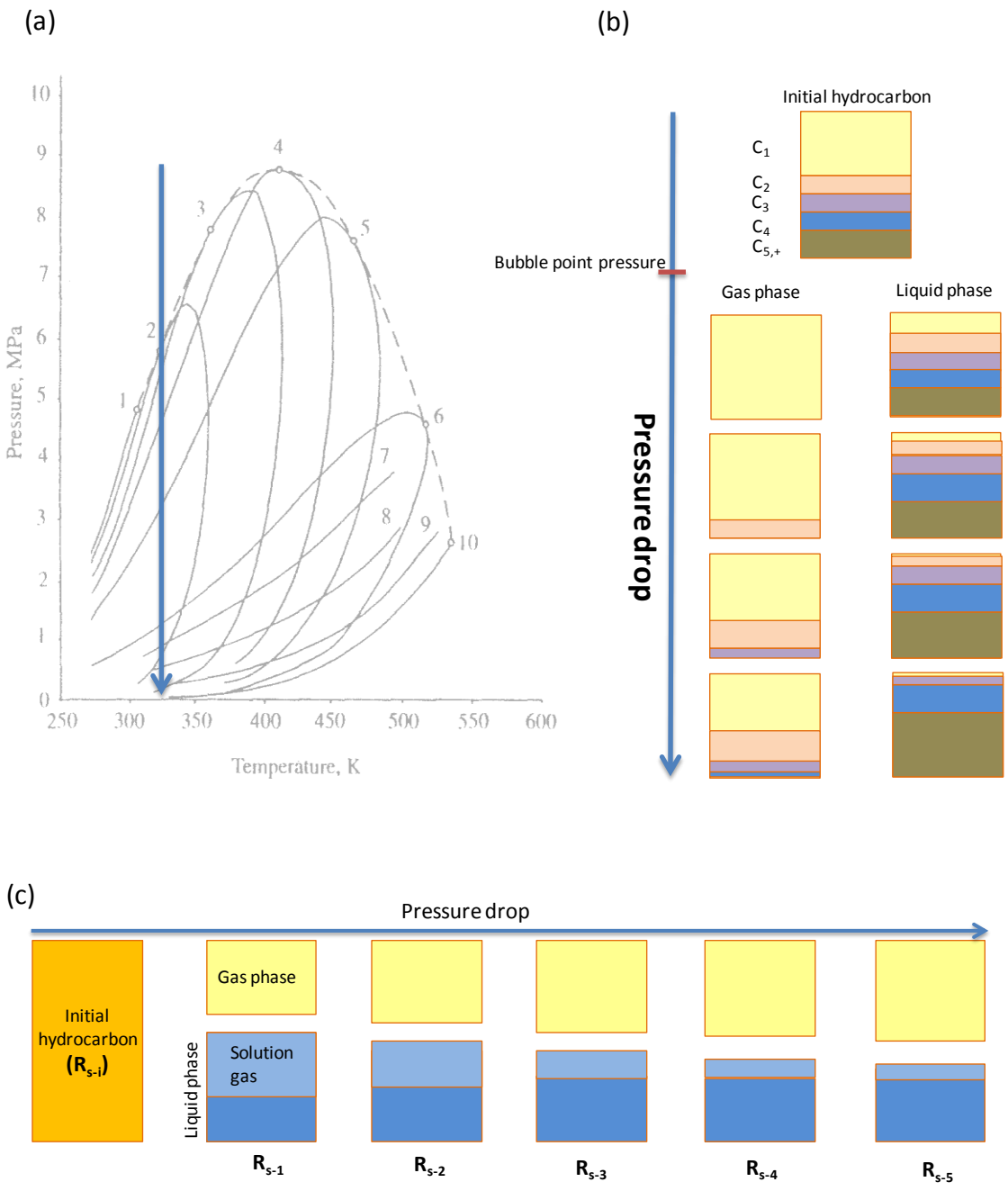

Figure 5.16 a) Phase diagrams of an ethane-heptane system (Danesh, 1998), b) and c) are the schematic modelling of the pressure drop and gas exsolution using the compositional and black oil concepts respectively. Volumes are schematic only.

time consuming, and needs more inputs than we may have access to (in the compositional modelling the percentage of the C_1 to C_n are calculated for both gas and fluid phases using equation of state (multi-component system), while in the

black oil modelling only the percentage of the gas and fluids are calculated (two-component system)).

To answer these questions, the composition of an oil has been received from the data provider. PVTi software is used for fluid simulation. The PR3 equation of state (three parameter Peng-Robinson, and the most popular in the PVT engineering domain), is employed in this procedure. Subsequently, the equation of state is fitted using the software. The resultant equations of state are validated by some accessible experiments (bubble point pressure and R_s values). Both flash liberation and differential liberation tests are implemented using the equation of state, but only the differential liberation test is used in the rest of the work. This is because we need to consider the effect of the maximum compositional change, and this test supports our aim. Under reservoir conditions, the compositional change is less than that given by the differential liberation test. This is because the liberated gas is mixed with the previously liberated gas. There is also production of both gas and oil, which alters the composition.

After simulating the pressure drop using the equation of state, the percentages of C_1 to C_n are extracted for both gas and liquid phases. Figure 5.17 illustrates the results for gas. As is expected, the percentage of C_2, C_3 and C_4 and other heavier components increase with pressure drop and, therefore, the percentage of C_1 decreases. The result of this phenomenon is that gas is heavier step by step with pressure decrease. This is consistent with the scenario presented in Figure 5.16-b. To quantify the magnitude of the compositional change on the gas phase, gas gravity and gas density are calculated (Figure 5.18-a and b). A small increase of the gas gravity (0.6% for a pressure drop of up to 1500 psi) is observed. The gas density variation by pressure (red line on Figure 5.18-b) is decomposed into the pressure and compositional effects. The pressure drop decreases the gas density (green line) as it enlarges the distance between the molecules. However, compositional change causes an increase of the gas density (blue line).

The density variation of the saturated rock is also calculated to examine the effect of the gas compositional change on the density of the saturated rock. A variation of less than 0.01% is observed, and this is too small to worry about in 4D seismic. It should be noted that, because of the use of the differential liberation test, this compositional variation is the

maximum variation. In conclusion, it appears that, by assuming a constant gas composition in the black oil model, we are safe enough.

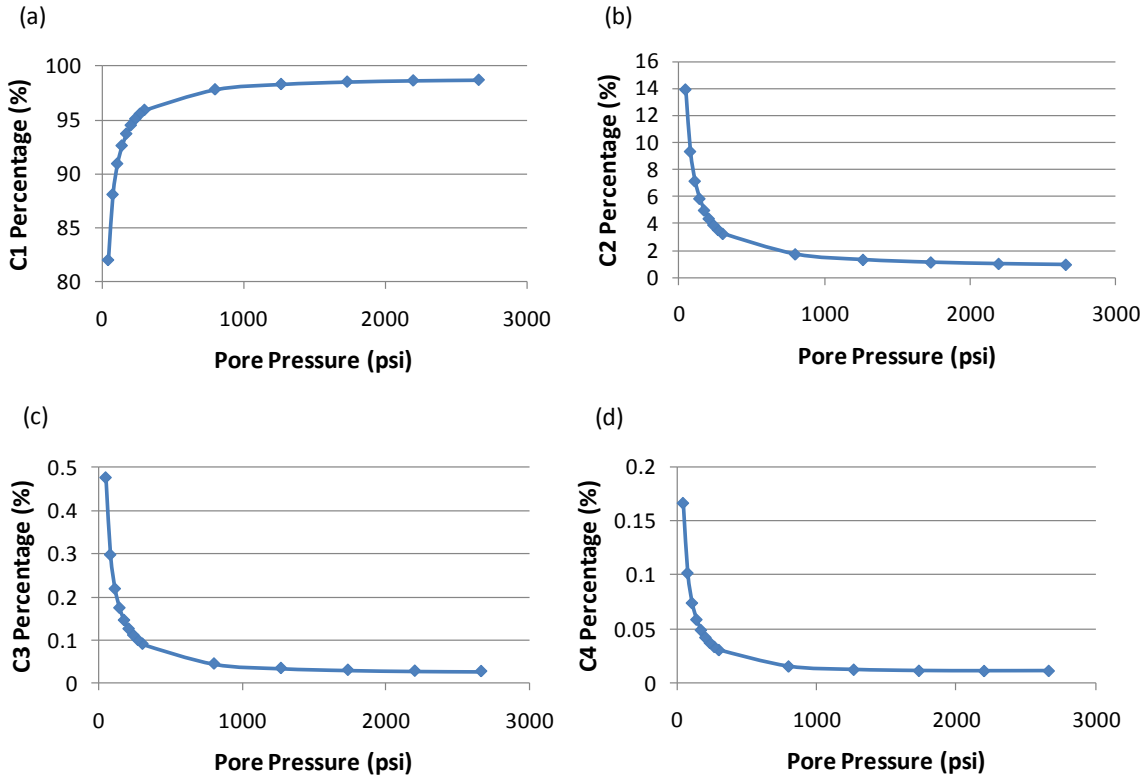

Figure 5.17 The variation of a) C_1, b) C_2, c) C_3, and d) C_4 with pressure drop in the gas phase.

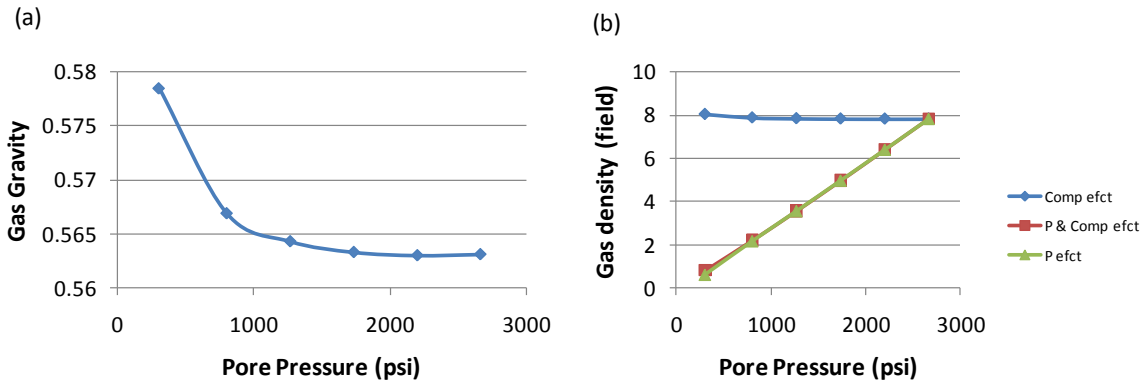

Figure 5.18 a) Gas gravity and b) gas density versus pressure variation. The effect of composition (blue line) and compressibility (red line) due to the pressure variation has been decomposed here.

The next stage of the modelling is the effect of the oil compositional change on the elastic properties. A percentage of C_1 to C_n are extracted from the liquid phase after simulating the pressure drop using the equation of state, with Figure 5.19 illustrating the results for oil. This is consistent with our interpretation and explanation of the phase diagram. As is expected, the percentage of C_1 goes down with pressure drop, the percentage of C_{3+} increases with pressure drop, however C2 shows a build up and then decline with pressure drop. The composition of the liquid phase changes from the lightest component during the primary stages to the heavier components in the last stages, so oil is going to be heavier step by step with decreasing pressure.

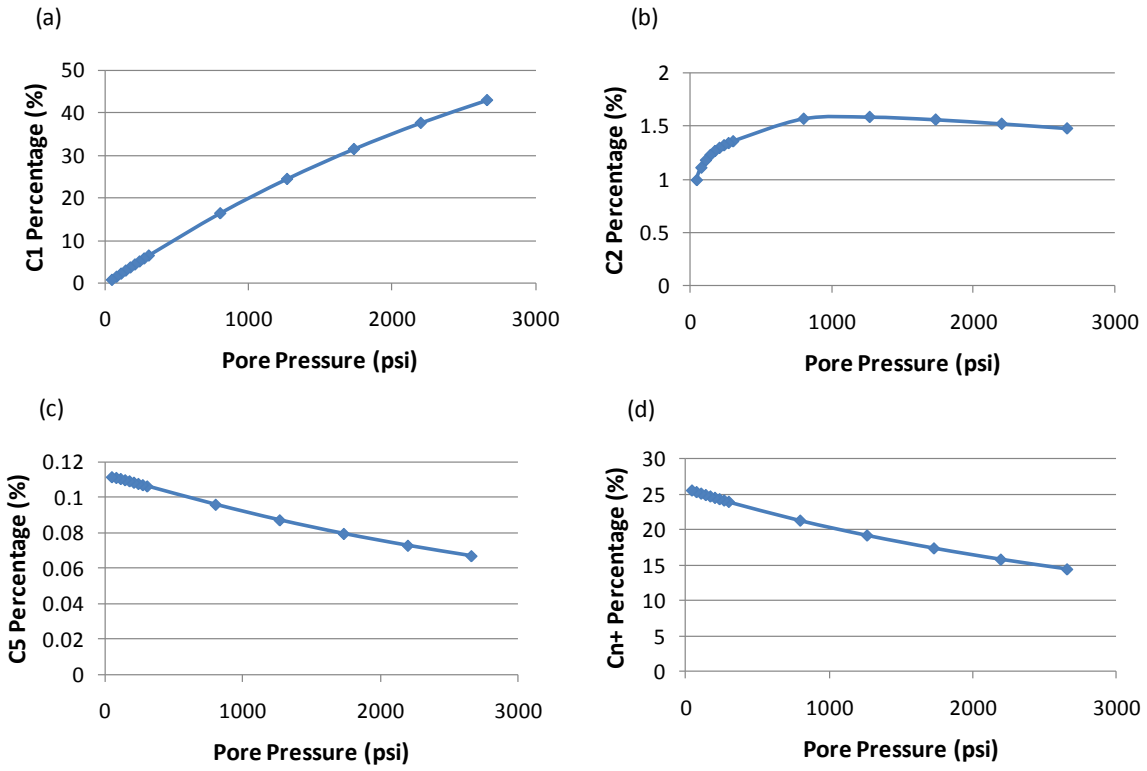

Figure 5.19 The variation of a) C_1, b) C_2, c) C_5, and d) C_n with pressure drop in the liquid phase. The combination of components highlights the increasing oil density with pressure drop, as the lighter components have decreased and the heavier ones have increased.

The oil molecular weight and density are calculated to quantify the order of the composition change (Figure 5.20-a and b). Oil molecular weight is affected by only compositional change, while the oil density is varied because of both pressure and

compositional change. As discussed earlier, the effect of these items is opposed, but compositional change wins. As a conclusion, a considerable compositional change is observed in the liquid phase that can affect the elastic properties. The question for oil is slightly different from gas, as the effect has been accommodated by the black oil model - the R_s concept tries to take into account this change (Figure 5.16-c). The question is, how valid is the R_s concept?

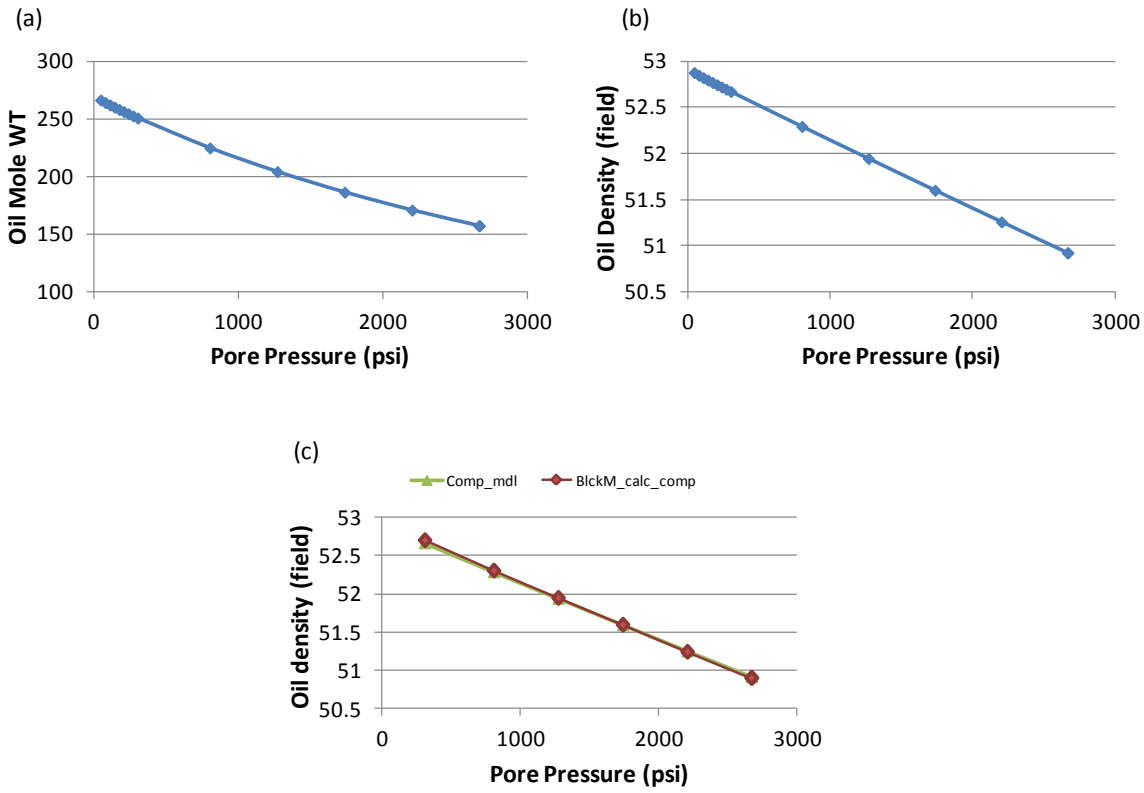

Figure 5.20 a) oil molecular weight and b) oil density versus pressure variation, c) oil density calculated from the black oil (red color) and compositional model (green color) plotted versus pressure variation.

To test the above, a black oil model was built using a compositional model to compare the oil density variation. After simulating the pressure drop, oil density is separately calculated for both compositional and the black oil model. Figure 5.20-c demonstrates the oil density calculated using the output of the compositional (green line) and black oil (red line) modelling. There is an excellent match and it can be stated as a conclusion that employment of the solution gas oil ratio in the black oil modelling can cover the oil compositional

change during gas exsolution stage adequately. However, as discussed in the Section (5.6), most of the seismic properties of live oil are related to R_s, so use of the proposed equations for calculation could be a source of error (Figure 5.13, 5.14 and 5.15). As is shown in Figure 5.14, there is a deviation by up to 25% for the oil density if the proposed equations in the literature are used for calculation of R_s. These equations are not valid at the gas dissolution stage. R_s and B_o should be directly extracted from laboratory measurements or from a good simulation model.

For gas	Composition of the gas changes during reservoir pressure drop.
	The compositional change of gas is negligible in the seismic domain (it is less than 0.01% of the density change of the saturated rock).
For oil	Compositional change of the oil is considerable during reservoir pressure drop.
	Solution gas-oil ratio (R_s) can properly cover this compositional change of the oil.
	R_s needs to be treated appropriately to cover the compositional change of the oil.
For gas condensate	A significant compositional change has been reported in the literature, so we need to take into account this compositional effect in gas condensate reservoirs.

Table 5.3 Summary of the discussion of compositional change for gas and oil.

The discussion provided here is valid for black oil and volatile oil reservoirs - more data sets are required to confirm it with certainty, but we believe that this can be generalised for reservoirs similar to those used here. However, gas condensate reservoirs are different, and the temperature and pressure of these reservoirs are above the critical point (C_p). In this case, the hydrocarbon is in the gas phase at reservoir conditions. With pressure drop, we reach the dew point line (not the bubble point line as previously). Now, the heaviest components are shifted from the gas phase to the liquid phase. The percentage of the liquid phase is increased with pressure drop. Gas releases its heavier components, so it becomes lighter step by step. The compositional change for the gas phase seems to be significant. Considerable variation of the elastic properties of gas condensate has been reported in the literature. Waggoner *et al.* (2002) observed a 3.6% drop in I_p with pressure drop.

Considerable variation of the elastic properties of gas condensate is reported by Hamdi *et al.* (2011). Our conclusion for the gas condensate is that compositional modelling, or a correction factor (like R_s in the black oil model), is probably necessary (is proposed for the future work). Table 5.3 summarizes the discussion above regarding compositional change of the gas and oil during reservoir pressure drop.

5.8 Summary

The basic concepts of gas liberation are understood using engineering literature. It is found that released gas migrates after arriving at the critical gas saturation, and this causes two sets of gas saturations in the reservoir: maximum gas saturation within the gas cap and critical or minimum gas saturation within the oil leg. Therefore, a similar saturation conclusion is reached as in the gas injection process discussed in previous chapters. Thus, the 4D seismic signal is due to the variation of the gas thickness. The effect of reservoir scale parameters on gas dissolution is also taken into account. It is found that it is not only the fluid type that impacts the gas when it goes back into solution, but also other reservoir properties such as relative permeability curves, transmissibility, K_v/K_h, and the injection/production plan.

Investigation of the effect of gas exsolution and dissolution on the pressure dependency of the fluid and rock highlights the fact that the pressure effect on fluid and rock has different signs. Furthermore, the laboratory based stress sensitivity of the sand is not valid in some cases in which the reservoir pressure drops below the bubble point pressure. In this situation, gas evolves and alters the pressure dependency of the saturated rock.

The solution gas oil ratio (R_s) is a main parameter that simulates the gas liberation in the black oil model, and is on the centre of the Petro elastic modelling. The proposed equation for calculation of the R_s introduces considerable error (up to 30%) on the seismic domain during gas exsolution. It is also noticed that these equations are not valid at the gas dissolution stage, as evolved gas has migrated and there is no gas to be dissolved in oil by pressure build up.

The magnitude of the compositional change is discussed as the last section of this chapter. The percentage of the heavier components in both gas and oil is raised with pressure drop. However, this variation is very small for the pressure drop range of our case study. The effect of compositional change is very small (perhaps negligible) in the seismic domain. Because of the low compositional change of the gas phase, it is found that employing a solution gas-oil ratio (R_s) to simulate gas liberation in the black oil model is still valid for the seismic domain.

Chapter 6

Adaptive scaling for an enhanced dynamic interpretation of 4D seismic data

In this study, importance is drawn to the role of engineering principles when interpreting dynamic reservoir changes from 4D seismic data. In particular, it is found that, in clastic reservoirs, the principal parameters controlling mapped 4D signatures are not the pressure and saturation changes *per se*, but these changes scaled by the corresponding thickness (or pore volume) of the reservoir volume that these effects occupy. For this reason, pressure and saturation changes cannot strictly be recovered by themselves, this being true for all data interpretation and inversion procedures. This understanding is validated both with numerical modelling and analytic calculation. Interestingly, the study also indicates that the impact of gas saturation on the seismic can be written using a linear term, but that inversion for gas saturation can yield at best only the total thickness/pore volume of the distribution. The above provides a basis for a linear equation that can readily and accurately be used to invert for pressure and saturation changes. Quantitative updates of the static and dynamic components of the simulation model can be achieved by comparing thickness or pore volume-scaled changes from the simulator with the corresponding quantities from the inverted observations.

6.1 Introduction

A widely recognised benefit of 4D seismic surveying is the ability to estimate reservoir pressure and saturation changes of the fluid constituents between wells and across the field. From the reservoir engineering perspective, this process is invaluable for updating the flow simulation model, as it can provide aerial information on reservoir connectivity, barriers and conduits. Indeed, there are many clastic reservoir examples where pressure up (Alsos *et al.*, 2009), pressure down (Fletcher, 2004) or saturation changes (Staples *et al.*, 2006) have been directly inferred from 4D seismic during production and recovery. In critical areas where pressure and saturation changes overlap their 4D seismic signatures significantly, specialised inversion techniques have also been developed to provide some degree of separation (for example: Tura and Lumley, 1999; Landrø, 2001; MacBeth *et al.*, 2004). Inversions are also possible in the presence of free gas (Floricich *et al.*, 2006) and, in this case, it is believed that a nonlinear gas saturation equation is required. In this current study, importance is drawn to the role of engineering principles when interpreting and estimating such dynamic information from the seismic. In particular, it is known that pressure spreads across and down through the reservoir at a faster rate than the fluids can move, and is relatively insensitive to net-to-gross variations, thus the vertical distribution of influence for each physical field is not the same. The thickness ranges over which pressure, water saturation or gas saturation effects spread are distinctly different, and may also not agree with the total reservoir (interval) thickness as defined geologically. It is therefore our understanding that the pressure and saturation changes influence the observed 4D signatures principally through their scaling with the corresponding vertical thickness distribution, or more correctly, their overall pore volume of influence. For amplitudes, this adaptive scaling phenomenon is loosely analogous to 4D tuning. It is shown here that an understanding of these overlapping effects and the scaled pressure and saturation changes as the controlling parameters for mapped time-lapse seismic can lead to a clearer, more quantitative, and linearised interpretation, and leads naturally to pressure and saturation change inversion.

6.2 Description of dataset

To study the phenomenon described above, we focus on a 4D seismic dataset from the North Sea, for which a well-founded, fine-scale reservoir simulation model is also available (Martin and MacDonald, 2010). The Schiehallion oil field, discovered in 1993, lies 200km west of the Shetland Islands in 350m water depth (Figure 6.1). The field has been operated by BP since field start-up in 1998. The reservoir comprises a complex Lower Tertiary (T25 to T35 age) sequence of deep marine siliciclastic turbidites (Martin and MacDonald, 2010). The field is segregated by a series of east-west trending normal faults, which divide the reservoir into five distinct segments with limited or no lateral communication. This character of the field enables us to select a single segment (segment 1, Figure 6.1) to act as a manageable dataset for our study.

The main geological interval, T30, was subdivided by the operator of the field into a number of sequences using the well and seismic data evaluation. Within these sequences there are three separate sandstone units, T31, T34 and T35 (Figure 6.1 and 6.2). It is these sandstone packages that form the reservoirs of the Schiehallion (Martin and MacDonald, 2010). Reservoir quality varies in character from thinly inter-bedded sands and shale to massive sands, with the massive sands being of better quality (high permeability and effective porosity). Typically, the sands are fine to medium grained (Smith *et al.*, 2000). Of particular interest here is the producing T31 interval (Figure 6.1), which forms a sheet-like unit, of typically 10 to 50m thick (Smith *et al.*, 2000), that can be mapped on the seismic over a large proportion of the chosen segment. The T31 exhibits large seismic amplitude variations (Figure 6.2 and 6.4) due to net sand thickness fluctuations, with the higher net-to-gross portions indentifying the multistory and multilateral channel complexes which run in the general direction southeast to northwest (Figure 6.2-c) (Martin and MacDonald, 2010). Most of the channels illustrate vertical and lateral stacking of channel storeys in the wells and in the seismic sections. These high NTG channels demonstrate up-dip and down-dip pinch-out (Smith *et al.*, 2000). The channels are sharply separated by areas of less than 0.2 NTG. The strong heterogeneity in vertical and lateral connectivity ultimately effects how the pressure and fluids spread across the reservoirs.

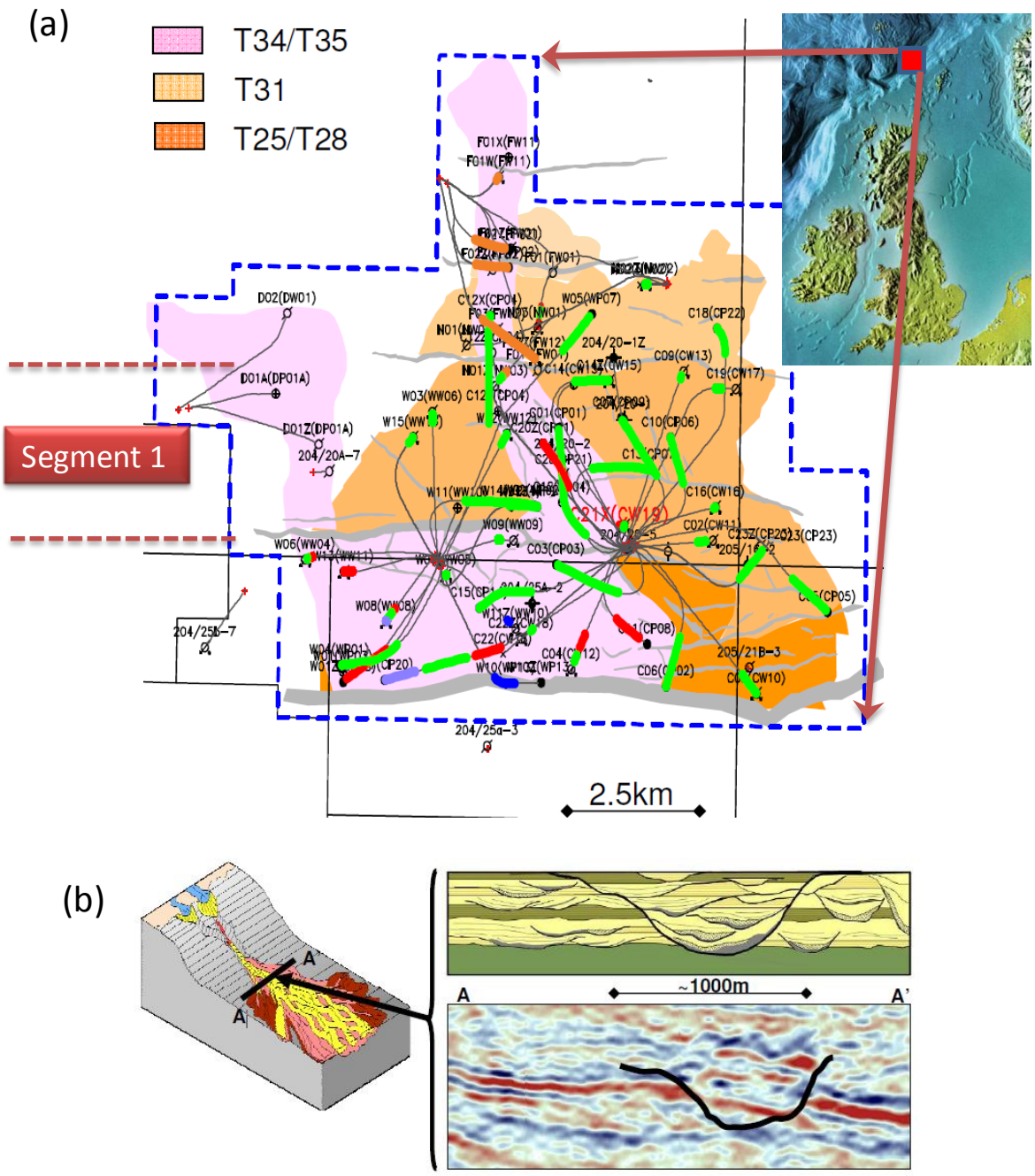

Figure 6.1 a) the location of Schiehallion oil field with the sedimentary layers (as label) overlain by faults (grey colour) and wells (black colour). The position of segment 1 is also shown. b) Channelised structure of the sediments (after Martin and MacDonald, 2010). These channels, which can be observed in the seismic data, are picked and directly imported into the geological model.

The Schiehallion reservoir fluid is single phase black oil with gravity in the range of 22 to 28 API. Initial reservoir pressure is 2907 psi (at 1940m TVDss). Bubble point pressure and gas oil ratio (GOR) are 2824 (at 1869 TVDss) and 340 scf/bbl respectively. Oil and water

viscosities are 3.5 cp and 0.5 cp respectively, at a temperature of 58 degrees centigrade (Martin and MacDonald, 2010). The considerable uncertainty in PVT properties obtained due to the difficulty in achieving single phase samples as the reservoir fluid is close to bubble point pressure, the imprecision of laboratory measurements, and a probable change in fluid composition with depth (Richardson *et al.*, 1997).

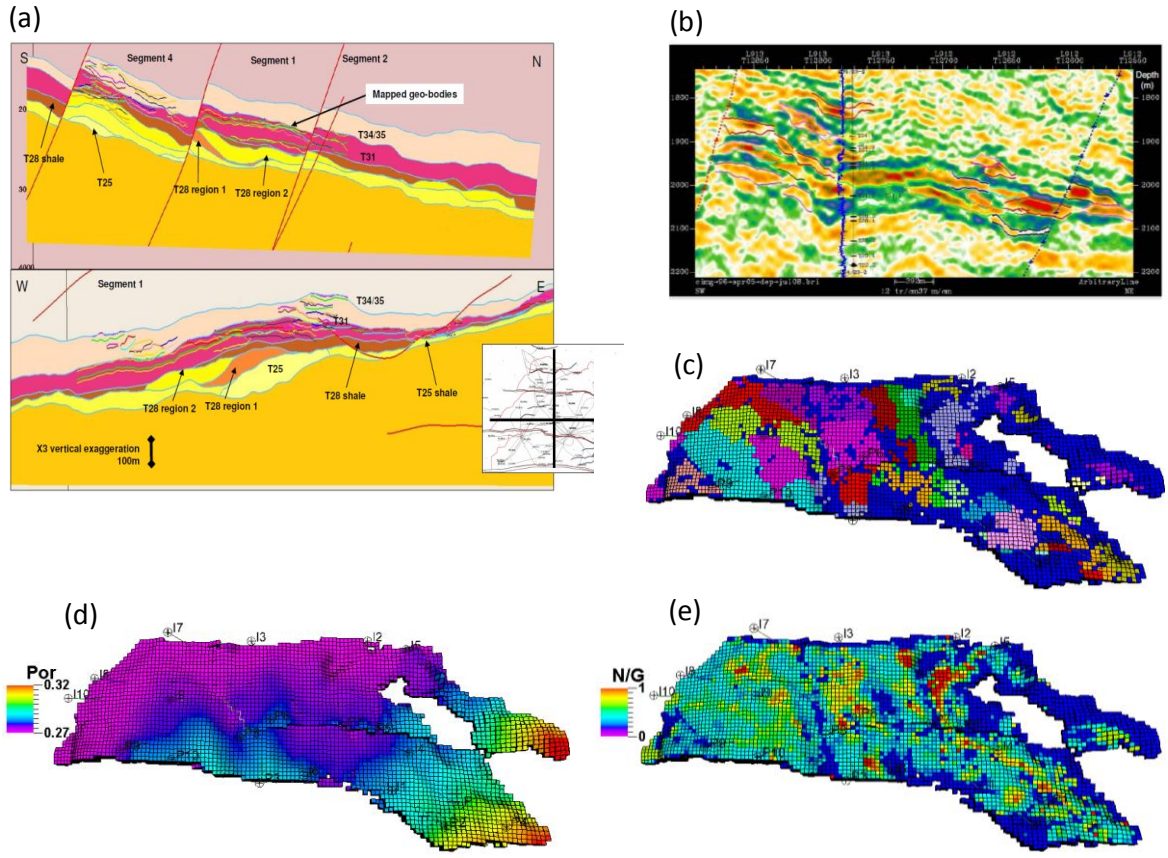

Figure 6.2 a) two geological cross sections with the sets of sealed faults that divide Schiehallion into different segments. By employing the seismic and well data b), the area was divided into different seismically identified 'geobodies' (after Martin and MacDonald, 2010). c) These seismically geobodies control the connectivity and fluid flow in the reservoir. d) and e) are the porosity and net to gross of the Segment 1 from the simulation model.

Connectivity between seismically geobodies (Figure 6.2-c) was a main challenge during the field life. The results from the Extended Well Test (EWT) in 1996 suggested that the field was well connected. However, it was later noticed that the EWT results were affected by an unrevealed gas cap close to the EWT well (Govan *et al.*, 2005). A few months after

production started, the connectivity was found poorer than expected. The large areas of the reservoir were not accessed by the preliminary development wells (Martin and MacDonald, 2010). It was rapidly noticed that various producers did not obtain sufficient pressure support. Accordingly, the gas oil ratio (GOR) climbed quickly. The reservoir management strategy was mainly about gas management for the first 3-4 years (Figure 6.3) (Govan *et al.*, 2005). By the efficient use of 4D seismic and pressure data to recognize connectivity, new wells were drilled and the injection plan was improved to recover the reservoir pressure and control the GOR (Govan *et al.*, 2005). The pressure regime and fluid flow were understood mainly by 4D seismic data over the field life of 14 years (up to date). A new Schiehallion model was built to capture reservoir compartments at completion interval scale (Martin and MacDonald, 2010). The interpretation of an integrated well log and seismic dataset allowed the operator to categorise the seismically geobodies that establish individual, intra-reservoir, pressure compartments.

Although there are multiple vintages of seismic shot across this field (Huang *et al.*, 2011), for the purposes of this work the baseline 1998 and monitor at 2002 are selected as they highlight large pressure changes in combination with gas out of solution. The seismic is a coloured inversion product provided by the operator, and thus is in essence relative impedance – the layers are observed as troughs in the seismic sections. The T31 interval can be further subdivided into the T31a and T31b, the latter of which does not fully cover the chosen segment. The top and base T31a and T31b were picked by the operator as zero crossings on the data in combination with wireline log data (Martin and MacDonald, 2010, see Figure 6.4). For the purposes of the analysis, the sum of the negative amplitudes between top T31a and base T31b is calculated separately in baseline and monitor seismic and a signed difference map obtained (Figure 6.4-c). In addition, mapped time-shifts for the T31 reservoir interval are also calculated by taking the difference between the time thicknesses of the top T31a to base T31b interval. For the synthetics considered below, this is achieved by using picked horizons common to both datasets. For the observed data, this is performed using code based on the work of Hale (2007), as implemented by Garcia *et al.* (2011).

Figure 6.3 illustrates the depth average maps of the pressure change, water saturation and gas saturation change between 2002 and 1998. Due to the lack of connectivity between

injection and production wells, pressure depletion has been observed in the seismically geobodies around the production wells (e.g., south-east, south and central parts) and pressure build up around the water injection wells (e.g., west, North-west and North). In general, there is good consistency between water saturation increasing and pressure build up anomalies as well as between pressure depletion and exsolved gas anomalies (Figure 6.3). Pressure depletion below bubble point pressure due to production has resulted with the gas coming out of solution (Figure 6.3-c).

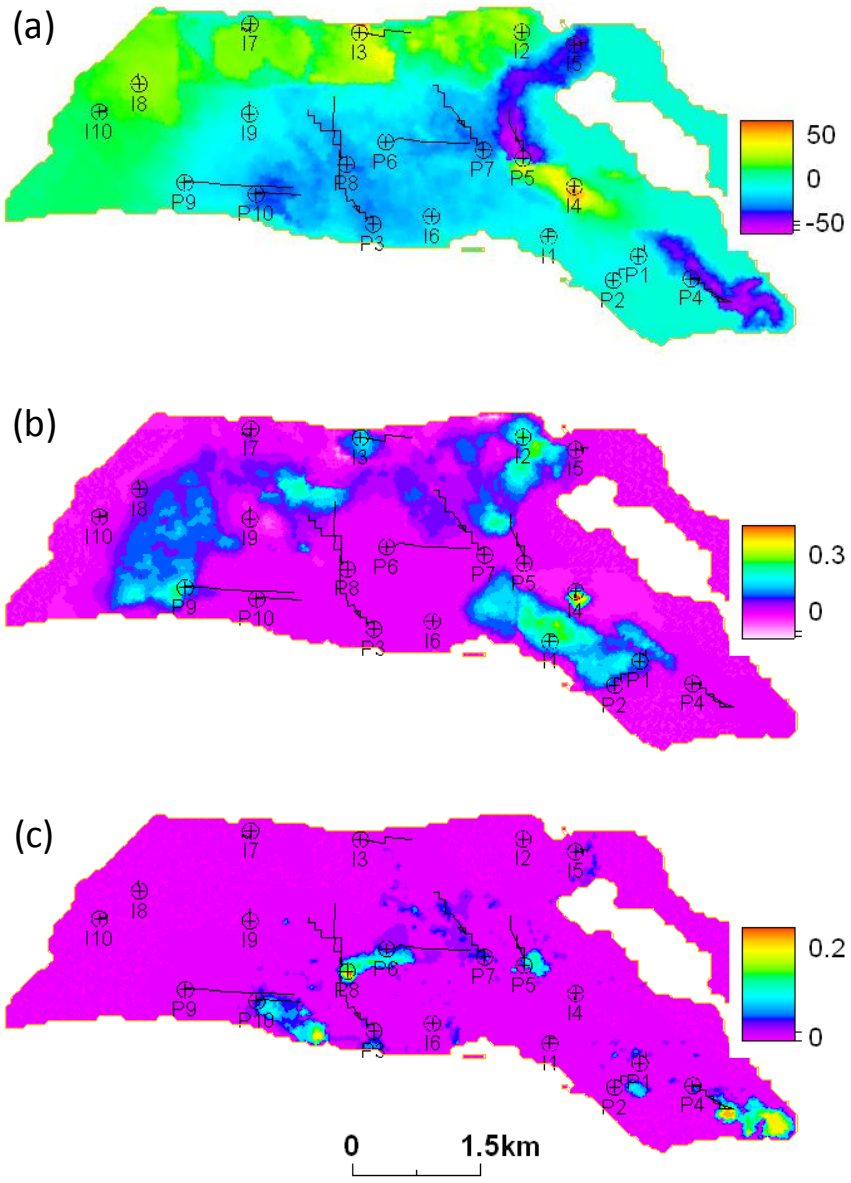

Figure 6.3 The depth average maps of the a) pressure change (bar), b) water saturation change (fraction), and c) gas saturation change (fraction) between 2002 and 1998.

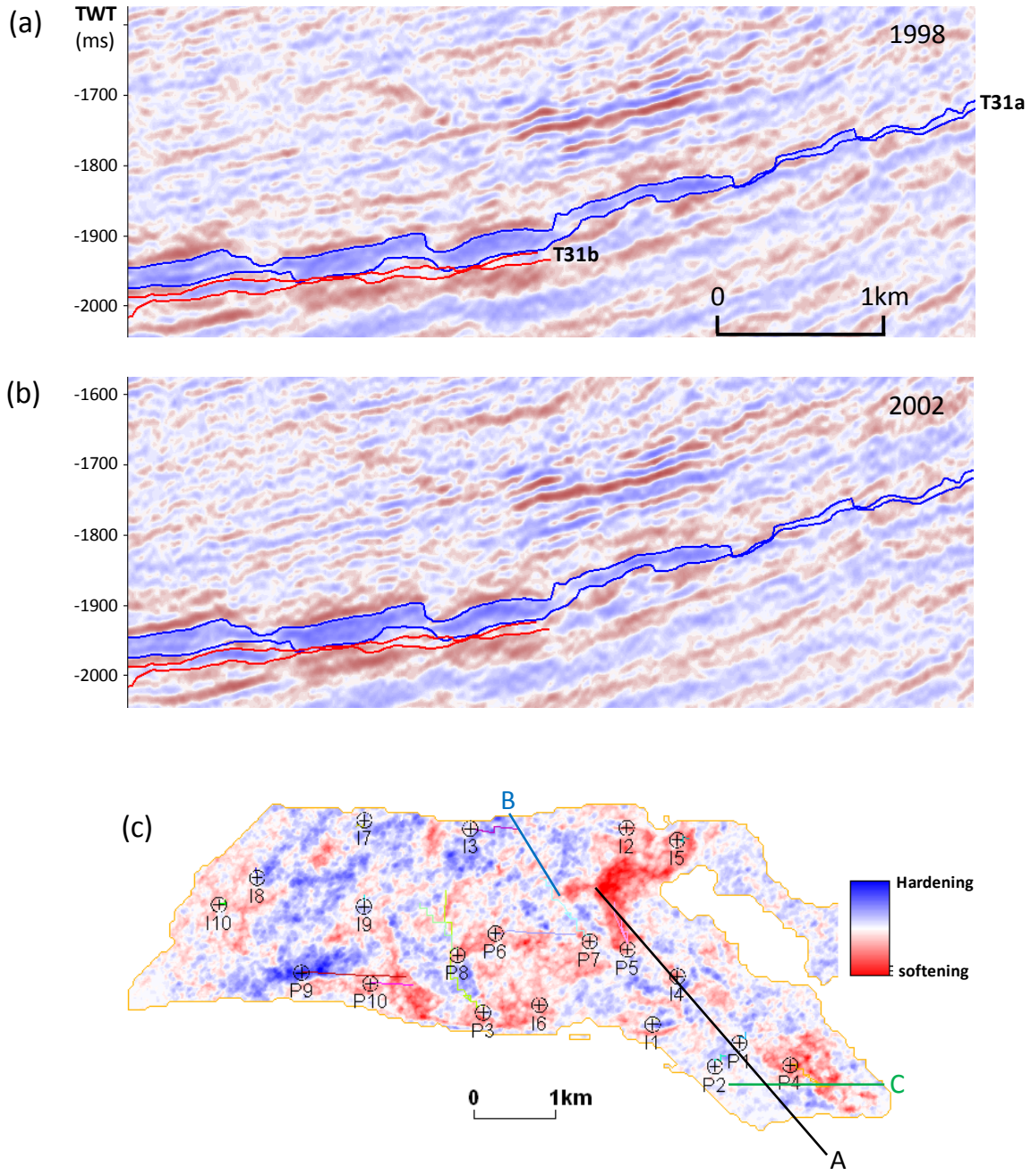

Figure 6.4 Seismic sections along line A on the a) 1998 (before production) and b) 2002 (4 years after production) in CIMG data with T31a and b horizons, c) 4D map of the sum of negative amplitude from top T31a to base T31b (between 2002 and 1998).

Qualitative interpretation of the 4D seismic maps point out good consistency with the general well activities (Figures 6.3 and 6.4). A gas-related (red softening response) signal is mainly observed around production wells P3, P4, P5 and P10 in the south, southeast and central portions of the segment. However, as the gas signal is a more localised

phenomenon, then it is usually surrounded by a more extensive blue hardening associated with the pressure down signal (see the south-eastern portion). Increases in water saturation cause a blue hardening response on the 4D seismic maps, which oppose the pressure up signal (red softening response) at the water injectors. However, the water saturation signal tends to dominate in this reservoir (Alvarez and MacBeth, 2011) and the blue hardening persists – see wells I2, I3, I7 and I10 in the north, northwest and western portions of the segment.

6.3 Relating pressure and saturation change to the 4D seismic signatures

Pressure and saturation changes are typically represented by reservoir engineers as absolute changes in a cellular model. For production-related measurements, the formation pressure change at the well is important. When these changes are visualised across the reservoir for management purposes, the depth average evaluated over the reservoir interval is mapped. Thus, for a particular location, if the pressure change occurs over a thickness h of the total reservoir interval H (Figure 6.5), the depth average $(h/H)\Delta P$ is visualised. Here, it is understood that h will vary with production time, as will ΔP, whilst H is a function of the reservoir geology. It has been the expectation of the seismic community that 4D seismic signatures must respond to this depth-averaged property and that this should therefore be used as an independent variable in seismic equations. This choice is rationalised by the fact that seismic, due to its wave behaviour, senses a depth-average of the reservoir properties and thus this definition appears at face value to be compatible. Indeed, time-lapse studies focussing on mapped changes have implicitly assumed depth average properties (for example, Landrø, 2001; Tura and Lumley, 1999; MacBeth *et al.*, 2004). Whilst such an approach appears encouraging, this particular choice is not the only one available, nor the most obvious choice. Another possibility as an independent variable is $h.\Delta P$. For this particular choice, the reservoir's geological variations are excluded. This is attractive in that the variable relates directly to production. In fact, the pressure change is scaled by its corresponding thickness. A third possibility is the $h.\phi.NTG.\Delta P$ where the change in pressure is now scaled by the pore volume, PV. Here ϕ is the sand porosity, NTG the net-to-gross of the reservoir interval occupied by pressure change. This is the proper physical

choice for both pressure and saturation, a fact well known in fundamental engineering literature (for example, Dake, 2002). Indeed, some evidence exists to indicate that *volumes* in general ('total fluid' or 'pore') are an important control on the 4D seismic signatures – for example, it has been recently shown that 4D seismic signatures are strongly correlated to well volume changes (Falahat *et al.*, 2011, Huang *et al.*, 2011). These arguments suggest the application of a principle of adaptive scaling to the principal parameters controlling the 4D seismic signature.

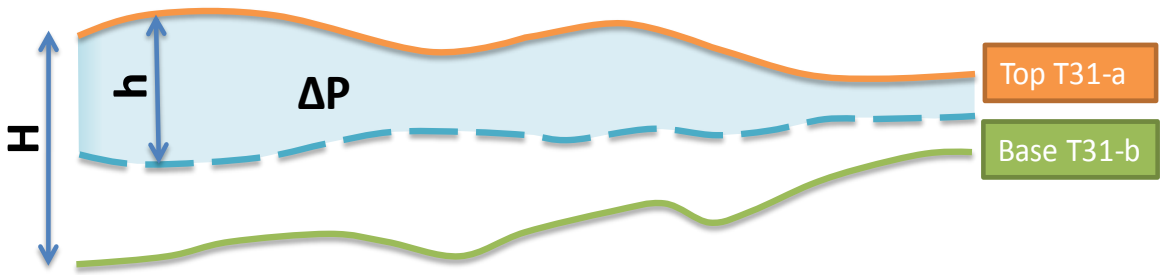

Figure 6.5 Schematic cross section representing two non-connective geobodies. Pressure change has spread over the upper geobody.

To understand how the suggested parameterisation above may relate to the seismic data, we now take a closer look at the way in which pressure and saturation behave. Figure 6.6 shows vertical cross-sections of the field simulation model for our area of study, together with the corresponding predictions of pressure, water saturation and gas saturation change between the 1998 (pre-production) and 2002 (post-production). Two cross-section locations are chosen in the reservoir to highlight the spatial variability. It is observed that the pressure change (Figures 6.6(a) and (e)) spreads uniformly both vertically and laterally across the reservoir, despite the obvious heterogeneity seen in the net-to-gross distribution (Figures 6.6(d) and (h)). Pressure changes typically occupy up to 75% of the total reservoir interval (up to 35m) due to vertical barriers. For the gas saturation (Figures 6.6(b) and (f)), however, the thickness occupied by the gas volume is a smaller proportion of the total vertical interval (30% or up to 13m) and much more variable across the segment. This effect is due to the timing of the gas exsolution relative to the seismic monitor, the volume of gas liberated from the oil, and the amount of gas produced at the well. For the water -

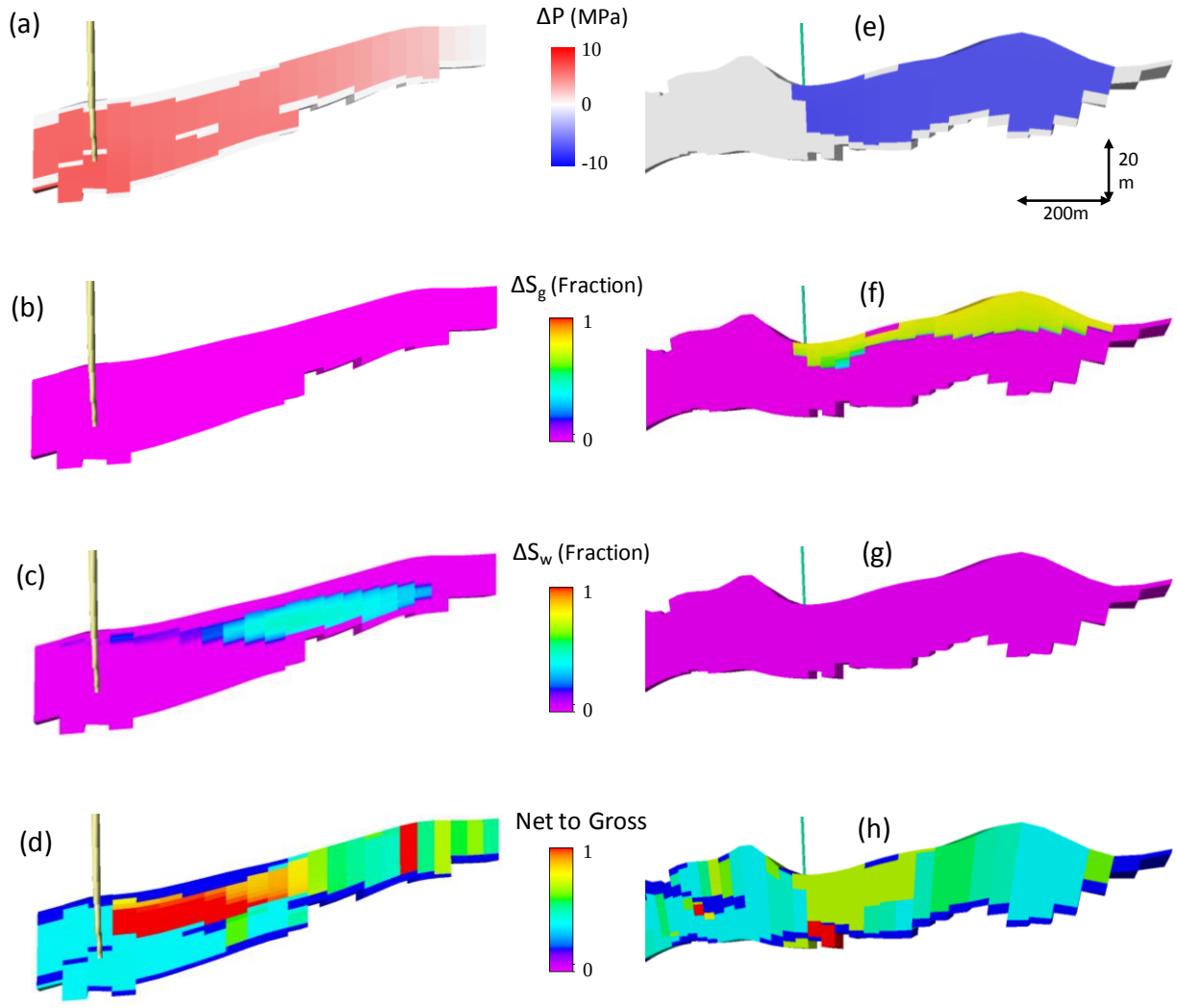

Figure 6.6 Simulated changes between the monitor (2002) and baseline (1998) for two vertical sections through the field, highlighting the thickness distributions associated with the pressure and saturation changes. (a) and (e) pressure change; (b) and (f) gas saturation; (c) and (g) water saturation and (d) and (h) NTG variation. Left column belong to the line B on Figure 6.4.c, and right column is for line C on that figure.

saturation (Figures 6.6(c) and (g)), the thickness of the accumulation is somewhat larger (55% or up to 27m), again due to different driving forces shaping the geometry of the saturated volume. Thus, in general, the volumes over which each of the physical change occurs are of different thickness, and overlap to different extents across the reservoir, depending on the mechanism and timing of the production and recovery processes. It is clear that the thicknesses used to create depth averaged changes vary depending on whether

we are dealing with pressure (h_P), water saturation (h_w) or gas saturation (h_g). Therefore, for a 4D seismic difference signature, in which the impact of these changes overlaps, this production-induced thickness scaling must be taken into account.

To analyse the above in more detail, synthetic seismic are modelled from the field simulation model using the procedure of Amini *et al.* (2011). In this approach, petroelastic parameters are firstly calibrated from the wireline logs and fluid properties obtained directly from PVT data. A convolutional model approach is then implemented, which captures the full range of offsets, and a data-derived (coloured inversion) wavelet (to ensure consistency with the observed seismic data). A data-derived wavelet of 24Hz peak frequency is used (giving a quarter wavelength of 32m). The workflow has proven to accurately capture the nature and character of the observed 4D seismic data for this field. Modelling provides us with a way to examine the impact of pressure, gas and water saturation changes on the seismic by independently isolating each of these controlling changes during the seismic modelling step.

To interpret the modelled 4D seismic signatures, we initially anticipate that the mapped seismic response might be decomposed linearly

$$\Delta A(\Delta P, \Delta S_g, \Delta S_w) = \Delta A(\Delta P,0,0) + \Delta A(0, \Delta S_g,0) + \Delta A(0,0, \Delta S_w) \quad (6.1)$$

where A represents mapped amplitude or time-shift, and ΔP, ΔS_w and ΔS_g are changes in pressure, water saturation and gas saturation respectively. This linearly additive behaviour has been tested by comparing the left hand side (all changes included) and right hand side (the addition of each change separately) of (6.1) (see Figure 6.7). It is found to be accurate across a wide range of geological and fluid conditions to within an error of 2% for both seismic amplitudes and the time shifts. Next, the time-lapse seismic responses corresponding to each change are cross-plotted against the three independent variables suggested above: that is, the depth averaged, production thickness scaled, and pore volume scaled quantity. Figures 6.8, 6.9 and 6.10 show the results for interval time-shifts and Figure 6.11 shows the corresponding results for the seismic amplitudes. The pore volume scaled variable is observed to show the strongest linear correlation with the seismic data, -

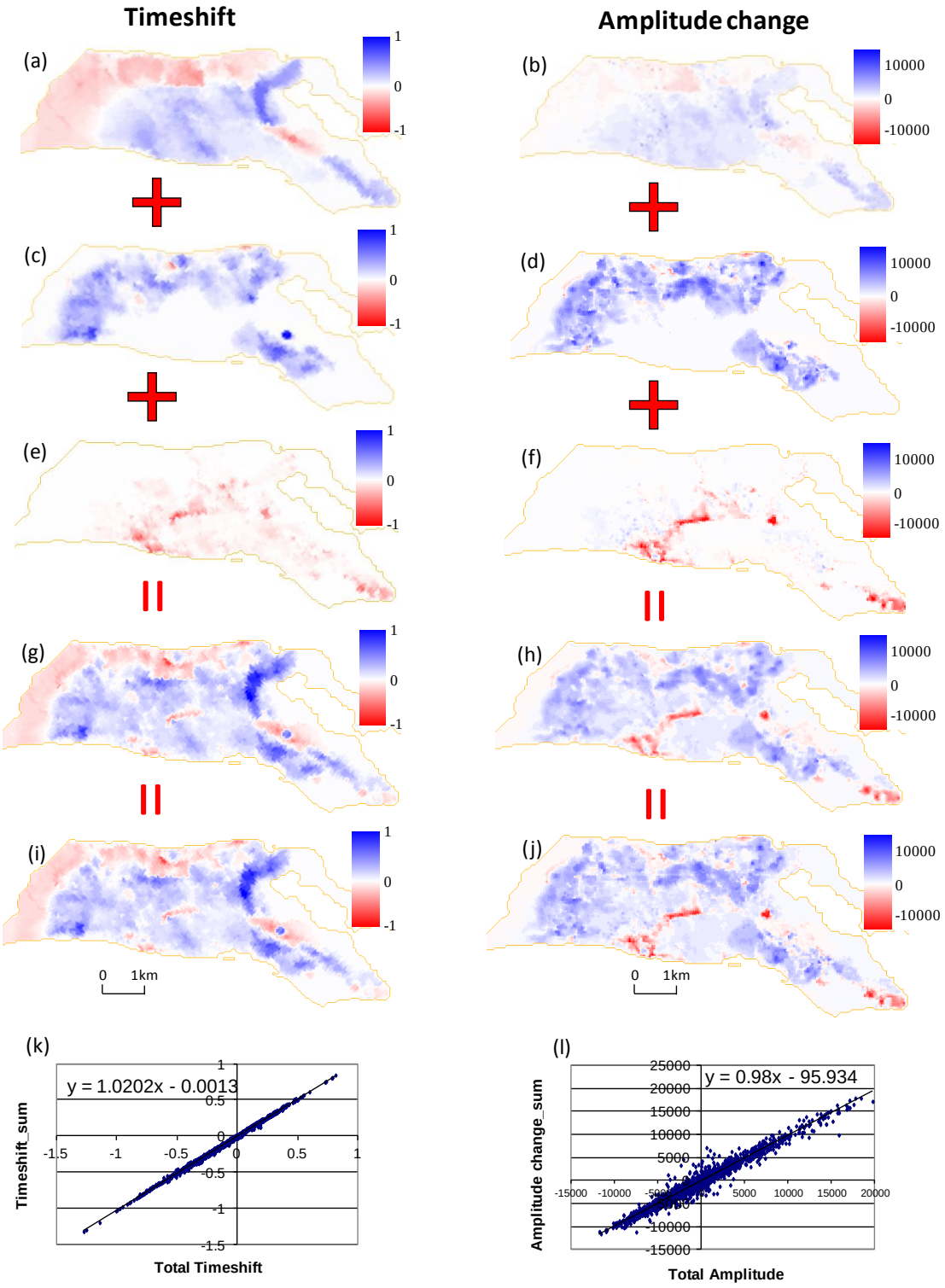

Figure 6.7 a), c) and e) Timeshifts for the effect of the pressure change, water and gas saturation change respectively. b), d) and f) amplitude changes for the effect of the pressure change, water and gas saturation change respectively, g) sum of a, c and e, h) sum of b, d and f. i) timeshifts for the effect of pressure change, water and gas saturation change together, j) amplitude changes for the effect of pressure change, water and gas saturation change together. k) g versus i and finally l) h versus j.

possessing a symmetric distribution about a mean linear trend and an average standard deviation of 1.2%. To extract the relationships at the right hand side of Equation 6.1, timeshift and amplitude change are separately discussed here.

Timeshift derivation

Consider a homogeneous reservoir sand with total thickness H, which is below the traditional tuning thickness of λ/4 (λ is wavelength), and a generic production scenario giving rise to gas out of solution and an upward movement of the oil-water contact. The reservoir is assumed to be surrounded by shale with an impedance of Z_{sh}. When pressure is depleted in the sand of thickness h_P, a thickness of exsolved gas (h_g) is formed at the top of the reservoir and water influx occupies a thickness h_w at the base of the reservoir (Figure 6.12). The velocities and impedances for these layers are: V_4 and Z_g (gas saturation and pressure change only region), V_3 and Z_p (pressure change only region), V_2 and Z_w (water saturation and pressure change only region), and V_1 and Z_n (the region with no change). For this situation, the time thickness change Δt of the reservoir at normal incidence can be written:

$$\frac{\Delta t}{2} = h_p\left(\frac{V_3 - V_1}{V_3 V_1}\right) + h_g\left(\frac{V_4 - V_3}{V_4 V_3}\right) + h_w\left(\frac{V_2 - V_3}{V_2 V_3}\right). \qquad (6.2)$$

By considering a linear approximation for each velocity as a function of their controlling parameters and the effective porosity ($\Delta V \propto \phi NTG$), it is possible now to write:

$$\frac{\Delta t}{2} \approx \left\{ a h_p (\phi NTG)_p \Delta P + b h_w (\phi NTG)_w \Delta S_w + c h_g (\phi NTG)_g \Delta S_g \right\} \qquad (6.3)$$

where *a*, *b* and *c* are the corresponding petroelastic parameters and the quantities in the curved brackets are averages taken over the reservoir volume affected by the particular change.

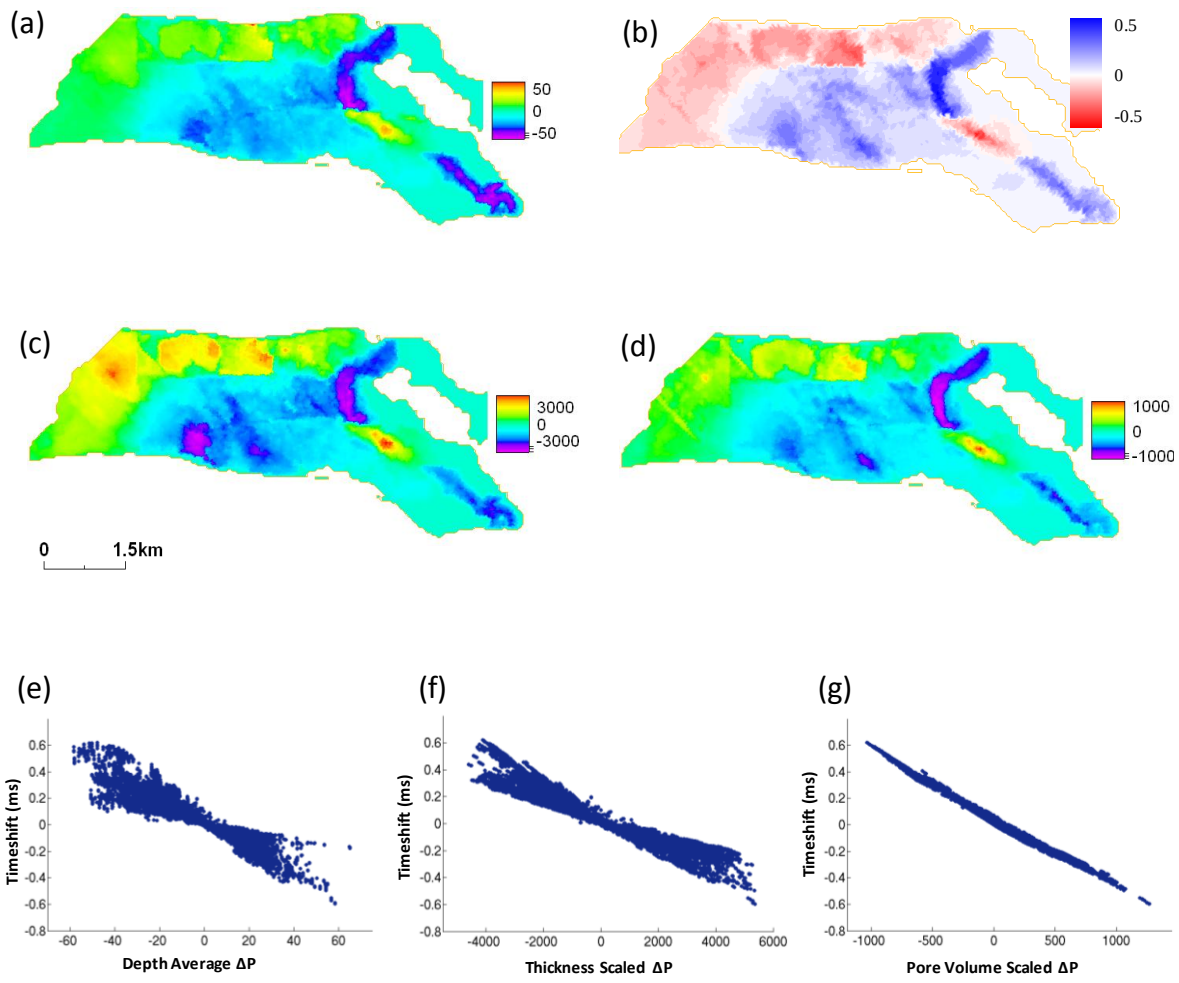

Figure 6.8 a) Depth average of pressure change, b) synthetic timeshift for pressure change only, c) thickness scaled pressure change and d) pore volume scaled pressure change. e, f and g) represents timeshift versus these changes.

Amplitude derivation

Consider the same reservoir as in the previous section. For the case before production, the composite reservoir reflectivity response R_{comp} in the frequency domain can be written:

$$R_{comp-b} = R_{top} + R_{base} e^{i\omega 2(\frac{H}{V})} \tag{6.4}$$

for long wavelengths relative to the reservoir thickness. Where ω is the angular frequency, and R_{top} and R_{base} are the reflection coefficients of the top and base respectively. Following

Falahat *et al.* (2011) and also Chapter 3, writing the reflection coefficients in full, converting to the time domain and including the wavelet *s(t)*, the composite amplitude response is

$$A_{comp-b} = \left\{ \left(\frac{Z_{sh} - Z_n}{\bar{Z}} \right) \left(\frac{H}{V} \right) \right\} . s'(t) \qquad (6.5)$$

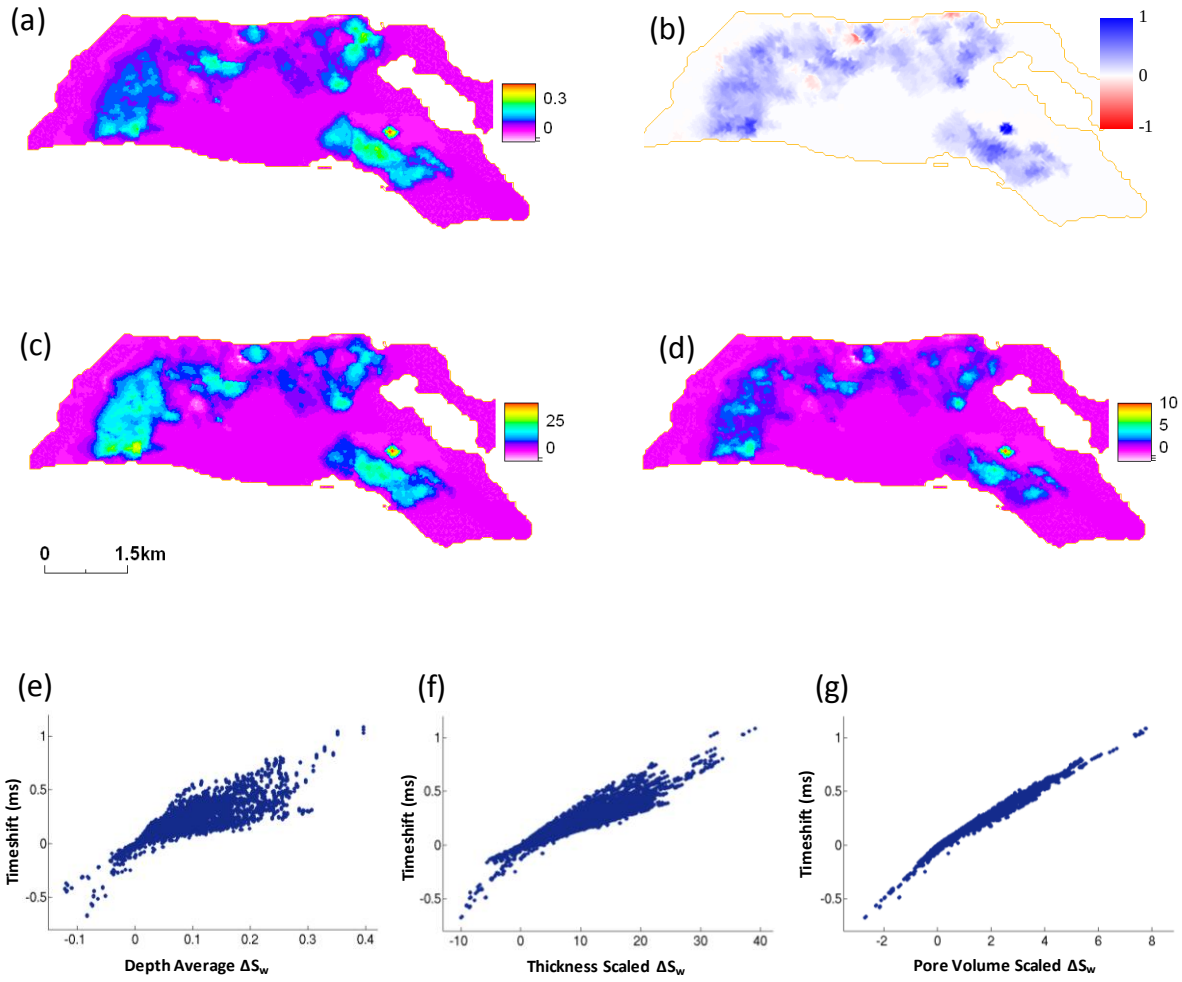

Figure 6.9 a) Depth average of water saturation change, b) synthetic timeshift for water saturation only, c) thickness scaled water saturation change and d) pore volume scaled water saturation change. e, f and g) represents timeshift versus these changes.

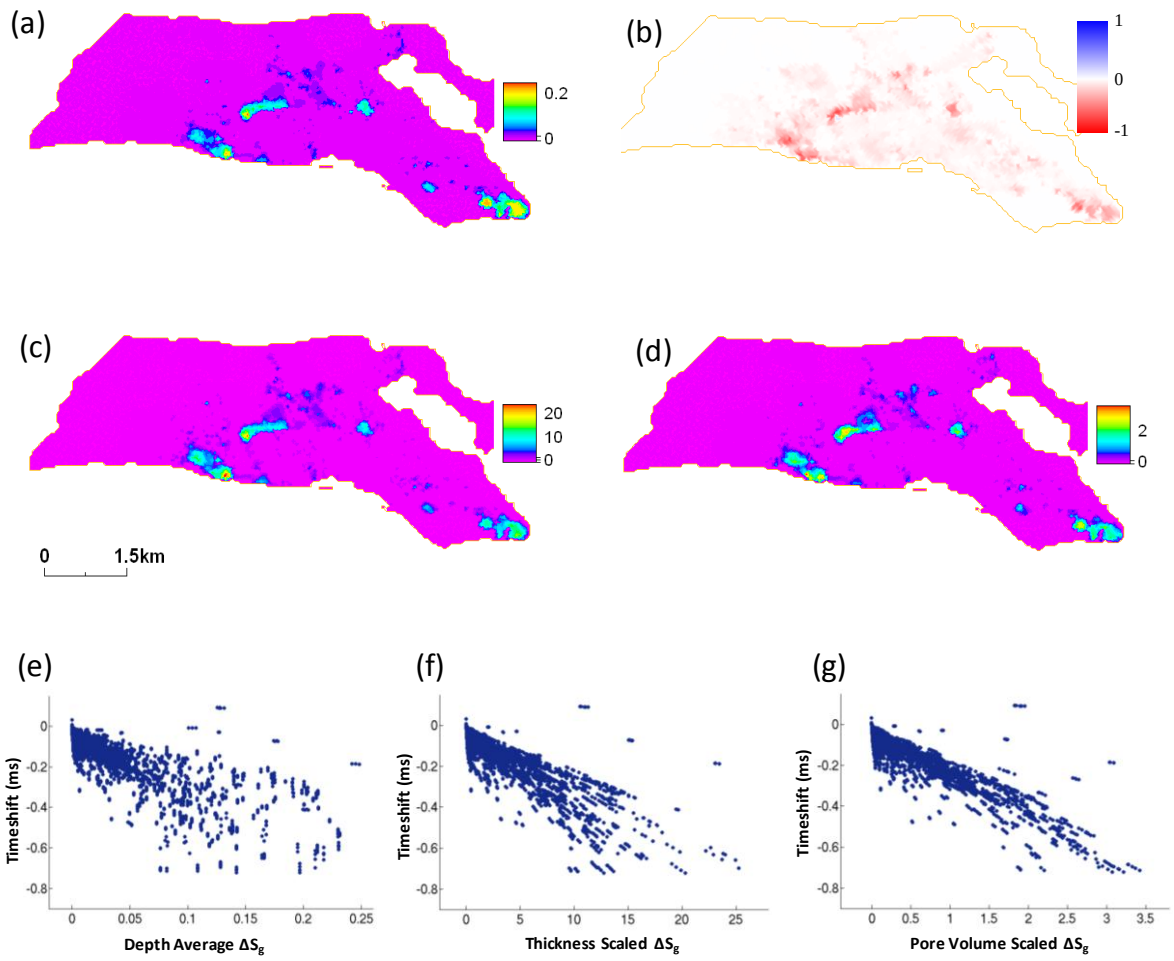

Figure 6.10 a) Depth average of gas saturation change, b) synthetic timeshift for gas saturation change only, c) thickness scaled gas saturation change and d) pore volume scaled gas saturation change. e, f and g) represents timeshift versus these changes.

where *s'(t)* is the time derivative of the wavelet. By considering a similar equation after production, with contributions coming from each layer, the time-lapsed amplitude response can be written:

$$\Delta A = \left\{ h_g \left[\left(\frac{Z_{sh} - Z_g}{2\bar{Z}V_4} \right) - \left(\frac{Z_{sh} - Z_p}{2\bar{Z}V_3} \right) \right] + h_p \left[\left(\frac{Z_{sh} - Z_p}{2\bar{Z}V_3} \right) - \left(\frac{Z_{sh} - Z_n}{2\bar{Z}V_1} \right) \right] + h_w \left[\left(\frac{Z_p - Z_{sh}}{2\bar{Z}V_3} \right) - \left(\frac{Z_{sh} - Z_w}{2\bar{Z}V_2} \right) \right] \right\} s'(t). \quad (6.6)$$

Finally, by assuming that the velocity and impedance obey a linear relation to the controlling perturbations in saturation and pressure, and also to the effective porosity

φ.NTG, then a linear equation identical to Equation 6.3 ensues but with different petroelastic parameters *d*, *e* and *f*:

$$\Delta A \approx \left\{ dh_p (\phi NTG)_p \Delta P + eh_w (\phi NTG)_w \Delta S_w + fh_g (\phi NTG)_g \Delta S_g \right\} s'(t). \qquad (6.7)$$

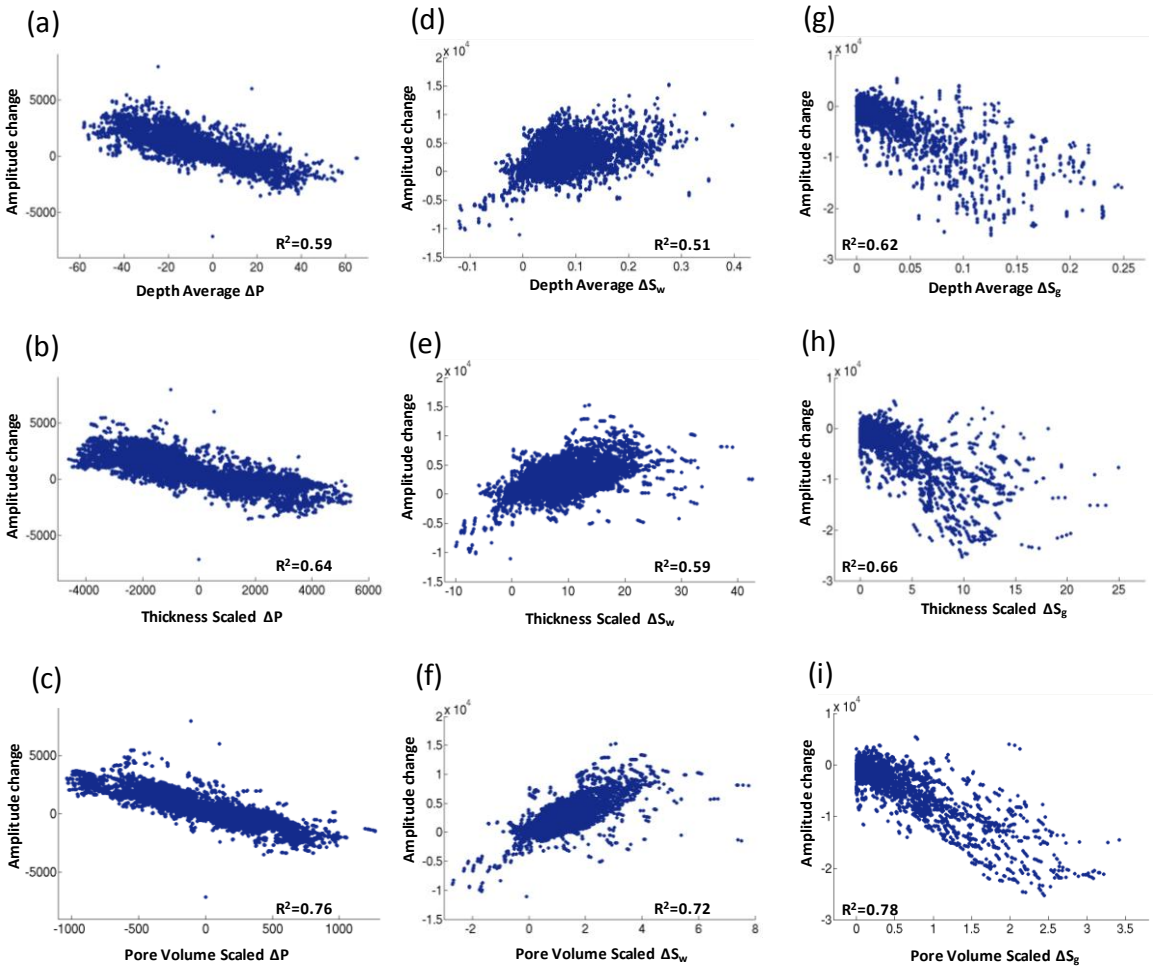

Figure 6.11 a), b) and c) Synthetic amplitude change versus the depth averaged, thickness scaled and pore volume scaled pressure change respectively. d), e) and f) Synthetic amplitude change versus the depth average, thickness scaled and pore volume scaled water saturation change respectively. g), h) and i) Synthetic amplitude change versus the depth average, thickness scaled and pore volume scaled gas saturation change respectively.

Equations 6.3 and 6.7 suggest that Equation 6.1 can be approximated by the following multi-linear equation in general:

$$\Delta A(\Delta P, \Delta S_g, \Delta S_w) \approx \left(ah_P[\phi NTG]_P \Delta P + bh_g[\phi NTG]_g \Delta S_g + ch_w[\phi NTG]_w \Delta S_w\right) \tag{6.8}$$

where the square bracketed terms refer to averages of the effective porosity ϕNTG over the depth range affected by the particular change. Thus, the mapped seismic response is dependent on the changes averaged over the total pore volume. The coefficients *a*, *b* and *c* represent the contributions from the petroelastic model. Material balance in the reservoir engineering domain or energy balance equations in the physics domain confirms the volumetric equation (Appendix A).

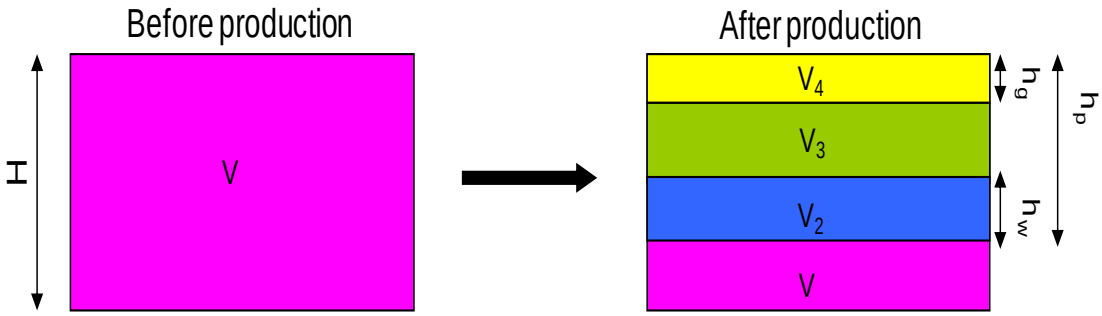

Figure 6.12 Idealised model of production used in this study.

Gas saturation distribution

Here, gas saturation deserves special attention as it is a departure from the expected non-linear behaviour. In fact, fluid flow considerations show that the change in gas saturation is a constant laterally and with depth for the reservoir, unlike ΔP and ΔS_w in general. The study of gas distribution within the reservoir is fundamental to understanding how it may in turn impact the 4D seismic signatures. In this work, this is investigated by simulating a sector of the full field simulation model with a fine-scale cell size of 12.5x12.5x0.18m. Here, particular care has been taken to ensure that the cell size is chosen to adequately represent the fluid physics and hence gas saturation values that would exist in the reservoir (Falahat *et al.*, 2011) without numerical artefacts. Two models are chosen, one capturing the expected reservoir heterogeneity and the other a homogeneous equivalent. As expected,

the modelling shows that, in response to pressure drop, gas liberated from solution migrates towards the upper parts of the reservoir when critical gas saturation (S_{gc}) has been exceeded in the oil. After this process, the saturation remains close to S_{gc} in the oil leg but higher values are present in the gas cap. Figure 6.13-a shows the gas saturation distribution taken from every cell of the model four years after production, when the bubble point pressure has been passed through. Two peaks in gas saturation can be observed in this histogram: one around the S_{gc} of 0.20% and the other around a maximum gas saturation (S_{gmax}) of 76%. The percentage of cells with values between these two saturations is small and, in the limit of a very fine model (and hence physical reality), the intermediate saturations will be negligible. A vertical section through the simulation model reveals that the gas saturations occupy two contiguous zones of constant gas saturation in the simulation model. Cells outside the depleted region are observed to contain zero gas saturation, as the pressure in these is still above the bubble point pressure. The nature of the particular saturation distribution described above has implications for the 4D seismic signature, as it is expected from laboratory studies that the seismic response with gas saturation should exhibit a strong non-linear behaviour (Domenico, 1974). However, as the gas saturation in the oil leg is very small for this particular field, the impact on the seismic is negligible when compared to the changes due to S_{gmax} in the gas cap (Figure 6.13-b). The seismic response is mainly controlled by seismic properties that are held fixed at one gas saturation S_{gmax}, and thus demonstrate instead a linear response to the gas cap thickness. These results do depend on the relative permeability curves and geological facies, and may thus vary from reservoir to reservoir. For very low permeabilities (e.g. tight gas reservoirs), there is a spread of saturations, and a nonlinear gas saturation response may also be taken into account in the inversion calculations in the text.

In this study, and for the conclusions developed above, a particular note shall be made of the care necessary with gas simulation studies to avoid scale-related effects. Thus, if coarser scale cells are used, it is found that there a considerable number of cells which have saturations intermediate between the two end member saturations, S_{gc} and S_{gmax}, described above. The coarse scale model now displays a range of apparent saturation states from cell to cell. This result is a consequence of the cell size, as it is simply not fine enough to capture the true gas distribution. In reality, gas continuously progresses across the reservoir filling each location up to S_{gmax}. The seismic response for the gas is predicted to be

controlled only by the total pore volume occupied by the gas change. An important conclusion of this work is that the presence of gas now appears as a linear term in gas pore volume only, rather than a non-linear function of gas saturation.

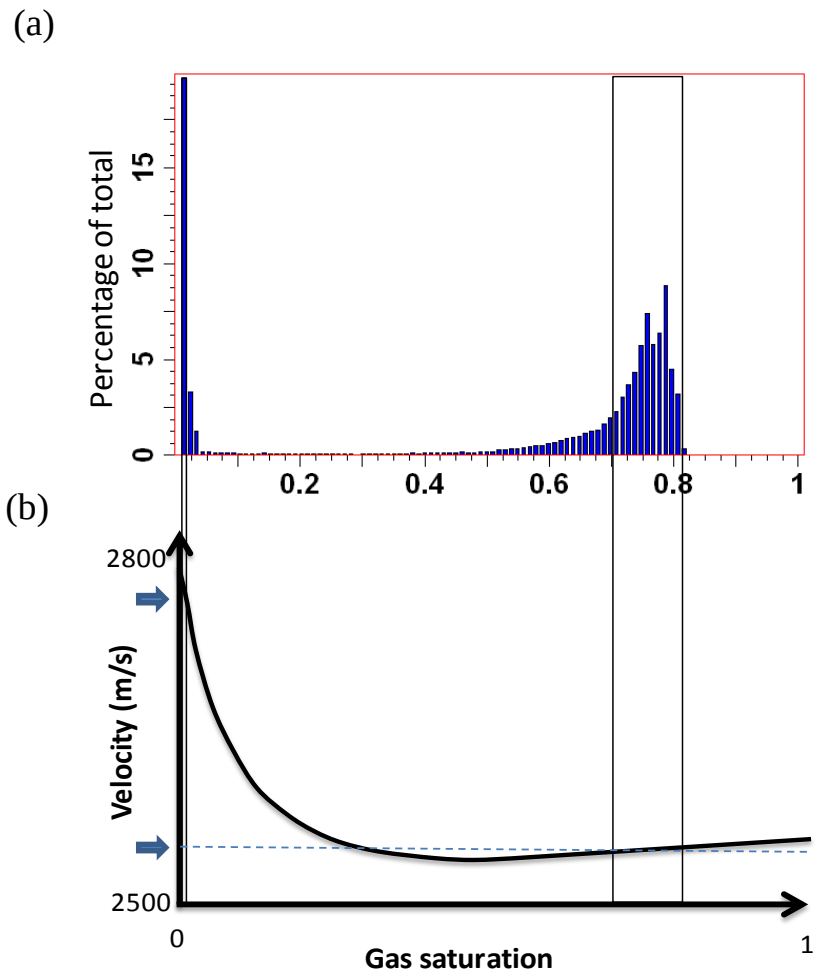

Figure 6.13 (a) Gas saturation histogram for the fine-scale simulation model. Here, zeros have been excluded to reveal the low saturation values at critical gas saturation. (b) Impact of the resultant saturation distribution on the seismic velocity. Note that, gas saturations higher than 80% do not exist in our simulation model (a) because of the S_{wir} of 20%. A homogeneous model produces similar results, but the distribution around maximum gas saturation is tighter.

Finally, for the seismic amplitudes (Figure 6.11), the above is also true but the scatter in the crossplots is observed to be slightly higher than for the time-shift attribute (Figures 6.8, 6.9 and 6.10). Further synthetic modelling (not shown) has revealed that the scatter present in

the results is due to the heterogeneity in the reservoir model – a control exercise using a homogeneous model yields a perfectly linear cross plot.

6.4 The principle of adaptive scaling applied to the observed data

To demonstrate how Equation 6.8 may be of value in quantitative interpretation, the observed seismic data were inverted for pressure and saturation changes using the principle above and the approach of MacBeth *et al.* (2004). For this purpose, four seismic attributes are considered: full angle stack, gradient stack, envelope weighted frequency, and finally time thickness. It is assumed that the adaptive scaling principle applies to these attributes also. According to this procedure, the unknown petroelastic coefficients (*a*, *b* and *c* in Equation 6.8) for each attribute are calibrated at thirteen wells in this segment for which changes in pressure and saturation are known with accuracy from fluid flow simulation prediction using the history matched simulation model. Unlike MacBeth *et al.* (2004), however, this well calibration involves the pore volume scaled pressure $h_p\varphi NTG\Delta P$ or saturation changes $h_w\varphi NTG\Delta S_w$ and $h_g\varphi NTG\Delta S_g$. After this stage, least squares inversion of all the selected attributes yields the desired results automatically (Figures 6.14, 6.15 and 6.16). These results are now the pore volume scaled pressure or saturation changes across the reservoir, and must therefore be compared with the corresponding values from the simulation model for updating purposes. Although there are twenty wells available in the chosen reservoir segment, thirteen are selected for the inversion and seven withheld for the purposes of cross-validation. In all, this leads to 77,520 sets of cross-validation error and, after computation, a mean error of 25% is found. It should be emphasised that these results are obtained by a *linear* inversion, and the reservoir effects include pressure, water and gas saturation, this only being possible because of the pore volume scaling. Higher order behaviour is assessed (i.e. quadratic terms in ΔP, ΔS_w and ΔS_g) but found to be unnecessary as they provide only a small overall contribution. Note that, as the product of the thickness of the affected volume, net-to-gross and porosity are not known with certainty in practice, it is not possible to convert the final results of this inversion immediately into absolute values of pressure and saturation changes. Instead, these products must be used to update the simulation model by comparing them with the corresponding simulation predictions of pore-volume scaled changes (these are shown in Figures 6.14, 6.15 and 6.16). This in turn

leads to the ambiguity of either dynamic or *static* model updates producing the desired match to the 4D seismic signatures. Figure 6.17 shows the baseline seismic amplitude map which may be correlated with net-to-gross, and the pore volume from the simulation model for reference in the 4D seismic results described below.

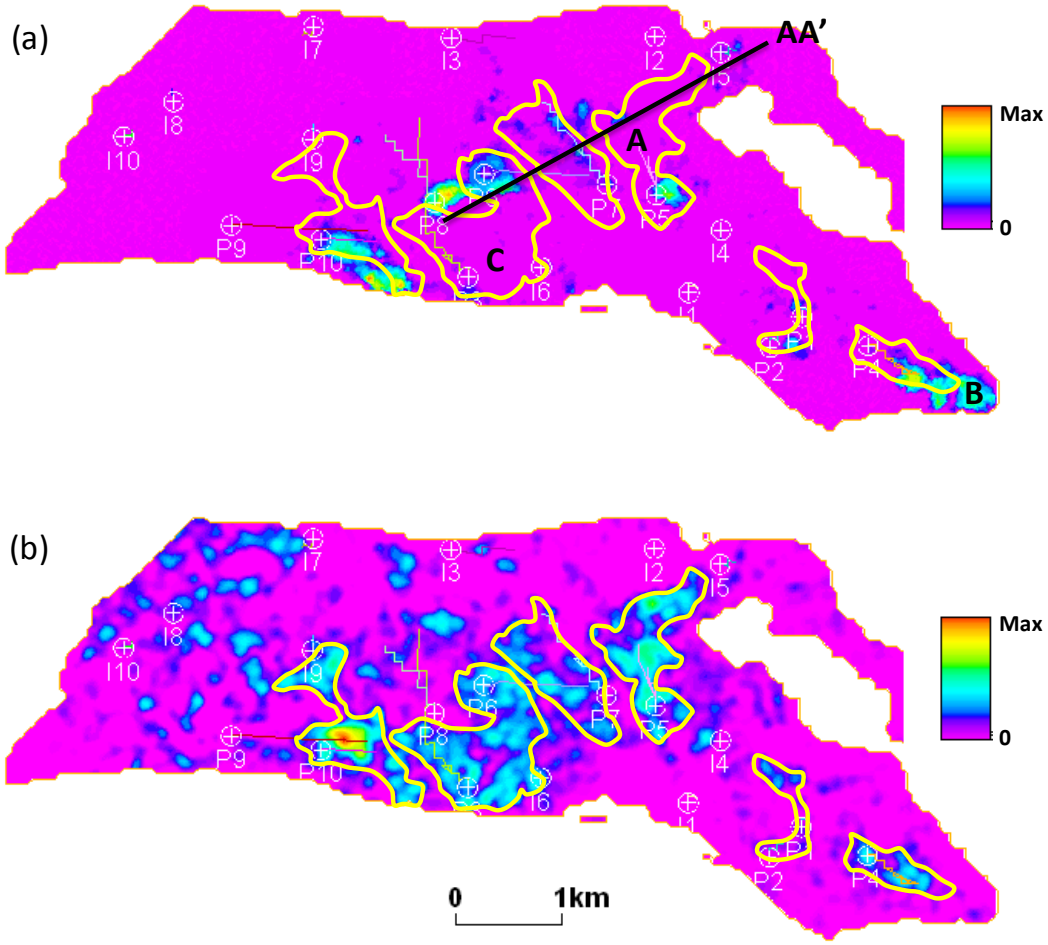

Figure 6.14 Pore volume scaled gas saturation change map from a) simulation model, and b) seismic inversion. Enclosed areas on the maps are drawn based on the seismic inversion map (b) and added to the simulation map (a) for comparison.

The pore volume scaled simulation model predictions are compared against the inverted observed seismic in Figures 6.14, 6.15 and 6.16, for scaled gas saturation, pressure and water saturation respectively. Indeed, the results show that the simulator does appear to predict the inverted seismic observations fairly accurately, however there are also some

noticeable differences which require some explanation. In the pore-volume scaled gas saturation maps for example (Figure 6.14), regions A, B and C are highlighted as major differences. The anomaly marked by A, detects a strong gas out of solution signature in the inversion result, that is consistent with the known pressure depletion in this area, but the simulated map shows significantly smaller gas than inversion. This interpretation is consistent with the amplitude change maps, which show a softening signal in this area (Figure 6.4). Inspection of a seismic section (Figure 6.18) taken through the anomaly reveals a discontinuity between two seismically geobodies, whereas in the simulation model a throughgoing connection allows migration of the gas away from this region. There

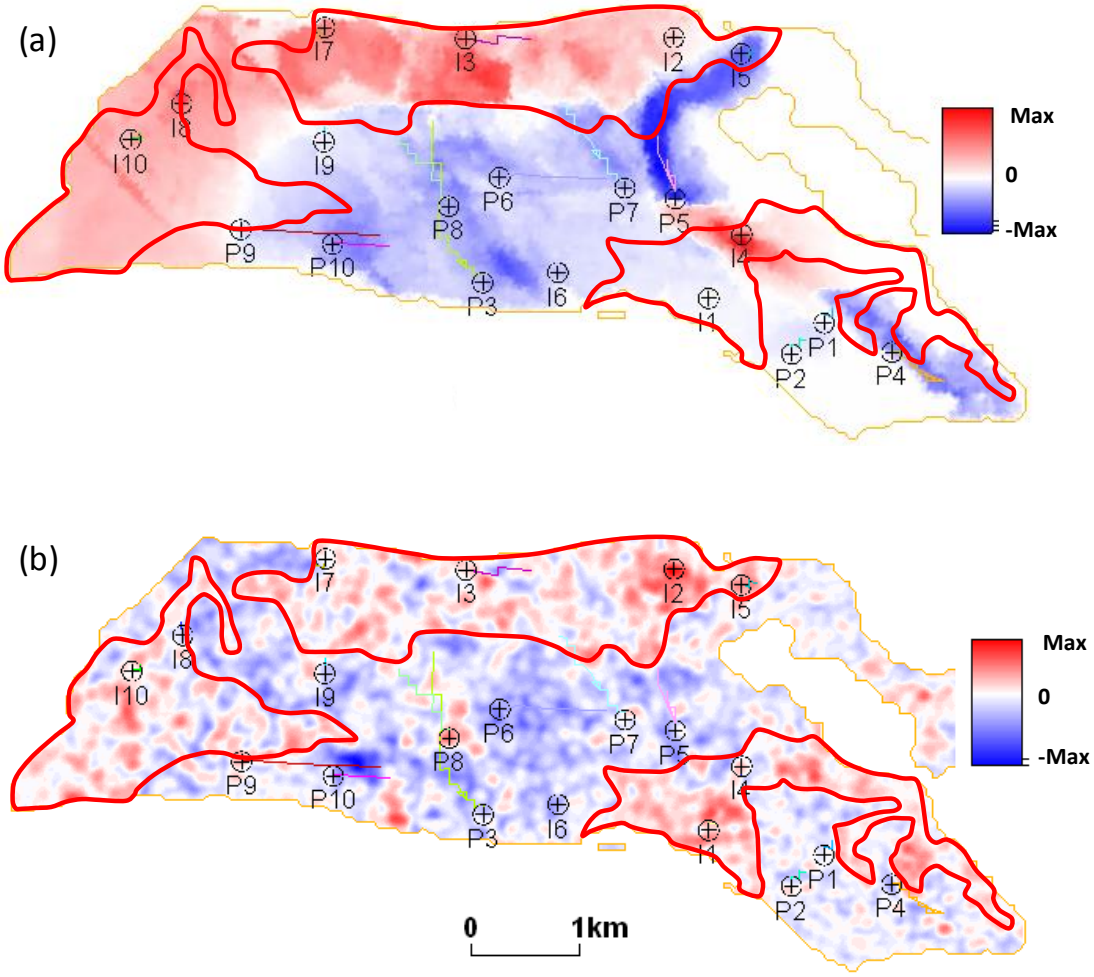

Figure 6.15 Pore volume scaled pressure change map from a) simulation model, and b) seismic inversion. Enclosed areas in the plot are drawn for reference. P8, I6 and I9 are inactive during the period of seismic monitoring.

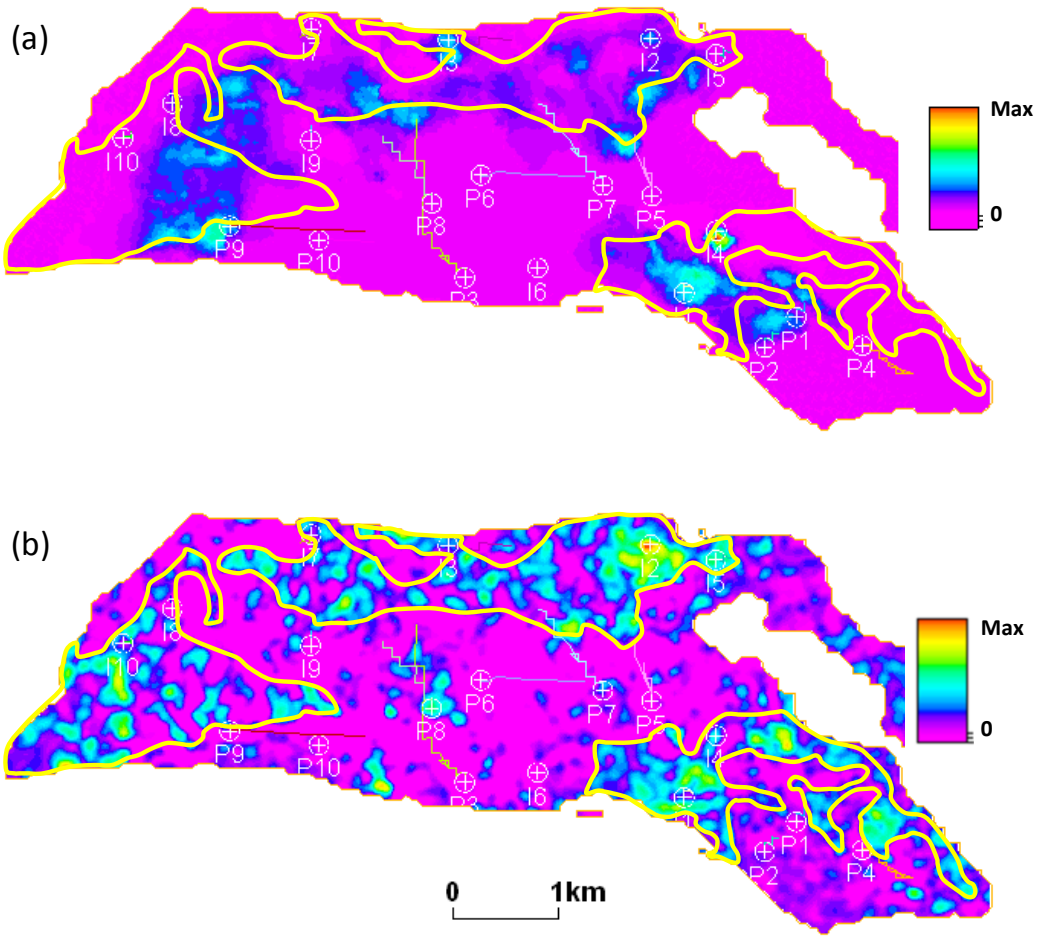

Figure 6.16 Pore volume scaled water saturation change map from a) simulation model, and b) seismic inversion. Enclosed areas in the plot are drawn for reference.

is a need to update the transmissibilities in the simulation model to take on board these conclusions. For anomaly B, injector I6 is not active until 2002 and so the pressure has dropped below bubble point. The inversion reveals an accumulation of gas in this area in a local high that is consistent with the pressure drop and geometry of the reservoir. For anomaly C, the reservoir top horizon has been smoothed in the simulation model, which prevents gas accumulation around the well, and makes unreal gas migration towards the south-east.

For the pressure compartmentalisation, there is excellent general agreement with the simulated and inverted results (Figure 6.15), but again some intriguing disparities. Pressure

is clearly seen to be controlled by the well activity and distribution and known barriers, and not by the net-to-gross (see also Figures 6.2-c and e and 6.6). Indeed, several contiguous pressure-up regions (for guidance only) can be drawn around the injectors, surrounding two regions of pressure depletion defined by the producers. It is satisfying to note that all of the injectors active between the 1998 to 2002 period are surrounded by areas of pressure-up (note that I6 and I9 were not active before 2002). In the east of the study area, the inversion results do not exhibit the strong arcuate pressure-up or -down features associated with the pore volume in the model. Interestingly, injector I1 shows no pressure change in the simulator, yet the inversion results indicate a pressure-up response consistent with the well pressure data, this signalling a need for a further model update and history match.

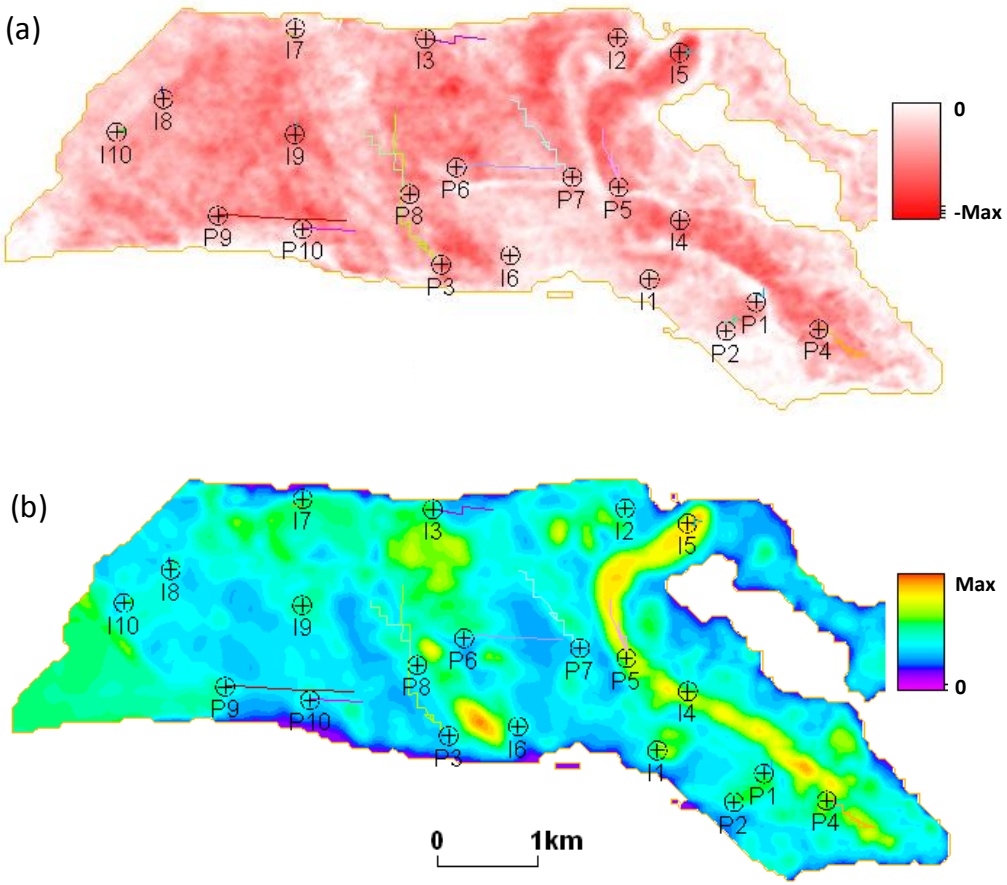

Figure 6.17 a) Seismic base line map, and b) pore volume map from the simulation model.

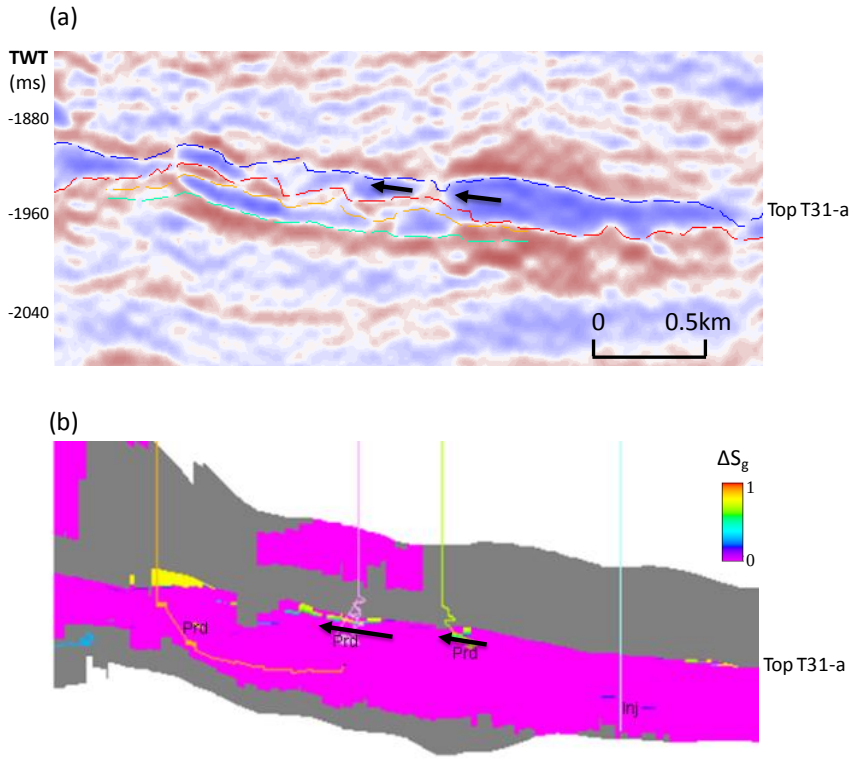

Figure 6.18 a) 2002 seismic section along line AA' in Figure 15, and b) vertical cross section from the simulation model for gas saturation change along the same section as in (a).

There is also a reasonable agreement between the predicted and simulated regions of water saturation change, which are distributed around the active injectors in a fairly heterogeneous fashion, and some observations can be drawn. Well I4 was only active three months before the acquisition of the monitor survey, and provides only a small amount of injected water. The pressure response is small and consistent with the injected results, whilst the simulation result gives a higher pressure. For well I7, injection stopped three months before shooting of the monitor survey and the pressure therefore dropped. In the northwest area of the study area, good connectivity to the central area containing the producing wells is probably the reason for the pressure drop (there is also the possibility of a connection with a neighbouring depleting segment). Around the producers P3 and P8 the inverted results show both a pressure and water saturation increase. Interestingly, P8 did not start to produce before 2002; however the neighbouring producer P3 started water production only a few months after the time of the monitor survey. Taken together, the

above observations suggest the need for some specific updates to the transmissibility multipliers (and hence barriers) and the net-to-gross distribution in the simulation model. These updates have been implemented in a separate piece of continuing work performed in collaboration with Sergey Kurelenkov (Heriot-Watt IPE, ETLP group), not included in this thesis.

6.5 Discussion and conclusions

The principal parameters controlling mapped 4D signatures are not pressure and saturation changes *per se*, but these changes scaled by the corresponding thickness (or more correctly the pore volume thickness) of the reservoir volume that these effects occupy. This understanding is consistent with our expectations from both seismic modelling and the fluid flow physics. It is a conclusion that is generally applicable for all data interpretation and inversion procedures that aim to infer or estimate pressure and saturation changes. The notion that it is the volumetric extent of the fluids that effect the seismic is consistent with our understanding derived from the constraining influence of the material balance equation (Dake, 2002). Indeed, this supports our past studies, that have shown that time-lapsed seismic signatures for multiply repeated seismic surveys are controlled strongly by the net cumulative volumes produced and injected (Falahat *et al.*, 2011, Huang *et al.*, 2011).

Interestingly, our studies also indicate that the impact of gas saturation on the seismic can be written using a linear term. This appears to follow directly from the gas properties for our field of study. For this field in particular, the critical gas saturation (the minimum movable gas saturation) is very small compared to the maximum gas saturation that is possible. The critical gas saturation is a function of the particular relative permeabilities used (Clark, 1969), which in turn are a function of the reservoir facies (Ali *et al.*, 2008). If for other reservoirs, there is a higher critical gas saturation, the gas term in Equation 6.8 will be decomposed into two linear terms which take account of the gas saturation in the oil leg as well as in the gas cap. However, calculations (not shown) have indicated that, in this case, the same expression for the seismic response to gas appears to exist, and thus the equations above may be regarded as a generality for most reservoirs.

Finally, the results in this work are proposed as the basis for a convenient linear Equation 6.8 that can be used to readily invert for pressure, gas and water saturation changes. The linear approximation for pressure and saturation changes is found to be valid for most reservoir conditions in this study. However, modelling has shown that it does break down for reservoirs of thickness greater than 40m and, at this point, a non-linear term for pressure is required. One possible drawback of the proposed linearised inversion is that simulation model updates can only be achieved by comparing the results with corresponding scaled dynamic changes from the simulator. There is, therefore, an inherent ambiguity when comparing predictions from the simulator with seismic inversion results. This prevents independent determination of the static and dynamic parameters, and places a strong emphasis on the need for assigning an appropriate static model before dynamic model updates can be implemented with accuracy. This comes as no surprise, as a similar conclusion has been reached by research into the seismic history match (Stephen and MacBeth, 2008).

Chapter 7

Conclusions, discussions and recommendations

Understanding accurate gas migration and distribution in the reservoir is the primary objective of this thesis. This achievement has given us a new perspective and improved knowledge of the reservoir scale seismic response to the injected or exsolved gas volume. This has led to a new volumetric approach to estimate the injected gas volume, using repeated seismic data. The exact mechanism of gas exsolution and dissolution is found to be important for an accurate interpretation of the 4D seismic signal. The principal parameters controlling mapped 4D signatures arising from gas saturation are considered and formulated. The thesis is structured into two parts: the first part, discussed in the Chapters 3 and 4, concentrated on gas injection; the second is provided in Chapters 5 and 6, where the main challenge is gas exsolution and dissolution in a depleted reservoir. This chapter summarizes the findings of this work, and provides a view to potential future research. Recommendations are made regarding some technical challenges that are relevant to the work but have not been possible to include. Opportunities to improve this research are also indicated.

7.1 Gas-related challenges in the engineering and seismic literature

Gas is injected into the reservoir for disposal, storage or IOR aims. The fate of the injected gas is a key point in continuing the project. In particular, leakage is one of the challenging issues in injection for disposal, whereas for storage the objective is to be able to re-produce the injected gas. Knowledge of the distribution and migration of the gas impacts decisions on whether to continue injection, stop the project or drill another well. Gas is also used in WAG (water alternating gas) projects in partnership with water injection, to control pressure and avoid bypassed oil. This process requires knowledge of the pressure regime inside the reservoir and the distribution of the injected gas and water. By accessing this understanding, the injection and production plan can be optimized. A drop of the oil production rate, due to the pressure decreasing below the bubble point pressure, on the other hand, is one of the main challenges in the engineering domain. Since gas is more mobile, it quickly arrives at the production well and surrounds it, so dropping oil rate. To overcome this problem, knowledge about the volume, shape and position of the liberated gas in the reservoir is vital to influence changes in the perforation depths. Management of produced gas is also important here. Liberated gas is present in the reservoir and it is not normally forced back into solution by pressure build up. It is produced during the life of the reservoir.

The problems and challenges of gas in the oil and gas industry highlight its importance as a topic for engineers and the management team. The complexity of the gas-related phenomena in the reservoir, and the non-applicability of some of the laboratory measurements at this scale, should encourage engineers to employ seismic data. These data provide valuable information spatially and between the wells. However, analysis of the literature on gas and seismic reveals some challenges that can cause problems for quantitative monitoring. For example, it is widely believed that a few percent of gas makes the pore fluid mixture very compressible. In the presence of gas, the fluid bulk modulus (κ) drops significantly, the P-wave velocity and impedance decreases sharply. The P-wave velocity demonstrates an extreme non-linear trend against gas saturation (see Figure 1.1). A few percent of gas has a dramatic effect on the P-wave velocity and cannot be distinguished from complete gas saturation. This suggests that seismic techniques cannot separate a water zone with small amounts of gas from economic gas reservoirs with high gas saturation. It is

concluded that 4D seismic is not able to quantitatively monitor the gas saturation variation (Lumley *et al.*, 2008).

In the 4D seismic literature, a different seismic response is proposed for gas saturation variation. The laboratory also shows the expected extreme non-linear response (e.g., Lumley, 2008, Dumont *et al.*, 2001, Rojas, 2005), but a linear seismic response is chosen by Huang *et al.* (2001). A linear response with positive gradient (opposite direction to Huang *et al.*, 2001) is employed by Dumont *et al.* (2001). An exponential relationship between gas saturation and 4D seismic changes is used by Floricich *et al.* (2006). Finally some intermediate variations are proposed by e.g. Sengupta and Mavko (2003), Wagner *et al.* (2004), Konishi *et al.* (2008). The diversity of these examples highlights the fact that there is as yet no accepted way of handling gas in the seismic domain. It is my belief that it is the reservoir scale gas distribution which is misunderstood. The literature has supported laboratory-based measurements, so these strange and probably invalid relationships are then re-applied at the reservoir scale. The main questions here are: does the seismic response follow a laboratory based trend at the reservoir scale?; is the gas distribution and migration at the reservoir scale the same as at the laboratory scale?

7.2 Reservoir-scale gas distribution

To determine the accurate reservoir-scale gas distribution, the capillary pressure literature has been studied. It is found that the transition zone is the only part of the reservoir with saturation variation (Figure 2.8)). The height of the transition zone is proportional to capillary pressure (Equation 2.19), which is related to the size of the pores (r_c) and the pores distribution, interfacial tension (σ), the wettability and inversely proportional to the fluid density difference ($\Delta\rho$). As a general statement, a small height of the transition zone is expected for gas injection or gas out of solution in a reservoir that contains a medium to high porosity and permeability. In these cases, the higher density difference between gas (mainly methane) and water, and also good pore size connections produce a negligible transition zone.

For gas injection into an aquifer, injected gas migrates toward the upper part of the

reservoir due to gravity. The gas saturation is the maximum gas saturation ($1-S_{wir}$) within the gas cap. The lower part of the reservoir contains 100% water saturation (Figure 2.12). Inside a specific thickness of the upper part of the reservoir (gas thickness), the magnitude of the gas saturation is constant. It is the gas thickness which varies horizontally. There are higher gas thicknesses around the injection well and a small thickness far from the well. The gas thickness is increased by continuing gas injection, but the gas saturation is approximately constant in that layer. Thus, the main factor in the seismic domain is gas thickness, and gas saturation *per se* remains approximately constant.

To capture the reservoir-scale gas distribution and validate the above, some fine-scale simulation models with different degrees of heterogeneity were built. It found out that the proposed description above is true, although there are some minor fluctuations. The standard deviation of the gas saturation inside the gas thickness is 0.04, 0.05 and 0.07 for homogeneous, vertically heterogeneous and totally heterogeneous models respectively (Figures 3.4, 3.5 and 3.7). Heterogeneity in the range of a typical North Sea reservoir increases the gas saturation variation by only 3%, and therefore does not break the understanding. At the reservoir scale, the absolute value of maximum gas saturation is influenced by the relative permeability curves, and the balance of viscous, gravitational and injection forces. The saturation equilibrium is reached very quickly (at less than a month) for the homogeneous model, while it takes slightly longer (around 6 months and less) for the heterogeneous model. This time scale is still less than normal 4D seismic repeat time. Note that a wider saturation distribution needs to be taken into account in LoF (Life of Field) 4D seismic projects.

The above results can also be generalised for reservoirs with a higher range of connectivity in terms of effective porosity and permeability, and this was investigated by building different models. However, I have reservations regarding the applicability of this description to reservoirs with very low permeability (e.g. tight gas reservoirs). The engineering data which are used in our synthetic modelling cannot be employed in these types of the reservoirs. They have a specific behaviour for the capillary pressure curve and relative permeability curves that may affect the gas saturation distribution. Nevertheless, it should be considered that reservoirs with medium to good connectivity were generally chosen for gas injection projects with the aim of storage or IOR (otherwise they will be

uneconomical). Therefore, our assumption can be easily generalised to most of the gas injection projects for storage, disposal or reservoir pressure maintenance.

By considering gas behaviour at the reservoir scale, the definition of 'gas saturation' is challenged and may need a new nomenclature. It seems that 'gas thickness' has more physical meaning at the reservoir scale. It is also representative of the changes for injected gas in the reservoir. However, the magnitude of the maximum gas saturation (or irreducible water saturation) is mainly dependent on the rock type, and different reservoirs contain different values (Morrow and Melrose, 1991). Therefore for a comparison of injection into reservoirs, it is possibly better to employ gas thickness multiplied by maximum gas saturation, and consider the gas in volumetric form.

7.3 The seismic response to gas

The seismic response to an injected gas volume was modeled analytically and numerically. For thin reservoirs (less than tuning thickness), both timeshift and amplitude change attributes show a linear trend versus gas volume (Figure 3.10). The linearity in the amplitude change is due to the tuning effect. The points mentioned in the previous sections are tested using synthetic simulation and seismic modelling, and linearity is indeed confirmed. The heterogeneity in our case studies gives only a few percent of scatter (less that 2%).

Despite observing a linear timeshift response versus gas volume for thick reservoirs, amplitudes become non-linear. It is the architecture of the reservoir that determines this amplitude response. It seems that timeshift is more stable than amplitude change. However, because thick reservoirs are normally the combination of intra reservoir thin sand and shale, interference effects produce a linear amplitude response (Figure 3.12). This linearity was also observed in my first case study (An'Teallach). To speed up the history matching process, intra-reservoir shale is normally mixed with the sand using the net to gross concept. The fluid flow is controlled by revising NTG and K_v/K_h, while it makes some challenging issues in the seismic domain. By including these thin layers, the interference effect will create a linear 4D seismic response even for realistically thick reservoirs. Our

suggestion is to include the intra-reservoir shale in both geological and simulation models.

We observed a deviation from the linear response with increasing simulation model cell size (especially in the vertical dimension). Gas saturation immediately arrives at the maximum gas saturation at the top of the reservoir for the fine scale model and then starts to increase the gas thickness as expected. However, for the upscaled models, gas saturation cannot arrive at the maximum gas saturation in the primary stages. More gas injection would be needed to increase the saturation of a large cell to the maximum value. As a consequence, a spurious gas saturation variation is observed during the injection process in the upscaled model (Figure 3.1). Prediction of a realistic gas saturation distribution is not possible with the upscaled model, and the expected linear response between 4D seismic attributes and the injected gas volume is not observed (Figure 3.14). To avoid this effect, it is proposed to use cell thicknesses of less than 2m in the simulation models.

The above problem is more challenging in the seismic domain than engineering domain. The main aim during history matching of the simulation model is accurate fluid flow prediction. This flow is controlled by some changes in the simulation model such as vertical equilibrium switches, pseudo relative permeability and capillary pressure curves, and changes in the transmissibility. These solutions fix the saturation front to be the same in the coarse scale and fine scale model, but the saturation variation is still present in the upscaled model. This variation is not an important issue for the engineers, but it prevents accurate calculation of the seismic response and misleads the geophysicist. As another issue, the simulation model and seismic data are normally converted into 2D maps to be compared and to make some seismic interpretations and reservoir model updates. This situation is the same as a completely upscaled model, in which the total reservoir thickness is assumed to be one cell. As the gas saturation variation is observed in these maps, geophysicists are encouraged to employ the laboratory extracted non-linear seismic response. Using the gas thickness or gas volume terms instead of gas saturation in the reservoir scale will solve this misunderstanding.

Using the concepts above, a technique was developed to calculate the volume of gas injected into a thick turbidite reservoir. The time-lapse seismic maps of both timeshift and amplitude change are thresholded to allow the definition of robust contiguous areas

influenced by the gas volume changes. The time-shift and amplitude changes remaining after the thresholding procedure describe an area on the change map. The formulations in Chapter 4 predict that the integration of the seismic attribute changes over the thresholded area is directly proportional to the total volume of injected gas V_{gas}. The pressure effect on the rock frame and fluids adds a positive constant to the equations, as pressure is fixed between monitors. The pressure effect and constants are estimated directly from the data by calibrating the time-lapse seismic with the known well injection data. Thus, the three combinations of integrated time-shift and amplitude change from the 2002-2000, 2002-1999 and 2000-1999 signatures are cross-plotted against the injected volumes independently from the 2002-1993, 2000-1993 and 1999-1993 signatures (Figure 4.5). This methodology can be generalized for the fairly homogeneous reservoirs in which the petrophysical properties vary slowly across $\sum$, so the spatial integral of S_g and ϕ_{eff} can be approximated by their average.

The gas volume is now calculated using both timeshift and amplitude change attributes. In our example, the two maps do appear to be reasonably close, but there are still regions of disparity (Figure 4.6). Calibrations using the well injectivity data and material balance are found to be excellent, and any differences between maps must be due to the inherent nature of the attributes themselves. This disparity was also reported in the literature, so an attempt was made to locate possible reasons. Synthetic data based on the reservoir model and further analysis of the observed data have been able to replicate some of these differences and identify them as due to inter-layer wave interference and 4D noise. It appears that amplitude estimates are reduced relative to those from the time-shifts, due to intra-reservoir wave interference. In addition, time-lapse seismic attributes are particularly susceptible to non-repeatability of the acquisition geometry when in the presence of overburden heterogeneity. Non-repeatability maps derived from the overburden are chosen separately for timeshift and amplitude change attributes as these represent the statistical measure of the noise. This is now rescaled, and then added to the synthetic amplitude map to simulate an observed dataset. Comparison of the original and noise contaminated synthetic with the observations indicates some interesting facts, particularly the repositioning of major anomalies in the amplitude change attribute. As another reason, amplitudes may shift laterally or vertically depending upon the velocity model and underlying structural dips.

The choice of migration combined with the heterogeneities in the velocity model can alter the spatial frequency content, continuity and smoothness of the amplitude maps. Inspection of the study area suggests structure as a possible cause of movement for the main amplitude changes. As a disparity between the results of amplitude and time-shift attributes has also been seen elsewhere, there is a need to carefully evaluate the impact of decisions made during acquisition and processing on the quantitative interpretation of 4D seismic, particularly when used for reservoir engineering purposes.

7.4 Gas exsolution and dissolution

Three phase reservoirs are the most challenging cases found in the literature. The saturation distribution was investigated using some synthetic fine-scale simulation models. The components of the oil are immediately decomposed and gas is exsolved upon arriving at the bubble point pressure. Since the gas saturation is below the critical saturation during the primary stages, it does not mobilise. After a greater pressure drop, more gas bubbles are liberated. These bubbles connect together, arrive at the critical saturation, and migrate upwards due to gravitational force (Figure 5.2 and 5.3). Migrated gas makes a gas cap at the top of the reservoir. Gas saturation is around maximum gas saturation in the gas cap, but it remains around the critical gas saturation in the oil leg. Therefore, two sets of gas saturation exist in the reservoir. By continuing the pressure drop, the thickness of the free gas cap increases.

The gas saturation contains a narrow variation at the reservoir scale. The standard deviations are 0.36% and 5.5% inside the oil leg and gas cap respectively (Figure 5.5). Therefore, only two end member saturations determine the seismic behaviour in addition to the gas thickness. However, for smaller time lines (less than 6 months), gas saturation does not reach the maximum gas saturation in the gas cap as earlier anticipated. This observation highlights the time required for the gas migration and stabilization at the gas cap, and may also signal to refine the cell thickness. Because the volume of migrated gas in the upper part of the reservoir is not large enough during the primary stages to fill the cells, a perceived variation of the gas saturation is apparent. This may be solved by choosing a smaller cell thickness, although this will lead to an increase in computational run time.

Note, however, that this point is not an important issue when working with normal 4D seismic time lines (one year and more), but it should be taken into account in highly repeated 4D seismic data (less than 6 months).

The gas dissolution process was also investigated at the reservoir scale using synthetic simulation models. Migration of liberated gas prevents dissolution of the entire evolved gas. There are three areas that have different stories (Figure 5.6): a) the gas in the oil leg (critical gas saturation) is entirely dissolved once pressure is slightly increased; b) in the gas cap two necessary conditions for the dissolution process already exist: pressure build up and free gas. However, since the oil saturation is very small in this region, gas cannot be completely dissolved in the oil; c) in the area close to the water injection well, water has moved the gas towards the production well, so there is no gas in this area to go back into solution. Therefore, despite the fact that pressure arrives back at the initial value (which is around the bubble point pressure), the gas has not dissolved completely and there is still around 65% free gas in the example studied.

The literature introduces the oil type as the main controller of the gas dissolution process. In 4D seismic interpretations, however, we are dealing with a specific reservoir and a narrow variation range of hydrocarbon type. Therefore, this parameter is not important in the 4D seismic interpretations. My investigations indicate that there are some reservoir scale parameters that have significant effects. Smaller K_v/K_h and transmissibility, and extreme non-linear relative permeability curves increase the volume of the dissolved gas (Figure 5.7). In these situations, it is harder for gas to move towards the upper part of the reservoir. Therefore a large volume of gas is in contact with the original oil. Subsequently, there is higher opportunity for this liberated gas to be dissolved by pressure build up. During 4D seismic interpretation, more careful attention is necessary to these reservoir scale parameters. On the other hand, the effect of the above parameters on the 4D seismic data can be used to indirectly extract parameter estimates from the seismic data to update the simulation model (e.g. reservoir scale relative permeability curves, transmissibility).

4D seismic was found to be a good tool to discriminate the different stages of the gas exsolution and dissolution process (Figure 5.8). Different stages of gas liberation at either pore scale or reservoir scale show timeshifts of more than 0.5ms and velocity changes of

more than 10%. This range sits close to the non-repeatability range for well-acquired and processed 4D seismic data. However, the scenario that belongs to the critical gas saturation shows a small 4D signal that is difficult to distinguish by seismic data. For reservoirs with high critical gas saturation, a significant seismic response can be expected, due to the known non-linear response. In this situation, on the other hand, discrimination between critical and maximum gas saturation is problematic. The effect on density may be employed here. A more in-depth investigation is proposed to take the effect of higher critical gas saturation into account.

The effects of pressure on the 4D seismic signals are typically interpreted using laboratory based measurements. These measurements illustrate an increase in the rockframe properties of the saturated rock with pore pressure drop (effective pressure build up). However, after a specific pressure, this variation is approximately constant. We noticed in this study that this understanding is not valid in the case in which the reservoir pressure drops below the bubble point pressure. In this situation, gas evolves and alters the pressure dependency of the saturated rock. Our investigation illustrates that a softening of the 4D seismic signal (decrease in the P-impedance) can be observed for reservoir pressure drop (Figure 5.12). It is the initial reservoir pressure that plays an important role here. This is important, as understanding the pressure signal in the 4D seismic data is one of the more challenging issues. It is also noted in this study that pressure has a different effect on samples from the oil leg and gas cap, so that the pressure dependency of the saturated rock is a function of saturation. However, because of the presence of two types of gas saturations (maximum and critical gas saturation), this effect is easy to handle in seismic interpretation.

In black oil modelling, R_s (the solution gas oil ratio) is normally employed to simulate different stages of the gas exsolution and dissolution process. This parameter is at the centre of petro-elastic modelling, so its validity is an important issue. A small deviation between the measured and calculated R_s and B_o was observed during the gas exsolution stage (pressure drop). However, when the calculated R_s and B_o are employed to calculate the seismic properties, a deviation by up to 25% and 30% for the oil density and bulk modulus is detected from the measured ones. Furthermore, the calculated R_s and B_o overestimates the pressure effect on the oil bulk modulus and density by up to 100% and 90% respectively (Figure 5.14). This is important, since the oil pressure dependency is the

main controlling factor for the saturated rock pressure dependency in the oil leg (as discussed in previous paragraph). During the gas dissolution stage, on the other hand, R_s is increased by pressure build up in the laboratory, but it is fixed at the reservoir scale due to gas migration. My investigation highlights the impact of this issue on the acoustic properties of the oil. The oil density and bulk modulus do not follow the same path as the exsolution stage. That may prevent employing the same stress sensitivity for the saturated rock for the pressure drop and pressure build up scenarios when below the bubble point pressure (Figure 5.15).

From the literature, a compositional change of the gas and oil is noted during gas exsolution. The effect of this change on the acoustic properties of the fluid was quantified in a North Sea example. After simulating the pressure drop using the equation of state, the percentages of C_1 to C_n are extracted for both gas and liquid phases. As expected, the percentage of lighter components goes down with pressure drop, conversely the percentage of the heavier components are increased for both gas and liquid phases (Figure 5.17). The result of this phenomenon is that gas and oil are heavier step by step with pressure decrease. However, the effect of this change is very small (less than 0.6%) for the gas phase. The variation is even smaller in the density of the saturated rock (less than 0.01%). Therefore, the effect of the gas compositional change is negligible in the 4D seismic.

On the other hand, the oil compositional change is found considerable, but it is already included in black oil modelling using the R_s concept. To investigate the accuracy of this concept to cover the compositional change, a black oil model is built from the compositional model. After simulating pressure drop, oil density is separately calculated for both models. There was an excellent match and it can be stated as a conclusion that employing the solution gas oil ratio in the black oil modelling can cover the oil compositional change during gas exsolution stage adequately. However, as discussed earlier, use of the proposed equations to calculate R_s could be a source of error. These equations are not valid at the gas dissolution stage. R_s and B_o should be directly extracted from laboratory measurements or from a good simulation model.

7.5 Adaptive scaling for an enhanced dynamic interpretation of 4D seismic data

In Chapter 6, importance is drawn to the role of engineering principles when interpreting and estimating dynamic information from seismic. It has been the expectation of the seismic community that 4D seismic signatures must respond to the depth-averaged property and that this should, therefore, be used as an independent variable in seismic equations. Indeed, time-lapse studies focusing on mapped changes have implicitly assumed depth average properties. Whilst such an approach appears encouraging, this particular choice is not the only one available, nor the most obvious choice. Other possibilities are independent variables that are thickness scaled ($h.\Delta P$) and pore volume scaled ($h.\phi.NTG.\Delta P$). In general, the volumes over which each of the physical changes occurs are of different thicknesses (h_P, h_w, and h_g for pressure, water and gas saturation respectively), and overlap to different extents across the reservoir depending on the mechanism and timing of the production and recovery processes (Figure 6.6). Therefore, for a 4D seismic difference signature in which the impact of these changes overlaps, this production-induced thickness scaling must be taken into account.

To analyse the above in more detail, synthetic seismic were modelled from the field simulation model. Modelling provides us with a way to examine the impact of pressure, gas and water saturation changes on the seismic, by independently isolating each of these controlling factors during the seismic modelling step. It was numerically proven that the mapped seismic response is decomposed linearly into the effect of the pressure, water and gas saturation (Figure 6.7). Next, the time-lapse seismic responses corresponding to each change are cross-plotted against the three independent variables suggested above: that is, the depth averaged, production thickness scaled, and pore volume scaled quantities. The pore volume scaled variable is observed to show the strongest linear correlation with the seismic data, possessing a symmetric distribution about a mean linear trend. The relationships for the timeshift and amplitude change attributes were separately extracted, and in general presented as the following multi-linear equation:

$$\Delta A(\Delta P, \Delta S_g, \Delta S_w) \approx \left(ah_P[\phi NTG]_P \Delta P + bh_g[\phi NTG]_g \Delta S_g + ch_w[\phi NTG]_w \Delta S_w\right) \qquad (7.1)$$

where the square bracketed terms refer to averages of the effective porosity ϕNTG over the depth range affected by the particular change. Thus, the mapped seismic response is dependent on the changes averaged over the total pore volume. The coefficients *a*, *b* and *c* represent the contributions from the petroelastic model. An important conclusion of this work is that the presence of gas now appears as a linear term in gas pore volume only, rather than a non-linear function of gas saturation. The gas saturation in the oil leg is very small for this particular field and the impact on the seismic is negligible when compared to the changes due to S_{gmax} in the gas cap. These results do depend on the relative permeability curves and geological facies, and may thus vary in detail from reservoir to reservoir. If, for other reservoirs, there is a higher critical gas saturation, the gas term in Equation 7.1 will be decomposed into two linear terms which take account of the gas saturation in the oil leg as well as in the gas cap.

To demonstrate how Equation 7.1 may be of value in quantitative interpretation, the observed seismic data are inverted for pressure and saturation changes using the principle above and the approach of MacBeth *et al.* (2004). For this purpose, four seismic attributes are considered. It is assumed that the adaptive scaling principle applies to these attributes also. According to this procedure, the unknown petroelastic coefficients (*a*, *b* and *c* in Equation 7.1) for each attribute are calibrated at wells in this segment for which changes in pressure and saturation are known with accuracy from fluid flow simulation prediction using the history matched simulation model. After this stage, least squares inversion of all the selected attributes yields the desired results automatically (Figures 6.14, 6.15 and 6.16). These results are now the pore volume scaled pressure or saturation changes across the reservoir, and must, therefore, be compared with the corresponding values from the simulation model for updating purposes. The results show that the simulator does appear to predict the inverted seismic observations fairly accurately; however, there are also some noticeable differences which require some specific updates to the transmissibility multipliers (and hence barriers) and the net-to-gross distribution in the simulation model.

The linear approximation for pressure and saturation changes is found to be valid for most reservoir conditions in this study. However, modelling has shown that it does break down for reservoirs of thickness greater than 40m and, at this point, a non-linear term for pressure is required. One possible drawback of the proposed linearised form is that simulation model

updates can only be achieved by comparing the results with corresponding scaled dynamic changes from the simulator. As the product of the thickness of the affected volume, net-to-gross and porosity are not known with certainty in practice it is not possible to convert the final results of this inversion immediately into absolute values of pressure and saturation changes. There is, therefore, an inherent ambiguity when comparing predictions from the simulator with seismic inversion results. This prevents independent determination of static and dynamic parameters, and places a strong emphasis on the need for assigning an appropriate static model before dynamic model updates can be implemented with accuracy. This comes as no surprise, as a similar conclusion has been reached by research into the seismic history match (Stephen and MacBeth, 2008).

7.6 Recommendations for future work

(a) Employing 4D seismic data to extract petrophysical and engineering data

The reservoir's petrophysical and engineering properties such as porosity, NTG, permeability, K_v/K_h and relative permeability curves are typically extracted from laboratory measurements or well data. 3D seismic data are also employed in this procedure. However, large uncertainty exists in the spatial distribution of these data. The scale problem sometimes prevents direct application of the laboratory and well data in the simulation model. 4D seismic can possibly be used to extract reservoir scale properties. As discussed in Chapter 5, these reservoir scale parameters have considerable impact on the gas dissolution process, and furthermore on the 4D seismic signal. For example, smaller K_v/K_h and transmissibility, and extreme non-linear relative permeability curves, increase the volume of dissolved gas. The effect of these parameters on the 4D seismic data can be used to indirectly extract parameter estimates from the seismic data to update the simulation model. This point is proposed as a future research topic.

(b) The effect of rock types

In my case studies, due to minor geological heterogeneity, the entire reservoir was assumed to be one facies by the data provider, so that fixed engineering properties such as relative permeability and capillary curves are used. Nonetheless, in some heterogeneous reservoirs, different facies and curves may are employed. This heterogeneity may impact the absolute

value of the maximum gas saturation. Therefore, different maximum gas saturation is possibly observed in these reservoirs. However, as the saturation is approximately constant inside each facies, it could be easily handled in the 4D seismic interpretations, and is proposed for further work.

The magnitude of the initial velocity and density is an important issue for the 4D seismic signal. My sensitivity analysis shows a higher 4D change for rocks that initially contain lower velocity and density. I selected identical pressure and saturation changes for different rocks, but 4D changes were not the same for these scenarios. The higher the initial velocity and density, the smaller 4D change. That is possibly why high velocity carbonate reservoirs demonstrate weak 4D signals. This effect should be included in reservoirs that contain a variety of facies with a large variation in seismic properties. More data sets are necessary to investigate the effect of the initial velocity and density on the magnitude of the 4D seismic signal.

(c) The effect of the critical gas saturation

Critical gas saturation is small in my case study, so gas is moveable at lower saturations. This property is a function of the rock and facies type, and it varies from field to field. The studies provided in Chapter 5 were guided by the case study. It is proposed to choose a range of saturation to find the impact of higher critical gas saturations. Because the non-linear response of velocity change to the gas saturation, high critical saturation may show the same signal as the maximum gas saturation. The density effect may be exploited to overcome this problem, but is proposed as further work.

(d) Gas distribution in very low permeable reservoirs

The gas saturation distribution found in this thesis depends on the rock permeability and transmissibility. As discussed in Chapters 2 and 3, in very low permeable reservoirs (e.g tight gas reservoirs) gas saturation may present as a large variation across the reservoir (both vertically and horizontally). Such a large variation could possibly break down the proposed linearity in the seismic domain and the hypothesis provided in this study, so it is recommended to do an investigation before applying my results to these reservoirs. The realistic engineering data (such as relative permeability and capillary pressure curves), specifically for these reservoirs, should be used in this research to quantify the order of the

saturation variation.

(e) Saturation distribution and seismic signal for the smaller time lines

My observations highlight the time required for gas migration and stabilization in the gas cap. This is true for both gas injection and exsolution cases. Saturation equilibrium is reached very quickly (less than a month) for the homogeneous model, while it takes slightly longer (less than 6 months) for the heterogeneous model. This point is not an important issue when working with normal 4D seismic time lines (one year and more), but it should be taken into account in highly repeated 4D seismic data (less than 6 months). The wider range of gas saturation variation may increase scattering in the seismic response that may, in turn, break down the expected linearity. Since the time between seismic repeats has become smaller in recent times, so the effect of the saturation equilibrium needs to be included. Research is proposed to quantify the magnitude of the saturation variations (both gas and water) at the smaller repeat times, and the impact of this variation in the seismic domain.

(f) Seismic signal around bubble point pressure

It is mainly believed that gas liberation makes a significant seismic change. When gas bubbles come out of solution, phase changes can be easily observed in the 4D seismic data, even for a few percent of gas. However, Han and Batzle (2000) and (2002) state that gas behaves like a fluid at high pressure. The liberated gas may not be detectable around the bubble point pressure using 4D seismic. A major pressure drop is necessary to identify the exsolved gas. Firoozabadi (1999) presented a few examples that support both of these statements, but most of his examples show considerable change of the acoustic wave properties close to the bubble point. A comprehensive literature review, as well as laboratory measurements, is proposed to discover the acoustic properties of the fluid close to the bubble point and dew point pressure. Different oil samples with different bubble points are necessary to detect the wave behaviour for a variety of pressures.

(g) Interaction between gas and oil

Interaction between gas and fluid, either oil or water, is a challenging subject. Using laboratory measurements, the harmonic averaging of the gas and oil bulk modulus has been regularly recommended to calculate the fluid bulk modulus. However, Firoozabadi (1999)

states that, due to the mass transfer between gas and oil, harmonic averaging may not valid, and the fluid bulk modulus may even be below the harmonic average. Research is proposed to investigate two phases (gas and oil) and three phases (gas, oil and water) fluid mixing laws. Interaction between the gas and fluid phases can be extracted using thermodynamic equations or laboratory measurements.

(h) How reliable is the amplitude change signal?

It is possible to have both destructive and constructive effects in the amplitude change response. My sensitivity analysis in a multi-layer reservoir shows that the location of the pressure and saturation change is important for the amplitude change signal. For example, when gas accumulates in the top layer, a softening signal is observed for gas. However, for gas accumulation in the second layer (when there is no gas in the first layer), an interference effect makes a hardening signal for gas that is completely contradictory to that expected. A destructive effect in amplitudes was also observed in the southern part of the An'Teallach field, which generates a negative or zero 4D signal for the injected gas. This is highlighted in reservoirs that contain a few thin layers, in which there is a pressure or saturation change inside only one of them. The 4D change (both magnitude and sign) depends on the position of that specific layer inside the reservoir. Timeshift is more reliable in these situations. Furthermore, heterogeneity of the overburden and underburden (immediately above or below the reservoir) has a significant impact on the 4D seismic signals. My sensitivity analysis shows that the presence of a small sand wedge model above the reservoir has a big impact on the 4D seismic signal due to the tuning effect. Therefore, it is suggested to construct different geological scenarios to investigate the effect of the structural heterogeneity (inside the reservoir, overburden and underburden) on the amplitude change.

(i) Gas injection for IOR

Gas injection into the aquifer for disposal aims and gas out of solution due to reservoir pressure drop were investigated in this project. Specific properties of gas injection for IOR make it different from the above case studies. Since the gas is injected to increase the reservoir pressure, solubility of gas in oil is an important issue. This phenomenon certainly alters the acoustic properties of the oil and gas. Solubility is normally assumed as negligible in the seismic domain (Han and Batzle, 2002, and Meadow, 2008), but it is an important issue in the PVT and thermodynamic literature (Danesh, 1998 and Firoozabadi, 1999).

Beside solubility, the phase change needs to be investigated using the literature and laboratory measurements. As pressure increases with gas injection, the bubble point pressure of the heavier components is perhaps reached, and this produces a phase change of these components.

(j) CO_2 injection for disposal or IOR

Specific properties of carbon dioxide make it different from methane or any other hydrocarbon gas. CO_2 is in a supercritical condition in the reservoir, so it behaves as either gas or fluid. Carbon dioxide in the fluid and gas phases has different acoustic properties (density and velocity) that impact the overall seismic signal. By including the solubility of the CO_2 in water or oil, a complicated system is reached. This phenomenon makes a six phase system (free CO_2 in gas or fluid phases, water and oil with dissolved CO_2, and finally free water and oil). Since each of these phases contains their specific acoustic properties, those effects must be included in 4D seismic interpretations. They also require a new fluid mixing law that includes the interaction between phases. In addition, as the density difference between CO_2 and water is not as large as methane and water, the transition zone that creates the different gas distributions discussed in this thesis is considerable. Because of the importance of the geological storage of carbon dioxide in reducing the environmental problems, and employment of 4D seismic to monitor injected gas, this case is suggested for further investigation.

Appendix A

Derivations from the material balance equations

Considering Equation 6.8, it is possible to derive such a volumetric equation by employing material balance in the reservoir engineering or energy balance equation in the physics. Here, a part of the reservoir in a black oil tank model is taken into account for this aim (Figure A.1). There are some changes after production in the reservoir; a) initial gas cap expansion due to the pressure drop, b) gas liberation and production, c) rock and connate water expansion, and finally d) there is some water in and some water out. The total change in volume is the original oil volume minus present oil volume, and it is equal to the summation of the liberated gas, gas cap expansion, water volume change, and rock and water expansion that can be written as below:

$$\begin{aligned}\text{Total changes in volume} &= N.B_{oi} - (N-N_p).B_o \\ &= [N.R_{si}-(N-N_p).R_s - G_{ps}].B_g + \\ &\quad (G-G_{pc}).B_g-G.B_{gi} + \\ &\quad (W_e - W_p).B_w + \\ &\quad N.B_{oi}(1+m).\Delta P.((C_wS_{wc}+C_f)/(1-S_{wc})) \end{aligned} \qquad (A.1)$$

where N and N_p refer to the initial oil in place and cumulative oil produced, B_o, B_w and B_g are formation volume factor for oil, water and gas respectively (subscript *i* refer to initial), R_{si} and R_s point to the initial and present solution gas oil ratio, G, G_{pc} and G_{ps} are initial gas cap volume, cumulative gas cap and solution gas produced respectively, W_e and W_p represent cumulative water influx and produced, C_w and C_f are water and pore compressibility factor, and finally *m* is ratio of initial gas volume to initial oil volume.

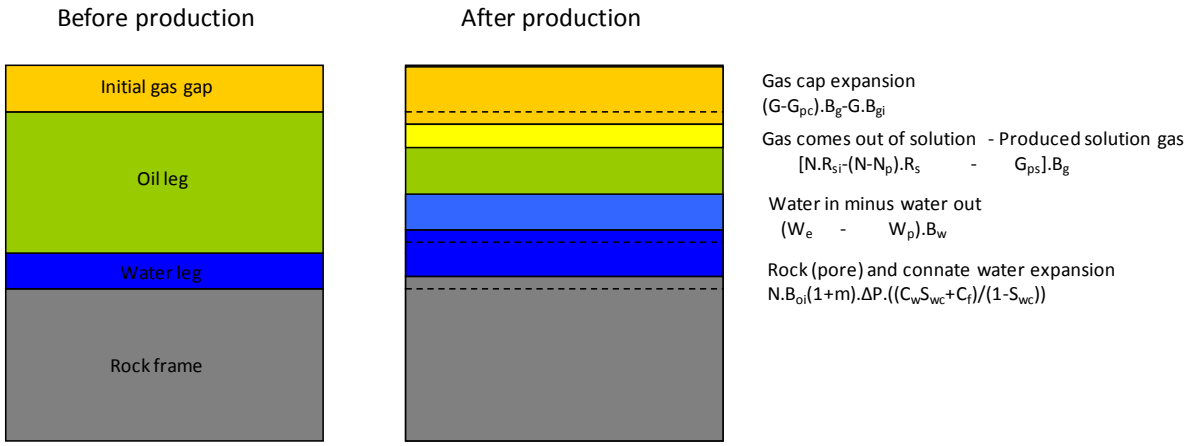

Figure A.1 A simple black oil model before production and after production with the equations representing the production related effects.

The first term is representative of the solution gas volume change in the reservoir conditions: $[N.R_{si}-(N-N_p).R_s - G_{ps}].B_g$ = (liberated gas – produced gas) = $\Delta V_g.B_g$. If we assume no free primary gas cap, so the second term will be zero: $(G-G_{pc}).B_g-G.B_{gi} = 0$. The third term is representative of the water volume change in the reservoir conditions: $(W_e - W_p).B_w = \Delta V_w.B_w$. For the fourth term, as there is no primary free gas cap, so m=0 and $(C_wS_{wc}+C_f)$ can be assumed as C_e which is representative of the compressibility factor. $N.B_{oi}/(1-S_{wc})$ is initial pore volume (V_{pv}). By rearrangement of the equations we arrive at:

$$\text{Total change in volume} = \Delta V_g.B_g + \Delta V_w.B_w + V_{pv}.\Delta P.C_e \qquad (A.2)$$

Pressure change scaled by pore volume represent the effect of pressure change in this equation $V_{pv}.\Delta P = \Delta P_v$. Therefore:

Total change in volume = $C_e.\Delta P_v + B_g.\Delta V_g + B_w.\Delta V_w$. (A.3)

Equation A.3 clearly illustrates that the total change is equal to the gas and water volume change at reservoir conditions plus the pressure change in volumetric form. This confirms, at a conceptual level, Equation 6.8 determined using analytical and numerical studies. The total change is equivalent to the 4D changes in the seismic domain, and these are therefore equal to the summation of the pore volume scaled gas and water saturation change and pressure change.

References

Aarre V., 2007. Estimating 4D Velocity Changes and Contact Movement on the Norne Field. Offshore technology conference, Houston, Texas, USA, OTC 19049.

Ali A., Taggart I., Mee B., Smith M., Gerhardt A. and Bourdon L, 2008. Integrating 4D seismic data with production related effects at Enfield, North West Shelf, Australia. SPE Asia Pacific oil and gas conference and exhibition, Perth, Australia, 116916.

Alsos T., Osdal B., and Høiås A., 2009. The Many Faces of Pressure Changes in 4D Seismic at the Svale Field and Its Implication on Reservoir Management. 71th EAGE Conference and Exhibition, Amsterdam, the Netherlands, 4 pages.

Alvarez, E. and MacBeth, C., 2011. An insightful parameterisation for the flatlander's interpretation of time-lapsed seismic data. Geophysical Prospecting, Submitted.

Amini H., MacBeth C., Shams A., 2011. Calibration of Simulator to Seismic Modelling for Quantitative 4D Seismic Interpretation. 73rd EAGE Conference and Exhibition, Vienna, Austria, 4 pages.

Arts R., Eiken O., Chadwick A., Zweigel P., van der Meer L and Zinszner B., 2004. Monitoring of CO2 injected at Sleipner using time-lapse seismic data. Energy, **29**, 1383–1392.

Backus G. E., 1962. Long-wave elastic anisotropy produced by horizontal layering. J. Geophys. Res., **67**, 4427-4440.

Batzle M. and Wang Z., 1992. Seismic properties of pore fluids. Geophysics, **57**, 1396-1408.

Bertrand A., McQuaid S., Bobolecki R., Leiknes S., Ro H. E., 2005. A high resolution workflow for 4D-friendly analysis: application to gas-oil contact monitoring at Troll West. 75th SEG Annual International Meeting, Expanded Abstracts.

Brie A., Pampur F., Marsala A. F. and Meazza O., 1995. Shear sonic interpretation in gas-bearing sands. SPE Annual Technical Conference, 30595.

Burdine N. T., 1953. Relative permeability calculations from pore size distribution data. Petroleum Transaction, **198**, 71-78.

Burnett M. D. and Castagna J. P., 2003. Application of spectral decomposition to gas basin in Mexico. The Leading Edge, 22, 1130-1141.

Castagna J. P., Sun S. and Siegfried R. W., 2003. Instantaneous spectral analysis: Detection of low-frequency shadows associated with hydrocarbons. The leading Edge, **22**, 120-127.

Castro S. A., Caers J., Otterlei C., Meisingset H., Hoye T., Gomel P. and Zachriassene E., 2009. Incorporating 4D seismic data into reservoir models while honouring production and geologic data: A case study. The Leading Edge, **28**, 1498-1506.

Chopra S. And Marfurt K. J., 2007. Seismic attributes for prospect identification and reservoir characterization. SEG Geophysical Development Series, 11, Society of exploration geophysicists, Tulsa, USA.

Clark, N.J., 1969. Elements of Petroleum Reservoirs. Society of Petroleum Engineers, H.L.Doherty Series, 0-89520-209-3.

Clark V. A., 1992. The properties of oil under in-situ conditions and its effect on the seismic properties of rocks. Geophysics, **57**, 894-901.

Corey A. T. and Rathjens C. H., 1956. Effect of stratification on relative permeability. Petroleum Transaction, AIME, 358-360.

Dake L. P., 2002. Fundamental of Reservoir Engineering. Nineteenth impression, ELSEVEIR Science B. V., Amsterdam, the Netherlands.

Danesh A., 1998. PVT and phase behaviour of petroleum reservoir fluids. ELSEVEIR Science B. V., Amsterdam, the Netherlands.

Domenico, S. N., 1974. Effect of water saturation on seismic reflectivity of sand reservoirs encased in shale. Geophysics, **39**, 759-769.

Domenico, S. N., 1976. Effect of brine-gas mixture on velocity in an unconsolidated sand reservoir. Geophysics, **41**, 882-894.

Domes, F. 2010. The influence of overburden on quantitative time-lapse seismic interpretation. PhD thesis, Institute of Petroleum Engineering, Heriot-Watt University.

Dumont M. H., Fayemendy C., Mari J. L., and Huguet F. 2001. Underground gas storage: estimating gas column height and saturation with time lapse seismic. Petroleum Geoscience **7**, 155-162.

Eiken O., Brevik I., Arts R., Lindeberg E. and Fagerviki K., 2000. Seismic monitoring of CO2 injected into a marine aquifer. 70th SEG Annual International Meeting, Expanded Abstracts.

Falahat R., Shams A., MacBeth C., 2011. Towards quantitative evaluation of gas injection using time-lapse seismic data. Geophysical Prospecting, **59**, 310–322.

Falahat R., Shams A. and MacBeth C., 2011. Adaptive engineering-based scaling for enhanced dynamic interpretation of 4D seismic. 73rd EAGE Conference and Exhibition, Vienna, Austria.

Falahat R., Shams A. and MacBeth C., 2011. Adaptive scaling for an enhanced dynamic interpretation of 4D seismic data. Geophysical Prospecting, Submitted.

Firoozabadi A., 1999. Thermodynamics of hydrocarbon reservoirs. McGraw-Hill Book Co., USA.

Firoozabadi A. and Ramey JR H. J., 1988. Surface tension of water-hydrocarbon system at reservoir conditions. Journal of Canadian Petroleum Technology, **27**, 41-48.

Fletcher J. 2004. Rock and fluid physics understanding the impact of pressure changes. SPE/EAGE Joint Workshop 'What Do Petroleum Engineers Expect from Time Lapse Seismic, and Do Geophysicists Answer The Right Questions?'. 23–25 March, Copenhagen, Denmark.

Floricich M., MacBeth C., Stammeijer J., Staples R., Evans A., and Dijksman C., 2006. A New Technique for Pressure – Saturation Separation from Time-Lapse Seismic - Schiehallion Case Study. 68th EAGE Conference and Exhibition, Vienna, Austria.

Folstad P. G. and Schoenberg M., 1992. Low frequency propagation through fine layering. SEG, ST2.7, 1279-1281.

Freeman P., Kelly S., Macdonald C., Milington J and Tothill M. 2008. The Schiehallion field: Lessons learned modelling a complex deepwater turbidite, the future of geological modelling in hydrocarbon development, the geological society. London, special publication **309**, 205-219.

Fulcher R. A., Ertekin T. and Stahl C. D., 1985. Effect of capillary number and its constituents on two-phase relative permeability curves. Journal of Petroleum Technology, February, 249-260.

Garcia, A., MacBeth, C., and Vejbaek, O., 2011. Estimation of effective stress changes in the reservoir from 4D seismic data. Geophysical Prospecting, Submitted.

Gassmann, F., 1951. Ueber die Elastizität poröser medien, Vierteljahrschrift der Naturforschenden Gesellschaft, Zürich, 96, 1-23 (English translation from http://sepwww.stanford.edu/sep/berryman/PS/gassmann.pdf).

Gei D. and Carcione J. M, 2003. Acoustic properties of sediments saturated with gas hydrate, free gas and water. Geophysical prospecting, **51**, 141-157.

Gestel J. P. V., Kommedal J. H., Barkved O.I., Mundal I., Bakke R, R., Best K. D., 2008. Continuous seismic surveillance of Valhall Field. The Leading Edge, **27**, 1616-1621.

Ghaderi, A., and Landrø, M. 2009. Estimation of thickness and velocity changes of injected carbon dioxide layers from prestack seismic data. Geophysics **74**, 17-28.

Govan A., Primmer T., Douglas C., Moodie N., Davis M. and Nieuwland, 2005. Reservoir management in a deepwater subsea field – the Schiehallion experience. SPE, Offshore Europe, Aberdeen, Scotland, UK, 96610.

Hale D., 2007. A method for estimating apparent displacement vectors from time lapse seismic images. Centre for Wave Phenomena Report 566.

Hamdi H., Amini H., Corbett P. W. M., MacBeth C. and Jamiolahmadi M., 2001. Application of compositional simulation in seismic modelling and numerical well testing for gas condensate reservoir. 73rd EAGE Conference and Exhibition, Vienna, Austria.

Han D. H. and Batzle M., 2000. Velocity, Density and Modulus of Hydrocarbon Fluids -- Empirical Modelling. 70th SEG Annual International Meeting, Expanded Abstracts.

Han D. H. and Batzle M., 2000. Velocity, Density and Modulus of Hydrocarbon Fluids -- Data Measurement. 70th SEG Annual International Meeting, Expanded Abstracts.

Han D. H. and Batzle M., 2002. Fizz water and low gas-saturated reservoirs. The Leading Edge, **21**, 395-398.

Han D. H. and Batzle M., 2004. Gassmann's equation and fluid-saturation effects on seismic velocities. Geophysics, **69**, 398-405.

Heggland R., 2004. Definition of geohazards in exploration 3-D seismic data using attributes and neural-network analysis. The American Association of Petroleum Geologists (AAPG), **88**, 857-868.

Holditch S. A., 1979. Factrors affecting water blocking and gas flow from hydraulically fractured gas wells. Journal of Petroleum Technology, December, 1515-1524.

Hodgson N., MacBeth C., Duranti L., Rickett J. and Nihei K., 2007. Inverting for reservoir pressure change using time-lapse time strain: Application to Genesis Field, Gulf of Mexico. The Leading edge, **26**, 649-654.

Huang X., Will R., Khan M., and Stanley L. 2001. Integration of time-lapse seismic and production data in a Gulf of Mexico gas field. The Leading Edge, **20**, 278-289.

Huang Y. and MacBeth C. 2011. Direct correlation of 4D seismic with well activity for a clarified dynamic reservoir interpretation. Accepted for publication in Geophysical Prospecting.

Huang, Y., MacBeth, C., Barkved, O. and van Gestel, J-P. 2011. Enhancing dynamic interpretation at the Valhall Field by correlating well activity to 4D seismic signatures. First Break, **29**, 37-44.

Hunt J. M., 1995. Petroleum geochemistry and geology. W. H. Freeman and Company, New York, USA.

Hwang L. F. and Lellis P. J., 1988. Bright spots related to high GOR oil reservoir in Green Canyon. 58th SEG Annual International Meeting, Expanded Abstracts.

Katz. D. L., Cornell. D., Vary. J. A., Kobayashi. R., Elenbaas. J. R., Poettmann F. H. and Weinaug, C. F., 1959. Handbook of natural gas engineering, McGraw-Hill Book Co., USA.
Keelan D. K.,1976. A Practical Approach to Determination of Imbibition Gas-Water Relative Permeability. Journal of petroleum technology, February, 199-204.

Knight R., Dvorkin J and Nur A., 1998. Acoustic signatures of partial saturation. Geophysics, **63**, 132-138.

Konishi C., Azuma H., Nabuoka D., Xue Z. and Watanabe J., 2008. Estimation of CO_2 saturation considering patchy saturation at Nagaoka. 70th EAGE Conference and Exhibition, Rome, Italy.

Koster K., Gabriels P., Hartung M., Verbeek J., Deinum G., and Staples R., 2000. Time-lapse seismic surveys in the North Sea and their business impact. The Leading Edge, **19**, 286-293.

Kumar A., Noh M., Pope G. A., Sepehrnoori K., Bryant S. and Lake L. W., 2004. Reservoir simulation of CO_2 storage in deep saline aquifers. SPE/DOE 14th Symposium on Improved Oil Recovery, Tulsa, USA, 89343.

Kvalheim, A.K., Sandø, I.A., Skogland, S.M., Vinje, V., and Carpenter, M. 2007. Impact of time and depth imaging methods on quantitative 4D reservoir management. EAGE 69th Conference and exhibition, London, UK.

Lal W. and Brandt H., 1988. A Pressure History-Matching Method for Determination of Relative PermeabiIities. SPE reservoir engineering, May, 651-661.

Lamers E. and Carmichael S. M. M. 1999. the Palaeocene deepwater sandstone play west of Shetland, petroleum geology of northwest Europe. Proceedings of the 5th conference, the geological society, London, 645-659.

Landrø M., 2001. Discrimination between pressure and fluid saturation changes from time-lapse seismic data. Geophysics, **66**, 836–844.

Langlais V., Mezghani M., and Lucet N. 2005. 4D monitoring of an underground gas storage using an integrated history matching technique. SPE 95838.

Lee M. W., 2004. Elastic velocities of partially gas-saturated unconsolidated sediments. Marine and Petroleum Geology, **21**, 641–650.

Link P. K., 2001. Basic petroleum geology, third edition. OGCI publications, Tulsa.

Lu S. and McMechan G. A., 2002. Estimation of gas hydrate and free gas saturation, concentration, and distribution from seismic data. Geophysics, **67**, 582-593.

Lumley D., Adams D., Wright R., Markus D. and Cole S., 2008. Seismic monitoring of CO2 geo-sequestration: realistic capabilities and limitations. 78th SEG Annual International Meeting, Expanded Abstracts.

MacBeth C., 2004. A classification for the pressure-sensitivity properties of a sandstone rock frame. Geophysics, **69**, 497-510.

MacBeth C., Hajnasser Y., Stephen K. and Gardiner A., 2011. Exploring the effect of meso-scale shale beds on a reservoir's overall stress sensitivity to seismic waves. Geophysical Prospecting, **59**, 90-110.

MacBeth, C., Soldo, J., Floricich, M., 2004, Going quantitative with 4D seismic. 74th SEG Annual International Meeting, Expanded Abstracts.

MacBeth C. and Stephen K, 2008. Seismic scale saturation relations in turbidite reservoirs undergoing waterflood. Geophysical Prospecting, **56**, 693–714.

MacCain Jr. W. D., 1990. The properties of petroleum fluids. PennWell Publishing Company, Tulsa, USA.

Martin K. and Macdonald C., 2010. Schiehallion Field: Applying a Geobody Modelling Approach to Piece Together a Complex Turbidite Reservoir. 7th European Production and Development Conference, Aberdeen, UK.

Mavko, G., Mukerji, T., and Dvorkin, J. 2003. The rock physics handbook: tools for seismic analysis in porous media. Cambridge University Press.

Meadows M. 2008. Time-lapse seismic modelling and inversion of CO2 saturation for storage and enhanced oil recovery. The Leading Edge, **27**, 506-516.

Meadows M. Adams D., Wright R., Tura A. and Cole S., 2005. Rock physics analysis for time-lapse seismic at Schiehallion field. Geophysical Prospecting, **53**, 205-213

Mehdizadeh H., Srivastava R. P., Vedanti N and Landro M. 2010. Seismic monitoring of in situ combustion process in a heavy oil field. Journal of geophysics and engineering, **7**, 16-29.

Mondal D., 2010. A critical analysis of pressure signal extraction from 4D seismic data. 23rd ETLP technical and sponsor meeting, November, Edinburgh, UK.

Morgan J. T. and Gordon D. T., 1970. Influence of pore geometry on water-oil relative permeability. Journal of Petroleum Technology, October, 1199- 1208.

Morrow N.R. and Melrose J.C. 1991. Application of capillary pressure measurements to the determination of connate water saturation. In: Interfacial Phenomena in Petroleum Recovery (ed. N.R. Morrow). 257–287. Marcel Dekker Inc., New York.

Mulyadi H., Amin R. and Kennaird A. F., 2001. Core Practical Approach to Determine Residual Gas Saturation and Gas-Water Relative Permeability. SPE Annual Technical Conference and Exhibition, New Orleans, USA, 71523.

Ng, H.T., Bentley, L.R., and Krebes, E.S. 2005. Monitoring fluid injection in a carbonate pool using time-lapse analysis: Rainbow Lake case study. The Leading Edge, **24**, 530-534.

O'Brien J., 2004. Seismic amplitudes from low gas saturation sands. The Leading Edge, **23**, 1236-1243.

Oyedele O., 2005. 3-D high resolution seismic imaging of deep water systems, SE Green Canyon, Sigsbee Escarpment, Golf of Mexico. M.S. thesis, University of Houston (From Chopra and Marfurt, 2007).

Pentland C. H., Al-Mansoory S., Iglauer S., Bijeljic B. and Blunt M. J. 2008. Measurements of non-wetting phase trapping in sand packs. SPE Annual Technical Conference and Exhibition, Denver, USA, September, 115697.

Pickup G.E. and Sorbie K.S., 1996. The scaleup of two-phase flow in porous media using phase permeability tensors. Society of Petroleum Engineers Journal, December, 369–381.

Richardson S. M., Herbert N. and Leach H. M., 1997. How well connected is the Schiehallion reservoir. SPE, Offshore Europe Conference, Aberdeen, Scotland, UK, 38560.

Rojas E, Davis T. L., Batzle M., Prasad M. And Michelena R. J., 2005. Vp-Vs ratio sensitivity to pressure, fluid, and lithology changes in tight gas sandstones. 75th SEG Annual International Meeting, Expanded Abstracts.

Sengupta M. and Mavko G, 2003. Impact of flow-simulation parameters on saturation scales and seismic velocity. Geophysics, **68**, 1267-1280.

Sengupta M., Mavko G. and Mukerji T., 2003. Quantifying subresolution saturation scales from time-lapse seismic data: A reservoir monitoring case study. Geophysics, **68**, 803-814.

Shams A., Macbeth C. and Gozalpour F., 2007. Determination of the Acoustic Properties of Hydrocarbon Rich Gases Using PVT Relations. EAGE 69th Conference & Exhibition, London, UK .

Sigit, R., Morse, P., and Kimber, K., 1999. 4-D seismic that works: A successful large scale application, Duri Steamflood, Sumatra, Indonesia. 69th SEG Annual International Meeting, Expanded Abstracts.

Smith A. A., MacGregor J. and Angert P., 2000. Reservoir geological modelling of the Schiehallion Field, west of Shetland, using IRAP-RMS: building the FFM2000 static model. BP internal report, unpublished.

Smith T. M., Sondergeld C. H. and Rai C. S., 2003. Gassmann fluid substitutions: A tutorial. Geophysics, **68**, 430-440.

Staples R., Cook A., Braisby J., Hodgson B., and Mabillard A., 2006. Integration of 4D seismic data and the dynamic reservoir model reveal new targets in Gannet C. The Leading Edge, **25**, 1126-1133.

Staple R., Hague P., Cooke G., Ashton P., Stammeijer J., Jolley S., Stevens T. and Marshall J 2002. Integrating 4D seismic to optimise production. SPE 13th European Petroleum Conference, Aberdeen, Scotland, UK.

Staple R., Stammeijer J., Jones S., Brain J., Smit F. and Hatchell P, 2006. Time-Lapse (4D) Seismic Monitoring - Expanding Applications. CSPG-CSEG-CWLS convention, 181-189.

Stephen K. D., and MacBeth C., 2008. Reducing reservoir prediction uncertainty by updating a stochastic model using seismic history matching. SPE Journal, December, 991-999.

Tiab D. And Donaldson E. C., 2004. Petrophysics, Theory and practice of measuring reservoir rock and fluid transport properties. Golf Professional Publishing, Elsevier, USA.

Timur A. 1968. An investigation of permeability, porosity and residual water saturation relation for sandstone reservoirs. The Log Analyst, **9**, 8-15.

Theune, U., Schmitt, D., and Rokosh, D., 2003. Feasibility study of time-lapse seismic monitoring for heavy oil reservoir development - The rock-physical basis. 73rd SEG Annual International Meeting, Expanded Abstracts.

Thomas L. K., Hankinson R. W. and Phillips K. A., 1970. Determination of Acoustic Velocities for Natural Gas. Journal of Petroleum Technology, July, 889-895.

Todd A., 2007. Reservoir Engineering. MSc Course notes, Institute of petroleum engineering, Heriot-Watt University.

Tonnessen R. K., ElOuair Y. And Alsos T., 2005. Comparing size of observed and modelled 4D effects. 67th EAGE Conference and Exhibition, Madrid, Spain.

Torskaya T., Jin G. and Torres-Verdın C., 2007. Pore-Level Analysis of the Relationship Between Porosity, Irreducible Water Saturation, and Permeability of Clastic Rocks. SPE Annual Technical Conference and Exhibition, Anaheim, USA, 109878.

Tsuneyama F. and Mavko G., 2007. Quantitative detection of fluid distribution using time-lapse seismic. Geophysical Prospecting, **55**, 169–184.

Tura, A., and Lumley, D. E., 1999. Estimating pressure and saturation changes from time-lapse AVO data. 69th SEG Annual International Meeting, Expanded Abstracts, 1655-1658.

Vidal S., Jardin A. and Huguet F., 2001. Feasibility Study of Time-Lapse Parameters Estimate for Mean Effective Stress and Saturation Changes in Gas Storage. 71st SEG Annual International Meeting, Expanded Abstracts.

Waggoner J. R., Cominelli A. and Seymour R, H., 2002. Improved reservoir modelling with time-lapse seismic in a Gulf of Mexico gas condensate reservoir. SPE Annual Technical Conference and Exhibition, 77514.

Wagner S., Pennington W. and MacBeth C., 2004. Gas Saturation Calculated from Patchy and Homogeneous Models at Foinaven Field. 74th SEG Annual International Meeting, Expanded Abstracts.

Walls J. and Dvorkin J, 2005. Effects of Pore Fluid Properties at High Pressure and Temperature on Seismic Response. 75th SEG Annual International Meeting, Expanded Abstracts.

Wang Z., Nur A. and Batzle M. L., 1988. Acoustic velocities in petroleum oils. 63rd Society of Petroleum Engineering Technology Conference, 18163.

Wyllie, M. R. J., Gregory, A. R., and Gardner, L. W., 1956. Elastic wave velocities in heterogeneous and porous media. Geophysics, **21**, 41-70.

Wyllie M. R. J. and Rose W. D., 1950. Some Theoretical Considerations Related to the Quantitative Evaluation of the Physical Characteristics of Reservoir Rock from Electric Log Data. Trans. AIME, **189**, 105-118.